Tuberculosis:
how different synthetic analogues of pathogen associated mycolates affect lipid homeostasis of murine host macrophages

by

ILKE VERMEULEN

Submitted in partial fulfilment of the requirements for the joint-degree

DOCTOR OF PHILOSOPHY
in
Biochemistry

In the Faculty of Natural & Agricultural Sciences
Department of Biochemistry
University of Pretoria
South Africa

and

DOCTOR OF SCIENCE
in
Biochemistry and Biotechnology

In the Faculty of Sciences
Department of Biomedical Molecular Biology
Ghent University
Belgium

December 2016

Tuberculosis: how different synthetic analogues of pathogen associated mycolates affect lipid homeostasis of murine host macrophages

by

Ilke Vermeulen[1,2]

Academic year: 2016

Promoters: Prof. Jan Verschoor[1] (University of Pretoria, South Africa)

Prof. Johan Grooten[2] (Ghent University, Belgium)

Examination of this dissertation was performed by external (unaffiliated) and independent internal examiners.

Examination committee: Prof. R. Benner[3]

Prof. C. J. Reinecke[4]

Prof. W.-D. Schubert[1]

Prof. P. Brouckaert[5]

[1]Department of Biochemistry, University of Pretoria, Pretoria, South Africa.
[2]Laboratory of Molecular Immunology, Department of Biomedical Molecular Biology, Ghent University, Ghent, Belgium.
[3]Middeldijk, Barendrecht, The Netherlands.
[4]Department of Biochemistry, North-West University, Potchefstroom, South Africa.
[5]Laboratory of Molecular Pathophysiology and Experimental Therapy, Department of Biomedical Molecular Biology, Ghent University, Ghent, Belgium.

SUBMISSION DECLARATION

I, Ilke Vermeulen declare that the thesis, which I hereby submit for the joint-degree *of Doctor of Philosophy in Biochemistry* at the University of Pretoria (Pretoria, South Africa) and of *Doctor of Science in Biochemistry and Biotechnology* at Ghent University (Ghent, Belgium), is my own work as has not previously been submitted by me for a degree at this or any other tertiary institution.

SIGNATURE: 

DATE: 6 December 2016

PLAGIARISM DECLARATION

Full name: Ilke Vermeulen

Student number: 27021476 (University of Pretoria) and 01101869 (Ghent University)

Title of work: **Tuberculosis: how different synthetic analogues of pathogen associated mycolates affect lipid homeostasis of murine host macrophages**

1. I understand what plagiarism entails and am aware of the University's policy in this regard.

2. I declare that this thesis is my own, original work. Where someone else's work was used (whether from a printed source, the internet or any other source) due acknowledgement was given and reference was made according to departmental requirements.

3. I did not make use of another student's previous work and submit it as my own.

4. I did not allow and will not allow anyone to copy my work with the intention of presenting it as his or her own work.

SIGNATURE: 

DATE: 6 December 2016

ETHICS STATEMENT

The Author, whose name appears on the title page of this thesis, has obtained, for the research described in this work, the applicable research ethics approval. The Author declares that she has observed the ethical standards required in terms of the **University of Pretoria's** and **Ghent University's** Code of Ethics for researchers and the Policy Guidelines for responsible research.

SIGNATURE: 

DATE: 6 December 2016

I dedicate this work to an exceptional man,

Hendrik Johannes Vermeulen

You exemplify strength, intelligence, commitment and integrity.
Your life story and success have profoundly inspired me.
Without you this, or any other academic pursuit, would not have been attainable.

I am grateful for your vision, trust and conviction in me, Dad.
This is for you.

ACKNOWLEDGEMENTS

First and foremost I would like to extend my sincere gratitude to my promoters, Professors Jan Verschoor and Johan Grooten, for their continuous support and supervision throughout the duration of this doctoral study. Johan, thank you for welcoming me into the Laboratory of Molecular Immunology (LMI) in Ghent where I conducted the experimental work, and for allowing me to train and grow as a young scientist under your skilful and kind-hearted supervision. The experience obtained in Belgium I deem immensely valuable. Prof. Jan, we make an excellent team! This past year especially is testament to that. You are an inspiration and it was a privilege working with such an intellectual and enthusiastic scientist. Though it entailed long hours, you always provided enough quality coffee to sustain each brain-storming or manuscript-grinding session. You taught me that PhD study is a process, not a destination. I am immensely appreciative for your encouragement and guidance.

To the director of the Antiviral Gene Therapy Research Unit (AGTRU) and my current place of work, Professor Patrick Arbuthnot, thank you for bearing with me throughout the writing-up period of my PhD thesis. Your continuous motivation and understanding of personal circumstances are surely appreciated.

To my past and present colleagues of the LMI (Sarah, Muriel, Charlotte, Ans, Thomas, Stefaan and Vimal) and AGTRU (Camilla, Kristie and Sam), I am thankful for your support. A few key people at the Flemish Institute of Biotechnology furthermore deserve my gratitude. Pieter Bogaert, Vera Goossens, Annelies Van Hecke, Bram Laukens, Evelyn Plets, Ann Meeus, Ann Schepens, Jannick Leoen, Chantal Eichperger, Saskia Lippens, Eef Parthoens, Evelien Van Hamme, Xavier Sealens, Chantal Bogaert, Daisy Ginneberge, Charly van Kuijck, Geert Versporten, Myriam Scherpereel and Marita Van Hauwermeiren: thank you for your kind assistance and friendly smiles during my doctoral studies. Also from the

Katholiek Universiteit Leuven, Professor Johan Swinnen and Dr Katarzyna Bloch, thank you for the productive lipidomics collaboration.

To the dear friends I made in Ghent, thank you for making Belgian life a pleasant and unforgettable experience. My Dutch friend Martje, coincidentally also a foreigner even if just from across the border, for all the memories made in Ghent and beyond - thank you for being there throughout. We survived Huis Begijnhoflaan, became prominent film festival goers and even enjoyed many a Belgian beer or South African wine together. I am immensely grateful for your and Joep's sincere friendship. All the best with the final year of your PhD. Sarah, you are one of the loveliest women I know. The immediate friendship we formed upon your return to the LMI was a true reflection of your benevolent nature. Lore and Elena are greatly blessed with a mother like you. Corinne, not only did we enjoy many exciting discussions, but you became a very dear friend. You are such a sophisticated woman, true to Swiss standard. I am humbled and delighted to have attended your and Oli's beautiful Lake Thun wedding. Good luck with completing the write-up of your PhD thesis. Veerle, Vie! You have an exuberant soul! You taught me a lot about Belgium and in particular, the strong sense of identity associated with the West-Vlaanderen way.

I would also like to thank Dr Erica Houthuys (Inflammation Research Center, Ghent) for provision of the BCG-dsRed, the Bio Imaging Core facility of the Flemish Institute of Biotechnology (Ghent) for microscopy training, Dr Marnik Vuylsteke (Gnomixx, Ghent) for statistical analysis guidance and Dr Jan-Åke Gustafsson (Karolinska Institute, Sweden) for the LXR-KO mice. Thank you to the funding bodies for financial support of this work, namely the National Research Foundation (South Africa) and Fund for Scientific Research (FWO, Belgium).

DANKWOORD

Daar is soveel ongelooflike mense wat deel gevorm het van die PhD periode in my lewe. Aan die vier sterk manne wat alles die moeite werd maak, dankie! Barend, niemand weet so goed soos jy hoeveel tyd en frustrasie saam só ‘n PhD studie gepaard gaan nie, want jy was daar van die begin tot die einde. Jy besit soveel onmeetbare eienskappe, en élkeen het my gedra deur hierdie tyd. Jou sagte geaardheid, begrip vir die vroeg uit-die-vere en ure aaneen agter die rekenaar; al die inkopies, ontbyt en aandetes wat jy voor gesorg het; en hoe jy altyd geduldig vir my gewag het om klaar te maak agter die rekenaar sodat ons ‘n braaitjie kon maak of ‘n glas wyn kon geniet. Jy is verby spesiaal, dankie vir ál jou ondersteuning en liefde. Pa Hen en boet Hen – absoluut die beste voorbeeld van die appel-en-die-boom – intilligent, gedrewe, staatmakers. Ek kan nie die lewe inbeeld sonder julle nie. Dad, waar begin ek? Géén woorde kan beskryf hoe dankbaar ek is vir Pa se leiding, ondersteuning, opheffing en aanmoediging. Pa is my rots en inspirasie, en bo die gevoel van verligting dat dié tesis nou afgesluit kan word, is die drywende krag wat dit bied om Pa trots te maak. Dankie, Dad. Hens, ek kyk só op na jou. Hoe jy volhard en suksesvol uitdraai in elke uitdagende situasie, is lofwaardig. Vir al die lewenslesse en dat jy áltyd daar is vir my, dankie. Jy is yster! Kaelan, jy is ‘n pragtige jong man en reeds bogemiddeld lewenswys. Wat ‘n voorreg om jou as deel van my lewe te hê. Dankie vir jou sin vir humor, nederigheid en liefde. Ek is geweldig trots op jou!

Aan die lewenskragtige en wonderlike vroue wat my inspireer en motiveer, wil ek opreg dankie sê vir al die liefde en ondersteuning. My pragtige mams, al bly ons so ver van mekaar af is dit so lekker om te weet ek kan enige tyd gesels. Dankie vir mam en Derek se bystand, elke spesiale herinnering, en al jul onvoorwaardelike liefde. Dieds, jou hart is goud. Jy is so ‘n sterk vrou en ek is baie dankbaar vir alles wat jy vir ons, Kaelan en Pa doen. Skoonsus Dori, ‘n absoluut geweldige moeder vir die drie orrelpypies (Mia, Hennie en Kelsie). Dankie

vir jul liefde. Aan my drie spesiale tannies, hoe geseënd is die lewe met jul daarin. Tan Riek, tan Meraai en Katryn - julle is juwele.

Ek is opreg dankbaar vir my dinamiese familie, skoonfamilie asook familie-vriende se ondersteuning. Aan almal van julle, julle is ongelooflik. Verál Suzette en Leslie, Japie en Susan, Wettie, Ferds en Rupert, Arno en Corné, Johann, Barry, ouma Helen, Estelle en André, Eben en Isabel, Zandri en Hanro, Elna en André – julle is almal uitsonderlike mense, baie dankie vir jul bystand. Aan my pragtige skoonfamilie: Karin en Johan, Margaux en Juan, Riaan en Lizaan, Marlene en Jayden – besónders dankie.

Ma Magda en Pa Johan, niks kan die leemte vul van jul skielike afsterwe 18 maande gelede… Die opregtheid van jul harte, was onmeetbaar. Ons mis julle elke dag.

Aan al my ongelooflike vriendinne en vriende, jul bystand en aanmoediging is só baie waardeer. Spesifiek die volgende mense: Cindy, Sean, Inge, Struan, Charanez, David, Mauritz, Laurene, Werries, Lilian, Lezaan, Ella, Elizabeth – vir al die ondersteuning, geselsies, braais en uithouvermoë (haha), dankie julle. Tenminste hoef daar nie meer gevra te word ‘wanneer kry jy klaar nie’. My hartsvriendinne Charanez, Cindy, Inge – baie dankie vir minstens twintig jaar van ondersteuning en liefde. Positiwiteit straal uit jul uit. Die miljoen boodskappies terwyl ek in België gewoon het en tydens die opskryf periode van die tesis, was opreg waardeer. Mau: Ctrl+P ☺

TABLE OF CONTENTS

APPENDIX I Exploration of comparative *ex vivo* cellular technologies

Note: The appendix is located on an additional compact disc provided with this thesis

LIST OF FIGURES AND TABLES

CHAPTER I

CHAPTER II

CHAPTER III

APPENDIX *(located on an additional compact disc provided with this thesis)*

LIST OF SUPPLEMENTAL DATA

Note: Supplemental data are located on an additional compact disc provided with this thesis

CHAPTER II

CHAPTER III

LIST OF MAIN ABBREVIATIONS

αMA | alpha mycolic acid
AA | arachidonic acid
ABCA1 | ATP-binding cassette transporter A1
ABCG1 | ATP-binding cassette transporter G1
ANOSIM | analysis of similarity
APC | antigen presenting cells
apoAI | apolipoprotein A-I
ATP | adenosine triphosphate

BCG | bacille Calmette-Guérin

Cer | ceramide

ER | endoplasmic reticulum
ESI-MS/MS | electrospray ionisation tandem mass spectrometry

GLM | generalised linear model

HDL | high density lipoprotein
HIV | human immunodeficiency virus
MA | mycolic acid
MA-bb | mycolic acid backbone
MA mix | natural mycolic acid mixture
MGC | multinucleated giant cell
mMA | methoxy mycolic acid
MHC | major histocompatibility complex
MOI | multiplicity of infection
Mtb | *Mycobacterium tuberculosis*
MUFA | monounsaturated fatty acids

NADH | nicotinamide adenine dinucleotide, reduced
NADPH | nicotinamide adenine dinucleotide phosphate, reduced
NO | nitric oxide

PAMP | pathogen-associated molecular pattern
PC | phosphatidylcholine
PE | phosphatidylethanolamine

IFNγ | interferon gamma
IL | interleukin
i.p. | intraperitoneal
i.t. | intratracheal

kMA | keto mycolic acid
KO | knockout

LD | lipid droplet
LDL | low density lipoprotein
LDLR | low density lipoprotein receptor
Lipo | liposome carrier
LPL | lysophospholipid
LPS | lipopolysaccharide
lysoPC | lysophosphatidylcholine
lysoPE | lysophosphatidylethanolamine
lysoPI | lysophosphatidylinositol
lysoPL | lysophospholipid
lysoPS | lysophosphatidylserine
LXR | liver X receptor

PEC | peritoneal exudate cells
PI | phosphatidylinositol
PI3K | phosphoinositide 3-kinase
PL | glycerophospholipid
PLA_2 | phospholipase A_2
PS | phosphatidylserine
PUFA | polyunsaturated fatty acids

SCD1 | stearoyl-CoA desaturase
SEM | standard error of the mean
SFA | saturated fatty acids
SIMPER | similarity percentage
SM | sphingomyelin

TAG | triacylglycerol
TB | tuberculosis
TLR | Toll-like receptor
TNFα | tumour necrosis factor alpha

WT | wild-type

ENGLISH ABSTRACT

Tuberculosis (TB) is characterised by infection of *Mycobacterium tuberculosis* (Mtb) living on a lipid diet within lung granulomas. The differentiation of macrophages into lipid-filled foam cells is a hallmark of the lung tubercle that forms in patients with active pulmonary TB. Mycolic acids (MAs), the abundant lipid virulence factors in the cell wall of Mtb, provide a hydrophobic interface for lipid nutrition and can induce this foam phenotype possibly as a way to perturb host cell lipid homeostasis to support the infection. It is not exactly clear how MAs allow differentiation of foam cells during Mtb infection. Chemically synthetic MAs, each with a defined stereochemistry, representing the major classes of natural Mtb MA, differentially steer host macrophages. Here we first investigated how chemically synthetic MAs, each with a defined stereochemistry similar to natural Mtb-associated mycolates, influence cell foamy phenotype and mycobacterial proliferation in murine host macrophages. Using light and laser-scanning-confocal microscopy, we assessed the influence of MA structure first on the induction of granuloma cell types, second on intracellular cholesterol accumulation, and finally on mycobacterial growth. While methoxy mycolates (mMA) effected multi-vacuolar giant cell formation, keto-MAs (kMA) induced abundant intracellular lipid droplets (LDs) that were packed with esterified cholesterol. Macrophages from mice treated with kMA were permissive to mycobacterial growth, whereas cells from mMA treatment were not. Alpha-MA (αMA) had no notable effect on macrophage physiology. This suggests a separate yet key involvement of oxygenated MAs in manipulating host cell lipid homeostasis to establish the state of TB.

We therefore hypothesised that the induction of phenotypically and functionally distinct macrophage populations by the oxygenated MAs could be accompanied by unique lipidome profiles. Next, we investigated how the peritoneal macrophage lipidome is affected by the

individual MAs, employing electrospray ionisation tandem mass spectrometry (ESI-MS/MS). Compared to placebo and αMA, oxygenated MA treatment elicited significantly more glycerophospholipid (PL), lysophospholipid (LPL) and sphingolipid synthesis. However, global PL synthesis and induction of eicosanoid potential was pronounced in phosphatidylcholine (PC) for mMA macrophages, and in phosphatidylethanolamine (PE) and phosphatidylserine (PS) for kMA macrophages. All lysoPC species were strongly upregulated by both oxygenated MAs. Finally, the occurrence of ceramide (Cer) and sphingomyelin (SM) with saturated acyl chains was mainly associated with mMA treatment, whereas unsaturated acyl chains and dihydrosphingomyelin were mostly associated with kMA treatment. Selective secretion of various ratios of oxygenated MAs may thus steer innate immunity through the lipidome of macrophages to establish persistent TB.

MAs assign a unique fingerprint to mycobacteria and display diverse biological functions. This work provided evidence for an improved understanding of the manifestation of TB. The keto and methoxy mycolates studied here, differentially interfere with host lipid homeostasis and materialisation of the TB disease phenotype. We clearly show that the type of oxygenated distal group of the meromycolic moiety influences foamy macrophage regulation, cholesterol accumulation and mycobacterial growth facilitation through the lipidome of its host cell. These are crucial findings, as the Mtb cell envelope displays significant structural variation in MA oxygenation class and proximal cyclopropane configuration, which is continuously remodelled in response to growth needs. Collectively this study provides a molecular basis by which the safety and mechanism of MA biolipids as plausible therapeutic agents may be assessed, and so to provide a starting-point for planning risk assessments for future development of nanomedicines for targeted drug delivery against macrophage borne infectious diseases, asthma and vaccine adjuvants.

NEDERLANDSTALIGE SAMENVATTING

Tuberculose (TB) is een aandoening van de longen die wordt gekenmerkt door ondermeer de aanwezigheid van *Mycobacterium tuberculosis* (Mtb) bacillen in long granulomen en levend op een dieet van lipiden. Een differentiatie van longmacrofagen tot zogenaamde schuimcellen, gevuld met lipiden, vormt een hoofdkenmerk van de long tuberkel die zich vormt in patiënten met actieve pulmonaire tuberculose. Mycolzuren (MZen) vormen de meest abundante lipide virulentiefactoren in de celwand van Mtb. Als hydrofobe interfase staan deze MZen mede in voor de aanlevering van lipide nutriënten en de opwekking van schuimcellen ter ondersteuning van de bacillaire infectie. Echter, het is alsnog onduidelijk hoe MZen aanleiding geven tot het ontstaan van schuimcellen bij infectie. Synthetische MZen, representatief voor de belangrijkste klassen van natuurlijk voorkomende Mtb MZen, oefenen een differentiële werking uit op macrofagen. In dit proefschrift hebben we in eerste instantie nagegaan in hoeverre verschillende synthetische MZen, chemisch overeenkomend met Mtb-geassocieerde MZen, al dan niet in staat zijn tot het opwekken van een schuimfenotype en in het ondersteunen van bacillaire groei in (muis) macrofagen. Gebruikmakend van 'laser scanning confocale microscopie' werd de invloed van de MZ-structuur op de opwekking van granuloom-geassocieerde celtypes, de intracellulaire accumulatie van cholesterol en intracellulaire bacteriële groei nagegaan. Terwijl methoxy-MZ (mMZ) de opwekking van multivacuolaire reuzencellen opwekte, ondersteunde keto-MZ (kMZ) de intracellulaire accumulatie van lipide druppels (LD) rijk aan veresterd cholesterol. Macrofagen van muizen behandeld met kMZ waren permissief voor mycobacteriële groei, terwijl macrofagen van proefdieren behandeld met mMZ geen versnelde mycobacteriële groei vertoonden. Alfa-MZ (aMZ) tenslotte oefende geen waarneembaar effect uit op de macrofaag fysiologie en functie. Deze waarnemingen wijzen op gedifferentieerde

sleutelfuncties uitgeoefend door geoxygeneerde MZen in het manipuleren van de lipide homeostase in de gastheercel bij het ontwikkelen van TB.

Aansluitend hierop werd de mogelijkheid onderzocht dat het opwekken van fenotypisch en functioneel onderscheiden macrofaagpopulaties door de verschillen MZen vergezeld gaat van wijzigingen in het lipidoomprofiel van de cellen. Aldus werd in een volgende stap lipidoomprofiel geanalyseerd aan de hand van 'electrospray ionisation tandem mass spectrometry' (ESI-MS/MS). Vergeleken met placebo- en aMZ-behandeling, vertoonden macrofagen behandeld met geoxygeneerde MZen significant verhoogde niveaus aan glycerofosfolipiden (FL), lysofosfolipiden (LFL) en sphingolipiden. Globale FL synthese en inductie van eicosanoied potentieel was meer uitgesproken in fosfatidylcholine (FC) bij mMZ macrofagen en in fosfatidylethanolamine (FE) and fosfatidylserine (FS) bij kMZ macrofagen. Alle lysoFC species vertoonden sterk verhoogde niveaus bij beide geoxygeneerde MZen. Tenslotte kwamen ceramide (Cer) en sfingomyeline (SM) met verzadigde acyl-ketens voornamelijk voor bij mMZ-behandeling terwijl onverzadigde acyl-ketens en dihydrosfingomyeline geassocieerd voorkomen met kMZ-behandeling. Wijzigingen in de verhoudingen aan MZ-klassen kan aldus een directe weerslag hebben op de natuurlijke immuniteit van de gastheer via het beïnvloeden van het lipidoom van de macrofaag.

De samenstelling aan MZen vormt een mycobacteriële vingerafdruk maar biedt tevens de mogelijkheid aan de bacillen om de gastheer immuun respons aan te sturen. De resultaten beschreven in dit doctoraatproefschrift bieden verdere inzichten in hoe de bestudeerde mycobacterium-geassocieerde MZ-klassen kunnen bijdragen tot de ontwikkeling van tuberculose via een differentieel interfereren met de gastheercel lipide homeostase. Aldus tonen onze data aan dat het type van geoxygeneerde distale meromycolgroep – keto of

methoxy – een weerslag heeft op de vorming van schuimcellen, de opname van cholesterol en intracellulaire mycobacteriële groei alsook op het lipidoom van de gastheercel. Deze bevindingen zijn belangrijk ondermeer in het kader van de beduidende structurele variatie in MZ oxygenatie klasse van de Mtb celwand onder verschillende groeicondities. Tevens levert deze studie een moleculaire basis aan voor het evalueren van de veiligheid en mechanisme van werking van MZ-biolipiden bij een potentiele toepassing als therapeutisch agens ondermeer voor de verdere ontwikkeling van nanomedicijnen voor een gerichte drugafgifte tegen aandoeningen waarin macrofagen een mediërende rol spelen zoals infectieziekten, astma en vaccin adjuvanten.

CHAPTER I |

General Introduction

1. Tuberculosis: an ancient, but persisting human infectious disease

1.1. The disease

Tuberculosis (TB) is a deadly airborne disease of mainly the respiratory organs which, according to archeopathologists, may well be the oldest bacterial infectious disease of humans[1]. The *Mycobacterium tuberculosis* (Mtb) causative agent is so well adjusted to its human host, that almost a third of all humans today are latently infected with TB[1]. Of the approximately 10 million new cases per annum, around 16% die and a further 5% develop multi-drug resistant TB[2]. This is compounded by simultaneous infection with human immunodeficiency virus (HIV), which hastens mortality from years to weeks and strongly correlates with diminished socio-economic standing. The prolonged anti-TB therapy that is required increases the probability of treatment non-compliance, with concomitant development of drug resistance[2]. In 2014, the World Health Organisation reported that the global TB incidence is most extensive in sub-Saharan Africa with more than 500 new cases reported per 100,000 people that year[2] (Fig. 1). In spite of the immense scale of global infection, less than 15% of individuals develop active disease. Immunocompetent patients are able to contain the Mtb bacillus in lung and tissue granulomas, but complete eradication is rarely attainable. Sometimes, latent bacilli can reinitiate active disease up to decades following initial exposure. Although the bacillus Calmette-Guérin (BCG) vaccine has been in use for almost a century with high efficacy in minors, it is less effective in adolescents and adults. As a result, chronic and latent TB infection remains a serious global health concern and a research focus for finding innovative solutions to manage the epidemic[3].

1.2 The tuberculosis pathogen

Mycobacteria are classified under the Order Actinomycetales, Suborder Corynebacterineae, and Family Mycobacteriaceae[4, 5]. The genus *Mycobacterium* is broadly divided into fast- and

slow-growing species. Some are purely environmental organisms, others opportunistic pathogens, but Mtb is classified among the host-adapted, pathogenic mycobacteria[6]. Mtb is a slow growing bacillus with a doubling time of ~18 hours. It forms part of the TB-complex of organisms, which is phylogenetically divided into eight lineages[7-9]. These include the human-adapted species *M. africanum* and *M. canetti* as well as the animal host subspecies *M. bovis*, *M. caprae*, *M. microti*, *M. pinnipedi*, *M. orygis* and *M. mungi*.

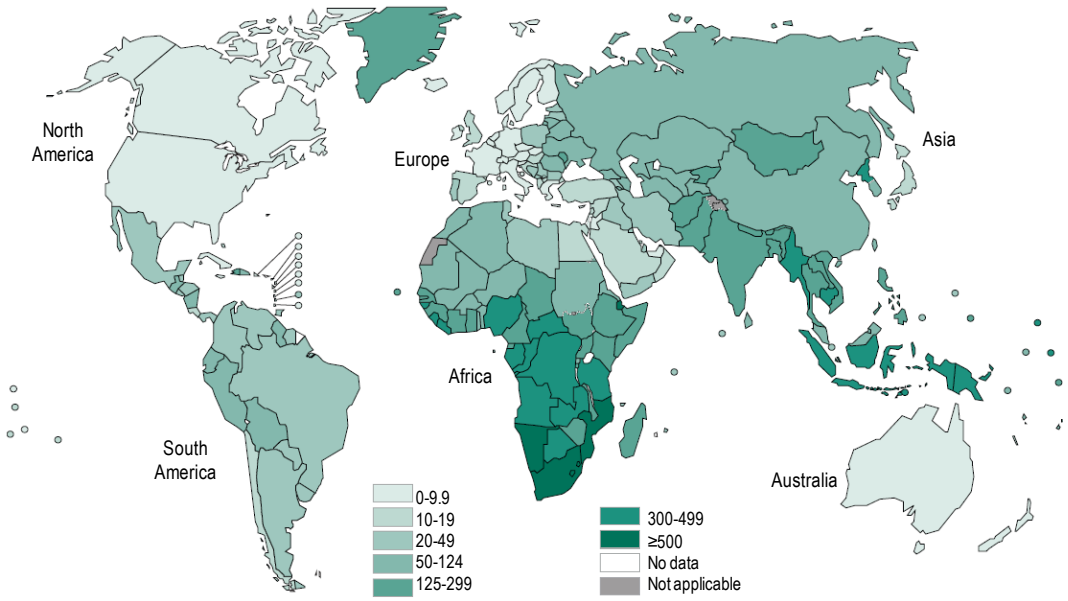

Figure 1 | Global estimated TB incidence rates in 2014 per 100,000 people[2].

The distinctive feature of Mtb is a waxy cell envelope that lends an acid fast property to the bacillus. A lipid-rich cell wall is essential for survival and virulence and provides protection against degradation by host immune defence chemicals and antibiotics[10]. The Mtb cell envelope contains multiple structural elements broadly divided into layers of peptidoglycan, arabinogalactan and mycolic acid (MA)[11, 12]. The peptidoglycan layer surrounds the inner plasma membrane and forms long polymer meshes of 4-3 and 3-3 peptide crosslinks between *N*-acetylglucosamine and *N*-acetylmuramic acid. Polymer modifications are interspersed and

comprise glycosylated *N*-acetylmuramic and amidated peptide side chain residues. The highly branched layer of arabinogalactan enfolds the peptidoglycan layer and mostly contains galactose and arabinose sugars. About 10% of the *N*-acetylglucosamine is covalently attached to repeated galactan disaccharides in the arabinogalactan layer[13]. Galactan chains are variably coupled to arabinan that may contain succinyl or non-*N*-acetylatedgalactosamine modifications. These modifications are characteristic of pathogenic mycobacteria and is associated with enhanced infectivity[13, 14]. Long-carbon chain MA monomers are ligated to arabinan by the fibronectin-binding proteins of the Mtb antigen 85 complex[15]. This layer forms the characteristic waxy lipid coat that contributes to cell wall impermeability.

1.3 The pathogenesis of tuberculosis

The biology and pathogenicity of TB has been widely reviewed[16-18]. Tubercle bacilli are dispersed from patients with active TB through aerosolised droplets that are inhaled into the lungs of uninfected individuals. Alveolar macrophages are first to phagocytose the bacilli, inducing a localised proinflammatory infiltration of blood-derived mononuclear cells. Macrophages represent the primary line of innate immune defence after which spontaneous healing, acute disease, or bacillary containment will result. In most healthy individuals with strong innate immune defences disease will not develop and early clearance and healing occur[19]. As there is a distinct regulation of immune effector machinery throughout Mtb infection[20], patients with compromised immune systems like those co-infected with HIV (~10% of cases) will suffer acute disease progression. Bacilli that are able to successfully resist host microbicidals or prevent phagolysosomal fusion may result in increased bacterial burden and dissemination through the bloodstream or lymphatics to other organs, tissues or immune cells. In the majority of cases, infected host macrophages trigger a secondary immune response through cytokine release or by degradation and shuttling of antigen

peptides to the cell surface. This is mediated by major histocompatibility complex (MHC) class II proteins that are recognised by T cells for immune activation[21]. The adaptive response then signals chemo- and cytokine-dependent recruitment and maintenance of other immune cells, such as neutrophils and lymphocytes, to migrate to the primary infection site. Granuloma formation marks the containment of the infection with limited noticeable disease indications. During this time, Mtb-infected patients do not transmit the disease. When containment fails due to host confounding factors, for example elderly, malnourished or immune-compromised patients, caseation of granulomas can occur. This is due to the release of bacteria from the necrotic centre into the airways of infected patients, leading to a productive cough and aerosolised spread of infectious bacilli.

2. Host response to Mtb infection

Mtb uptake occurs through specific receptors that influence successive host cell signalling pathways[20, 22-24]. During bacterial internalisation, germ line-encoded host pattern recognition receptors (PRRs) are expressed in the cytosol, at the cell surface or lysosome and endosome membranes to detect pathogen-associated molecular patterns (PAMPs). PAMPs are conserved microbial-specific small molecule motifs. Important bacterial PAMPs include lipopolysaccharide (LPS), mannose and peptidoglycan carbohydrates, nucleic acids and flagellin peptides. The PRRs expressed by immune cells directed at innate activation include the Toll-like (TLR; e.g. TLR2/4/9), C-type lectin (e.g. Dectin-1) and Nod-like (e.g. NOD2) receptors. Key receptors that are responsible for mediating attachment, engulfment and internalisation of Mtb via phagocytosis consist of the scavenger, mannose and complement receptors[20].

Although numerous mediators have been implicated in the host response upon Mtb infection, those strongly associated with disease progression reflect an interplay of host and/or pathogen genetic predisposition with environment[25]. The establishment of a primary infection mostly depends on the virulence of the mycobacterium and the state of activation of resident host cells responsible for pathogen uptake. Macrophage microbicidal activity is strongly enhanced by cytokine stimulation of mainly interferon-gamma (IFNγ) and tumour necrosis factor alpha (TNFα), which rapidly constrain bacilli to the endocytic pathway and exposes them to phagosome acidification and destruction by reactive oxygen or nitrogen[26]. Bacterial pathogens however, have evolved numerous escape and survival tactics[27]. This is more so for Mtb which, being among the most ancient of human bacterial pathogens, holds the edge in manipulating the immune system of its host to benefit the pathogen. Thus, Comas *et al*. reported that human T cell epitopes of Mtb are hyperconserved[8], even to a larger extent than the so-called essential genes, indicating that Mtb has co-evolved a host-pathogen relationship that is even more critical for its survival than its own metabolic pathways. The ability of Mtb to avoid destruction by host microbicidal machinery, combined with its ability to manipulate host immunity will consequently result in the formation of a granuloma.

Granulomas are the signature histopathology of pulmonary TB and the product of an adaptive cell-mediated immune response to the inhalation of aerosolised Mtb[28]. It represents a balance between ongoing bacillary replication (active TB) and a strong immune cell-induced growth suppression towards latent TB, which happens in more than 90% of Mtb infections[29]. Granulomas are structured cellular complexes enclosing a caseous core rich in debris and lipids and containing necrotic infected macrophages and extracellular bacilli (Fig. 2). The macrophage-rich zone of the granuloma consists of epitheloïd macrophages, multinucleated giant cells (MGC) and lipid-laden foam cells, all of which can contain Mtb bacilli. Additional

immune cell infiltration and migration occurs towards the periphery of mainly dendritic cells (DC), neutrophils and natural killer (NK) cells[18]. Concentric layers of fibroblasts and leukocytes enclose the granuloma, segregating the infection to prevent bacterial dissemination (Fig. 2).

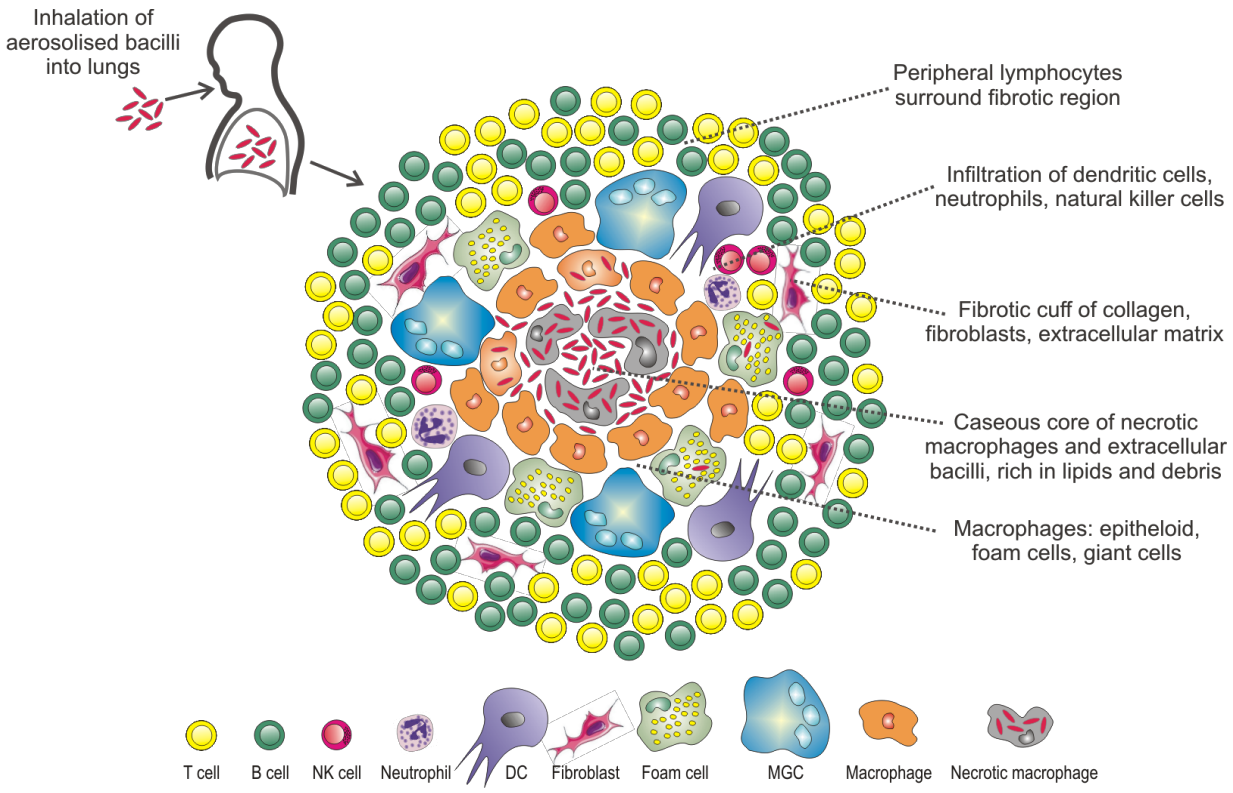

Figure 2 | Cellular composition of the Mtb-induced granuloma. Following aerosolised Mtb inhalation into the lungs, bacilli are internalised by alveolar macrophages (granuloma core). Subsequent T cell stimulation results in cytokine-dependent macrophage activation to the lipid-laden foam phenotype (granuloma periphery). Mature granulomas morphologically comprise a necrotic core with extracellular bacilli surrounded by concentric layers of apoptotic, infected, foamy and epitheloïd macrophages. As part of a localised infection, granulomas are also characterised by aggregates of multinucleated giant cells (MGC), neutrophils, and natural killer (NK) and dendritic (DC) cells.

A study by Tsai and colleagues assessed with flow cytometry the influx of cells in murine lungs to convert from the acute to the chronic phase of Mtb infection[30]. At 2-week post infection, macrophages ($F4/80^+$) and neutrophils ($Ly6G^+$) represented the most abundant cells of the acute phase at 36-37% each of the total leukocyte population ($CD45^+$). Macrophages remained at this proportion during the 12- and 27-week post infection chronic stages, while the neutrophil population was reduced in the lungs by half at both time points. The $CD3^+$ T lymphocytes became the dominant leukocyte population four weeks post infection and remained an important cell type throughout the chronic stages (35-47%). T helper cells ($CD4^+$, 60-69%) comprised the major subset of the T lymphocyte population throughout infection with cytotoxic T cells ($CD8^+$, 17-32%) contributing a lesser portion. The B lymphocytes ($CD19^+$) made up the minor population of all the CD45+ leukocytes during the acute phase (<2%), but increased 4-fold from 4-weeks post infection. Though the numbers of DCs ($DEC205^+$) per lung slightly increased over the six month assessment period, they stably represented 3-4% of the total lung leukocyte population. Neutrophils and macrophages thus predominate during the early acute phase of Mtb infection, representing the initial antimicrobial defences. In addition to macrophages remaining in the lungs, the $CD3^+$ T cell population becomes important during the maintenance of chronic infection.

Though reported here for a murine model of Mtb infection, which may by far removed from the case of human TB, the mouse model remains a powerful tool. Mice are inexpensive and easy to handle or manipulate genetically[31]. Murine and human granulomas are characterised by similar leukocyte populations that will follow an ordered sequence of events upon infiltration into the lungs[30, 32]. Many similarities exist, in particular at the level of the macrophage populations. Both acute and chronic phases of infection can be followed in mice[33-35]. Animal *in vitro* and *ex vivo* models of Mtb infection thus present ideal

opportunities for understanding the complex host-pathogen dynamics in the Mtb granuloma and may allow for the development of novel TB therapeutics.

3. Current anti-TB therapy

Apart from an immense effort into the development of vaccines, diagnostics and anti-TB drug treatments, the rise in human populations led to the evolution of modern virulent strains causing global TB epidemics[36]. To effectively eradicate TB, new therapeutics and treatment regimes are urgently needed. TB drugs are broadly classified based on their efficacy and comprise the first, second, and third-line drugs[37]. The first-line drugs are widely used and are most effective against susceptible (non-resistant) TB strains, including Rifampicin, Isoniazid, Ethambutol and Pyrazinamide[37, 38]. Isoniazid targets and eradicates actively growing bacteria, while Rifampicin has an additional sterilising effect as potent bactericidal agent. Ethambutol significantly slows bacterial replication while Pyrazinamide, though weakly bactericidal, is effective against non-replicating bacteria in acidic environments (i.e. inside macrophages or at acute inflammation sites)[38]. Second-line drugs are primarily used when bacilli become resistant to first-line therapies. These drugs may be inaccessible in developing regions (e.g. Fluoroquinolones) or have toxic side-effects (e.g. Cycloserine) and poor efficacy (e.g. Para-aminosalicylic acid)[37]. Third-line drugs are the least effective or well characterised (e.g. Clarithromycin and Clofazimine)[39].

Drug-susceptible, active TB can be 90% successfully treated in HIV-negative patients with an intensive six-month antibiotic regimen[38]. This comprises an initial two-month treatment with the four major first-line drugs followed by maintenance with Isoniazid and Rifampicin for a further four months. However, various acquired resistance, for example in multidrug, extensively and totally-drug resistant strains, can develop as a result of poor drug quality,

interrupted supply and irregular drug use[40]. The bacterial mechanisms of action for acquiring resistance include decreased permeability barriers, degrading or inactivating enzymes, modification of drug activation or metabolism pathways and drug target amplification or modification (i.e. chromosomal mutations)[41]. The mycobacterial envelope comprises multiple layers of lipids with interspersed sugars and protein and provides the hydrophobic character that protects against chemotherapeutic agents. The Mtb cell wall is biologically active and thus largely responsible for its virulence, pathogenicity and persistence. Key components comprise the genes and proteins involved in fatty acid synthesis and lipid metabolism[42]. Novel TB therapies should hence stem from research that focuses on understanding the functional diversity of key virulence lipids, like the MAs.

4. Mycolic acids

4.1 General structure of mycolic acid

A key feature of intrinsic antibiotic resistance is the low permeability of MA-containing bacterial cell walls from the phylum Actinobacteria, which includes species of *Corynebacterium*, *Nocardia*, *Rhodococcus* and *Mycobacterium*[43, 44]. The Mtb cell envelope comprises intricate layers of peptidoglycan, arabinogalactan, glycolipids, MA (*α*-alkyl, *β*-hydroxy fatty acids) and lipoproteins, with MA being the dominant constituent[12, 14]. The structural and biochemical properties of MAs have been reviewed recently[45]. In short, these wax-like hydrophobic lipids comprise a mycolic motif with long non-functionalised alkyl chain and a meromycolate chain with up to two functional groups that can be either oxygenated (distal group) or unoxygenated (distal or proximal group; Fig. 3A). Three main Mtb MA classes exist: the most abundant unoxygenated alpha-MA (αMA), the less abundant oxygenated methoxy- (mMA) and the least abundant keto-MA (kMA). Though some *trans*- may be present, αMA essentially exists in *cis*-cyclopropane configuration while mMA and

kMA contain either *cis*- or *trans*-cyclopropanation with an adjoining methyl branch[12]. A major advance towards understanding the functional diversity of MAs in TB was made since 2005 in the development and manufacture of synthetic analogues of representatives of each of the major MA classes[46-48] (Fig. 3B).

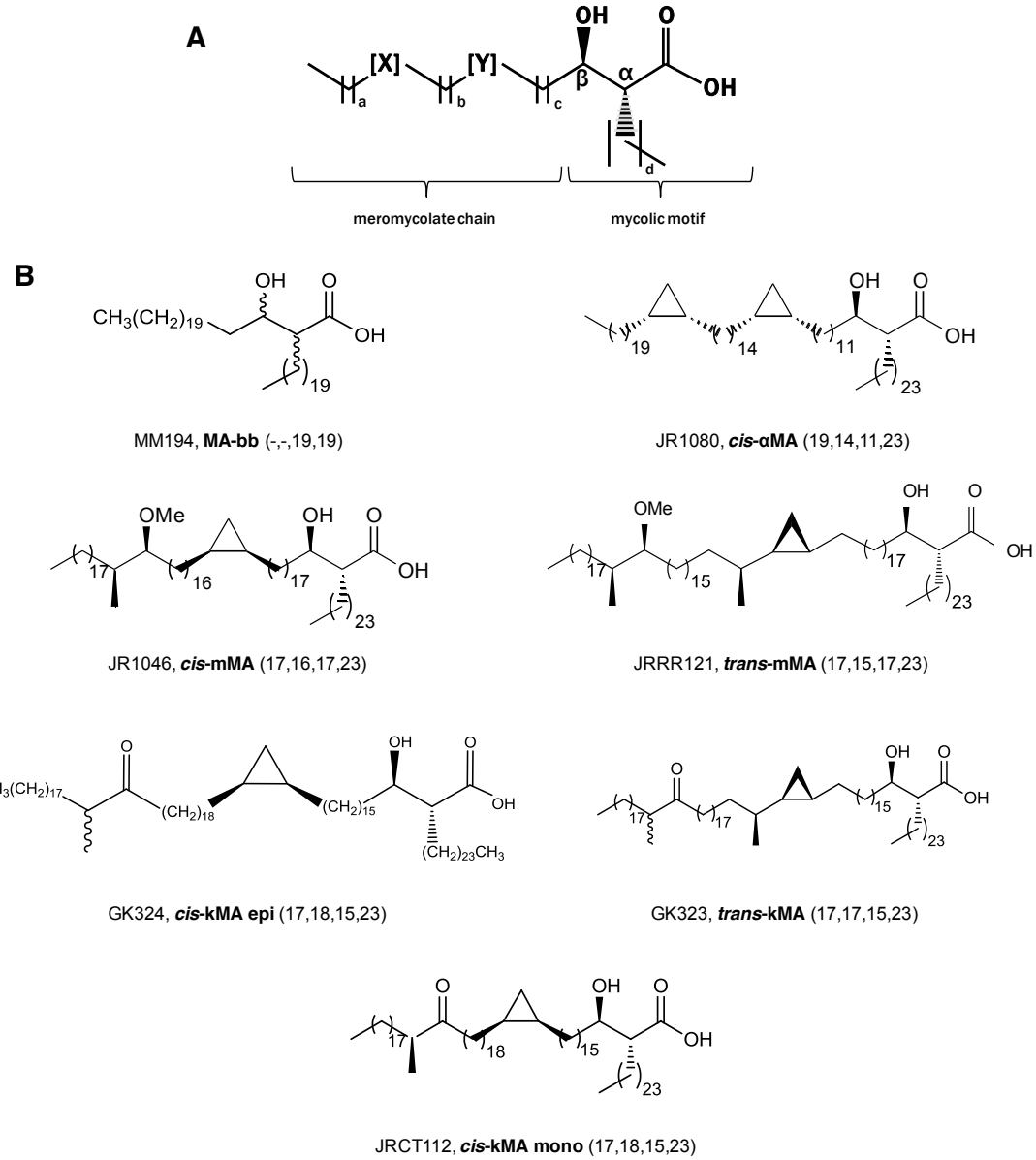

Figure 3 | Mycolic acid structures. The biochemical structures are given of the ***A***, general MA, where X and Y represents the distal and proximal groups, respectively; and a-d are varying lengths of methylene chains[45] and ***B***, synthetic MAs: MA lipid backbone (MM194), *cis*-alpha (JR1080), *cis*-methoxy- (JR1046), *trans*-methoxy (JRRR121), the epimeric (GK324) and monomeric (JRCT112) isomers of *cis*-keto and *trans*-keto (GK323). Numbers in brackets represent carbon chain lengths and wiggly line indicates a mixture of stereoisomers at that position.

4.2 Mycolic acid and host-pathogen interactions

Mtb closely regulates its proliferation in macrophage host cells, owing most of its virulence to a highly structured cell wall of which MA makes up a substantial portion[12]. In nature the inflammatory neutral αMA (fixed at ~50%) and proinflammatory mMA and kMA (variable, totalling ~50%) in the Mtb bacillus cell wall can be tuned to complement growth and proliferation[10, 49]. While most Mtb PAMPs are TLR agonists[50], the MA biolipid was identified as a PAMP eliciting innate responses similar to Mtb infection, but independent of TLR[51]. In a murine model of lung exposure to MA, Korf and team[51] recorded the induction of lipid-filled alveolar foam cells and inhibition of TNFα production. This would likely support intracellular Mtb growth whilst allowing escape from host cell destruction. MA treatment of mice also caused cell infiltration and cytokine expression involved in containment of Mtb infection; observed by a rapid neutrophilic infiltration to MA-exposed murine lungs and production of the proinflammatory cytokines IL-6 and IL-12. A conditioning of macrophages was observed with MA treatment that enabled antimicrobial TNFα, IFNγ and myeloperoxidase production upon subsequent treatment of the cells with LPS as a secondary innate stimulus[51]. Release of IL-12 and IFNγ by host cells activates a Th1 response, leading to bactericidal functions through recruitment of $CD4^+$ T cells and nitric oxide (NO) production[52]. As key membrane lipid of the Mtb bacillus, MA may thus contribute to a role of steering the innate host-pathogen response to establish active TB.

A striking feature of MA treatment is the induction of macrophage giant cell and foamy phenotypes in murine peritoneal and alveolar macrophages[51, 53, 54] that closely represents the characteristic foam cell in lung granulomas of TB patients[34]. Key features of foam cells include enlarged (giant) size and the accumulation of intracellular vacuoles and neutral lipid droplets (LDs), mainly comprising cholesterol esters and/or triacylglycerol (TAG)[54, 55]. MAs

have been shown to bind cholesterol-specific antibodies and the sterol-binding agent amphotericin B, suggesting that the three-dimensional structure of MA has cholesteroid structural properties[56]. Cholesterol, a common structural component of mammalian cell envelopes present within lipid rafts, is involved in diverse cellular processes[57]. Cholesterol can therefore be an attractive target for pathogens to infect host cells or modulate their dynamics. Mycobacteria in particular utilise cholesterol for entry, inhibition of phagolysosomal fusion and persistence[58-60]. It is thus clear that free MAs regulate mycobacterial pathogenesis, but it is unclear how this happens. Further study using these long carbon chain fatty acids in disease models is therefore necessary. The recent availability of chemically synthetic MAs provided the opportunity to make this happen, to which this thesis aimed to contribute.

5. Macrophages as central host cell of the Mtb bacillus

Macrophages are associated with every phase of TB progression from the establishment of a primary infection to latent persistence in the granuloma, and the potential reactivation up to decades later[18, 61]. As facultative intracellular pathogen, Mtb targets these macrophage mononuclear phagocytes, which are instrumental in mediating both the innate and adaptive protective immune functions[62].

5.1 Macrophage phenotype, function and polarisation

Innate immune cells like macrophages regulate their polarisation as a result of interaction with extracellular stimuli and the adjacent microenvironment[63-65]. As macrophages display abundant biological activity they differentiate along a spectrum into proinflammatory (classical M1) and regenerative or immune-regulatory (alternative M2) lineages[66]. The switch into the M1 or M2 modes is mediated by haematopoietic growth factors, cytokines, and

multiple small glucose and lipid metabolites[67, 68]. M1 macrophages are primed by IFNγ, but need stimulation by a second signal for instance TNFα or bacterial virulence factors, to become efficient antigen presenting cells (APCs) with enhanced synthesis of proinflammatory cytokines and reactive nitrogen or oxygen species[69]. Classically-activated M1 macrophages display strong microbicidal and tumouricidal capacity. Conversely, secretion of IL-4 and IL-13 by type-2 T helper cells converts macrophages to the anti-inflammatory, alternatively activated M2 phenotype[70]. Alternatively activated macrophages have reduced MHC class II expression and are thus less efficient towards antigen presentation or elimination of intracellular pathogens. M2 macrophages are more effective in tissue repair and resolution of inflammation. Though the importance of innate immune cells in inflammatory activation or resolution has been well characterised, specific metabolic pathways involved in directing the various stages of macrophage activation has only recently obtained serious attention.

5.2 Macrophage metabolism and mycolic acids

Macrophage activation and metabolism are related (reviewed in[71-75]). Biswas and Mantovani[69] summarised key intrinsic metabolic features of the M1 (proinflammatory) and M2 (anti-inflammatory) modes. Polarised macrophages exhibit diverse plasticity in glucose, lipid and amino acid metabolism as well as distinct regulation of iron storage and redox balance. Macrophage redox state is linked to intracellular glutathione. High glutathione levels drive a reductive M1 state and low levels bring forth an oxidative M2 mode. M1 relates to the phenotype of aerobic glycolysis (Warburg effect), which is typical of active proliferating or cancerous cells[76], while M2 relates to a tissue repair phenotype with a metabolic state that favours oxidative phosphorylation. High aerobic glycolysis in malignant tumours is characterised by increased cellular glucose import, *de novo* fatty acid synthesis and a

preference for lactate fermentation to produce cellular energy[77]. A noteworthy justification for this altered metabolic state is the provision of important biosynthetic substrates required for cell proliferation other than just ATP[78]. Similarly, in LPS-activated innate immune cells a metabolic transition towards aerobic glycolysis confirmed that proinflammatory signals can skew cellular metabolism towards anabolic mode[79]. Regulation of L-arginine metabolism is effected by nitric oxide synthase 2 (NOS2) and arginase 1 (ARG1): M1 macrophages ($NOS2^{high}$) synthesise reactive nitrogen intermediates from L-arginine to augment microbicidal and tumouricidal function, whereas M2 macrophages ($ARG1^{high}$) catalyse L-arginine to L-ornithine and polyamines for matrix remodelling[80]. While iron is a crucial cofactor in cellular processes, Mtb expresses essential iron-storage proteins for growth and protection against host oxidative stressors[81]. The M1 phenotype ($Ferritin^{high}$) mainly upholds iron storage to reduce its availability to pathogens and to enhance proinflammatory activity, while M2 ($Ferroportin^{high}$) promote iron export for tissue repair and immune regulation. The capacity of macrophages to alter metabolic profiles and activation state in response to microenvironment and cellular stimuli thus drives inflammation mediation or resolution.

There are important lipid regulators of macrophage functional dynamics as well. For example, prostaglandin-endoperoxidase synthase (PTGS), a key enzyme generating prostaglandins and thromboxanes from arachidonic acid, is differentially expressed in M1 and M2 macrophages. While M2 cells induce the expression of the PTGS1 isoform, M1 cells upregulate PTGS2 in response to stimulatory factors. There is also distinct induction of fatty acid uptake and oxidation genes in M2, but not M1 macrophages.

Vander Beken *et al*. recently assessed the effect of MA chemical structure on the induction of pulmonary inflammation in murine macrophages[53]. Phosphatidylcholine liposomes loaded

with examples of methoxy and keto mycolates caused inflammation with distinctly more total cells and neutrophils in bronchoalveolar infiltrate as compared to an empty liposome control treatment. Gene induction analyses by RT-qPCR showed elevated expression of proinflammatory genes (Il6, Il12b and Ccl2) in $CD11c^{+}$ cells from oxygenated MA-treated mice (opposed to control phosphatidylcholine liposomes). Interestingly, the anti-inflammatory cytokine IL-10 was 6-fold higher in mMA-treated lungs (versus kMA). While the M1 activation marker NOS2 was only upregulated in mMA-treated cells, the M2 marker ARG1 was induced under all MA conditions (except αMA). Oxygenated MAs furthermore did not induce expression of TNFα. It has been shown that TNFα and IL-10 have opposing roles in Mtb infection. While TNFα induces NO-dependent apoptosis in Mtb-infected macrophages, IL-10 inhibits inflammatory cytokine release and NO production, permitting intracellular bacterial growth[82]. Increased cellular infiltration and proinflammatory gene expression in cells exposed to oxygenated MAs signify M1 activation. Yet oxygenated MA treatment also induced select M2 markers. Assessment of the differential innate immune activity of MA by Vander Beken *et al*. did not clarify which synthetic oxygenated MA stimulates either M1 or M2 activation[53], as cells from mice exposed to these mycolates exhibited traits of both modes. Research suggests that macrophage activation changes throughout TB development. A recent study of macrophage polarisation in an *in vitro* model of tuberculous granuloma formation identified a mixed macrophage M1/M2 orientation[83]. Following Mtb infection, macrophage polarisation markers changed from predominately M1 (CXCL11 and iNOS) during the early phase to M2 (CD206, CCL17 and CCL18) at the later stage of granuloma formation. Polarisation status was further assessed in lung tissues from patients with pulmonary TB by immunohistochemistry and qPCR for induction of M1 and M2 markers. In Mtb-infected tissues mixed M1/M2 markers were recorded ($iNOS^{high}$/$CD206^{high}$ and $CXCL11^{high}$/$CCL17^{high}$/$CCL18^{high}$), but M2 markers

(iNOS^{low}/CD206^{high}) dominated in tissues from patients with active TB. Though speculative, the mixed M1/M2 immune orientation induced by oxygenated MAs likely correlates with a phase-dependent contribution during TB progression of each of these classes to the Mtb cell wall composition, thus warranting further investigation.

6. Cholesterol homeostasis in macrophages

6.1 Transcriptional regulation of cellular cholesterol

The genetic regulator of systemic and cellular cholesterol homeostasis is the liver X receptor (LXR). LXRs are transcription factors that regulate the expression of cholesterol associated-target genes, and act as cholesterol sensors to maintain the fine balance of uptake and export of cholesterol[84]. The two LXR isoforms, LXRα (NR1H3) and LXRβ (NR1H2), share ~80% homology in DNA- and ligand-binding sequences[85], but are differentially expressed. LXRα is predominately expressed in metabolically active tissues like the liver, intestines, adipose tissue and peripheral macrophages, whereas LXRβ is ubiquitously expressed at low to moderate levels throughout the body[86]. The endogenous ligands of LXR are oxidised cholesterol derivatives (oxysterols) and intermediates of the cholesterol biosynthesis pathway such as desmosterol[87]. The most common oxysterol ligands are 22(R)-hydroxycholesterol (steroid hormone biosynthesis metabolite), 24(S)-hydroxycholesterol (brain and plasma), the most potent agonist 24(S),25-epoxycholesterol (located in liver), 20(S)-hydroxycholesterol, and 27-hydroxycholesterol (macrophages and plasma)[85].

To regulate gene expression in a ligand-dependent manner, LXRs must form obligate heterodimers with the retinoid X receptor (RXR) α, β or γ. LXRs are master cholesterol sensors that in the absence of a ligand, reside in the nucleus bound to LXR response elements at target gene promoters[85]. LXR-RXR heterodimers interact with corepressor complexes that

suppress transcription. Upon binding of an endogenous oxysterol agonist, conformational changes in the ligand-binding pocket initiate recruitment of coactivator complexes that lead to transcriptional activation of target genes. Cellular cholesterol levels are tightly controlled by not only the LXRs for cholesterol efflux, but also the sterol regulatory element-binding proteins (SREBP) 1c and 2 for fatty acid and cholesterol biosynthesis and transport, respectively[85, 88]. When cellular cholesterol levels are low, precursor SREBPs are processed to active transcription factors for protein expression of enzymes (e.g. HMG CoA reductase) and receptors (e.g. low density lipoprotein receptor, LDLR) involved in cholesterol production and uptake[88]. The LXR-RXR heterodimers will remain suppressed by corepressors to inhibit cholesterol efflux. When cellular cholesterol rises, coactivators are recruited upon binding of oxysterol ligands that initiate transcription for proteins mediating cholesterol efflux or induce genes involved in LDLR degradation[86, 88]. The degradation of the LDLR involves the E3 ubiquitin ligase, inducible degrader of LDLR, which targets the LDLR for ubiquitination and eventual lysosomal destruction[89]. Without the LDLR, macrophages would not be able to internalise plasma-derived native LDL particles.

6.2 Cellular cholesterol transport

For macrophages to be converted to foam cells a distinct dysregulation in the flow of LDL in and out of the cell, will be evident. VLDL and LDL are important transporters of cholesterol from the liver and intestines to peripheral tissues like macrophages[90]. Cholesterol-rich LDL can then be internalised via the LDLR, while modified LDL (oxidised or acetylated) is taken up by the scavenger receptors SR-A or cluster of differentiation 36 (CD36) integral membrane proteins (Fig. 4). CD36 is also known as fatty acid translocase (FAT/CD36) due to its role in cellular long chain fatty acid transport[91]. LDL particles are predominately composed of phospholipids, esterified cholesterol and TAG, which are largely metabolised

by the cell[92]. Cholesterol imported into the cytosol after LDL breakdown is then either esterified for storage into LDs or sequestered into high density lipoprotein (HDL). ATP-binding cassette transporter A1 (ABCA1) and G1 (ABCG1) are the exporters of cellular cholesterol (Fig. 4). Any genetic deficiency or interference in the transcriptional pathways of ABCA1 and ABCG1 may result in increased foam cell formation.

The plasma cholesterol acceptors, apolipoprotein A-I (apoAI) and HDL particles, collectively regulate cholesterol export along with the transporters ABCA1 and ABCG1. The membrane transporter ABCA1 transfers cholesterol to extracellular lipid-poor apoAI for priming into nascent HDL particles (apoAI-HDL). The endogenous secretion of apoE, known to mediate cholesterol release to the lipid-free cholesterol acceptor apoAI, cohesively modulates macrophage cholesterol levels along with plasma apoAI and the membrane transporter ABCA1[93]. Furthermore, the LXR target gene ADP-ribosylation factor-like 7 functions with ABCA1 to move cholesterol from inside the cell to extracellular apolipoproteins[94]. ABCG1 is primarily an intracellular transporter that translocates to the plasma membrane for extracellular formation of mature HDL particles[95, 96]. Inside the cell, ABCG1 distributes cholesterol to endocytic vesicles before redirecting them away from the endoplasmic reticulum (ER), where esterification of LDs occurs, to the cell membrane for capture into the apoAI-HDL particles (Fig. 4). Mature HDL particles are then sequestered from peripheral tissues, like macrophages, to the liver where they are processed or excreted during the process of reverse cholesterol transport[92].

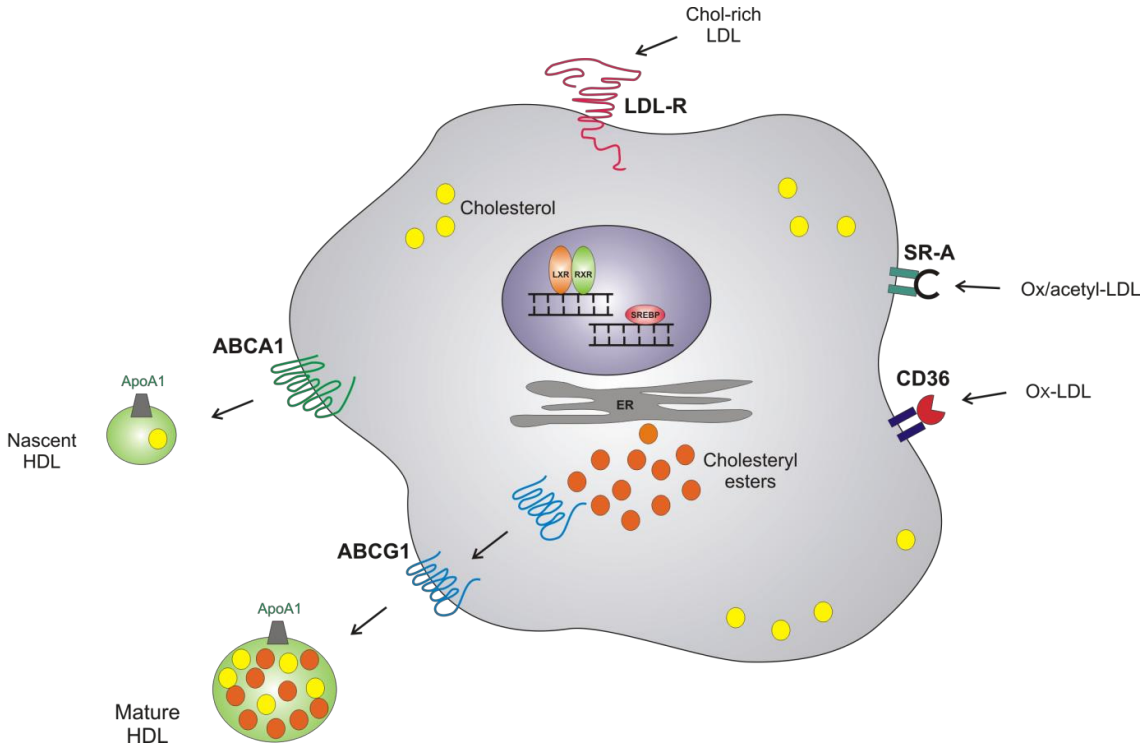

Figure 4 | Cholesterol transport in macrophages. When cellular cholesterol is low, sterol regulatory element-binding protein (SREBP) precursors become active transcription factors that mediate expression of proteins necessary for cholesterol synthesis and uptake through the low density lipoprotein receptor (LDLR). Liver X receptor-retinoid X receptor (LXR-RXR) heterodimers are bound by corepressors and expression of cholesterol efflux is suppressed. Upon increase of cellular cholesterol, oxysterols bind the LXR transcription factor that recruits coactivators to mediate transcription of cholesterol efflux genes. The ATP-binding cassette transporters A1 (ABCA1) and G1 (ACBG1) are responsible for movement of intracellular cholesterol to the plasma lipid acceptor apolipoprotein A-I (ApoAI) where they are primed to mature HDL complexes for transport away from peripheral tissues to the liver.

6.3 Macrophage foam cell formation

Fat-laden foam cells are widely implicated in disease pathologies like atherosclerosis and vascular disease. As a result, the broadest body of knowledge on foam cell formation relates to this field[97-100]. Mtb infection, however, also drives macrophage differentiation to the foamy phenotype[54, 101]. The provision of a safe, nutrient-rich harbour for the lipid metabolising bacilli is facilitated by an alteration of the host macrophage to accrue LDs[55]. As macrophages are key phagocytes of the innate immune system their role in disease pathogenesis stems from a normal protective function, which Mtb exploits to its own benefit.

The generally accepted view on foam cell formation is that SR-mediated uptake of modified (oxidised or acetylated) LDL will result in lipid-loaded macrophages[102]. Though scavenger receptors class A and B (CD36) knockout mouse models have shown substantially reduced lipid uptake, this did not abrogate foam cell formation[103, 104]. Other important receptors implicated in foam cell formation are the PPAR nuclear receptors and those associated with eicosanoid biosynthesis, for example the lipoxygenase and leukotriene receptors[105, 106]. Whereas the SRs mediate uptake of LDL, the PPARs partly regulate SR function to which the eicosanoids form natural PPAR ligands[107]. LDs, which are abundantly induced during foam cell formation, are far more than inert fat storage compartments[108, 109]. They have dynamic functions in immunity, cellular physiology and lipid homeostasis[110]. The formation of LDs in leukocytes is in fact an important event associated with innate immune activation[111].

6.4 Cholesterol and the Mtb bacillus

As facultative intracellular pathogen constrained by a host-derived phagosome, Mtb bacilli are challenged to acquire nutrients for survival and replication. Precisely what nutrients are assimilated during the various stages of infection and how they are attained remain ill-defined, but host lipids are an essential source. Initial evidence for this was highlighted by an enhanced respiration of Mtb bacilli isolated from murine lungs following growth on fatty acids, rather than carbohydrates[112]. Subsequently Cole *et al*. in their work on deciphering the Mtb genome identified a profound coding capacity associated with lipid biosynthesis and degradation[113]. Cholesterol is the abundant structural sterol of cell membranes[114] and is essential for Mtb virulence and pathogenesis[115, 116]. The catabolism by Mtb of cholesterol involves extensive sets of enzymes for steroid ring degradation or *β*-oxidation of the branched-chain fatty acids[117]. In particular, 35 of the ~80 genes associated with cholesterol metabolism encode for members of the acyl-CoA dehydrogenase family, which are the

principal enzymes responsible for truncation of the cholesterol side-chain[118-120]. Whereas catabolism of the steroid rings produces pyruvate and propionate, complete β-oxidation of the side-chain yields a 17-keto steroid intermediate (androstendione) and the metabolites acetyl-CoA and propionyl-CoA[121]. Acetyl-CoA and propionyl-CoA are then respectively further oxidised by the tricarboxylic acid (TCA) and methyl citrate cycles[122]. When fatty acids are the sole carbon source, acetyl-CoA is directed through the glyoxylate cycle for anapleurosis of TCA intermediates like oxaloacetate[122]. Alternatively, malonyl-CoA can be generated by carboxylation of acetyl-CoA for biosynthesis of long-carbon chain MAs in the Mtb fatty acid synthase-II enzyme pathway[12]. Propionyl-CoA, a precursor of potentially toxic metabolites to Mtb, is either directed into the methyl citrate or methylmalonyl pathways for generation of succinate or succinyl-CoA, respectively; or is carboxylated to yield methylmalonyl-CoA[123]. This latter metabolite can then be incorporated into methyl-branched fatty acids for generation of bacterial envelope lipids[123].

7. The major mammalian membrane lipids

Lipids are distinct carbon (C), hydrogen (H) and oxygen (O) containing compounds that are hydrophobic and soluble in organic solvents or other lipids[90]. The building blocks of lipids, namely fatty acids, comprise linear hydrocarbon chains with an organic acid group or carboxyl (-COOH) at one end. Chain length and degree of saturation with H atoms significantly influence the structural properties and functioning of fatty acids[124]. Fatty acids with single covalent bonds between C atoms are saturated (SFA) whereas those containing one or more double bonds are monounsaturated (MUFA) and polyunsaturated (PUFA), respectively. The common lipid classes that make up mammalian cells include the glycerophospholipids (PL) and derivative lysophospholipids (LPL), sphingolipids, triglycerides, sterols, eicosanoids and lipoproteins[90].

Besides structural and energy storage functions, lipids are important in membrane organisation, trafficking and signalling dynamics[125-127]. Lipid organisation in cells is largely achieved by the bulk lipid classes, particularly those organised within membranes, while the function and behaviour of the myriad minor lipids complement the dynamic cellular organisation of the major species. Four distinct metabolic pathways regulate the majority of lipid interactions in eukaryotic cells including the PLs, sphingolipids, glycerolipids and non-esterified (free) fatty acids[128]. Lipid metabolism networks have been well studied (reviewed in[128-130]). As a result, quantitative alterations in lipid class or species can reveal changes to enzyme activity or gene expression involved with regulating cellular lipid turnover. Understanding how lipid biosynthesis and degradation pathways function or change following physiological perturbations, can therefore allow the identification of mechanisms responsible for disease pathogenesis[128].

7.1 Glycerophospholipids

PLs form key components of cellular membranes and participate in plasma lipid transport[90]. Phosphoglycerides consist of two fatty acyl chains attached to a glycerol backbone ($C_3H_8O_3$) containing a phosphorylated alcohol head group[124]. Major PL classes are defined by the structure of the head group, but PL diversity in eukaryotic cell membranes (i.e. more than 1000 types) is ascribed to distinct molecular species classified according to the variation in fatty acyl chains esterified to the glycerol backbone at the *sn1* and *sn2* positions[124, 127] (Fig. 5). These fatty acids normally contain 14 to 24 carbon atoms and zero to six double bonds[130]. Generally, the *sn1* alkyl chain is saturated or monounsaturated while the *sn2* position is polyunsaturated[130]. Without the alcohol the parent compound is phosphatidic acid, an important precursor of PL biosynthesis present at low levels in all cells[124]. The polar (alcohol) moiety that is choline, ethanolamine, inositol or serine, can be esterified to the *sn3*

hydroxyl of glycerol through phosphoric acid (H_3PO_4) – thus giving rise to the lipids phosphatidylcholine (PC), phosphatidylethanolamine (PE), phosphatidylinositol (PI) and phosphatidylserine (PS)[127] (Fig. 5). The amphipathic nature of PLs that form unique membrane bilayers is attributed to the interaction of the hydrophobic (nonpolar) hydrocarbon fatty acyl tails with the hydrophilic (polar), negatively charged phosphorus-containing head regions. As the hydrocarbon chain linkage at the *sn2* position is always an ester, the subclass referring to *phosphatidyl* results from an ester bond (in contrast to an ether or vinylether) at the *sn1* position of the glycerol moiety[128].

Mammalian plasma membranes are characterised by asymmetric distribution of PLs, glycolipids (comprising lipid moieties with an adjoined sugar) and cholesterol[131]. The distribution and quantity of lipid components vary with important implications for membrane fluidity and function[132]. While PC is highly abundant constituting ~50% of total PL content, PE comprises 20-50%, PS ~10% with minor contributions of PI[127, 133]. Choline-containing PLs (i.e. PC) are mainly located on the exoplasmic leaflet while the acidic PI and the amino-PLs (i.e. PE and PS) are enriched on the cytoplasmic leaflet[133, 134]. PLs have important structural and physiological functions and primarily define the permeability barrier of cell or organelle membranes by forming PL mono- or bilayers[124]. PLs do not have inherent catalytic activity, but influence a wide range of membrane-related cellular processes[135]. In particular PS, PI and PI phosphates (PIPs) form essential enzyme substrates for many signalling processes involving specific protein interactions. Cell bilayer matrices house many proteins involved in cell recognition, energy and signal transduction, solute transport and secretion, DNA replication, and provision of donor particles for synthesis of macromolecules[136]. The lateral and transverse lipid assembly into membranes are closely linked to their biosynthesis

in the ER, translocation from the ER lumen to the cell cytosol, and movement between the organelle compartments, endo- and ectoplasm[137].

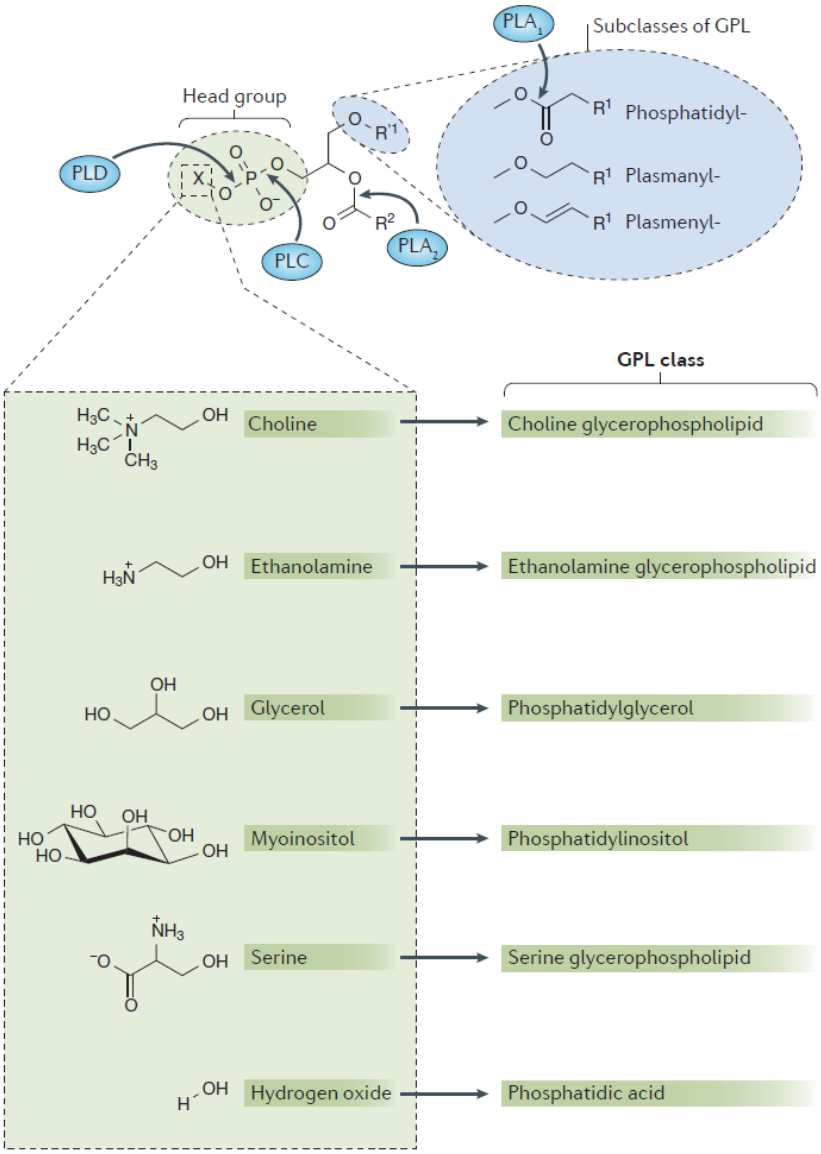

Figure 5 | Composition of mammalian glycerophospholipids. Representation of the chemical configurations of the glycerophospholipids (PLs) in mammalian cell membranes. PL classes are defined by the polar moiety (X) attached to the phosphate head group. An ester, ether or vinylether linked to the hydroxy group of the glycerol backbone at *sn1*, respectively specifies the phosphatidyl, plasmanyl or plasmenyl subclasses. Molecular species are generated through variation in carbon atom number, and location and number of double bonds of the chains at R^1, R^{-1} and R^2. Phospholipase (PLA, PLC, PLD) cleavage sites are indicated[128].

Owing to the diversity of membrane PL species and their important biological functions, lipid compositions must be carefully controlled. Membrane PL homeostasis is regulated by the processes of biosynthesis, remodelling, degradation and interorganelle trafficking, each the product of distinct enzymatic pathways. A comprehensive body of literature exists regarding PL synthesis, remodelling and degradation in mammalian cells[128, 130, 138]. Cellular levels of phosphatidic acid, the precursor of all PLs, are important for maintaining PL pools. Synthesis of phosphatidic acid entails *sn1* acylation of glycerol-3-phosphate (by acyl-CoA:glycerol-3-phosphate acyltransferase) to generate lysophosphatidic acid, which is further acylated (by lysophosphatidic acid acyltransferase) to produce phosphatidic acid *de novo* (Fig. 6). Phosphatidic acid may also be generated through diacylglycerol (DAG) phosphorylation by DAG-kinase or by enzymatic degradation (discussed later). PL synthesis using phosphatidic acid then follows either of two pathways: dephosphorylation of DAG (by phosphatidic acid phosphatase) for generation of PC, PE, PS or TAG; or conversion of phosphatidic acid to cytidine diphosphate (CDP)-DAG (by CDP-DAG synthase) for synthesis of the acidic PI, phosphatidylglycerol, or cardiolipin (Fig. 6).

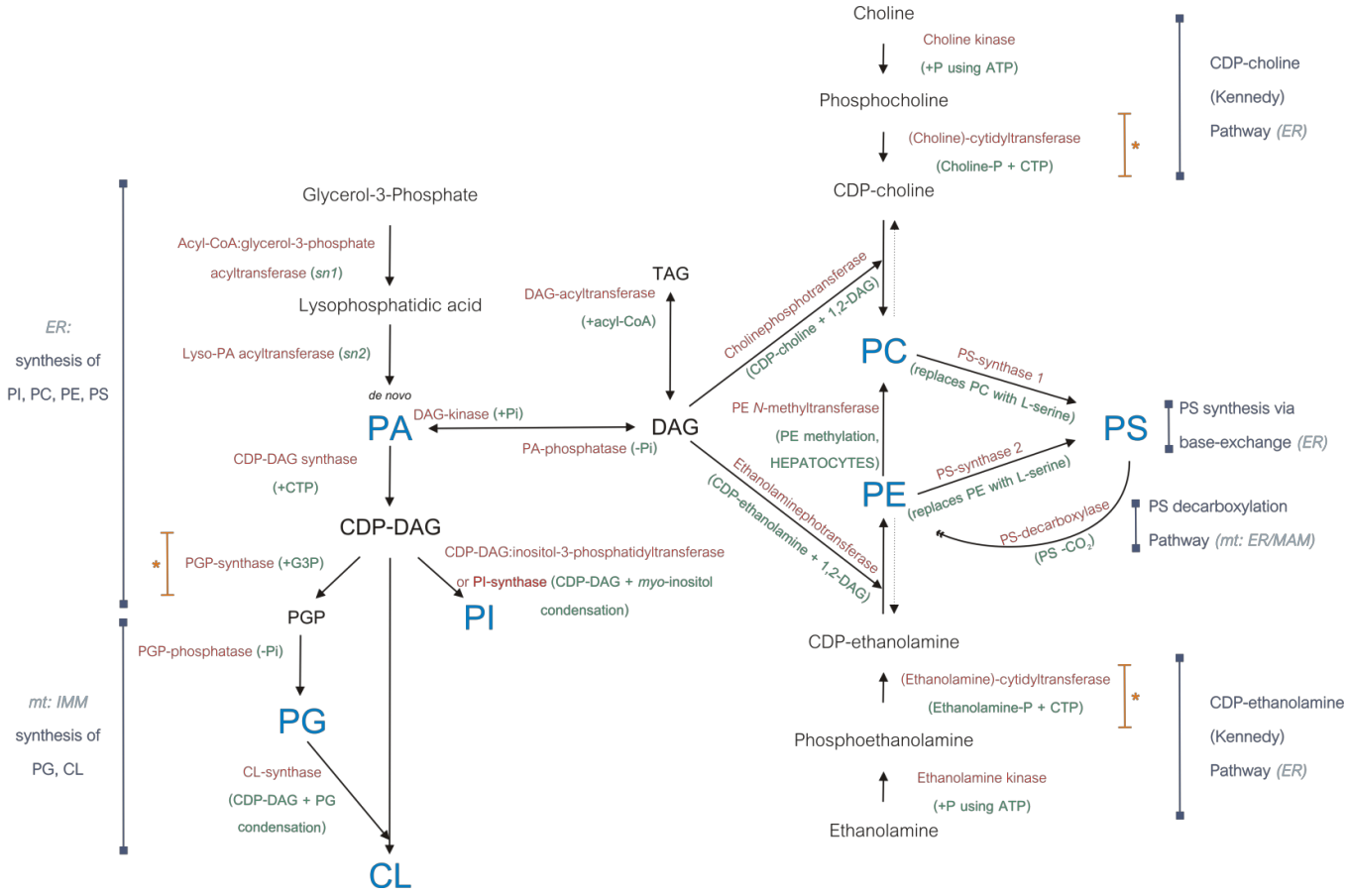

Figure 6 | *De novo* synthesis of mammalian glycerophospholipids. *De novo* glycerophospholipid synthesis (Kennedy Pathway) uses acyl-CoA as donor molecules. The key lipid metabolites (blue capitals) and enzymes (red) catalysing the respective reactions (green) from diverse substrates (black), are indicated. Orange asterisks illustrate potential rate-limiting steps along the pathway. ATP, adenosine triphosphate; CDP, cytidine diphosphate; CL, cardiolipin; -CO_2, carboxylation; CTP, cytidine triphosphate; DAG, diacylglycerol; ER, endoplasmic reticulum; ER/MAM, region of ER named mitochondria-associated membrane, which transiently tethers to the mitochondrion; G3P, glycerol-3-phosphate; IMM, inner mitochondrial membrane; mt, mitochondrion; PA, phosphatidic acid; PC, phosphatidylcholine; PE, phosphatidylethanolamine; PG, phosphatidylglycerol; PI, phosphatidylinositol; +/-Pi, phosphorylation/ dephosphorylation; PS, phosphatidylserine; *sn1*/*sn2*, fatty acyl position on glycerol moiety; TAG, triacylglycerol.

De novo synthesis of PC occurs exclusively through the sequential activity of choline kinase, cytidyltransferase and cholinephosphotransferase via the CDP-choline (Kennedy) pathway (Fig. 6). PC can also be generated via methylation of PE by PE-*N*-methyltransferase, but this occurs primarily in hepatocytes[139-141]. Two pathways are involved in PE synthesis, namely CDP-ethanolamine and PS decarboxylation[142]. The CDP-ethanolamine pathway is analogous to that of PC generation, but with ethanolamine, not choline, as substrate. The cytidine triphosphate (CTP) phosphocholine or phosphoethanolamine cytidyltransferase reaction limits PC or PE synthesis via the Kennedy pathway. PE formation mediated by PS-decarboxylase occurs in the inner mitochondrial membrane, but as PS is synthesised in the ER, evidence suggests that translocation of PE through the cell and to other membranes may be rate-limiting[143]. PS-synthase 1 and 2, respectively substitutes the PC and PE head groups via base-exchange with L-serine in the mitochondria-associated membrane compartment of the ER to produce PS[142]. PI is generated via a two-step process[144]. CDP-DAG is synthesised from phosphatidic acid and CTP by CDP-DAG synthase, which then undergoes condensation with *myo*-inositol by either CDP-DAG:inositol-3-phosphatidyltransferase or PI synthase to generate PI (Fig.6).

Remodelling of *de novo* generated PLs, or the Lands' cycle, maintains PL homeostasis and molecular species composition and involves cycles of deacylation and reacylation catalysed by the coordinated reactions of phospholipase A (PLA), acyl-CoA synthases, transacylases and LPL-acyltransferases (reviewed in[145, 146]). PL remodelling also mediates arachidonic acid (AA) signalling, enzyme activation in the inner mitochondrial membrane, oxidised PL repair and maintenance of functional alveolar surfactant[130]. Acyl chain removal from the glycerol backbone by PLA catalyses the committing step along the pathway. In particular, PLA_1 and PLA_2 respectively hydrolyse the acyl chain from the *sn1* or *sn2* positions of the glycerol

moiety. Following PLA-mediated acyl chain cleavage, a different fatty acid may be reacylated by the activity of acyltransferases, which catalyses the transacylation of an acyl group from acyl-CoA to various acceptors.

The degradation of PLs has two important functions: As a result of the rapid yields of many PL species, degradation pathways maintain basal PL turnover, but also generates second messengers involved in signalling following stress or inflammatory stimuli[147, 148]. According to the broad body of literature available on PL synthesis, much less is known regarding cellular PL degradation mechanisms. However, the enzymes known as phospholipases mediate cleavage of mammalian PL substrates[149]. Three major phospholipases are described based on their sites of cleavage, namely phospholipases A, C and D (PLA, PLC and PLD) (Fig. 5). PLA mediated acyl-chain removal from the *sn1* or *sn2* positions yields 2-acyl- or 1-acyl-LPL respectively, and a free fatty acid. Both PLC and PLD are considered phosphodiesterases[148]. PLC cleaves the bond before the phosphate of the glycerol backbone, thus forming DAG and a phosphorylated head group. The activity of PLC is essential for generating second messengers involved in signal transduction, for example inositol-3-phosphate. Cleavage of the bond after the phosphate of the glycerol moiety is mediated by PLD, which produces phosphatidic acid and an alcohol head group[150]. PLD-catalysed hydrolysis of primarily PC is a third example of cellular phosphatidic acid generation. Even though levels of phosphatidic acid are transitory, these diacyl-glycerophospholipids serve essential functions in lipid biosynthesis, membrane curvature and signalling[151]. PLB exhibits both *sn1* and *sn2* fatty acyl ester hydrolysis, thus generating LPLs; but it can also act upon the acyl chain of LPLs as lysophospholipases (which is how PLB is commonly referred to)[149].

7.2 Lysophospholipids

LPLs are major products of the Lands' cycle, which is primarily regulated by the concerted activities of PLA and LPL-acyltransferases (LPLAT)[145, 152]. The activity of PLA_1 and PLA_2 thus generates LPLs, which may be reacylated to form intact PLs or hydrolysed by lysophospholipases to produce a PL backbone and a fatty acid. LPLAT, the key enzyme completing the remodelling process, is responsible for acylating the LPLs generated by $PLA_{1/2}$. LPLs are thus bioactive PL metabolites that regulate important cellular functions and disease processes[153, 154]. With chemical structures similar to the glycerol-derived PLs, LPLs consist of a phosphate head group linked to a glycerol backbone at the *sn3* carbon, but differ from PLs in that a single hydroxyl group is acylated at the *sn1* or *sn2* position[155, 156] (Fig. 7). LPLs are *de novo* biosynthesised via the activity of phospholipases or acyltransferases from glycerol-3-phosphate and fatty acyl-CoA, or by PL fatty acid hydrolysis from either of the acyl chain positions[155]. Despite a simple structure and low abundance in cell membranes, LPLs display broad biological activity in numerous cell types and tissues involving neoplasia and immunity[153, 157], inflammation[158], cancer[159, 160], and metabolic disorders like atherosclerosis[161]. Lysophospholipidomic interpretation is still in its infancy, but is a rapidly growing field of knowledge[162]. As a consequence, a clear understanding of the biological functions of lysophosphatidylcholine (lysoPC), -ethanolamine (lysoPE), -inositol (lysoPI) and -serine (lysoPS), remains to be elucidated[155].

LysoPC is derived from PC and reacylated by lysoPC acyltransferases (LPCAT)[163]. LPCAT2 is strongly expressed in macrophages and along with lysoPC, which acts as chemoattractant to inflammation sites, contribute to an overall proinflammatory effect[163, 164]. The proinflammatory activity of lysoPC involves modulation of T cell functions[165, 166], enhancing expression of proinflammatory cytokines[166, 167] and conversion of pro-cytokines to their

biologically active forms by caspase-1 following lysoPC-dependent NADPH oxidase stimulation and reactive oxygen species (ROS) production[168]. LysoPE, a metabolite from PE hydrolysis by PLA_2, is largely understudied. LysoPE has been implicated in cancer as marker metabolites in hepatocellular carcinoma[169] and through chemotactic migration and invasion of ovarian cancer cells[170], though anti-inflammatory activity has also been reported[171]. LysoPC and lysoPE can also form major constituents of oxidised LDL particles and LDs[172, 173].

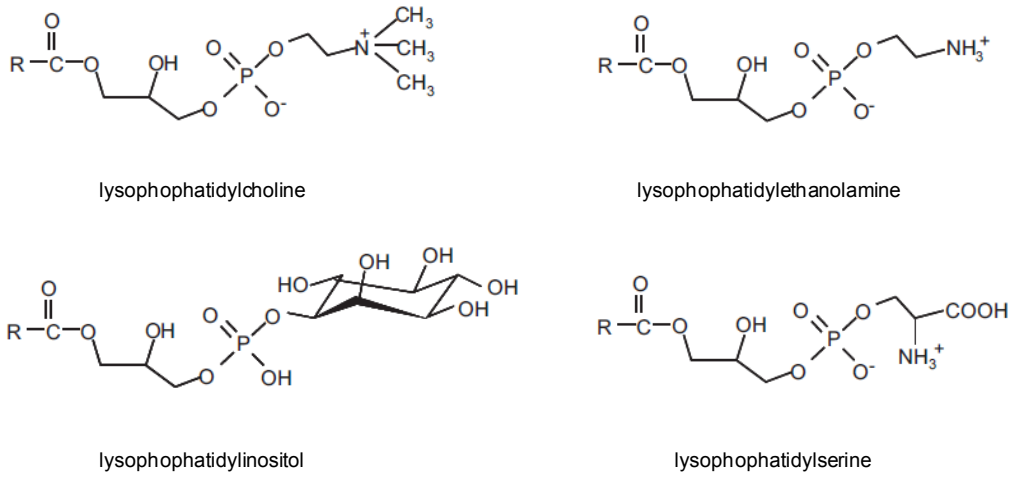

Figure 7 | Chemical structure of glycerol-based lysophospholipids. Representation of the chemical structures of the glycerol-derived lysophospholipids. R, fatty acyl chain[155].

7.3 Sphingolipids

Another class of important structural mammalian cell membrane lipids are the sphingolipids. Sphingolipids contain three key structural elements, namely an 18C alkane (i.e. sphinganine) or alkene (i.e. sphingosine) sphingoid long-chain base (lcb), a fatty acid attached to the *sn2* carbon of the lcb via an amide-bond, and a hydrophilic head group linked to the *sn1* hydroxyl[174-176]. Head groups comprising sugars produce the glycosphingolipids, whereas phosphorylcholine generates sphingomyelin (SM), which represents the sphingolipid

analogue of PC (Fig. 8). Ceramides (Cer) consist of the sphingoid lcb and the *sn2*-linked fatty acid of variable length only, thus forming the backbone of all complex membrane sphingolipids[177] (Fig. 8). Apart from the core moiety, structurally diverse sphingolipids are classified according to the free non-acylated sphingoid lcb (i.e. sphingosine), *N*-acylated sphingoid base or the complex *N*-acylated sphingoid base with polar moiety at the *sn1* position[175]. Sphingosine (d18:1) is the most abundant sphingoid base in animal tissues. It contains *sn1* and *sn3* hydroxyl groups, and an amine and *trans*-double bond in *sn2* and *sn4* positions, respectively[176]. SM is largely located on the outer plasma leaflet (like PC), where it exerts diverse biological activities[133].

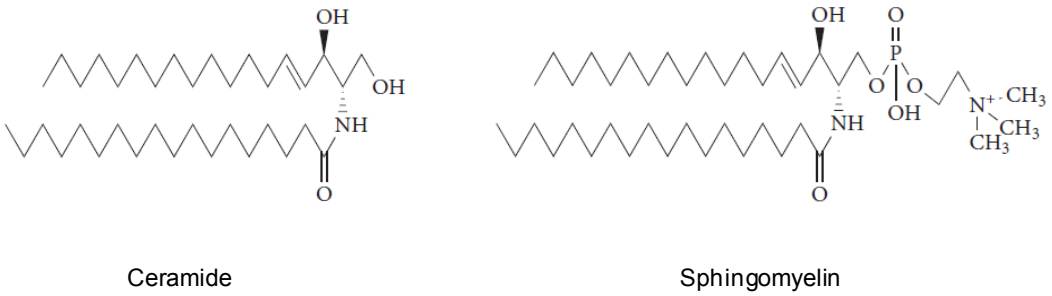

Figure 8 | Chemical structure of sphingolipids. Representation of the chemical structures of the ceramide and sphingomyelin sphingolipids in mammalian membranes. Ceramide comprises a sphingosine base with amide-linked fatty acid and forms the hydrophobic backbone of the phosphorylcholine-containing sphingomyelin[135].

Important membrane associated sphingolipids that function in signalling and metabolism like Cer and SM, exhibit great structural diversity attributed to an excess of 20 identified fatty acid species in mammalian cells that differ in chain length and degree of saturation and hydroxylation[178, 179]. Cer can be generated in mammalian cells from the activity of SMase hydrolysis in the cell membrane, via the salvage pathway where complex sphingolipids are catabolised to sphingoid bases and reacylated to form Cer, or through *de novo* synthesis in the ER by enzymatic reactions using precursor molecules[180]. *De novo* Cer synthesis follows the condensation of palmitoyl-CoA (16:0) with L-serine to form 3-keto-sphinganine, which is

further reduced to sphinganine, *N*-acylated to dihydroceramide and after addition of a 4,5-*trans* double bond by dihydroceramide desaturase, produces Cer[180, 181]. The reactions catalysed by serine palmitoyltransferase (generating 3-keto-sphinganine) and Cer synthase (CerS, catalysing fatty acyl-CoA addition to sphinganine generating the saturated Cer precursor) are the major regulatory steps along the *de novo* pathway[181]. Cer synthesised in the ER is then delivered to the Golgi apparatus by vesicular transport or Cer transport proteins (CERT). The conversion of Cer to complex sphingolipids or metabolites in the Golgi entails metabolism by Cer kinase to ceramide-1-phosphate, or by CerS for generation of glucosyl- or lactosylceramide[126]. Conversion of Cer to SM is mediated by SM synthase that transfers phosphorylcholine from PC, thus producing SM and DAG. In contrast, SM to Cer conversion occurs through the activity of SMase, which releases the phosphorylcholine head group from the *sn1* position of the sphingoid base[179]. Interestingly, *de novo* generated Cer may also undergo degradation in the ER by either neutral or alkaline ceramidases, accordingly sustaining the balance of SM versus sphingosine and sphingosine derivatives[182].

The salvage pathway of Cer accumulation is primarily associated with late endosome or lysosomal compartments, which delivers 50 to 90% of the Cer pool[183]. Following the hydrolytic release of sphingolipids from the plasma membrane and internalisation by the endocytic or lysosomal compartments, acidic forms of SMase and glycosidase degrade SM or glycosphingolipids to Cer, which is further metabolised by acidic ceramidases to produce sphingosine[126]. Recycled sphingosine can then be directed towards glycerolipid synthesis or be reutilised for sphingolipid generation. Sphingosine kinases that catalyse ATP-dependent phosphorylation of sphingosine substrates leaving endosomes or lysosomes, generate sphingosine-1-phosphate (S1P)[184]. S1P is a pro-survival cell growth lipid that suppresses programmed cell death[185]. Conversely, S1P degradation is mediated by either S1P

phosphatase dephosphorylation back to sphingosine (reversible reaction), or by S1P lyase that produces hexadecenal and phosphoethanolamine (irreversible reaction). Both of the S1P lyase products are then reused for the production of PE[184].

Mammalian CerS consists of a six-member enzyme family (CerS1-CerS6) that are integral membrane proteins of the ER catalysing the acylation of sphinganine by *N*-acyltransferase (reviewed in[126, 182, 186, 187]). Each CerS displays specific catalytic activity towards acyl chains of defined length ranging from 14 to 26 carbon atoms that are saturated or monounsaturated. Research into the regulation of the CerS isoforms is limited. However, acyl-CoA specificity for each of the CerS enzymes have been identified: C18 for CerS1, C20 to C26 for CerS2, C22 to C26 for CerS3, C18 to C22 for CerS4, C16 for CerS5, and C14 and C16 for CerS6[186]. As Cer levels are affected by numerous sphingolipid enzymes and proteins regulating CerS stability and activity, identifying the precise contributions of each of the CerS enzymes to cellular Cer metabolism becomes challenging[186]. Nevertheless, what is clear is that Cer with specific acyl chain lengths and/or saturation display unique membrane biophysical properties and mediate diverse cellular processes in signal transduction and disease[188].

7.4 Cholesterol

The nonpolar sterol lipids in mammalian cells largely comprise cholesterol and its derivatives[124]. As a subgroup of steroids, cholesterol is a key integral lipid in plasma membranes and the trans-Golgi compartments and also exhibit important biosynthetic precursor and signalling functions[57]. Steroids consist of a core structure of C17 atoms fused into a four-ringed organic compound of three cyclohexane rings and a single cyclopentane[124]. The oxidation of, and variation in, functional groups attached to the four-ring core ascribes diversity to the steroid lipids. Cholesterol is the most abundant sterol in mammalian cells

with unique biophysical properties that influence membrane organisation, fluidity and signalling[114]. In addition to a role in membrane trafficking, esterified cholesterol is an essential component of cellular LDs[189]. LDs not only provide important nutrient reservoirs, but are dynamic cell organelles involved in diverse biological processes[110].

7.5 Eicosanoids

Eicosanoids are primarily derived from C20 fatty acids known as AA (20:4n-6) and have wide-ranging transcellular and physiologic functions in homeostasis and inflammation[190, 191]. Biosynthesis of eicosanoids is dependent on the levels of free AA. The Lands' cycle is instrumental to the generation of PUFA-containing PLs, which also constitute major sources of lipid mediators including eicosapentaenoic acid, docosapentaenoic acid and AA. Arachidonate is esterified to the *sn2* hydroxyl of glycerol-derived PLs, in particular to PI. Upon cleavage of the ester bond by PLA_2, a LPL and an AA is released. Distinct PI metabolic cascades may also generate free AA through the activity of PLC on AA-containing DAG backbones. For example, PLC will cleave the phosphodiester bond before the phosphate of PI-4,5-bisphosphonate (PIP_2), yielding PI-1,4,5-trisphosphate (PIP_3) after hydrolysis of the 1,2-cyclic phosphodiester, and DAG as products. The activity of DAG lipase then catalyses the *sn2* removal of arachidonate from the glycerol moiety, thereby liberating a monoglyceride (MAG). Arachidonate can then be steered towards either of three pathways for synthesis of eicosanoids. Enzymatic conversion of AA by cyclooxygenase (COX), lipoxygenase (LOX) and cytochrome P450-monooxygenase (CYP450) will respectively generate the prostaglandins and thromboxanes, leukotrienes and lipoxins, and epoxyeicosatrienoic and hydroxyeicosatetraenoic acids[192, 193].

8. Lipidomics: profiling of cellular lipid pathways and networks

Lipidomics entail the comprehensive study of the organisation, activity and biological pathways of cellular lipids[194]. To investigate the lipid metabolome and its myriad metabolites, different analytical platforms should be employed. Dependent on the type of analysis method, various output levels can be obtained such as information on the lipid class, fatty acid sum composition, location of fatty acid attachment to the glycerol backbone, or position of the fatty acid double bond[195]. High performance liquid chromatography (HPLC) or gas chromatography (GC) methods are well-established and can analyse numerous lipid extracts. However, detection may be of moderate resolution or throughput capacity and may require the use of volatile compounds or radioactive *in vivo* labelling[196]. Though a relatively recent field when compared with proteomics or genomics, major progress in lipidomics research over the last decade was achieved by novel applications of chromatographic and spectrometry technologies[197].

Whereas traditional lipidomic strategies showed great promise, detailed lipid profiling has demonstrated rapid analysis of individual molecular species directly from biological extracts without pre-separation into lipid class[198, 199]. Advances in mass spectrometric techniques like nuclear magnetic resonance (NMR), electrospray ionisation (ESI) and tandem mass spectrometry (MS/MS) have greatly improved earlier limitations and now allow robust and reliable analysis of complex lipid mixtures[200, 201]. ESI is a highly suited method for characterising polar lipids in ion-containing solvents, such as PLs, glycolipids and sphingolipids, which results in singly charged molecular ions[202]. Addition of serial-separation (e.g. MS/MS) greatly simplified limitations in sample purification and derivatisation of GC-MS methods[199]. ESI-MS/MS that utilises the precursor ion and neutral loss scanning capability of MS/MS is performed on minute quantities of unfractionated biological sample

extracts, and will quantify molecular species based on carbon number and saturation[202]. In the ESI-MS/MS method, collision-activated dissociation of the head group of each lipid will result in the formation of common fragments that are either charged or uncharged. Charged fragments will undergo positive or negative precursor ion scans while uncharged common fragments are exposed to neutral loss scanning. Continuous sample infusion and sequential precursor or neutral loss scanning will yield a complete lipid profile of all molecular species in a lipid class through a series of distinct mass spectra[203]. For quantitative results, the spectrometer setup (in precursor and neutral loss scanning mode) necessitates calibration for mass and energy of fragmentation as well as the addition of numerous internal standards. A drawback however, is the lack of distinction between acyl chains that make up the total carbon and double bonds of each molecular species, with the outcome that combined-acyl chain species are reported[202, 203].

8.1 Macrophage lipidomics

Macrophages effortlessly phagocytose and eliminate invading microbes through production of reactive nitrogen and oxygen intermediates and by shuttling microbes to acidic and hydrolytic lysosomes[204]. Pathogenic Mtb, however, is one of the most successful intracellular bacterial species that has evolved numerous mechanisms of host manipulation. By subverting phagosome maturation and destruction from lysosomal hydrolases, Mtb-restrained vacuoles remain fusion-competent and are able to derive nutrients from the recycling endosomal network[205, 206]. The block in phagolysosomal fusion is mediated by Mtb membrane lipids[207]. The importance of PI and its phosphorylated derivates in signal transduction, cytoskeletal organisation and as substrates for modifying-enzymes is well demonstrated[208, 209]. Moreover, phosphatidylinositides are important mediators of discrete membrane trafficking events during organelle biogenesis following phosphorylation of the inositol head-group at the 3, 4

or 5 position (or in combination)[210, 211]. In particular, PI3P is required in abundance on endosome and phagosome membranes to mediate maturation through recruitment of distinct fusion proteins[212]. As calcium flux is also important for phagosome maturation, Mtb can inhibit this through suppression of sphingosine kinase activity[213].

While the physiological functions of single lipid mediators have been more studied[214, 215], lipid profiles of host cells in the context of bacterial invasion are less documented. Yet since 2008 a few important reports on macrophage lipidomics emerged[216-221]. LPS is a major membrane lipoglycan of Gram-negative bacteria with important endotoxic properties that activate immune cells via TLR4[222]. As a result, native or synthetic LPS (i.e. Kdo_2-lipid A; KLA) stimulation in macrophages has been studied widely as *in vitro* or *ex vivo* models of bacterial immune cell activation[216, 217, 219, 223]. By developing robust LC-MS/MS platforms, the groups of Buczynski[223] and Norris[219] quantitatively described the eicosanoid profiles of diverse murine macrophages. In particular, Norris *et al*. examined KLA-dependent TLR4 activation in murine resident alveolar, thiogycolate-elicited, bone marrow-derived and RAW264.7 macrophages[219]. Their results identified unique COX metabolism between KLA-treated and -untreated cells, but also among macrophage types. All TLR4-activated cells expressed substantially more COX-derived species (5- to 188-fold; versus untreated cells) while the metabolite prostaglandin D2 (PGD_2) was significantly elevated in immortalised (~250 pmol/µg DNA) compared to primary macrophages (<10 pmol/µg DNA)[219].

Dennis and co-workers[217], in a model of LPS challenged RAW264.7 macrophages, assessed lipidome changes effected by bacterial inflammatory insult and pharmacological perturbation of the sterol pathway. Following KLA treatment, more than 400 molecular species were identified that reflected alterations in PL, sterol, and eicosanoid lipid profiles. While total PL

content remained unchanged over 24 hr in KLA-treated cells, reduced levels were recorded in control cells after 12 and 24 hours of treatment. In KLA-treated cells, a 7-fold increase was recorded in the phosphatidic acid species 32:0, 34:0, 34:1, 36:0 and 36:1. Saturated species of PI were elevated whereas species with polyunsaturation (i.e. 38:4) were reduced by 50% compared to control cells. Saturated free fatty acids and acyl-CoA increased in KLA-stimulated cells. This coincided with a downregulation in elongase or desaturase transcriptional machinery. For example, low abundances of stearoyl-CoA desaturase (SCD1) mRNA reflected less monounsaturated acyl-CoA species. SCD1 is a key lipogenesis enzyme that forms the double bond in stearoyl-CoA to produce monounsaturated from saturated fatty acids[224]. In particular palmitoleic (16:1n-7) and oleic (18:1n-9) acid from palmitic (16:0) and stearic (18:0) acid, respectively[224]. In spite of being a key regulator of metabolism, SCD1 has been implicated in atherosclerosis, cancer and inflammation (e.g. loss of SCD1 attenuates inflammation in adipocytes)[225, 226]. Dennis *et al*. further recorded distinct changes in cellular sterols after 24 hours of KLA treatment[217]. Substantial elevation in cholesterol 25-hydroxylase mRNA coincided with up to 8-fold enrichment of the precursor intermediates desmosterol and lanosterol. 25-Hydroxylase is an essential enzyme catalysing the reaction for 25-hydroxycholesterol generation, a potent antiviral oxysterol implicated in cell membrane rearrangements that inhibit viral entry[227]. Interestingly, after KLA treatment the majority of sterol biosynthesis genes decreased with the exception of 3-hydroxy-3-methylglutaryl-CoA reductase (HMGCR)[217], the rate-limiting enzyme of the mevalonate pathway responsible for NADPH-dependent generation of cholesterol and isoprenoids[228]. Elevated expression of HMGCR coupled with 2-fold more cholesterol in KLA-treated cells (versus control) suggested sterol synthesis. In addition, important changes in sphingolipid profiles were reported following KLA treatment in RAW264.7 macrophages. Compared with control cells, levels of SM, glycosphingolipids, Cer and the potent signalling metabolite S1P, were

elevated. The rise in sphingolipid abundance was linked to *de novo* biosynthesis as early intermediates in the pathway increased (sphinganine and dihydroceramide) and the primary biosynthesis enzyme (serine palmitoyltransferase) was upregulated. Cer species with very long-chain fatty acids were not affected by KLA treatment (i.e. C24:0 and C24:1). Yet, fatty acids and mRNA of SM and glycosylceramides were induced. A substantial increase in sulphated galactosylceramides was reported that might have been as a function of macrophage phagocytosis, but also as an anti-inflammatory signal since sulfatides are known suppressors of proinflammatory cytokines[229]. The researchers also recorded an early 10-fold upregulation of COX mRNA in KLA-treated cells. COX converts free AA, mobilised from the glycerol backbone *sn2* position of membrane PLs or lysoPLs by PLA_2, to precursor PGH2[230]. Whereas free arachidonate levels decreased after an initial spike (possibly due to elevated COX activity), several COX-derived metabolites ($PGF_{2\alpha}$, PGE and PGD_2) were detected in culture media that were strongly correlated with upregulation of prostaglandin synthesis genes (Ptgs2 and Ptges)[217].

Dennis *et al*. furthermore assessed changes to macrophage lipid profiles after pharmacological inhibition of sterol biosynthesis[217]. Statin treatment prevented the KLA-induced rise in biosynthetic intermediates, but had little effect on global cholesterol or 25-hydroxycholesterol content (possibly as these molecules can be derived from uptake of cholesterol-rich lipoproteins[114]). In response to sterol pathway inhibition, distinct increases in eicosanoid species (i.e. PGD_2 and PGE_2) were associated with elevated mRNA of coinciding synthesis enzymes. Crosstalk between the sterol and eicosanoid pathways was independent of the LXR, an interesting finding as LXRs are key regulators of cellular cholesterol homeostasis[231]. This suggested involvement of an alternative conduit to the sterol-eicosanoid coupling. As the first documented study on quantitative immune cell lipidome dynamics it

greatly contributed to a better understanding of lipid profile changes following inflammatory activation and inhibition of a metabolic pathway.

8.2 Significance of studying macrophage lipid metabolism during mycobacterial infection

Intracellular pathogens like Mtb may target any of the unique lipid features of its host to manipulate cellular functioning for bacillus uptake, replication and persistence[232, 233]. Lipid profile analysis of the most abundant lipids within MA-induced foam cells is thus necessary to identify a possible structure-function involvement of lipids in cell signalling and membrane trafficking during TB. Therefore, studying the contribution of lipids in macrophages and how they change after treatment with various pathogen-associated MAs will allow us to better understand the role of MAs in TB.

9. Aims

Mtb cell wall MAs that are important pathogen virulence factors, are proven PAMPs and immune response steering agents. However, Mtb MAs display extensive structural variation in oxygenation class and proximal cyclopropane configurations influencing antigenicity, but are continuously remodelled depending on growth needs. To gain a better understanding of the biological function of each of the major MA classes, we investigated in this study the induction of foamy macrophage phenotypes and how their lipidomic regulation influenced the facilitation of intracellular mycobacterial growth. The objectives for each chapter are reported on as follows in this thesis:

9.1 Chapter II: Mycolates of Mycobacterium tuberculosis modulate the flow of cholesterol for bacillary proliferation in murine macrophages

To better understand the mechanisms responsible for the establishment of active TB related granulomas, we investigated how *in vivo* treatment of mice with chemically synthetic MAs, each with a defined stereochemistry representing the separate major classes of Mtb mycolates, influence cell differentiation and support of mycobacteria in peritoneal macrophages. We assessed the influence of MA structure first on the induction of foamy macrophages and multinucleated giant cells identified by light and laser-scanning-confocal microscopy, second on cholesterol accumulation and finally on intracellular mycobacterial growth.

9.2 Chapter III: Lipidome immunomodulation of murine macrophages by chemically synthetic mycobacterial mycolates

In Chapter II of this thesis, we report how MAs differentially change the phenotype of macrophages to facilitate mycobacterial survival and proliferation. By using individual chemically synthetic MAs, each with a defined stereochemistry, representative of the three main classes of natural MA, mMA was found to cause vacuolation while kMA induced cholesteryl ester rich LD accumulation in murine macrophages. Only macrophages associated with kMA, but not mMA treatment, could sustain intracellular mycobacterial growth. αMA had no notable effect on macrophage physiology. We therefore hypothesised that the induction of phenotypically and functionally distinct macrophage populations by the oxygenated MAs could be accompanied by unique lipidome profiles. Employing an ESI-MS/MS lipidomics approach, we therefore studied changes in the lipidome of murine peritoneal macrophages following *in vivo* treatment with chemically synthetic representatives of the major classes of Mtb MAs. We report here on changes in the composition of PLs, LPLs and sphingolipids among the lipidomes of murine peritoneal macrophages differentially treated with each of the MA classes.

9.3 Chapter IV: General Discussion

In the final chapter of this thesis, we discuss the potential impact of the results obtained in the experimental chapters and how this may relate to the future development of novel anti-TB therapies and research.

9.4 Appendix: Exploration of comparative ex vivo cellular technologies

Considering the complex and diverse nature of immunological responses and the need for animal models to simulate human immune response models, extensive optimisation of experimental conditions and protocols were required. In the Appendix we thus outline the optimised conditions for this research project and the resulting observations that led to our eventual working experimental models as employed and described in the Materials and Methods in Chapters II and III.

10. References

1. Comas, I., M. Coscolla, T. Luo, S. Borrell, K. E. Holt, M. Kato-Maeda, J. Parkhill, B. Malla, S. Berg, G. Thwaites, D. Yeboah-Manu, G. Bothamley, J. Mei, L. Wei, S. Bentley, S. R. Harris, S. Niemann, R. Diel, A. Aseffa, Q. Gao, D. Young and S. Gagneux. 2013. Out-of-Africa migration and Neolithic coexpansion of *Mycobacterium tuberculosis* with modern humans. *Nat. Genet.* **45**: 1176-1182.

2. WHO. 2015. *Global Tuberculosis Report*. 20th ed. World Health Organization, Geneva. pp 204

3. Kaufmann, S. H. E. 2011. Fact and fiction in tuberculosis vaccine research: 10 years later. *Lancet Infect. Dis.* **11**: 633-640.

4. Raven, P. H., G. B. Johnson, J. B. Losos and S. R. Singer. 2005. *Biology*, 7th ed., McGraw-Hill, New York. pp 1250.

5. Fu, L. M. and C. S. Fu-Liu. 2002. Is *Mycobacterium tuberculosis* a closer relative to Gram-positive or Gram-negative bacterial pathogens? *Tuberculosis* **82**: 85-90.

6. Broset, E., C. Martin and J. Gonzalo-Asensio. 2015. Evolutionary landscape of the *Mycobacterium tuberculosis* complex from the viewpoint of PhoPR: implications for virulence regulation and application to vaccine development. *MBio* **6**: e01289-01215.

7. Wirth, T., F. Hildebrand, C. Allix-Beguec, F. Wolbeling, T. Kubica, K. Kremer, D. van Soolingen, S. Rusch-Gerdes, C. Locht, S. Brisse, A. Meyer, P. Supply and S. Niemann. 2008. Origin, spread and demography of the *Mycobacterium tuberculosis* complex. *PLoS Pathog.* **4**: e1000160.

8. Comas, I., J. Chakravartti, P. M. Small, J. Galagan, S. Niemann, K. Kremer, J. D. Ernst and S. Gagneux. 2010. Human T cell epitopes of *Mycobacterium tuberculosis* are evolutionarily hyperconserved. *Nat. Genet.* **42**: 498-503.

9. Gill, W. P., N. S. Harik, M. R. Whiddon, R. P. Liao, J. E. Mittler and D. R. Sherman. 2009. A replication clock for *Mycobacterium tuberculosis*. *Nat. Med.* **15**: 211-214.

10. Glickman, M. S., J. S. Cox and W. R. Jacobs, Jr. 2000. A novel mycolic acid cyclopropane synthetase is required for cording, persistence and virulence of *Mycobacterium tuberculosis*. *Mol. Cell* **5**: 717-727.

11. Minniken, D. E., L. Kremer, L. G. Dover and G. S. Besra. 2002. The methyl-branched fortifications of *Mycobacterium tuberculosis*. *Chem. Biol.* **9**: 545-553.

12. Jankute, M., J. A. Cox, J. Harrison and G. S. Besra. 2015. Assembly of the mycobacterial cell wall. *Annu. Rev. Microbiol.* **69**: 405-423.

13. McNeil, M., M. Daffe and P. J. Brennan. 1990. Evidence for the nature of the link between arabinogalactan and peptidoglycan of mycobacterial cell walls. *J. Biol. Chem.* **265**: 18200-18206.

14. Riley, L. W. 2006. Of mice, men and elephants: *Mycobacterium tuberculosis* cell envelope lipids and pathogenesis. *J. Clin. Invest.* **116**: 1475-1478.

15. Daffe, M. 2000. The mycobacterial antigens 85 complex – from structure to function and beyond. *Trends Microbiol.* **8**: 438-440.

16. Delogu, G., M. Sali and G. Fadda. 2013. The biology of *Mycobacterium tuberculosis* infection. *Mediterr. J. Hematol. Infect. Dis.* **5**: 10.4084/MJHID.2013.4070.

17. Russell, D. G. 2001. *Mycobacterium tuberculosis*: here today, and here tomorrow. *Nat. Rev. Mol. Cell Biol.* **2**: 1-9.

18. Pieters, J. 2008. *Mycobacterium tuberculosis* and the macrophage: maintaining a balance. *Cell Host Microbe* **3**: 399-407.

19. Verrall, A. J., M. G. Netea, B. Alisjahbana, P. C. Hill and R. van Crevel. 2013. Early clearance of *Mycobacterium tuberculosis*: a new frontier in prevention. *Immunology* **141**: 506-513.

20. Rajaram, M. V., B. Ni, C. E. Dodd and L. S. Schlesinger. 2014. Macrophage immunoregulatory pathways in tuberculosis. *Semin. Immunol.* **26**: 471-485.

21. Duque, C., L. Arroyo, H. Ortega, F. Montufar, B. Ortiz, M. Rojas and L. F. Barrera. 2014. Different responses of human mononuclear phagocyte populations to *Mycobacterium tuberculosis*. *Tuberculosis* **94**: 111-122.

22. Hossain, M. M. and M. N. Norazmi. 2013. Pattern recognition receptors and cytokines in *Mycobacterium tuberculosis* infection - the double-edged sword? *Biomed. Res. Int.* **2013**: 1-18.

23. van Crevel, R., T. H. M. Ottenhoff and J. W. M. van der Meer. 2002. Innate Immunity to *Mycobacterium tuberculosis*. *Clin. Microbiol. Rev.* **15**: 294-309.

24. Kleinnijenhuis, J., M. Oosting, L. A. Joosten, M. G. Netea and R. Van Crevel. 2011. Innate immune recognition of *Mycobacterium tuberculosis*. *Clin. Dev. Immunol.* **2011**: 1-12.

25. Behar, S. M. and C. M. Sasetti. 2014. Fixing the odds against tuberculosis. *Nature* **511**: 39-40.

26. Etna, M. P., E. Giacomini, M. Severa and E. M. Coccia. 2014. Pro- and anti-inflammatory cytokines in tuberculosis: a two-edged sword in TB pathogenesis. *Semin. Immunol.* **26**: 543-551.

27. Finlay, B. B. and G. McFadden. 2006. Anti-immunology: evasion of the host immune system by bacterial and viral pathogens. *Cell* **124**: 767-782.

28. Kaufmann, S. H. E. 2001. How can immunology contribute to the control of tuberculosis? *Nat. Rev. Immunol.* **1**: 20-30.

29. Kumar, D. and K. V. Rao. 2011. Regulation between survival, persistence, and elimination of intracellular mycobacteria: a nested equilibrium of delicate balances. *Microbes Infect.* **13**: 121-133.

30. Tsai, M. C., S. Chakravarty, G. Zhu, J. Xu, K. Tanaka, C. Koch, J. Tufariello, J. Flynn and J. Chan. 2006. Characterization of the tuberculous granuloma in murine and human lungs: cellular composition and relative tissue oxygen tension. *Cell. Microbiol.* **8**: 218-232.

31. Guirado, E. and L. S. Schlesinger. 2013. Modeling the Mycobacterium tuberculosis Granuloma - the Critical Battlefield in Host Immunity and Disease. *Front. Immunol.* **4**: 1-7.

32. Ghosn, E. E., A. A. Cassado, G. R. Govoni, T. Fukuhara, Y. Yang, D. M. Monack, K. R. Bortoluci, S. R. Almeida, L. A. Herzenberg and L. A. Herzenberg. 2010. Two physically, functionally, and developmentally distinct peritoneal macrophage subsets. *Proc. Natl. Acad. Sci. U. S. A.* **107**: 2568-2573.

33. Davis, J. M. and L. Ramakrishnan. 2009. The role of the granuloma in expansion and dissemination of early tuberculous infection. *Cell* **136**: 37-49.

34. Caceres, N., G. Tapia, I. Ojanguren, F. Altare, O. Gil, S. Pinto, C. Vilaplana and P. J. Cardona. 2009. Evolution of foamy macrophages in the pulmonary granulomas of experimental tuberculosis models. *Tuberculosis* **89**: 175-182.

35. Munoz-Elias, E. J., J. Timm, T. Botha, W. T. Chan, J. E. Gomez and J. D. McKinney. 2005. Replication dynamics of *Mycobacterium tuberculosis* in chronically infected mice. *Infect. Immun.* **73**: 546-551.

36. Gagneux, S. 2012. Host-pathogen coevolution in human tuberculosis. *Philos. Trans. R. Soc. Lond. B Biol. Sci.* **367**: 850-859.

37. Zumla, A. I., S. H. Gillespie, M. Hoelscher, P. P. J. Philips, S. T. Cole, I. Abubakar, T. D. McHugh, M. Schito, M. Maeurer and A. J. Nunn. 2014. New antituberculosis drugs, regimens, and adjunct therapies: needs, advances, and future prospects. *Lancet Infect. Dis.* **14**: 327-340.

38. Lienhardt, C., M. Raviglione, M. Spigelman, R. Hafner, E. Jaramillo, M. Hoelscher, A. Zumla and J. Gheuens. 2012. New drugs for the treatment of tuberculosis: needs, challenges, promise, and prospects for the future. *J. Infect. Dis.* **205 Suppl 2**: S241-249.

39. Bailo, R., A. Bhatt and J. A. Ainsa. 2015. Lipid transport in *Mycobacterium tuberculosis* and its implications in virulence and drug development. *Biochem. Pharmacol.* **96**: 159-167.

40. Gandhi, N. R., A. Moll, A. W. Sturm, R. Pawinski, T. Govender, U. Lalloo, K. Zeller, J. Andrews and G. Friedland. 2006. Extensively drug-resistant tuberculosis as a cause of death in patients co-infected with tuberculosis and HIV in a rural area of South Africa. *Lancet* **368**: 1575-1580.

41. Cohen, K. A., W. R. Bishai and A. S. Pym. 2014. Molecular Basis of Drug Resistance in *Mycobacterium tuberculosis*. *Microbiol. Spectr.* **2**: MGM2-0036-2013.

42. Forrellad, M. A., L. I. Klepp, A. Gioffre, J. Sabio y Garcia, H. R. Morbidoni, M. de la Paz Santangelo, A. A. Cataldi and F. Bigi. 2013. Virulence factors of the *Mycobacterium tuberculosis* complex. *Virulence* **4**: 3-66.

43. Zuber, B., M. Chami, C. Houssin, J. Dubochet, G. Griffiths and M. Daffe. 2008. Direct visualization of the outer membrane of mycobacteria and corynebacteria in their native state. *J. Bacteriol.* **190**: 5672-5680.

44. Liu, J., C. E. Barry, 3rd, G. S. Besra and H. Nikaido. 1996. Mycolic acid structure determines the fluidity of the mycobacterial cell wall. *J. Biol. Chem.* **271**: 29545-29551.

45. Verschoor, J. A., M. S. Baird and J. Grooten. 2012. Towards understanding the functional diversity of cell wall mycolic acids of *Mycobacterium tuberculosis*. *Prog. Lipid Res.* **51**: 325-339.

46. Al Dulayymi, J. a. R., M. S. Baird and E. Roberts. 2005. The synthesis of a single enantiomer of a major α-mycolic acid of *M. tuberculosis*. *Tetrahedron* **61**: 11939-11951.

47. Koza, G. and M. S. Baird. 2007. The first synthesis of single enantiomers of ketomycolic acids. *Tetrahedron Lett.* **48**: 2165-2169.

48. Al Dulayymi, J. a. R., M. S. Baird, E. Roberts, M. Deysel and J. Verschoor. 2007. The first syntheses of single enantiomers of the major methoxymycolic acid of *Mycobacterium tuberculosis*. *Tetrahedron* **63**: 2571-2592.

49. Dubnau, E., J. Chan, C. Raynaud, V. P. Mohan, M.-A. Laneelle, K. Yu, A. Quemard, S. Smith and M. Daffe. 2000. Oxygenated mycolic acids are necessary for virulence of *Mycobacterium tuberculosis* in mice. *Mol. Microbiol.* **36**: 630-637.

50. Tobian, A. A. R., N. S. Potter, L. Ramachandra, R. K. Pai, M. Convery, W. H. Boom and C. V. Harding. 2003. Alternate Class I MHC Antigen Processing Is Inhibited by Toll-Like Receptor Signaling Pathogen-Associated Molecular Patterns: *Mycobacterium tuberculosis* 19-kDa Lipoprotein, CpG DNA, and Lipopolysaccharide. *J. Immunol.* **171**: 1413-1422.

51. Korf, J., A. Stoltz, J. Verschoor, P. De Baetselier and J. Grooten. 2005. The *Mycobacterium tuberculosis* cell wall component mycolic acid elicits pathogen-associated host innate immune responses. *Eur. J. Immunol.* **35**: 890-900.

52. McNab, F. W., J. Ewbank, A. Howes, L. Moreira-Teixeira, A. Martirosyan, N. Ghilardi, M. Saraiva and A. O'Garra. 2014. Type I IFN induces IL-10 production in an IL-27-independent manner and blocks responsiveness to IFN-gamma for production of IL-12 and bacterial killing in *Mycobacterium tuberculosis*-infected macrophages. *J. Immunol.* **193**: 3600-3612.

53. Vander Beken, S., J. R. Al Dulayymi, T. Naessens, G. Koza, M. Maza-Iglesias, R. Rowles, C. Theunissen, J. De Medts, E. Lanckacker, M. S. Baird and J. Grooten. 2011. Molecular structure of the *Mycobacterium tuberculosis* virulence factor, mycolic acid, determines the elicited inflammatory pattern. *Eur. J. Immunol.* **41**: 450-460.

54. Russell, D. G., P. J. Cardona, M. J. Kim, S. Allain and F. Altare. 2009. Foamy macrophages and the progression of the human tuberculosis granuloma. *Nat. Immunol.* **10**: 943-948.

55. Peyron, P., J. Vaubourgeix, Y. Poquet, F. Levillain, C. Botanch, F. Bardou, M. Daffe, J. F. Emile, B. Marchou, P. J. Cardona, C. de Chastellier and F. Altare. 2008. Foamy macrophages from tuberculous patients' granulomas constitute a nutrient-rich reservoir for *M. tuberculosis* persistence. *PLoS Pathog.* **4**: e1000204. doi:1000210.1001371/journal.ppat.1000204.

56. Benadie, Y., M. Deysel, D. G. Siko, V. V. Roberts, S. Van Wyngaardt, S. T. Thanyani, G. Sekanka, A. M. Ten Bokum, L. A. Collett, J. Grooten, M. S. Baird and J. A. Verschoor. 2008. Cholesteroid nature of free mycolic acids from *M. tuberculosis*. *Chem. Phys. Lipids* **152**: 95-103.

57. Ikonen, E. 2008. Cellular cholesterol trafficking and compartmentalization. *Nat. Rev. Mol. Cell Biol.* **9**: 125-138.

58. Gatfield, J. and J. Pieters. 2000. Essential role for cholesterol in entry of mycobacteria into macrophages. *Science* **288**: 1647-1650.

59. de Chastellier, C. and L. Thilo. 2002. Pathogenic *Mycobacterium avium* remodels the phagosome membrane in macrophages within days after infection. *Eur. J. Cell Biol.* **81**: 17-25.

60. de Chastellier, C. and L. Thilo. 2006. Cholesterol depletion in *Mycobacterium avium*-infected macrophages overcomes the block in phagosome maturation and leads to the reversible sequestration of viable mycobacteria in phagolysosome-derived autophagic vacuoles. *Cell. Microbiol.* **8**: 242-256.

61. Cooper, A. M. 2009. Cell-mediated immune responses in tuberculosis. *Annu. Rev. Immunol.* **27**: 393-422.

62. Glickman, M. S. and W. R. Jacobs, Jr. 2001. Microbial pathogenesis of *Mycobacterium tuberculosis*: dawn of a discipline. *Cell* **104**: 477-485.

63. Lawrence, T. and G. Natoli. 2011. Transcriptional regulation of macrophage polarization: enabling diversity with identity. *Nat. Rev. Immunol.* **11**: 750-761.

64. Mosser, D. M. and J. P. Edwards. 2008. Exploring the full spectrum of macrophage activation. *Nat. Rev. Immunol.* **8**: 958-969.

65. Hume, D. A. 2015. The Many Alternative Faces of Macrophage Activation. *Front. Immunol.* **6 (370)**: 1-10.

66. Liddiard, K. and P. R. Taylor. 2015. Understanding local macrophage phenotypes in disease: shape-shifting macrophages. *Nat. Med.* **21**: 119-120.

67. Mantovani, A., A. Sica, S. Sozzani, P. Allavena, A. Vecchi and M. Locati. 2004. The chemokine system in diverse forms of macrophage activation and polarization. *Trends Immunol.* **25**: 677-686.

68. Biswas, S. K., M. Chittezhath, I. N. Shalova and J. Y. Lim. 2012. Macrophage polarization and plasticity in health and disease. *Immunol. Res.* **53**: 11-24.

69. Biswas, S. K. and A. Mantovani. 2012. Orchestration of metabolism by macrophages. *Cell Metab.* **15**: 432-437.

70. Becker, M., M. A. De Bastiani, M. M. Parisi, F. T. Guma, M. M. Markoski, M. A. Castro, M. H. Kaplan, F. M. Barbe-Tuana and F. Klamt. 2015. Integrated Transcriptomics Establish Macrophage Polarization Signatures and have Potential Applications for Clinical Health and Disease. *Sci. Rep.* **5 (13351)**: 1-12.

71. Murray, P. J. and T. A. Wynn. 2011. Protective and pathogenic functions of macrophage subsets. *Nat. Rev. Immunol*. **11**: 723-737.

72. Murray, P. J. and T. A. Wynn. 2011. Obstacles and opportunities for understanding macrophage polarization. *J. Leukoc. Biol*. **89**: 557-563.

73. McGettrick, A. F. and L. A. O'Neill. 2013. How metabolism generates signals during innate immunity and inflammation. *J. Biol. Chem*. **288**: 22893-22898.

74. Kelly, B. and L. A. O'Neill. 2015. Metabolic reprogramming in macrophages and dendritic cells in innate immunity. *Cell Res*. **25**: 771-784.

75. Mills, E. L. and L. A. O'Neill. 2016. Reprogramming mitochondrial metabolism in macrophages as an anti-inflammatory signal. *Eur. J. Immunol*. **46**: 13-21.

76. Vander Heiden, M. G., L. C. Cantley and C. B. Thompson. 2009. Understanding the Warburg effect: the metabolic requirements of cell proliferation. *Science* **324**: 1029-1033.

77. Dakubo, G. D. 2010. The Warburg Phenomenon and other metabolic alterations of cancer cells. In *Mitochondrial Genetics and Cancer*, Springer-Verlag, Heidelberg Germany. pp 39-66.

78. Asgari, Y., Z. Zabihinpour, A. Salehzadeh-Yazdi, F. Schreiber and A. Masoudi-Nejad. 2015. Alterations in cancer cell metabolism: the Warburg effect and metabolic adaptation. *Genomics* **105**: 275-281.

79. Krawczyk, C. M., T. Holowka, J. Sun, J. Blagih, E. Amiel, R. J. DeBerardinis, J. R. Cross, E. Jung, C. B. Thompson, R. G. Jones and E. J. Pearce. 2010. Toll-like receptor-induced changes in glycolytic metabolism regulate dendritic cell activation. *Blood* **115**: 4742-4749.

80. Rath, M., I. Muller, P. Kropf, E. I. Closs and M. Munder. 2014. Metabolism via Arginase or Nitric Oxide Synthase: Two Competing Arginine Pathways in Macrophages. *Front. Immunol*. **5 (532)**: 1-10.

81. Reddy, P. V., R. V. Puri, A. Khera and A. K. Tyagi. 2012. Iron storage proteins are essential for the survival and pathogenesis of *Mycobacterium tuberculosis* in THP-1 macrophages and the guinea pig model of infection. *J. Bacteriol*. **194**: 567-575.

82. Rojas, M., M. Olivier, P. Gros, L. F. Barrera and L. F. Garcia. 1999. TNFa and IL-10 modulate the induction of apoptosis by virulent *Mycobaterium tuberculosis* in murine macrophages. *J. Immunol*. **162**: 6122-6133.

83. Huang, Z., Q. Luo, Y. Guo, J. Chen, G. Xiong, Y. Peng, J. Ye and J. Li. 2015. *Mycobacterium tuberculosis*-induced polarization of human macrophage orchestrates the formation and development of tuberculous granulomas i*n vitro*. *PLoS One* **10**: e0129744. doi:0129710.0121371/journal.pone.0129744.

84. Jakobsson, T., E. Treuter, J. A. Gustafsson and K. R. Steffensen. 2012. Liver X receptor biology and pharmacology: new pathways, challenges and opportunities. *Trends Pharmacol. Sci*. **33**: 394-404.

85. Zhao, C. and K. Dahlman-Wright. 2010. Liver X receptor in cholesterol metabolism. *J. Endocrinol*. **204**: 233-240.

86. Zelcer, N. and P. Tontonoz. 2006. Liver X receptors as integrators of metabolic and inflammatory signaling. *J. Clin. Invest*. **116**: 607-614.

87. Wojcicka, G., A. Jamroz-Wisniewska, K. Horoszewicz and J. Beltowski. 2007. Liver X receptors (LXRs). Part I: structure, function, regulation of activity, and the role in lipid metabolism. *Postepy Hig. Med. Dosw*. **61**: 736-759.

88. Ignatova, I. D., J. Angdisen, E. Moran and I. G. Schulman. 2013. Differential regulation of gene expression by LXRs in response to macrophage cholesterol loading. *Mol. Endocrinol*. **27**: 1036-1047.

89. Zelcer, N., C. Hong, R. Boyadjian and P. Tontonoz. 2009. LXR regulates cholesterol uptake through Idol-dependent ubiquitination of the LDL receptor. *Science* **325**: 100-104.

90. Marieb, E. N. and K. Hoehn. 2010. *Human Anatomy & Physiology*, Eighth ed., Pearson Benjamin Cummings, San Francisco, CA. pp 1114.

91. Qiao, L., C. Zou, P. Shao, J. Schaack, P. F. Johnson and J. Shao. 2008. Transcriptional regulation of fatty acid translocase/CD36 expression by CCAAT/enhancer-binding protein alpha. *J. Biol. Chem.* **283**: 8788-8795.

92. Michael, J. and S. Sircar. 2011. *Fundamentals of Medical Physiology*, Thieme Medical Publishers, Inc., New York. pp 648.

93. Yancey, P. G., H. Yu, M. F. Linton and S. Fazio. 2007. A pathway-dependent on apoE, ApoAI, and ABCA1 determines formation of buoyant high-density lipoprotein by macrophage foam cells. *Arterioscler. Thromb. Vasc. Biol.* **27**: 1123-1131.

94. Schmitz, G. and M. Grandl. 2009. The molecular mechanisms of HDL and associated vesicular trafficking mechanisms to mediate cellular lipid homeostasis. *Arterioscler. Thromb. Vasc. Biol.* **29**: 1718-1722.

95. Tarling, E. J. and P. A. Edwards. 2011. ATP binding cassette transporter G1 (ABCG1) is an intracellular sterol transporter. *Proc. Natl. Acad. Sci. U. S. A.* **108**: 19719-19724.

96. Wang, N., M. Ranalletta, F. Matsuura, F. Peng and A. R. Tall. 2006. LXR-induced redistribution of ABCG1 to plasma membrane in macrophages enhances cholesterol mass efflux to HDL. *Arterioscler. Thromb. Vasc. Biol.* **26**: 1310-1316.

97. Yu, X. H., Y. C. Fu, D. W. Zhang, K. Yin and C. K. Tang. 2013. Foam cells in atherosclerosis. *Clin. Chim. Acta* **424**: 245-252.

98. Gui, T., A. Shimokado, Y. Sun, T. Akasaka and Y. Muragaki. 2012. Diverse roles of macrophages in atherosclerosis: from inflammatory biology to biomarker discovery. *Mediators Inflamm.* **2012 (693083)**: 1-14.

99. Moore, K. J. and I. Tabas. 2011. Macrophages in the pathogenesis of atherosclerosis. *Cell* **145**: 341-355.

100. Khan, S., H. N. Rahman, T. Okamoto, T. Matsunaga, Y. Fujiwara, T. Sawa, J. Yoshitake, K. Ono, K. A. Ahmed, M. M. Rahaman, K. Oyama, M. Takeya, T. Ida, Y. Kawamura, S. Fujii and T. Akaike. 2014. Promotion of atherosclerosis by Helicobacter cinaedi infection that involves macrophage-driven proinflammatory responses. *Sci. Rep.* **4 (4680)**: 1-12.

101. Singh, V., S. Jamwal, R. Jain, P. Verma, R. Gokhale and K. V. Rao. 2012. *Mycobacterium tuberculosis*-driven targeted recalibration of macrophage lipid homeostasis promotes the foamy phenotype. *Cell Host Microbe* **12**: 669-681.

102. Rahaman, S. O., D. J. Lennon, M. Febbraio, E. A. Podrez, S. L. Hazen and R. L. Silverstein. 2006. A CD36-dependent signaling cascade is necessary for macrophage foam cell formation. *Cell Metab.* **4**: 211-221.

103. Makinen, P. I., J. P. Lappalainen, S. E. Heinonen, P. Leppanen, M. T. Lahteenvuo, J. V. Aarnio, J. Heikkila, M. P. Turunen and S. Yla-Herttuala. 2010. Silencing of either SR-A or CD36 reduces atherosclerosis in hyperlipidaemic mice and reveals reciprocal upregulation of these receptors. *Cardiovasc. Res.* **88**: 530-538.

104. Manning-Tobin, J. J., K. J. Moore, T. A. Seimon, S. A. Bell, M. Sharuk, J. I. Alvarez-Leite, M. P. de Winther, I. Tabas and M. W. Freeman. 2009. Loss of SR-A and CD36 activity reduces atherosclerotic lesion complexity without abrogating foam cell formation in hyperlipidemic mice. *Arterioscler. Thromb. Vasc. Biol.* **29**: 19-26.

105. Chinetti, G., S. Lestavel, V. Bocher, A. T. Remaley, B. Neve, I. P. Torra, E. Teissier, A. Minnich, M. Jaye, M. Duverger, H. B. Bewer, J. C. Fruchart, V. Clavey and B. Staels. 2001. PPAR-α and PPAR-ψ activators induce cholesterol removal from human macrophage foam cells through stimulation of the ABCA1 pathway. *Nat. Med.* **7**: 53-58.

106. Funk, C. D. and T. Cyrus. 2001. 12/15-Lipoxygenase, oxidative modification of LDL and atherogenesis. *Trends Cardiovasc. Med.* **11**: 116-124.

107. Shashkin, P., B. Dragulev and K. Ley. 2005. Macrophage differentiation to foam cells. *Curr. Pharm. Des.* **11**: 3061-3072.

108. Ouimet, M. and Y. L. Marcel. 2012. Regulation of lipid droplet cholesterol efflux from macrophage foam cells. *Arterioscler. Thromb. Vasc. Biol.* **32**: 575-581.

109. Olofsson, S. O., P. Bostrom, L. Andersson, M. Rutberg, J. Perman and J. Boren. 2009. Lipid droplets as dynamic organelles connecting storage and efflux of lipids. *Biochim. Biophys. Acta* **1791**: 448-458.

110. Walther, T. C. and R. V. Farese, Jr. 2012. Lipid droplets and cellular lipid metabolism. *Annu. Rev. Biochem.* **81**: 687-714.

111. Weller, P. F., S. J. Ackerman, A. Nicholson-Weller and A. M. Dvorak. 1989. Cytoplasmic lipid bodies of human neutrophilic leukocytes. *Am. J. Pathol.* **135**: 947-959.

112. Segal, W. and H. Bloch. 1955. Biochemical differentiation of *Mycobacterium tuberculosis* grown *in vivo* and *in vitro*. *J. Bacteriol.* **72**: 132-141.

113. Cole, S. T., R. Brosch, J. Parkhill, T. Garnier, C. Churcher, D. Harris, S. V. Gordon, K. Eigleimer, S. Gas, C. E. Barry, F. Tekaia, K. Badcock, D. Basham, D. A. Brown, T. Chillingworth, R. Connor, R. Davies, K. Devlin, T. Feltwell, S. Gentles, N. Hamlin, S. Holroyd, T. Hornsby, K. Jagels, A. Krogh, J. McLean, S. Moule, L. Murphy, K. Oliver, J. Osborne, M. A. Qual, M.-A. Rajandream, J. Rogers, S. Rutter, K. Seeger, J. Skelton, S. Squares, J. E. Sulston, K. Taylor, S. Whitehead and B. G. Barrell. 1998. Deciphering the biology of *Mycobacterium tuberculosis* from the complete genome sequence. *Nature* **393**: 537-544.

114. Maxfield, F. R. and G. van Meer. 2010. Cholesterol, the central lipid of mammalian cells. *Curr. Opin. Cell Biol.* **22**: 422-429.

115. Pandey, A. K. and C. M. Sassetti. 2008. Mycobacterial persistence requires the utilization of host cholesterol. *Proc. Natl. Acad. Sci. U. S. A.* **105**: 4376-4380.

116. Brzostek, A., J. Pawelczyk, A. Rumijowska-Galewicz, B. Dziadek and J. Dziadek. 2009. *Mycobacterium tuberculosis* is able to accumulate and utilize cholesterol. *J. Bacteriol.* **191**: 6584-6591.

117. Thomas, S. T., B. C. VanderVen, D. R. Sherman, D. G. Russell and N. S. Sampson. 2011. Pathway profiling in *Mycobacterium tuberculosis*: elucidation of cholesterol-derived catabolite and enzymes that catalyze its metabolism. *J. Biol. Chem.* **286**: 43668-43678.

118. Wipperman, M. F., M. Yang, S. T. Thomas and N. S. Sampson. 2013. Shrinking the FadE proteome of *Mycobacterium tuberculosis*: Insights into cholesterol metabolism through identification of an $alpha_2beta_2$ heterotetrameric acyl coenzyme A dehydrogenase family. *J. Bacteriol.* **195**: 4331-4341.

119. Thomas, S. T. and N. S. Sampson. 2013. *Mycobacterium tuberculosis* utilizes a unique heterotetrameric structure for dehydrogenation of the cholesterol side chain. *Biochemistry* **52**: 2895-2904.

120. Van der Geize, R., K. Yam, T. Heuser, M. H. Wilbrink, H. Hara, M. C. Anderton, E. Sim, L. Dijkhuizen, J. E. Davies, W. W. Mohn and L. D. Eltis. 2007. A gene cluster encoding cholesterol catabolism in a soil actinomycete provides insight into *Mycobacterium tuberculosis* survival in macrophages. *Proc. Natl. Acad. Sci. U. S. A.* **104**: 1947-1952.

121. Yang, M., R. Lu, K. E. Guja, M. F. Wipperman, J. R. St Clair, A. C. Bonds, M. Garcia-Diaz and N. S. Sampson. 2015. Unraveling cholesterol catabolism in: ChsE4-ChsE5 alphabeta Acyl-CoA Dehydrogenase Initiates beta-Oxidation of 3-Oxo-cholest-4-en-26-oyl CoA. *ACS Infect. Dis.* **1**: 110-125.

122. Munoz-Elias, E. J., A. M. Upton, J. Cherian and J. D. McKinney. 2006. Role of the methylcitrate cycle in *Mycobacterium tuberculosis* metabolism, intracellular growth, and virulence. *Mol. Microbiol.* **60**: 1109-1122.

123. Yang, X., N. M. Nesbitt, E. Dubnau, I. Smith and N. S. Sampson. 2009. Cholesterol metabolism increases the metabolic pool of propionate in *Mycobacterium tuberculosis*. *Biochemistry* **48**: 3819-3821.

124. Garrett, R. H. and C. M. Grisham. 1995. *Biochemistry*, 2nd ed., Saunders College Publishing, Orlando, Florida. pp 1127.

125. Norris, P. C. and E. A. Dennis. 2014. A lipidomic perspective on inflammatory macrophage eicosanoid signaling. *Adv*. *Biol*. *Regul*. **54**: 99-110.

126. Maceyka, M. and S. Spiegel. 2014. Sphingolipid metabolites in inflammatory disease. *Nature* **510**: 58-67.

127. Chaurio, R. A., C. Janko, L. E. Munoz, B. Frey, M. Herrmann and U. S. Gaipl. 2009. Phospholipids: key players in apoptosis and immune regulation. *Molecules* **14**: 4892-4914.

128. Han, X. 2016. Lipidomics for studying metabolism. *Nat*. *Rev*. *Endocrinol*. **12**: 668-679.

129. Nagao, K. and T. Yanagita. 2008. Bioactive lipids in metabolic syndrome. *Prog*. *Lipid Res*. **47**: 127-146.

130. Hermansson, M., K. Hokynar and P. Somerharju. 2011. Mechanisms of glycerophospholipid homeostasis in mammalian cells. *Prog*. *Lipid Res*. **50**: 240-257.

131. Berg, J. M., J. L. Tymoczko and L. Stryer. 2002. *Biochemistry*, 5th ed., W H Freeman, New York. pp 1100.

132. Rysman, E., K. Brusselmans, K. Scheys, L. Timmermans, R. Derua, S. Munck, P. P. Van Veldhoven, D. Waltregny, V. W. Daniels, J. Machiels, F. Vanderhoydonc, K. Smans, E. Waelkens, G. Verhoeven and J. V. Swinnen. 2010. *De novo* lipogenesis protects cancer cells from free radicals and chemotherapeutics by promoting membrane lipid saturation. *Cancer Res*. **70**: 8117-8126.

133. Van Meer, G. and A. I. P. M. de Kroon. 2011. Lipid map of the mammalian cells. *J*. *Cell Sci*. **124**: 5-8.

134. Hazarosova, R., A. Momchilova, K. Koumanov, D. Petkova and G. Staneva. 2015. Role of Aminophospholipids in the Formation of Lipid Rafts in Model Membranes. *J Fluoresc* **25**: 1037-1043.

135. van Meer, G., D. R. Voelker and G. W. Feigenson. 2008. Membrane lipids: where they are and how they behave. *Nat*. *Rev*. *Mol*. *Cell Biol*. **9**: 112-124.

136. Dowhan, W. 1997. Molecular basis for membrane phospholipid diversity: why are there so many lipids? *Annu*. *Rev*. *Biochem*. **66**: 199-234.

137. Bishop, W. B. 1988. Assembly of phospholipids into cellular membranes: biosynthesis, transmembrane movement and intracellular translocation. *Annu*. *Rev*. *Cell Biol*. **4**: 579-610.

138. Holthuis, J. C. and A. K. Menon. 2014. Lipid landscapes and pipelines in membrane homeostasis. *Nature* **510**: 48-57.

139. Cui, Z., J. E. Vance, M. H. Chen, D. R. Voelker and D. E. Vance. 1993. Cloning and expression of a novel phosphatidylethanolamine *N*-methyltransferase. *J*. *Biol*. *Chem*. **268**: 16655-16663.

140. Li, Z., L. B. Agellon, T. M. Allen, M. Umeda, L. Jewell, A. Mason and D. E. Vance. 2006. The ratio of phosphatidylcholine to phosphatidylethanolamine influences membrane integrity and steatohepatitis. *Cell Metab*. **3**: 321-331.

141. Jacobs, R. L., Y. Zhao, D. P. Koonen, T. Sletten, B. Su, S. Lingrell, G. Cao, D. A. Peake, M. S. Kuo, S. D. Proctor, B. P. Kennedy, J. R. Dyck and D. E. Vance. 2010. Impaired *de novo* choline synthesis explains why phosphatidylethanolamine *N*-methyltransferase-deficient mice are protected from diet-induced obesity. *J*. *Biol*. *Chem*. **285**: 22403-22413.

142. Vance, J. E. and G. Tasseva. 2013. Formation and function of phosphatidylserine and phosphatidylethanolamine in mammalian cells. *Biochim*. *Biophys*. *Acta* **1831**: 543-554.

143. Vance, J. E. 2008. Phosphatidylserine and phosphatidylethanolamine in mammalian cells: two metabolically related aminophospholipids. *J. Lipid Res.* **49**: 1377-1387.

144. Nuwayhid, S. J., M. Vega, P. D. Walden and M. E. Monaco. 2006. Regulation of *de novo* phosphatidylinositol synthesis. *J. Lipid Res.* **47**: 1449-1456.

145. Shindou, H., D. Hishikawa, T. Harayama, K. Yuki and T. Shimizu. 2009. Recent progress on acyl CoA: lysophospholipid acyltransferase research. *J. Lipid Res.* **50 Suppl**: S46-51.

146. Hishikawa, D., T. Hashidate, T. Shimizu and H. Shindou. 2014. Diversity and function of membrane glycerophospholipids generated by the remodeling pathway in mammalian cells. *J. Lipid Res.* **55**: 799-807.

147. Darios, F., E. Connell and B. Davletov. 2007. Phospholipases and fatty acid signalling in exocytosis. *J. Physiol.* **585**: 699-704.

148. Farooqui, A. A. and L. A. Horrocks. 2005. Signaling and interplay mediated by phospholipases A2, C, and D in LA-N-1 cell nuclei. *Reprod. Nutr. Dev.* **45**: 613-631.

149. Aloulou, A., Y. B. Ali, S. Bezzine, Y. Gargouri and M. H. Gelb. 2012. Phospholipases: An Overview. In *Lipases and Phospholipases: Methods and Protocols* (Sandoval, G. ed.), 1 Ed., Humana Press, New York. pp 63-85.

150. Cazzolli, R., A. N. Shemon, M. Q. Fang and W. E. Hughes. 2006. Phospholipid signalling through phospholipase D and phosphatidic acid. *IUBMB Life* **58**: 457-461.

151. Foster, D. A., D. Salloum, D. Menon and M. A. Frias. 2014. Phospholipase D and the maintenance of phosphatidic acid levels for regulation of mammalian target of rapamycin (mTOR). *J. Biol. Chem.* **289**: 22583-22588.

152. Shindou, H. and T. Shimizu. 2009. Acyl-CoA:lysophospholipid acyltransferases. *J. Biol. Chem.* **284**: 1-5.

153. Oz-Arslan, D., W. Ruscher, D. Myrtek, M. Ziemer, Y. Jin, B. B. Damaj, S. Sorichter, M. Idzko, J. Norgauer and A. A. Maghazachi. 2006. IL-6 and IL-8 release is mediated via multiple signaling pathways after stimulating dendritic cells with lysophospholipids. *J. Leukoc. Biol.* **80**: 287-297.

154. Birgbauer, E. and J. Chun. 2006. New developments in the biological functions of lysophospholipids. *Cell. Mol. Life Sci.* **63**: 2695-2701.

155. Grzelczyk, A. and E. Gendaszewska-Darmach. 2013. Novel bioactive glycerol-based lysophospholipids: new data -- new insight into their function. *Biochimie* **95**: 667-679.

156. D'Arrigo, P. and S. Servi. 2010. Synthesis of lysophospholipids. *Molecules* **15**: 1354-1377.

157. Huang, M.-C., M. Graeler, G. Shankar, J. Spencer and E. J. Goetzl. 2002. Lysophospholipid mediators of immunity and neoplasia. *Biochim. Biophys. Acta* **1582**: 161-167.

158. Qin, X., C. Qiu and L. Zhao. 2014. Lysophosphatidylcholine perpetuates macrophage polarization toward classically activated phenotype in inflammation. *Cell. Immunol.* **289**: 185-190.

159. Monet, M., D. Gkika, V. Lehen'kyi, A. Pourtier, F. Vanden Abeele, G. Bidaux, V. Juvin, F. Rassendren, S. Humez and N. Prevarsakaya. 2009. Lysophospholipids stimulate prostate cancer cell migration via TRPV2 channel activation. *Biochim. Biophys. Acta* **1793**: 528-539.

160. Sutphen, R., Y. Xu, G. D. Wilbanks, J. Fiorica, E. C. Grendys, J. P. LaPolla, H. Arango, M. S. Hoffman, M. Martino, K. Wakeley, D. Griffen, R. W. Blanco, A. B. Cantor, Y.-j. Xiao and J. P. Krischner. 2004. Lysophospholipids are potential biomarkers of ovarian cancer. *Cancer Epidemiol. Biomarkers Prev.* **13**: 1185-1191.

161. Nishikawa, M., M. Kurano, H. Ikeda, J. Aoki and Y. Yatomi. 2015. Lysophosphatidylserine has bilateral effects on macrophages in the pathogenesis of atherosclerosis. *J. Atheroscler. Thromb.* **22**: 518-526.

162. Makide, K., A. Uwamizu, Y. Shinjo, J. Ishiguro, M. Okutani, A. Inoue and J. Aoki. 2014. Novel lysophosphoplipid receptors: their structure and function. *J. Lipid Res.* **55**: 1986-1995.

163. Moessinger, C., L. Kuerschner, J. Spandl, A. Shevchenko and C. Thiele. 2011. Human lysophosphatidylcholine acyltransferases 1 and 2 are located in lipid droplets where they catalyze the formation of phosphatidylcholine. *J. Biol. Chem.* **286**: 21330-21339.

164. Chen, X., B. A. Hyatt, M. L. Mucenski, R. J. Mason and J. M. Shannon. 2006. Identification and cahracterisation of lysophosphatidylcholine acyltransferase in alveolar type II cells. *Proc. Natl. Acad. Sci. U. S. A.* **130**: 11724-11729.

165. Fox, L. M., D. G. Cox, J. L. Lockridge, X. Wang, X. Chen, L. Scharf, D. L. Trott, R. M. Ndonye, N. Veerapen, G. S. Besra, A. R. Howell, M. E. Cook, E. J. Adams, W. H. Hildebrand and J. E. Gumperz. 2009. Recognition of lyso-phospholipids by human natural killer T lymphocytes. *PLoS Biol.* **7**: e1000228.

166. Hasegawa, H., J. Lei, T. Matsumoto, S. Onishi, K. Suemori and M. Yasukawa. 2011. Lysophosphatidylcholine enhances the suppressive function of human naturally occurring regulatory T cells through TGF-beta production. *Biochem. Biophys. Res. Commun.* **415**: 526-531.

167. Nishi, E., N. Kume, Y. Ueno, H. Ochi, H. Moriwaki and T. Kita. 1998. Lysophosphatidylcholine enhances cytokine-induced interferon gamma expression in human T lymphocytes. *Circ. Res.* **83**: 508-515.

168. Schilling, T. and C. Eder. 2010. Importance of lipid rafts for lysophosphatidylcholine-induced caspase-1 activation and reactive oxygen species generation. *Cell. Immunol.* **265**: 87-90.

169. Tan, Y., P. Yin, L. Tang, W. Xing, Q. Huang, D. Cao, X. Zhao, W. Wang, X. Lu, Z. Xu, H. Wang and G. Xu. 2012. Metabolomics study of stepwise hepatocarcinogenesis from the model rats to patients: potential biomarkers effective for small hepatocellular carcinoma diagnosis. *Mol. Cell. Proteomics* **11**: M111 010694.

170. Park, K. S., H. Y. Lee, S. Y. Lee, M. K. Kim, S. D. Kim, J. M. Kim, J. Yun, D. S. Im and Y. S. Bae. 2007. Lysophosphatidylethanolamine stimulates chemotactic migration and cellular invasion in SK-OV3 human ovarian cancer cells: involvement of pertussis toxin-sensitive G-protein coupled receptor. *FEBS Lett.* **581**: 4411-4416.

171. Hung, N. D., M. R. Kim and D. E. Sok. 2011. 2-Polyunsaturated acyl lysophosphatidylethanolamine attenuates inflammatory response in zymosan A-induced peritonitis in mice. *Lipids* **46**: 893-906.

172. Bartz, R., W. H. Li, B. Venables, J. K. Zehmer, M. R. Roth, R. Welti, R. G. Anderson, P. Liu and K. D. Chapman. 2007. Lipidomics reveals that adiposomes store ether lipids and mediate phospholipid traffic. *J. Lipid Res.* **48**: 837-847.

173. Tauchi-Sato, K., S. Ozeki, T. Houjou, R. Taguchi and T. Fujimoto. 2002. The surface of lipid droplets is a phospholipid monolayer with a unique fatty acid composition. *J. Biol. Chem.* **277**: 44507-44512.

174. Merrill, A. H., Jr., M. C. Sullards, J. C. Allegood, S. Kelly and E. Wang. 2005. Sphingolipidomics: high-throughput, structure-specific, and quantitative analysis of sphingolipids by liquid chromatography tandem mass spectrometry. *Methods* **36**: 207-224.

175. Haynes, C. A., J. C. Allegood, H. Park and M. C. Sullards. 2009. Sphingolipidomics: methods for the comprehensive analysis of sphingolipids. *J. Chromatogr. B Analyt. Technol. Biomed. Life Sci.* **877**: 2696-2708.

176. Sullards, M. C., Y. Liu, Y. Chen and A. H. Merrill, Jr. 2011. Analysis of mammalian sphingolipids by liquid chromatography tandem mass spectrometry (LC-MS/MS) and tissue imaging mass spectrometry (TIMS). *Biochim. Biophys. Acta* **1811**: 838-853.

177. Uchida, Y. 2014. Ceramide signaling in mammalian epidermis. *Biochim. Biophys. Acta* **1841**: 453-462.

178. Hannun, Y. A. and L. M. Obeid. 2008. Principles of bioactive lipid signalling: lessons from sphingolipids. *Nat. Rev. Mol. Cell Biol.* **9**: 139-150.

179. Futerman, A. H. and H. Riezman. 2005. The ins and outs of sphingolipid synthesis. *Trends Cell Biol.* **15**: 312-318.

180. Morad, S. A. and M. C. Cabot. 2013. Ceramide-orchestrated signalling in cancer cells. *Nat. Rev. Cancer* **13**: 51-65.

181. Merrill, A. H., Jr. 2002. *De novo* sphingolipid biosynthesis: a necessary, but dangerous, pathway. *J. Biol. Chem.* **277**: 25843-25846.

182. Wegner, M. S., S. Schiffmann, M. J. Parnham, G. Geisslinger and S. Grosch. 2016. The enigma of ceramide synthase regulation in mammalian cells. *Prog. Lipid Res.* **63**: 93-119.

183. Gillard, B. K., R. G. Clement and D. M. Marcus. 1998. Variations among cell lines in the synthesis of sphingolipids in *de novo* and recycling pathways. *Glycobiology* **8**: 885-890.

184. Spiegel, S. and S. Milstien. 2003. Sphingosine-1-phosphate: an enigmatic signalling lipid. *Nat. Rev. Mol. Cell Biol.* **4**: 397-407.

185. Mendelson, K., T. Evans and T. Hla. 2014. Sphingosine 1-phosphate signalling. *Development* **141**: 5-9.

186. Levy, M. and A. H. Futerman. 2010. Mammalian ceramide synthases. *IUBMB Life* **62**: 347-356.

187. Stiban, J., R. Tidhar and A. H. Futerman. 2010. Ceramide Synthases: Roles in Cell Physiology and Signaling. In *Sphingolipids as signaling and regulatory molecules* (Chalfant, C. E.andDel Poeta, M. eds.), Springer-Verlag, New York. pp 60-71.

188. Merrill, A. H., Jr., T. H. Stokes, A. Momin, H. Park, B. J. Portz, S. Kelly, E. Wang, M. C. Sullards and M. D. Wang. 2009. Sphingolipidomics: a valuable tool for understanding the roles of sphingolipids in biology and disease. *J. Lipid Res.* **50 Suppl**: S97-102.

189. Krahmer, N., Y. Guo, R. V. Farese, Jr. and T. C. Walther. 2009. SnapShot: Lipid Droplets. *Cell* **139**: DOI 10.1016/j.cell.2009.1011.1023.

190. Funk, C. D. 2001. Prostaglandins and leukotrienes: advances in eicosanoid biology. *Science* **294**: 1871-1875.

191. Folco, G. and R. C. Murphy. 2006. Eicosanoid transcellular biosynthesis: from cell-cell interactions to in vivo tissue responses. *Pharmacol. Rev.* **58**: 375-388.

192. Harizi, H., J. B. Corcuff and N. Gualde. 2008. Arachidonic-acid-derived eicosanoids: roles in biology and immunopathology. *Trends Mol. Med.* **14**: 461-469.

193. Spector, A. A. and A. W. Norris. 2007. Action of epoxyeicosatrienoic acids on cellular function. *Am. J. Physiol. Cell Physiol.* **292**: C996-C1012.

194. van Meer, G. 2005. Cellular lipidomics. *EMBO J.* **24**: 3159-3165.

195. Ekroos, K. 2012. Lipidomics perspective: From molecular lipidomics to validated clinical diagnostics. In *Lipidomics*, First Ed., Wiley VCH, Weinheim, Germany. pp 1-19.

196. Wenk, M. R. 2005. The emerging field of lipidomics. *Nat. Rev. Drug Discov.* **4**: 594-610.

197. Ivanova, P. T., S. B. Milne, D. S. Myers and H. A. Brown. 2009. Lipidomics: a mass spectrometry based systems level analysis of cellular lipids. *Curr. Opin. Chem. Biol.* **13**: 526-531.

198. Milne, S., P. Ivanova, J. Forrester and H. Alex Brown. 2006. Lipidomics: an analysis of cellular lipids by ESI-MS. *Methods* **39**: 92-103.

199. Ho, C. S., M. H. M. Chan, R. C. K. Cheung, L. K. Law, L. C. W. Lit, K. F. Ng, M. W. N. Suen and H. L. Tai. 2003. Electrospray ionisation mass spectrometry: Principles and clinical applications. *Clin. Biochem. Rev.* **24**: 3-12.

200. Han, X. and R. W. Gross. 2003. Global analyses of cellular lipidomes directly from crude extracts of biological samples by ESI mass spectrometry: a bridge to lipidomics. *J. Lipid Res.* **44**: 1071-1079.

201. Layre, E. and D. B. Moody. 2013. Lipidomic profiling of model organisms and the world's major pathogens. *Biochimie* **95**: 109-115.

202. Brugger, B., G. Erben, R. Sandhoff, F. T. Wieland and W. D. Lehmann. 1997. Quantitative analysis of biological membrane lipids at the low picomole level by nano-electrospray inoization tandem mass spectrometry. *Proc. Natl. Acad. Sci. U. S. A.* **94**: 2339-2344.

203. Draper, J., A. J. Lloyd, R. Goodacre and M. Beckmann. 2012. Flow infusion electrospray ionisation mass spectrometry for high throughput, non-targeted metabolite fingerprinting: a review. *Metabolomics* **9**: 4-29.

204. Aderem, A. A. and D. M. Underhill. 1999. Mechanisms of phagocytosis in macrophages. *Annu. Rev. Immunol.* **17**: 593-623.

205. Sturgill-Koszycki, S., U. E. Schaible and D. G. Russell. 1996. *Mycobacterium*-containing phagosomes are accessible to early endosomes and reflect a transitional state in normal phagosome biogenesis. *EMBO J.* **15**: 6960-6968.

206. Wagner, D., J. Maser, B. Lai, Z. Cai, C. E. Barry, K. Honer zu Bentrup, D. G. Russell and L. E. Bermudez. 2005. Elemental analysis of *Mycobacterium avium*-, *Mycobacterium tuberculosis*-, and *Mycobacterium smegmatis*-containing phagosomes indicates pathogen-induced microenvironments within the host cell's endosomal system. *J. Immunol.* **174**: 1491-1500.

207. Beatty, W. L., E. R. Rhoades, H.-J. Ullrich, J. Chatterjee, J. E. Heuser and D. G. Russell. 2000. Trafficking and release of mycobacterial lipids from infected macrophages. *Traffic* **1**: 235-247.

208. Engelman, J. A., J. Luo and L. C. Cantley. 2006. The evolution of phosphatidylinositol 3-kinases as regulators of growth and metabolism. *Nat. Rev. Genet.* **7**: 606-619.

209. Engelman, J. A. 2009. Targeting PI3K signalling in cancer: opportunities, challenges and limitations. *Nat. Rev. Cancer* **9**: 550-562.

210. Downes, C. P., A. Gray and J. M. Lucocq. 2005. Probing phosphoinositide functions in signaling and membrane trafficking. *Trends Cell Biol.* **15**: 259-268.

211. Di Paolo, G. and P. De Camilli. 2006. Phosphoinositides in cell regulation and membrane dynamics. *Nature* **443**: 651-657.

212. Fratti, R. A., J. M. Backer, J. Gruenberg, S. Corvera and V. Deretic. 2001. Role of phosphatidylinositol 3-kinase and Rab5 effectors in phagosomal biogenesis and mycobacterial phagosome maturation arrest. *J. Cell Biol.* **154**: 631-644.

213. Malik, Z. A., G. M. Denning and D. J. Kusner. 2000. Inhibition of Ca^{2+} signaling by *Mycobacterium tuberculosis* is associated with reduced phagosome-lysosome fusion and increased survival within human macrophages. *J. Exp. Med.* **191**: 287-302.

214. Kiss, L., Y. Roder, J. Bier, N. Weissmann, W. Seeger and F. Grimminger. 2008. Direct eicosanoid profiling of the hypoxic lung by comprehensive analysis via capillary liquid chromatography with dual online photodiode-array and tandem mass-spectrometric detection. *Anal. Bioanal. Chem.* **390**: 697-714.

215. Hong, S., T. F. Porter, Y. Lu, S. F. Oh, P. S. Pillai and C. N. Serhan. 2008. Resolvin E1 metabolome in local inactivation during inflammation-resolution. *J. Immunol.* **180**: 3512-3519.

216. Quehenberger, O., A. Armando, D. Dumlao, D. L. Stephens and E. A. Dennis. 2008. Lipidomics analysis of essential fatty acids in macrophages. *Prostaglandins Leukot. Essent. Fatty Acids* **79**: 123-129.

217. Dennis, E. A., R. A. Deems, R. Harkewicz, O. Quehenberger, H. A. Brown, S. B. Milne, D. S. Myers, C. K. Glass, G. Hardiman, D. Reichart, A. H. Merrill, Jr., M. C. Sullards, E. Wang, R. C. Murphy, C. R. Raetz, T. A. Garrett, Z. Guan, A. C. Ryan, D. W. Russell, J. G. McDonald, B. M. Thompson, W. A. Shaw, M. Sud, Y. Zhao, S. Gupta, M. R. Maurya, E. Fahy and S. Subramaniam. 2010. A mouse macrophage lipidome. *J. Biol. Chem.* **285**: 39976-39985.

218. Balgoma, D., A. M. Astudillo, G. Perez-Chacon, O. Montero, M. A. Balboa and J. Balsinde. 2010. Markers of monocyte activation revealed by lipidomic profiling of arachidonic acid-containing phospholipids. *J. Immunol.* **184**: 3857-3865.

219. Norris, P. C., D. Reichart, D. S. Dumlao, C. K. Glass and E. A. Dennis. 2011. Specificity of eicosanoid production depends on the TLR-4-stimulated macrophage phenotype. *J. Leukoc. Biol.* **90**: 563-574.

220. Dalli, J. and C. N. Serhan. 2012. Specific lipid mediator signatures of human phagocytes: microparticles stimulate macrophage efferocytosis and pro-resolving mediators. *Blood* **120**: e60-e72.

221. Dinasarapu, A. R., S. Gupta, M. Ram Maurya, E. Fahy, J. Min, M. Sud, M. J. Gersten, C. K. Glass and S. Subramaniam. 2013. A combined omics study on activated macrophages--enhanced role of STATs in apoptosis, immunity and lipid metabolism. *Bioinformatics* **29**: 2735-2743.

222. Rhee, S. H. 2014. Lipopolysaccharide: basic biochemistry, intracellular signaling, and physiological impacts in the gut. *Intest Res* **12**: 90-95.

223. Buczynski, M. W., D. S. Dumlao and E. A. Dennis. 2009. Thematic Review Series: Proteomics. An integrated omics analysis of eicosanoid biology. *J. Lipid Res.* **50**: 1015-1038.

224. Paton, C. M. and J. M. Ntambi. 2009. Biochemical and physiologial function of stearoyl-CoA desaturase. *Am. J. Physiol. Endocrinol. Metab.* **297**: E28-E37.

225. Ntambi, J. M. 1999. Regulation of stearoyl-CoA desaturase by polyunsaturated fatty acids and cholesterol. *J. Lipid Res.* **40**: 1549-1558.

226. Liu, X., M. Miyazaki, M. T. Flowers, H. Sampath, M. Zhao, K. Chu, C. M. Paton, D. S. Joo and J. M. Ntambi. 2010. Loss of Stearoyl-CoA desaturase-1 attenuates adipocyte inflammation: effects of adipocyte-derived oleate. *Arterioscler. Thromb. Vasc. Biol.* **30**: 31-38.

227. Liu, S. Y., R. Aliyari, K. Chikere, G. Li, M. D. Marsden, J. K. Smith, O. Pernet, H. Guo, R. Nusbaum, J. A. Zack, A. N. Freiberg, L. Su, B. Lee and G. Cheng. 2013. Interferon-inducible cholesterol-25-hydroxylase broadly inhibits viral entry by production of 25-hydroxycholesterol. *Immunity* **38**: 92-105.

228. Istvan, E. S. and J. Deisenhofer. 2001. Structural mechanism for statin inhibition of HMG-CoA reductase. *Science* **292**: 1160-1164.

229. Bruun, J. M., A. Roeske-Nielsen, B. Richelsen, P. Fredman and K. Buschard. 2007. Sulfatide increases adiponectin and decreases TNF-alpha, IL-6, and IL-8 in human adipose tissue in vitro. *Mol. Cell. Endocrinol.* **263**: 142-148.

230. Dennis, E. A. 2000. Phospholipase A2 in eicosanoid generation. *Am. J. Respir. Crit. Care Med.* **161**: S32-S35.

231. Laurencikiene, J. and M. Ryden. 2012. Liver X receptors and fat cell metabolism. *Int. J. Obes. (Lond.)* **36**: 1494-1502.

232. van der Meer-Janssen, Y. P., J. van Galen, J. J. Batenburg and J. B. Helms. 2010. Lipids in host-pathogen interactions: pathogens exploit the complexity of the host cell lipidome. *Prog*. *Lipid Res*. **49**: 1-26.

233. Divangahi, M., D. Desjardins, C. Nunes-Alves, H. G. Remold and S. M. Behar. 2010. Eicosanoid pathways regulate adaptive immunity to *Mycobacterium tuberculosis*. *Nat*. *Immunol*. **11**: 751-758.

CHAPTER II |

Mycolates of *Mycobacterium tuberculosis* modulate the flow of cholesterol for bacillary proliferation in murine macrophages

---

Ilke Vermeulen[1,2], Mark Baird[3], Juma Al-Dulayymi[3], Muriel Smet[1], Jan Verschoor[2], and Johan Grooten[1]

[1]Laboratory of Molecular Immunology, Department of Biomedical Molecular Biology, Ghent University, Technologiepark 927, Ghent Zwijnaarde 9052, Belgium

[2]Department of Biochemistry, University of Pretoria, Pretoria 0002, South Africa

[3]School of Chemistry, Bangor University, Bangor, Gwynedd, Wales, LL57 2UW, UK

Manuscript accepted for publication in the *Journal of Lipid Research* (IF = 4.56).

First published online on 13 February 2017 (doi: 10.1194/jlr.M073171) - *In Press*.

Author contributions: IV conducted the experimental work, analysed the results, compiled the figures and wrote the complete first draft of the manuscript. JG and JV conceptualised the research. MB oversaw the MA synthesis and JAD provided the synthetic MAs. MS provided constructive critiques.

Mycolates of *Mycobacterium tuberculosis* modulate the flow of cholesterol for bacillary proliferation in murine macrophages

Ilke Vermeulen,*,† Mark Baird,§ Juma Al-Dulayymi,§ Muriel Smet,* Jan Verschoor,† and Johan Grooten[1,*]

Laboratory of Molecular Immunology,* Department of Biomedical Molecular Biology, Ghent University, Ghent Zwijnaarde 9052, Belgium; Department of Biochemistry,† University of Pretoria, Pretoria 0002, South Africa; and School of Chemistry,§ Bangor University, Bangor LL57 2UW, United Kingdom

Abstract The differentiation of macrophages into lipid-filled foam cells is a hallmark of the lung granuloma that forms in patients with active tuberculosis (TB). Mycolic acids (MAs), the abundant lipid virulence factors in the cell wall of *Mycobacterium tuberculosis* (Mtb), can induce this foam phenotype possibly as a way to perturb host cell lipid homeostasis to support the infection. It is not exactly clear how MAs allow differentiation of foam cells during Mtb infection. Here we investigated how chemically synthetic MAs, each with a defined stereochemistry similar to natural Mtb-associated mycolates, influence cell foamy phenotype and mycobacterial proliferation in murine host macrophages. Using light and laser-scanning-confocal microscopy, we assessed the influence of MA structure first on the induction of granuloma cell types, second on intracellular cholesterol accumulation, and finally on mycobacterial growth. While methoxy-MAs (mMAs) effected multi-vacuolar giant cell formation, keto-MAs (kMAs) induced abundant intracellular lipid droplets that were packed with esterified cholesterol. Macrophages from mice treated with kMA were permissive to mycobacterial growth, whereas cells from mMA treatment were not. This suggests a separate yet key involvement of oxygenated MAs in manipulating host cell lipid homeostasis to establish the state of TB.—Vermeulen, I., M. Baird, J. Al-Dulayymi, M. Smet, J. Verschoor, and J. Grooten. **Mycolates of *Mycobacterium tuberculosis* modulate the flow of cholesterol for bacillary proliferation in murine macrophages. *J. Lipid Res.* 2017.** 58: ■■■–■■■.

Supplementary key words confocal microscopy • foam cell • infection • lipid droplets • liver X receptor • mycolic acid • tuberculosis

Mycobacterium tuberculosis (Mtb), the etiological agent of tuberculosis (TB), infects approximately two to three billion people globally (1). Though only a minority of infected individuals (<15%) will develop pulmonary disease during their lifetime, most remain prolonged asymptomatic carriers that may develop active disease later on (1). In this instance, bacilli are not entirely cleared, but remain in a state of dormancy inside the host. Throughout this period, Mtb resides inside lung granulomas, the main histopathology of TB (2). The granuloma milieu is characterized by a multifaceted host immune response of containment and destruction, yet Mtb bacilli are able to counteract and evade host defenses (3–5). During active TB, granulomas are characterized by large cell aggregates of lymphocytes, neutrophils, dendritic cells, and peripheral fibroblasts (6). The key effector cells of granuloma formation are macrophages, which can differentiate into vacuolar multinucleated giant cells (MGCs) or lipid-laden foam cells (7). Tuberculous bacilli may reside in foam cells or escape into the cell-free caseous center of the granuloma (2, 7). The biochemical signaling pathways involved in foamy phenotype regulation remain understudied. Growing evidence indicates that an advanced metabolic network stands at the center of the unique adaptation of Mtb in its host macrophage (8–10), regulating the manifestation of latent, chronic, or acute TB.

The Mtb cell envelope comprises intricate layers of peptidoglycan, arabinogalactan, glycolipids, mycolic acids (MAs; α-alkyl, β-hydroxy fatty acids) and lipoproteins, with MAs being the dominant constituent (11, 12). The structural and biochemical properties of MAs have been reviewed

This work was supported by National Research Foundation Grant 73931 and Fonds Wetenschappelijk Onderzoek Grant 73931. Additional support was provided by the TBVAC2020 consortium from the EU H2020 initiative to support the joint PhD research programme of I.V. at Ghent University and the University of Pretoria. The authors declare no conflict of interest regarding this work. [AQ1]

Manuscript received 11 November 2017 and in revised form 28 January 2017.

Published, JLR Papers in Press, February 13, 2017
DOI 10.1194/jlr.M073171

Abbreviations: αMA, α-mycolic acid; BCG, *Mycobacterium bovis* bacille Calmette-Guérin; BCG-dsRed, *Mycobacterium bovis* bacille Calmette-Guérin expressing the dsRed fluorescent protein; GLM, generalized linear model; kMA, keto-mycolic acid; LD, lipid droplet; Lipo, liposome carrier without synthetic mycolic acid; LXR, liver X receptor; MA, mycolic acid; MGC, multinucleated giant cell; mMA, methoxy-mycolic acid; MOI, multiplicity of infection; Mtb, *Mycobacterium tuberculosis*; PEC, peritoneal exudate cell; TB, tuberculosis; V+, vacuole-positive. [AQ2]

[1]To whom correspondence should be addressed.
e-mail: Johan.Grooten@irc.ugent.be

1. Introduction

Mycobacterium tuberculosis (Mtb), the aetiological agent of tuberculosis (TB), infects approximately 2-3 billion people globally[1]. Though only a minority of infected individuals (<15%) will develop pulmonary disease during their lifetime, most remain prolonged asymptomatic carriers that may develop active disease later on[1]. In this instance bacilli are not entirely cleared, but remain in a state of dormancy inside its host. Throughout this period, Mtb resides inside lung granulomas, the main histopathology of TB[2]. The granuloma milieu is characterised by a multifaceted host immune response of containment and destruction, yet Mtb bacilli are able to counteract and evade host defences[3-5]. During active TB, granulomas are characterised by large cell aggregates of lymphocytes, neutrophils, dendritic cells and peripheral fibroblasts[6]. Key effector cells of granuloma formation are macrophages, which can differentiate into vacuolar multinucleated giant cells (MGCs) or lipid-laden foam cells[7]. Tuberculous bacilli may reside in foam cells or escape into the cell-free caseous centre of the granuloma[2, 7]. The biochemical signalling pathways involved in foamy phenotype regulation remain understudied. Growing evidence indicates that an advanced metabolic network stands at the centre of the unique adaptation of Mtb in its host macrophage[8-10], regulating the manifestation of latent, chronic or acute TB.

The Mtb cell envelope comprises intricate layers of peptidoglycan, arabinogalactan, glycolipids, mycolic acids (MAs; α-alkyl, β-hydroxy fatty acids) and lipoproteins, with MAs being the dominant constituent[11, 12]. The structural and biochemical properties of MAs have been reviewed recently[13]. In short, these wax-like hydrophobic lipids comprise a mycolic motif with long non-functionalised alkyl chain and a meromycolate chain with up to two functional groups that can be either oxygenated (distal group) or unoxygenated (distal or proximal group)[13]. Three main Mtb MA classes exist: the most abundant unoxygenated

alpha-MA (αMA), the less abundant oxygenated methoxy- (mMA) and the least abundant keto-MA (kMA; Fig. 1)[14, 15]. Orientation of the proximal cyclopropane differs. αMA essentially exists in *cis*- configuration (though a small amount of *trans*- may be present), whereas mMA and kMA contain either *cis*- or *trans*-cyclopropanation with an adjoining methyl branch[11]. Whilst the level of αMA is fixed at ~53% and oxygenated MA at ~47%, the ratio between the two oxygenated MAs varies with methoxy at 32-40% and keto at 7-15%[16], depending on the growth stage of the bacilli[17-19]. Mtb envelope derived lipids potently influence host immunity[20-22], while host cell lipidomes are exploited by intracellular pathogens like Mtb to gain entry and replicate[23]. The work by Cole *et al*. on deciphering the Mtb genome identified two distinct sets of complex enzymatic machinery for successive biosynthesis of fatty acids, meromycolates and long carbon chain MAs[24]. A MA-rich cell wall that can be altered depending on physiological requirements is essential for Mtb virulence[17, 18]. We previously showed that *in vivo* MA treatment induced peritoneal and alveolar macrophages of the foam phenotype in mice[25, 26], similar to that in macrophages from the TB granuloma[27]. At the onset of TB infection, foam cells form that are characteristically enlarged and filled with multiple lipid droplets (LD) and vacuoles[28, 29]. Cholesterol is abundantly distributed across cell membranes and forms a major constituent of LDs[30, 31]. It also plays a unique role in Mtb virulence and pathogenesis. Mtb preferentially catabolises cholesterol as nutrient source whilst its acquisition, through a unique Mtb import system, is necessary to establish and maintain persistent infection[32, 33]. In macrophages, the genetic regulator of cellular cholesterol homeostasis is the liver X receptor (LXR)[34]. LXRs are transcription factors that act as cholesterol sensors and that maintain the balance of cholesterol uptake and export through regulation of expression of cholesterol-associated target genes[35].

2. Research aims

- To better understand the mechanisms responsible for the establishment of active TB related granulomas, we investigated how *in vivo* treatment of mice with chemically synthetic MAs, each with a defined stereochemistry representing the separate major classes of Mtb mycolates, influence cell differentiation and support of mycobacteria in peritoneal macrophages. We assessed the influence of MA structure first on the induction of foamy macrophages and MGCs identified by light and laser-scanning-confocal microscopy, second on cholesterol accumulation and finally on intracellular mycobacterial growth.

- To determine how foam cells brought about by non-tuberculous means compares to foam cells induced by the different mycolates, we also investigated cholesterol accumulation and mycobacterial growth of peritoneal macrophages from LXR-deficient mice.

Our results show that Mtb mycolates differentially steer host macrophages to either an enlarged vacuolar or a lipid-laden foamy phenotype. We report it is kMA that induces mainly cholesterol ester accumulation and intracellular LDs to sustain facilitation of Mycobacterium bovis bacille Calmette-Guérin (BCG) proliferation. mMA was found to induce vacuolation with no change in cholesterol ester levels and no improvement in the ability to sustain and facilitate mycobacterial growth. αMA treatment had a negligible effect on these parameters. In macrophages with a deficiency in LXR activity that is characterised by perturbed cholesterol transport or export, we recorded foam cells with abundant cholesterol ester-containing LDs that showed elevated BCG replication.

3. Materials and methods

3.1 Mycolic acids

Natural MA mixture was isolated and single synthetic MAs synthesised as previously described[16, 36-38]. The single MAs used for *in vivo* murine treatment in this study all contained *cis*-cyclopropanation, referring to the orientation of the proximal cyclopropane. MA treatments comprised *cis*-αMA, *cis*-mMA, *cis*-kMA consisting of a mixture of both epimers of the distal α-methyl-ketone group with S- and R-stereochemistry, and a natural isolated mixture of all three MA classes (each as a complex mixture of homologues) similar to the natural composition of MAs in the Mtb cell wall (MA mix) (Fig. 1), i.e. ~53% αMA, ~38% mMA and ~9% kMA.

3.2 Animals

Mice used were specific pathogen-free C57BL/6 WT females, aged eight to twelve weeks (Janvier Labs, France). C57BL/6Bom WT and LXR$\alpha^{-/-}\beta^{-/-}$ mice[39] were bred in the animal facility of Ghent University. Animals were housed individually in a temperature- and light-controlled facility and received mixed ration feed and water *ad libitum*. Experiments were preapproved by the Ghent University Ethical Committee for Animal Experimentation in accordance with current European laws regarding the welfare and humane use of animals.

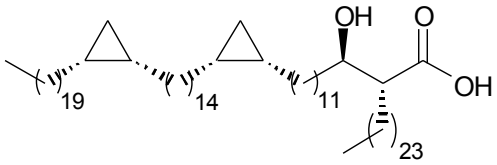

JR1080, **αMA** (19,14,11,23)

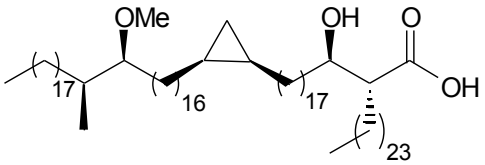

JR1046, **mMA** (17,16,17,23)

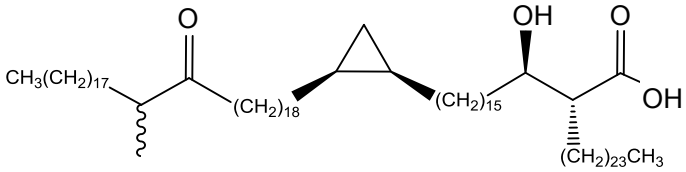

GK324, **kMA** (17,16,17,23)

Figure 1 | Mycolic acid structures. The biochemical structures of the synthetic MAs are given for examples of the alpha (αMA; JR1080), methoxy (mMA; JR1046) and keto (kMA; GK324) classes containing *cis*-cyclopropanation. Numbers in brackets represent carbon chain lengths and wiggly line indicates a mixture of stereoisomers at that position.

3.3 Experimental design

Mice were treated intraperitoneally (i.p.) with various control or MA solutions two days prior to harvesting of peritoneal exudate cells (PEC). Macrophages from PEC were cultured for three days and live cells fluorescently labelled for foam cell markers and examined by laser-scanning-confocal microscopy on each day (0 h, 24 h and 48 h time points; Supplementary Fig. S1). The mycobacterial model was similar to the foam cell model except that following overnight adherence, cells were infected for 6 h with *M. bovis* bacille Calmette-Guérin expressing the dsRed fluorescent protein (BCG-dsRed; a gift from Prof. Ben Appelmelk from the Department of Medical Microbiology and Infection Control at the Vrije Universiteit University Medical Centre in Amsterdam via the Unit of Medical Biotechnology at the Inflammation Research Center in Ghent). After three washes with endotoxin-free PBS (Lonza), the cells were stained with fluorescent markers for confocal microscopy (0 h) to assess macrophage morphotype or left for up to five days to measure mycobacterial growth (48 h and 96 h). The LXR model was similar to the mycobacterial model apart from mice were not treated with MAs prior to harvesting PEC.

3.4 Mycobacterial culture and infection

BCG-dsRed has been described previously[40]. The BCG strain Copenhagen (Danish 1331) was used here [41], which has no mMA, but similar quantities each of αMA and kMA[42]. Bacterial cultures were grown in Middlebrook 7H9 broth (Difco) supplemented with 0.2% glycerol, 0.05% Tween-80 and 10% Middlebrook AODC enrichment containing oleic acid, albumin, dextrose and catalase (Becton Dickinson). BCG expanded to an OD_{600nm} of 0.8-1.0 was used to infect cells *ex vivo* at a multiplicity of infection (MOI) of 1 bacterium per cell for 6 h. Following the 6 h infection, cells were washed three times with warm endotoxin-free PBS and cultured at 37°C and 5% CO_2.

3.5 Injectable solutions and macrophage isolation

Liposomes were used as carrier to deliver the highly hydrophobic MA compounds to target cells. As a first step, L-α-Phosphatidylcholine (PC, Sigma) powder was dissolved in chloroform at 100 mg/ml (10% w/v). PC and MA dissolved in chloroform were vortexed and heated before undergoing dehydration on a heat block (90°C) and the dried lipids recovered in endotoxin-free PBS. Solutions underwent a series of vortex and sonication steps at 65°C until homogenous milky consistency. Mice were immediately treated *in vivo* by i.p. injection (25 µg MA/100 µl/mouse). A liposome control (Lipo) was formulated as described for the MA solutions, but without the addition of any synthetic MA. Two days after *in vivo* treatment, mice were euthanized via cervical dislocation and PECs harvested by peritoneal lavage. Mouse abdomens were decontaminated with 70% ethanol and 10 ml ice cold endotoxin-free PBS injected i.p. Following a short abdominal massage, PECs were removed into sterile 15 ml tubes and kept on ice until further processing by centrifugation (1200 rpm, 4°C, 10 min) and red blood cell lysis (ACK lysing buffer, Lonza; 50% v/v). PECs were seeded in 250 µl culture medium ($5x10^5$ cells) in µ-Slide 8-well microscopy plates (Ibidi). Culture medium consisted of RPMI 1640 (Gibco) supplemented with LPS-free and heat-inactivated FCS (10%), sodium pyruvate (2 mM), non-essential amino acids (1%), penicillin/streptomycin antibiotics (0.2%), and β-mercaptoethanol (0.1%). Cultures were enriched for macrophages by overnight adherence. All cells were cultured at 37°C and 5% CO_2.

3.6 Light and laser-scanning-confocal microscopy

An aliquot of cell suspension equal to $5x10^4$ to $1x10^5$ cells was taken for cytospin analysis. The cytospin filter was primed with 100 µl PBS (300 rpm, 1 min) before addition of 200 µl cell suspension (300 rpm, 5 min). After an overnight drying step, cells were fixed in methanol

for 30 min at -20°C and dried for 2 h. Cells were stained with undiluted May-Grünwald for 5 min (granular stain), washed in PBS, and stained for 20 min in 20x diluted Giemsa (nuclear stain). Cells received a final wash with bi-distilled water and were left to dry overnight. At least 200 cells were counted per treatment with a standard light microscope.

Live cells were stained with fluorescent markers for confocal microscopy at the time points specified in culture medium without amines and serum at 37°C for 30 min. Nuclear DNA was stained with Hoechst (1 μM), cellular cytoplasm with CellTrackerRed or CellTrackerBlue (10 μM) and neutral LDs with Bodipy493/503 (8 μg/ml; Molecular Probes). Cells were washed three times in warm endotoxin-free PBS to remove unbound probe and fixed consecutively for 15 min in 2% then 4% paraformaldehyde. Macrophages were classified as enlarged vacuole-positive (V+) when their cell size was ≥24 μm and multiple large vacuoles were present. Fluorescently labelled cells were viewed on a Leica TCS SP5 AOBS inverted confocal microscope with a 63x HCX PL Apo 1.4 oil objective and stacked images taken at 0.42 μm slices with a spectral photomultipliers DFC320 colour camera (36-bit, 7 megapixels, non-confocal). Training and technical support was provided by the Bio Imaging Core facility of the Flemish Institute of Biotechnology (Ghent).

3.7 Quantification of intracellular cholesterol content

Macrophage intracellular cholesterol was quantified using the Calbiochem cholesterol/cholesteryl ester quantitation kit (Merck Millipore, Cat. No.428901). Cell pellets ($1x10^6$ cells) were freeze-thawed five times in liquid nitrogen, homogenised with pestle in 200 μl chloroform:isopropanol:NP40 (7:11:0.1, v/v/v) and centrifuged for 10 min at 14,000 rpm. The organic lower phase was transferred to a clean microcentrifuge tube and air-dried at 50°C. To remove any residual chloroform, samples were further vacuum-dried for 30 min at

45°C. The dried lipids were dissolved in 200 µl cholesterol reaction buffer at 40°C for two cycles of heating (10 min) and vortexing with a final vortex of 5 min. All extracted samples and standards were added to a volume of 50 µl in a black 96-well plate followed by 50 µl of reaction mix 1 (with cholesterol esterase) or 2 (without cholesterol esterase) for determination of total cholesterol and free cholesterol, respectively. The assay plate was incubated at 37°C for 60 min; then fluorometrically measured on a FLUOstar OMEGA microplate reader (~535/590 nm). Cholesterol standards were plotted against relative fluorescence units and the concentration of total, free and esterified cholesterol (free subtracted from total) calculated as µg/10^6 cells.

3.8 Statistical analyses

The number of mice used for experiments comprised a minimum of five mice per treatment. Data were obtained from at least three independent experiments or 500 cells from no less than five separate microscopy images. The distribution of all data was determined by a Shapiro-Wilk (*W*) normality test. Nonparametric Mann-Whitney *U* or Kruskal-Wallis one-way analysis of variance tests (*H*; with Dunn's ranked sum multiple comparisons) were used to assess the proportion of foam cells in PEC cytospins and cellular cholesterol content (dependent variables) for each treatment or cholesterol fraction (categorical variables). Generalised linear model analyses (GLM: Poisson distribution with sequential Sidak pairwise comparisons) were used to assess counts of the number of cellular vacuoles, LDs, and bacilli (dependent variables) for each treatment or MOI at specified time points (predictors). Image processing and quantification of cellular markers for confocal microscopy were conducted with Volocity 3D Image Analysis Software (PerkinElmer Inc.). All other statistical analyses were performed with IBM SPSS Statistics 23 (IBM, Chicago IL, USA) and GraphPad Prism

5 (GraphPad Software, Inc.). Results were presented as mean ± standard error of the mean (SEM) and were considered significant at $P \leq 0.05$.

4. Results

4.1 Mycolic acids of the methoxy oxygenation class promote the formation of multi-vacuolar foam cells

To assess the influence of MA structure on the induction of multi-vacuolar giant foam cells, mice were i.p. injected with 25 µg of various MAs (alpha, methoxy or keto) (Fig. 1) or control compounds (PBS or liposome carrier without synthetic MA). PECs were harvested two days after treatment. Macrophages were examined by cytospin analysis and laser-scanning-confocal microscopy. PEC from mice treated with PBS, liposome carrier without synthetic MA (Lipo) and αMA-containing liposomes contained <10% vacuolar foam cells (Fig. 2A-B). In contrast, PEC from mice treated with liposomes containing kMA or mMA showed ~15% and 27-30% vacuolar foam cells, respectively. GLM analysis showed a clear difference among the treatments in their ability to induce vacuoles (Supplementary Table S1). mMA clearly effected vacuole formation with significantly more enlarged vacuole-positive (V+) cells (25-35%) as compared to kMA (5-10%) and other treatments (<5%) (Fig. 2C-D). In addition, the proportion of enlarged V+ cells from the mMA cell population remained significantly elevated over time when kept in culture. At the 48 h time point, the macrophages from mMA treatment remained enlarged, while all other treatments resulted in macrophages returning to normal size (<5% enlarged V+ cells) (Fig. 2C). MGCs were seen mainly among the enlarged V+ cells induced by mMA (Fig. 2E).

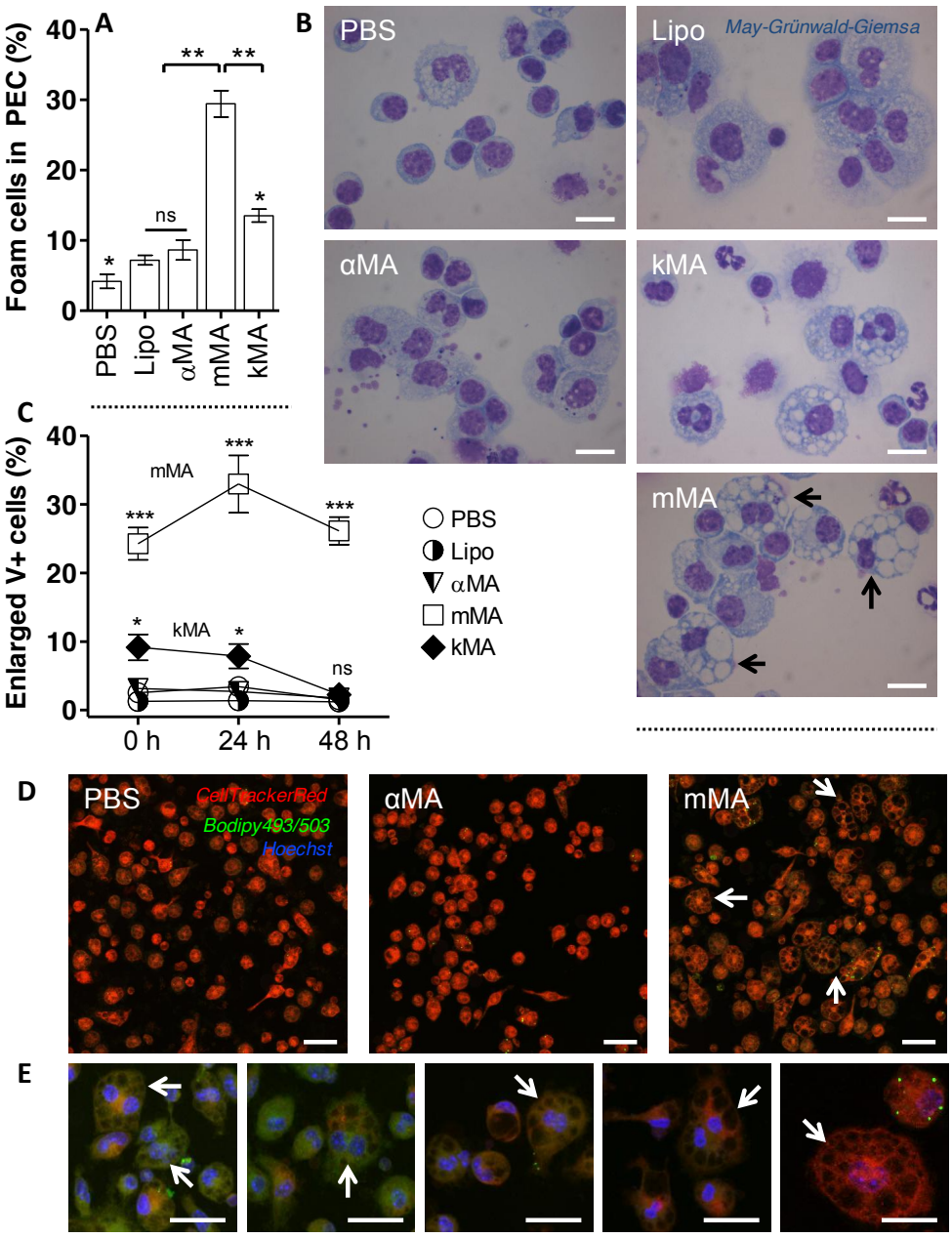

Figure 2 | Mycolic acids of the methoxy oxygenation class promote the formation of multi-vacuolar foam cells. The proportion of vacuole-rich macrophages was determined by light microscope images of May-Grünwald-Giemsa stained cells on cytospins and by laser-scanning-confocal microscopy (mean ± SEM). (A) Percentage of foam cells in PEC fraction from the control (PBS and Lipo), αMA, mMA and kMA treatments. (Shapiro-Wilk: $W = 0.801$, $^{**}P < 0.01$; Kruskal-Wallis: $H = 12.100$, $^{*}P < 0.05$, $df = 4$, $n = 3$ independent experiments; ns, not significant). (B) Light microscope images of cytospins showing vacuolar foam cells in PEC fraction. Images were taken at 100x oil magnification. Arrows indicate multinucleated giant cells (MGCs). Scale bar: 10 µm. (C) Induction of enlarged vacuole-positive (V+) cells is shown for control (PBS and Lipo) and the various MA-treated mouse peritoneal macrophages over time, as measured by laser-scanning-confocal microscopy (GLM: Wald Chi-Square = 753.924, $^{***}P < 0.001$, $df = 14$, $n = 5$ per time point; ns, not significant). (D-E) Laser scanning confocal microscopy images showing enlarged V+ cells for PBS, αMA and mMA treatments. Arrows indicate MGCs. Stacked images, 63x oil objective. Scale bar: 20 µm. (E) Zoomed images from the mMA treatment in D.

4.2 Mycolic acids of the keto oxygenation class induce foam cells rich in cholesterol-laden lipid droplets

A clear difference was observed among treatments in their ability to induce LD accumulation (Fig. 3; Supplementary Table S2). kMA significantly induced LDs, up to 3-fold higher in comparison to all other treatments (Fig. 3A). Clearly, kMA was the strongest inducer of intracellular lipids in peritoneal mouse macrophages at all time points assayed. In order to normalise for LDs involved in regular macrophage metabolic activity, the LD number in PBS-treated cells was selected as baseline value against which relative increases or decreases of LDs in other treatments were compared. From this relative analysis, kMA again emerged as the MA class that significantly and prominently induced an increment in LDs in the macrophages (Fig. 3B-C). To further substantiate and quantify the accumulation of LDs in kMA-treated macrophages, the levels of intracellular active cholesterol and stored cholesteryl ester was determined in peritoneal macrophages isolated two days after oxygenated mMA or kMA treatment (Supplementary Table S3). Macrophages from the kMA treatment contained substantial intracellular esterified cholesterol, which also accounted for 77% of the total cholesterol content (Fig. 3D). Thus, the ratio of esterified-to-free cholesterol was distinctly elevated in the LD inducing kMA treatment and not in vacuole inducing mMA treated cells (Fig. 3D-E).

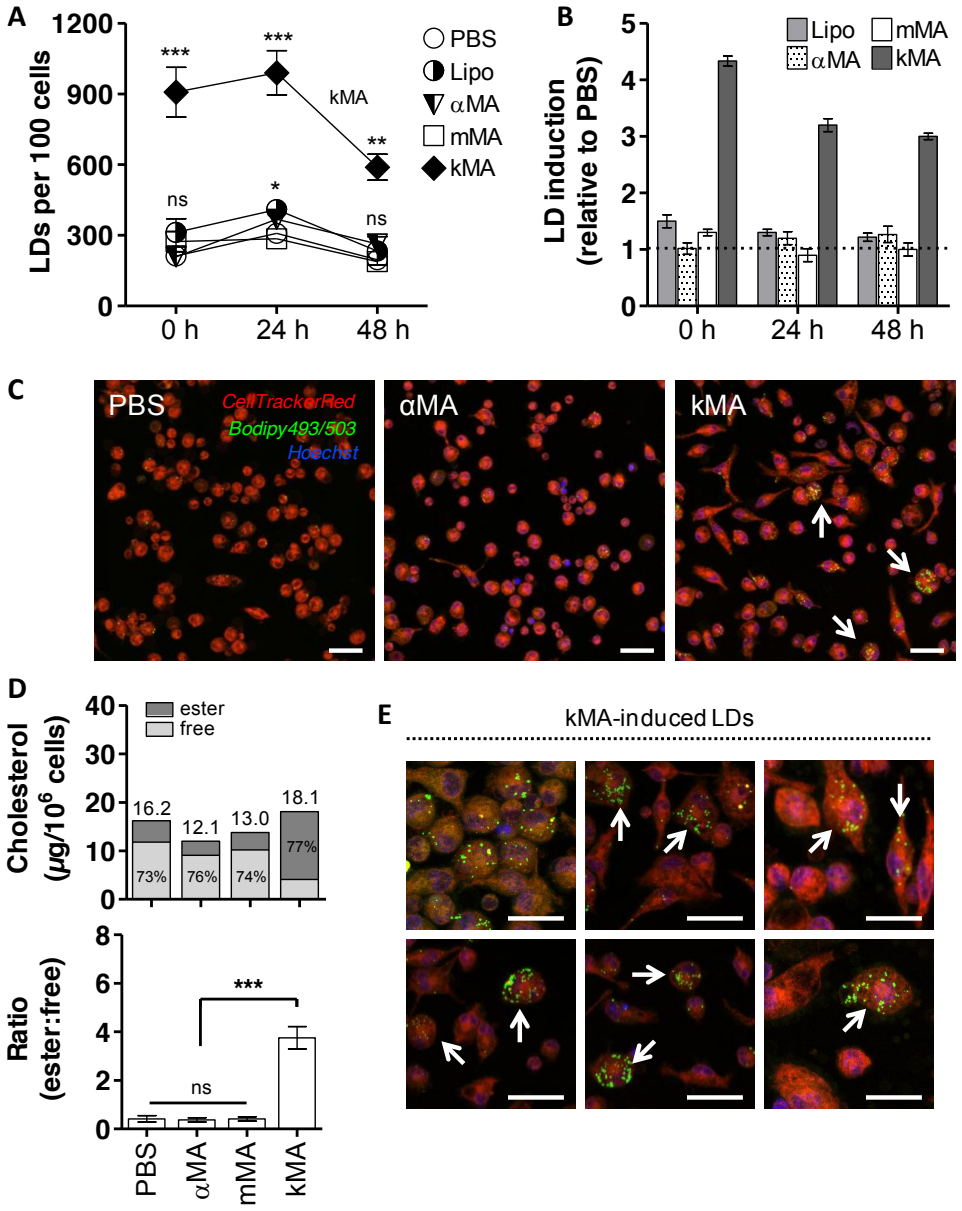

Figure 3 | Mycolic acids of the keto oxygenation class induce foam cells rich in cholesterol-laden lipid droplets. The induction of LDs is shown for peritoneal macrophages from control (PBS and Lipo) and αMA, mMA and kMA-treated mice (mean ± SEM). (A) LD accumulation in murine macrophages harvested at specified time points following the control and various MA treatments (GLM: Wald Chi-Square = 353.662, $P < 0.001$, df =14, n = 5 per time point). (B) Relative induction of LDs over time as compared to PBS (broken line). (C) Laser-scanning-confocal microscopy images depicting variation in LD induction for PBS, αMA and kMA treatments. Arrows indicate LD filled cells. (D) Cellular cholesterol content of variously treated cells. Bars represent total cholesterol, subdivided in the amount of free and esterified cholesterol for each of the treatments (µg/10^6 cells). Upper panel, fraction percentages of free and esterified cholesterol are shown in the bars (n = 12 mice; Shapiro-Wilk: W = 0.813, $P < 0.05$; Kruskal-Wallis: H = 24.726, $P < 0.001$, df = 3). Lower panel, the ratio of esterified-to-free cholesterol is given for the various treatments (Kruskal-Wallis: H = 26.554, $P < 0.001$, df = 3). (E) kMA induced LDs in peritoneal macrophages as identified by the neutral lipid probe Bodipy®493/503. (C, E) Stacked images, 63x oil objective. Scale bar: 20 µm. Significant P values were ranked as $P < 0.05$ (*), $P < 0.01$ (**) and $P < 0.001$ (***); ns, not significant.

4.3 Mycolic acid induced lipid droplet accumulation in macrophages promotes BCG proliferation

In order to determine to what extent LD induction by kMA or vacuole induction by mMA may affect mycobacterial growth, peritoneal macrophages from mice treated with kMA or mMA were infected with BCG-dsRed and cultured for five days (Fig. 4A). Control groups again consisted of peritoneal macrophages isolated from mice injected with PBS (placebo) or the unoxygenated αMA. Infection of the macrophages with BCG did not abrogate the accumulation of LDs in kMA-treated macrophages and did not induce, as such, an accumulation of LDs in placebo- or mMA-treated macrophages (Fig. 4B, upper panel). Strikingly, BCG replication was strongly enhanced in the kMA-treated macrophages (Fig. 4C), resulting in a near 3-fold increment in BCG numbers compared to the placebo-treated macrophages or macrophages treated with mMA (Fig. 4B, lower panel; Fig. 4D; Supplementary Table S4-S5). Macrophages from mice treated with a natural mixture of MA made up of αMA (~53%), kMA (~9%) and mMA (~38%) showed an intermediate induction of LDs as well as BCG replication (Fig. 4B), indicating that the presence of either mMA and/or αMA does not inhibit the LD-inducing and BCG proliferative biological function of kMA.

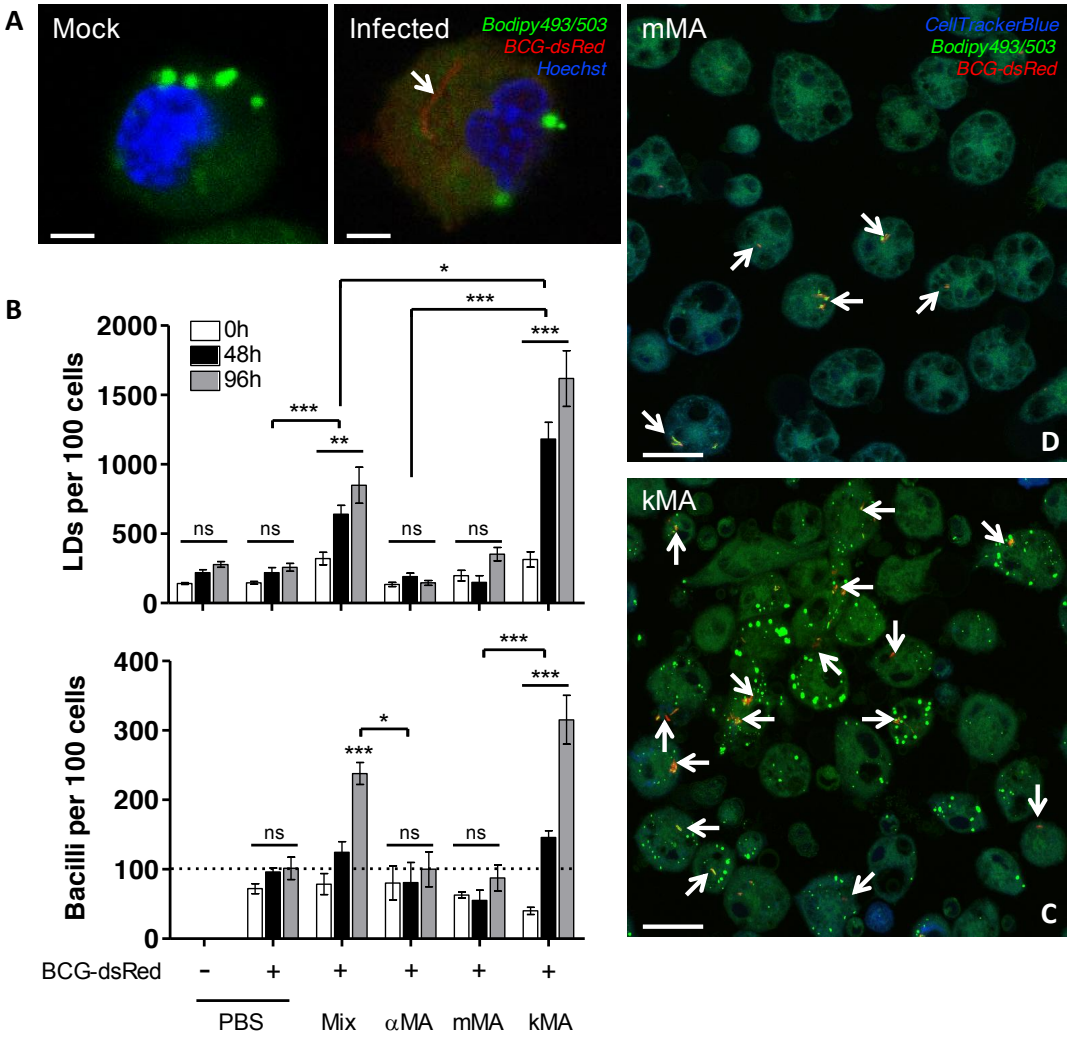

Figure 4 | Mycolic acid induced lipid droplet accumulation in macrophages promotes BCG proliferation. Following *in vivo* treatment with MA, peritoneal macrophages were infected *ex vivo* with BCG-dsRed (MOI 1, broken line) and cultured until timed interval measurements were taken by laser-scanning-confocal microscopy (mean ± SEM). (A) Laser-scanning-confocal microscopy images (zoomed) showing macrophages from mock or BCG infections. The presence of a BCG-dsRed bacillus can be clearly distinguished. Scale bar: 2.5 µm. (B) Upper panel, LD accumulation in peritoneal macrophages over time (GLM: Wald Chi-Square = 636.496, $P < 0.001$, $df = 17$, $n = 5$ per time point). Lower panel, proliferation of BCG bacilli over time (GLM: Wald Chi-Square = 250.303, $P < 0.001$, $df = 17$, $n = 5$ per time point). On the X-axis, "Mix" denotes a natural purified MA extract consisting of ~53% αMA, ~38% mMA and ~9% kMA. (C-D) Laser-scanning-confocal microscopy images depicting a clear difference in the presence of BCG-dsRed bacilli in peritoneal macrophages from mice treated with either kMA or mMA. Stacked images, 63x oil objective. Scale bar: 20 µm. Arrows indicate BCG-dsRed bacilli. Significant P values were ranked as $P < 0.05$ (*), $P < 0.01$ (**) and $P < 0.001$ (***); ns, not significant.

4.4 Assessment of mycobacterial growth in lipid droplet-accumulating macrophages from LXR-deficient mice

In order to determine whether foamy macrophages brought about by non-tuberculous means would also display elevated intracellular mycobacterial growth similar to kMA-treated macrophages, we investigated this parameter in peritoneal macrophages from LXR-deficient KO mice. Macrophages deficient in LXR contained abundant LDs sustained over time (Fig. 5A; Supplementary Fig. S2). This was accompanied with intracellular accumulation of esterified-to-free cholesterol at a ratio of ~8:1 in KO mice (Fig. 5B). Strikingly, these LD-accumulating macrophages, elicited by a deficiency in LXR activity, also showed a significantly increased mycobacterial growth as compared to macrophages from WT mice (Fig. 5C; Supplementary Table S6-S7).

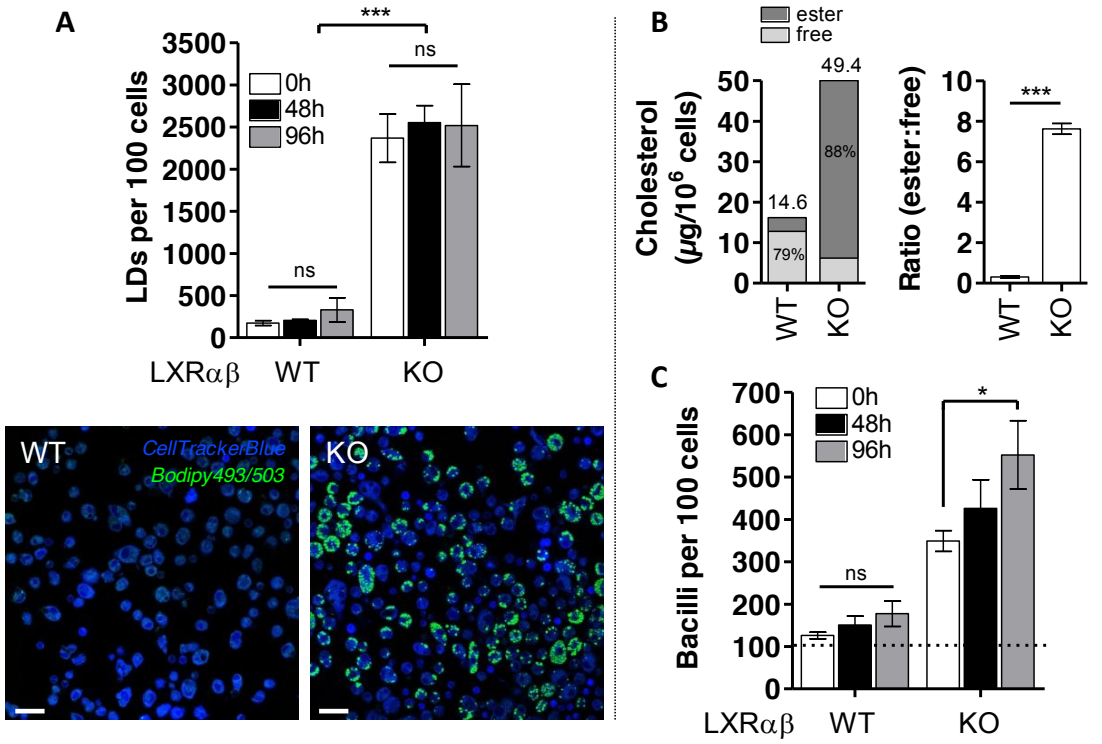

Figure 5 | Mycobacterial growth in lipid droplet accumulating macrophages from LXR-deficient mice. (A) Macrophages from WT and LXR-deficient mice were cultured for five days and the intracellular LD prevalence analysed by laser-scanning-confocal microscopy. KO-cells contained ~10-fold more cellular LDs in comparison to WT-cells, though no significant change in the number of LDs per 100 cells was observed over time (GLM: Wald Chi-Square = 99.093, $P < 0.001$, $df = 5$, $n = 4$ per time point; sequential Sidak pairwise comparisons $P > 0.05$). Laser-scanning-confocal microscopy images depicting clear morphological differences in LD prevalence between WT and KO macrophages. Scale bar: 20 μm. (B) Cholesteryl esters accounted for 88% of total cholesterol in LXR-deficient cells (left panel) that also contained significantly elevated ratios of intracellular esterified-to-free cholesterol (right panel; Mann-Whitney: $U = 144.000$, $P < 0.001$, $df = 1$, $n = 12$ mice). (C) Macrophages from WT and KO mice were infected *ex vivo* for 6 h with BCG-dsRed (MOI 1, broken line) and cultured for five days. Mycobacterial growth was measured by laser-scanning-confocal microscopy at specified time points, and was significantly increased in LXR-deficient cells over time (GLM: Wald Chi-Square = 576.689, $P < 0.001$, $df = 17$; $n = 6$ per time point; sequential Sidak pairwise comparisons $P < 0.05$). Data represent mean ± SEM. Significant P values were ranked as $P < 0.05$ (*) and $P < 0.001$ (***); ns, not significant.

5. Discussion

The hallmark response to Mtb infection is the formation of granulomas that, in spite of being crucial to host protection, are exploited by mycobacteria for survival and persistence[43]. Granulomas contain distinct macrophage populations of which foam cells loaded with neutral lipids and giant cells containing abundant vacuoles are characteristic[44]. It was shown previously that natural, purified Mtb MA induces cellular features similar to those observed in granuloma cell populations[25]. However, as MAs are heterogeneous, we determined in this study to what extent examples of individual MA classes sustain the foamy and/or vacuolar giant cellular traits in macrophages. The clear difference reported here between mMA and kMA treatment in murine macrophages – a distinct induction by mMA of vacuoles without LDs and an upregulation of LDs without vacuoles by kMA – indicates the occurrence of independent triggers for giant versus foamy cell phenotypes during Mtb infection. The pathophysiological significance of these independent macrophage responses possibly reflects a strategy by Mtb to persist inside the key immune effector cell responsible for its elimination[45-47]. In nature, the inflammatory neutral αMA class makes up approximately 50% of all MAs whereas the ratio of pro-inflammatory mMA to kMA classes in the Mtb bacillus cell wall is variable and may be tuned to complement growth and persistence[13, 17, 18]. Korf *et al*.[25] previously showed that macrophages from mice treated with the natural MA mixture (similar to the MA mix used in this study) containing approximately 32-40% methoxy mycolates, accumulated large intracellular vacuoles like those reported by us here after treatment with pure (100%) mMA. Our results furthermore showed that the macrophages harvested from mice after natural MA mix treatment, which contains 7-15% keto mycolates, significantly accumulated intracellular LDs and allowed for mycobacterial growth, comparable to the macrophages from the pure (100%) kMA treatment group, but reduced by

about half. One could therefore anticipate that the changes brought about by regulation of the MA class composition by Mtb will not be extreme.

LDs are widespread cell organelles dedicated to the storage of neutral lipids like cholesteryl esters[48]. Numerous studies have reported on the close association of this distinctive lipid organelle with Mtb pathogenesis[28, 46, 49-52]. The dynamic interaction of the LD with the Mtb-containing vacuole was recorded in an *in vitro* granuloma model by Peyron and team[28]. Electron microscopy analyses of foam cells showed that phagosomes containing bacilli migrated towards LDs and eventually engulfed them. D'Avila *et al*.[53] observed in a murine model of TB using the vaccine strain BCG, a dose-response in LD formation over time. Close associations between LDs and phagosomes were recorded in BCG-infected treatments, with significant LD induction observed after 24 hours that remained elevated for about two weeks after infection. Cytoskeleton arrangement and phosphatidylinositol-3-kinase, an enzyme involved in cellular regulation of proliferation, trafficking and metabolism[54], were identified to play key roles in the LD recruitment to bacilli-enclosed phagosomes[55]. It is thus clear that pathogenic mycobacteria regulate biogenesis or accumulation of host cell lipids into LD-confined organelles, which may be further manipulated to intimately associate with the phagosomes enclosing the bacilli. An important question is the pathophysiological relevance of this association. Research suggests that the LD-phagosome interaction serves a dual purpose: at one end to benefit the microorganism and at the other to aid the host cell in microbe elimination[28, 32, 56]. LDs may serve as a nutrient source to the bacillus through direct assimilation of host cell lipids [28] or as nutrient reservoir during latency[32]. In contrast, host cells employ LDs to disseminate important anti-bacterial factors as was recorded in an *in vitro* study of latex bead phagosomes and pathogenic mycobacteria[56]. Phagosomes infected with Mtb and exposed to distinct lipids (i.e. arachidonate, ceramide and sphingomyelin)

induced actin assembly in macrophages, a process involved in microtubule organisation and LD trafficking[55]. Lipid exposure also effected phagolysosomal fusion and decreased phagosome pH, events indicative of phagosome maturation and engagement of bactericidal machinery[56]. It was noted that the kMA induced LD accumulation in macrophages tended to rapidly return to normal after removing the kMA stimulation, while the mMA induced vacuolation of the macrophage was maintained after removal of mMA. Enlarged intracellular vacuoles, like those induced after treatment with mMA, represent structures formed by invagination of the external cell membrane phospholipid bilayer into the cytosol[57]. These double-layered vacuoles form stable structures that essentially provide a compartment for upholding the bacterium. LDs are phospholipid monolayer organelles critically involved in cellular lipid metabolism[58]. As dynamic structures mediating lipid exchange or consumption, removal of the LD-inducing stimulus can be expected to coincide with rapid turnover and/or catabolism of the LDs by cellular machinery.

As indicated above, we confirmed that αMA is functionally neutral and showed that the oxygenated MAs effected pronounced changes with remarkable segregation of foam cell features: mMA induced enlarged multi-vacuolar cells whereas kMA stimulated cells to accumulate LDs with most of its cholesterol converted to the cholesteryl ester storage form. We next verified the relevance of these responses to intracellular growth of mycobacteria. Using kMA-induced foamy cells and mMA-induced giant cells, we infected these macrophages *ex vivo* with BCG-dsRed and measured replication of the bacilli over time. Our results showed that intracellular growth was promoted in kMA-induced foamy macrophages, but not in mMA-induced giant cells. Macrophages classically convert into foam cells through a dysregulation in the balance between influx and efflux of cholesterol. Cholesterol is transported to peripheral macrophages in LDL that are taken up by the cell through the LDL

receptor, or in the oxidized form, through scavenger receptors SRA and CD36. Cholesterol efflux is mediated by the transporters ABCA1 and ABCG1 that load the cholesterol on HDL for transfer to the liver, a mechanism known as reverse cholesterol transport. These processes are regulated by the lipid sensing nuclear receptors LXR and PPARγ. A direct role for LXR in mycobacterial foam cell formation has not been reported. However, mice deficient in LXR show spontaneous foam cell formation[59]. LXR-deficient macrophages may be considered a cell model of the late stage of Mtb infection, where the macrophage has been modified to shut off its cholesterol export without limiting cholesterol import, aiming at providing a rich sterol nutrition source for mycobacterial growth and replication. We therefore investigated whether foam cells generated through a non-infectious condition, namely a deficiency in LXR activity, would also facilitate growth and proliferation of BCG bacilli. Similar to macrophages from mice treated with kMA, LXR-deficient macrophages accumulated cholesteryl ester-rich LDs and were facilitative towards mycobacterial growth. LXR-deficient macrophages contained more than double the amount of cholesterol compared to what could be induced with kMA and facilitated proliferation to almost double the number of BCG mycobacteria per 100 cells after 96 hours. These results suggest that LXR may indirectly function as a negative regulator of mycobacterial foam cell formation and mycobacterial growth. Although speculative, this proposition is in line with a previous report showing that LXR-activity suppresses the outgrowth of Mtb bacilli in a mouse model of pulmonary Mtb infection[60].

Our study addressed the individual contribution that examples of each of the three main classes of MAs from Mtb makes towards the induction of foam cells and multi-vacuolar giant cells as well as towards the facilitation of intracellular mycobacterial proliferation. All three features are important elements of the manifestation of TB in human lungs and were elicited

to varying degrees by the individual MA classes studied. Thus, we showed here that it is kMA that induces mainly cholesterol ester accumulation within intracellular LDs and facilitates mycobacterial BCG proliferation. In contrast, mMA was found to induce vacuole formation, characteristic of giant cells found in Mtb lung granulomas, with however no change in cholesteryl ester content or an improved ability to sustain and facilitate mycobacterial growth. Finally, αMA treatment exerted a negligible effect on all three parameters. These findings suggest separate important roles for keto and methoxy oxygenated MA classes in manipulating the host macrophage response during the establishment of TB. This new insight may assist in deciphering and targeting the Achilles' heel of the tubercle bacillus according to an approach recently reviewed by Nataraj *et al*.[61], relying on the most recent understanding of how MA is synthesised and differentiated into classes by Mtb. Cyclopropanation provides the minimum functionalisation associated with MA virulence[17]. Dubnau *et al*.[18] provided evidence that cyclopropanation or functionalisation of the distal group of the meromycolic chain represents the first step of a common pathway responsible for generating methoxy and keto mycolates. Differential regulation of this single mechanism can thus allow mycobacteria to manipulate MA class composition of alpha, methoxy and keto mycolates during growth progression. Evidence for this was provided by Yuan *et al*.[19], who showed that keto mycolates are more abundant during the early stage of mycobacterial infection, but gives way to methoxy mycolates that become more abundant in the later phase of infection. Our results imply that much may be accomplished by attempting to control the switch between methoxy and keto mycolates as a principle of drug treatment to combat TB. One argument for this was provided by Slama *et al*.[62] who showed that mMA was much more abundant in the virulent Mtb H37Rv strain than in the attenuated Mtb H37Ra strain. This has to be understood in the wider context that other differences between the H37Rv and H37Ra strains were also identified, but the researchers then achieved better resolution of the

evidence[62]: A recombinant Mtb H37Rv was generated with a single gene KO of a protein involved in the late stage of MA biosynthesis, namely HadC. HadC is a dehydratase that is not catalytically active, but holds the longer form of the elongating merochain of MA in a complex with HadB, which catalyses dehydration of a β-hydroxyacyl in the merochain to an enoyl. The *hadC* KO Mtb H37Rv showed a reduction in the abundance of mMA similar to that found in Mtb H37Ra[62]. It accordingly also had lower virulence, approximating that of Mtb H37Ra, lost its cording and biofilming ability and its envelope integrity, thus making it more susceptible to the hydrophobic drug rifampicin. It should be noted that these biological effects could not only be ascribed to the lowering of the abundance of mMA, because the *hadC* KO Mtb H37Rv also had a larger degree of unsaturation in the merochain and could not produce the small amount of extra-long chain MAs of all three classes that are present in the WT Mtb H37Rv.

Whereas the group of Slama[62] demonstrated the advantage of being able to reduce the abundance of mMA in Mtb, our results could imply that even more may be achieved by interfering with kMA production in Mtb. However, Dubnau *et al*.[18] managed to create a *hma*-KO mutant Mtb H37Rv that produced no oxygenated MA at all. The mutant Mtb also showed severe loss of virulence, but was still able to grow and multiply in a monocytic cell line or in lungs and spleen of infected mice. Thus, kMA seems not to be essential for survival of Mtb and is hence not a prime target for the conceptualisation of a new anti-TB drug; although we have demonstrated here how kMA allows the mycobacterium to thrive, but not survive, in the target host cell.

6. Conclusion

Our study addressed the individual contribution that examples of each of the three main classes of MAs from Mtb makes towards the induction of foam cells and multi-vacuolar giant cells as well as towards the facilitation of intracellular mycobacterial proliferation. All three features are important elements of the manifestation of TB in human lungs and were elicited to varying degrees by the individual MA classes studied. Thus, we showed here that it is kMA that induces mainly cholesterol ester accumulation and intracellular LDs and facilitates mycobacterial BCG proliferation. In contrast, mMA was found to induce vacuole formation, characteristic of giant cells found in Mtb lung granulomas, with however no change in cholesteryl ester content or an improved ability to sustain and facilitate mycobacterial growth. Finally, αMA treatment exerted a negligible effect on all three parameters. These findings suggest separate important roles for keto and methoxy oxygenated MA classes in manipulating the host macrophage response during the establishment of TB.

7. Supplemental data

All supplemental data pertaining to this study have been compiled as an additional chapter, which is provided on a separate compact disc along with this thesis.

7.1 List of supplemental data

Table S1 | Sequential Sidak pairwise comparisons showing within- and between-group differences in the proportion of enlarged vacuole-positive (V+) cells induced by MA

Table S2 | Sequential Sidak pairwise comparisons showing within- and between-group differences in the induction of LDs by MA

Table S3 | Cellular cholesterol levels of murine peritoneal macrophages

Table S4 | Sequential Sidak pairwise comparisons showing differences among treatments in LD induction and mycobacterial replication of murine peritoneal macrophages

Table S5 | Sequential Sidak pairwise comparisons showing within- and between-group differences in LD induction and mycobacterial replication of murine peritoneal macrophages

Table S6 | Sequential Sidak pairwise comparisons showing differences in LD induction and mycobacterial growth at various MOIs of WT and LXR-deficient mouse macrophages

Table S7 | Sequential Sidak pairwise comparisons depicting within- and between-group differences in mycobacterial MOI over time for WT and LXR-deficient macrophages

Figure S1 | Schematic overview of the experimental design of the foam cell and mycobacterial models

Figure S2 | Fluorescently-labelled macrophages from WT and LXR-deficient mice after five days of culture

7.2 Additional experiments

Screen for LXR target genes and ER stress markers in MA-treated macrophages

Figure S3 | LXR target genes

Figure S4 | ER stress markers

8. References

1. WHO. 2015. *Global Tuberculosis Report*. 20th ed. World Health Organization, Geneva. pp 204

2. Pieters, J. 2008. *Mycobacterium tuberculosis* and the macrophage: maintaining a balance. *Cell Host Microbe* **3**: 399-407.

3. Jamwal, S. V., P. Mehrotra, A. Singh, Z. Siddiqui, A. Basu and K. V. Rao. 2016. Mycobacterial escape from macrophage phagosomes to the cytoplasm represents an alternate adaptation mechanism. *Sci. Rep.* **6**: 1-9.

4. Banerjee, S. K., M. Kumar, R. Alokam, A. K. Sharma, A. Chatterjee, R. Kumar, S. K. Sahu, K. Jana, R. Singh, P. Yogeeswari, D. Sriram, J. Basu and M. Kundu. 2016. Targeting multiple response regulators of *Mycobacterium tuberculosis* augments the host immune response to infection. *Sci. Rep.* **6**: 25851; doi: 25810.21038/srep25851.

5. Blischak, J. D., L. Tailleux, A. Mitrano, L. B. Barreiro and Y. Gilad. 2015. Mycobacterial infection induces a specific human innate immune response. *Sci. Rep.* **5**: 16882; doi: 16810.11038/srep16882.

6. Tsai, M. C., S. Chakravarty, G. Zhu, J. Xu, K. Tanaka, C. Koch, J. Tufariello, J. Flynn and J. Chan. 2006. Characterization of the tuberculous granuloma in murine and human lungs: cellular composition and relative tissue oxygen tension. *Cell. Microbiol.* **8**: 218-232.

7. Ramakrishnan, L. 2012. Revisiting the role of the granuloma in tuberculosis. *Nat. Rev. Immunol.* **12**: 352-366.

8. Yang, M., R. Lu, K. E. Guja, M. F. Wipperman, J. R. St Clair, A. C. Bonds, M. Garcia-Diaz and N. S. Sampson. 2015. Unraveling cholesterol catabolism in: ChsE4-ChsE5 alphabeta Acyl-CoA Dehydrogenase Initiates beta-Oxidation of 3-Oxo-cholest-4-en-26-oyl CoA. *ACS Infect. Dis.* **1**: 110-125.

9. Lee, W., B. C. VanderVen, R. J. Fahey and D. G. Russell. 2013. Intracellular *Mycobacterium tuberculosis* exploits host-derived fatty acids to limit metabolic stress. *J. Biol. Chem.* **288**: 6788-6800.

10. Griffin, J. E., A. K. Pandey, S. A. Gilmore, V. Mizrahi, J. D. McKinney, C. R. Bertozzi and C. M. Sassetti. 2012. Cholesterol catabolism by *Mycobacterium tuberculosis* requires transcriptional and metabolic adaptations. *Chem. Biol.* **19**: 218-227.

11. Jankute, M., J. A. Cox, J. Harrison and G. S. Besra. 2015. Assembly of the mycobacterial cell wall. *Annu. Rev. Microbiol.* **69**: 405-423.

12. Riley, L. W. 2006. Of mice, men and elephants: *Mycobacterium tuberculosis* cell envelope lipids and pathogenesis. *J. Clin. Invest.* **116**: 1475-1478.

13. Verschoor, J. A., M. S. Baird and J. Grooten. 2012. Towards understanding the functional diversity of cell wall mycolic acids of *Mycobacterium tuberculosis*. *Prog. Lipid Res.* **51**: 325-339.

14. Watanabe, M., Y. Aoyagi, M. Ridell and D. E. Minniken. 2001. Separation and characterization of individual mycolic acids in representative mycobacteria. *Microbiology* **147**: 1825-1837.

15. Watanabe, M., Y. Aoyagi, H. Mitome, T. Fujita, H. Naoki, M. Ridell and D. E. Minniken. 2002. Location of functional groups in mycobacterial meromycolate chains; the recognition of new structural principles in mycolic acids. *Microbiology* **148**: 1881-1902.

16. Ndlandla, F. L., V. Ejoh, A. C. Stoltz, B. Naicker, A. D. Cromarty, S. van Wyngaardt, M. Khati, L. S. Rotherham, Y. Lemmer, J. Niebuhr, C. R. Baumeister, J. R. Al-Dulayymi, H. Swai, M. S. Baird and J. A. Verschoor. 2016. Standardization of natural mycolic acid antigen composition and production for use in biomarker antibody detection to diagnose active tuberculosis. *J. Immunol. Methods* **435**: 50-59.

17. Glickman, M. S., J. S. Cox and W. R. Jacobs, Jr. 2000. A novel mycolic acid cyclopropane synthetase is required for cording, persistence and virulence of *Mycobacterium tuberculosis*. *Mol. Cell* **5**: 717-727.

18. Dubnau, E., J. Chan, C. Raynaud, V. P. Mohan, M.-A. Laneelle, K. Yu, A. Quemard, S. Smith and M. Daffe. 2000. Oxygenated mycolic acids are necessary for virulence of *Mycobacterium tuberculosis* in mice. *Mol. Microbiol.* **36**: 630-637.

19. Yuan, Y., Y. Zhu, D. D. Crane and C. E. Barry, 3rd. 1998. The effect of oxygenated mycolic acid composition on cell wall function and macrophage growth in *Mycobacterium tuberculosis*. *Mol. Microbiol.* **29**: 1448-1458.

20. Ishikawa, E., T. Ishikawa, Y. S. Morita, K. Toyonaga, H. Yamada, O. Takeuchi, T. Kinoshita, S. Akira, Y. Yoshikai and S. Yamasaki. 2009. Direct recognition of the mycobacterial glycolipid, trehalose dimycolate, by C-type lectin Mincle. *J. Exp. Med.* **206**: 2879-2888.

21. Moody, D. B., G. S. Besra, I. A. Wilson and S. A. Porcelli. 1999. Molecular basis of CD1-mediated presentation of lipid antigens. *Immunol. Rev.* **172**: 285-296.

22. Karakousis, P. C., W. R. Bishai and S. E. Dorman. 2004. *Mycobacterium tuberculosis* cell envelope lipids and the host immune response. *Cell. Microbiol.* **6**: 105-116.

23. van der Meer-Janssen, Y. P., J. van Galen, J. J. Batenburg and J. B. Helms. 2010. Lipids in host-pathogen interactions: pathogens exploit the complexity of the host cell lipidome. *Prog. Lipid Res.* **49**: 1-26.

24. Cole, S. T., R. Brosch, J. Parkhill, T. Garnier, C. Churcher, D. Harris, S. V. Gordon, K. Eigleimer, S. Gas, C. E. Barry, F. Tekaia, K. Badcock, D. Basham, D. A. Brown, T. Chillingworth, R. Connor, R. Davies, K. Devlin, T. Feltwell, S. Gentles, N. Hamlin, S. Holroyd, T. Hornsby, K. Jagels, A. Krogh, J. McLean, S. Moule, L. Murphy, K. Oliver, J. Osborne, M. A. Qual, M.-A. Rajandream, J. Rogers, S. Rutter, K. Seeger, J. Skelton, S. Squares, J. E. Sulston, K. Taylor, S. Whitehead and B. G. Barrell. 1998. Deciphering the biology of *Mycobacterium tuberculosis* from the complete genome sequence. *Nature* **393**: 537-544.

25. Korf, J., A. Stoltz, J. Verschoor, P. De Baetselier and J. Grooten. 2005. The *Mycobacterium tuberculosis* cell wall component mycolic acid elicits pathogen-associated host innate immune responses. *Eur. J. Immunol.* **35**: 890-900.

26. Korf, J. E., G. Pynaert, K. Tournoy, T. Boonefaes, A. Van Oosterhout, D. Ginneberge, A. Haegeman, J. A. Verschoor, P. De Baetselier and J. Grooten. 2006. Macrophage reprogramming by mycolic acid promotes a tolerogenic response in experimental asthma. *Am. J. Respir. Crit. Care Med.* **174**: 152-160.

27. Russell, D. G., P. J. Cardona, M. J. Kim, S. Allain and F. Altare. 2009. Foamy macrophages and the progression of the human tuberculosis granuloma. *Nat. Immunol.* **10**: 943-948.

28. Peyron, P., J. Vaubourgeix, Y. Poquet, F. Levillain, C. Botanch, F. Bardou, M. Daffe, J. F. Emile, B. Marchou, P. J. Cardona, C. de Chastellier and F. Altare. 2008. Foamy macrophages from tuberculous patients' granulomas constitute a nutrient-rich reservoir for *M. tuberculosis* persistence. *PLoS Pathog.* **4**: e1000204. doi:1000210.1001371/journal.ppat.1000204.

29. Caceres, N., G. Tapia, I. Ojanguren, F. Altare, O. Gil, S. Pinto, C. Vilaplana and P. J. Cardona. 2009. Evolution of foamy macrophages in the pulmonary granulomas of experimental tuberculosis models. *Tuberculosis* **89**: 175-182.

30. Maxfield, F. R. and G. van Meer. 2010. Cholesterol, the central lipid of mammalian cells. *Curr. Opin. Cell Biol.* **22**: 422-429.

31. Guo, Y., K. R. Cordes, R. V. Farese, Jr. and T. C. Walther. 2009. Lipid droplets at a glance. *J. Cell Sci.* **122**: 749-752.

32. Pandey, A. K. and C. M. Sassetti. 2008. Mycobacterial persistence requires the utilization of host cholesterol. *Proc. Natl. Acad. Sci. U. S. A.* **105**: 4376-4380.

33. Brzostek, A., J. Pawelczyk, A. Rumijowska-Galewicz, B. Dziadek and J. Dziadek. 2009. *Mycobacterium tuberculosis* is able to accumulate and utilize cholesterol. *J. Bacteriol.* **191**: 6584-6591.

34. Jakobsson, T., E. Treuter, J. A. Gustafsson and K. R. Steffensen. 2012. Liver X receptor biology and pharmacology: new pathways, challenges and opportunities. *Trends Pharmacol. Sci.* **33**: 394-404.

35. A-Gonzalez, N. and A. Castrillo. 2011. Liver X receptors as regulators of macrophage inflammatory and metabolic pathways. *Biochim. Biophys. Acta* **1812**: 982-994.

36. Al Dulayymi, J. a. R., M. S. Baird and E. Roberts. 2005. The synthesis of a single enantiomer of a major α-mycolic acid of *M. tuberculosis*. *Tetrahedron* **61**: 11939-11951.

37. Al Dulayymi, J. a. R., M. S. Baird, E. Roberts, M. Deysel and J. Verschoor. 2007. The first syntheses of single enantiomers of the major methoxymycolic acid of *Mycobacterium tuberculosis*. *Tetrahedron* **63**: 2571-2592.

38. Koza, G. and M. S. Baird. 2007. The first synthesis of single enantiomers of ketomycolic acids. *Tetrahedron Lett.* **48**: 2165-2169.

39. Alberti, S., G. Schuster, P. Parini, B. Feltkamp, U. Diczfalusy, M. Rudling, B. Angelin, I. Björkhem, S. Pettersson and J.-Å. Gustafsson. 2001. Hepatic cholesterol metabolism and resistance to dietary cholesterol in LXRbeta-deficient mice. *J. Clin. Invest.* **107**: 565-573.

40. Abadie, V., E. Badell, P. Douillard, D. Ensergueix, P. J. Leenen, M. Tanguy, L. Fiette, S. Saeland, B. Gicquel and N. Winter. 2005. Neutrophils rapidly migrate via lymphatics after *Mycobacterium bovis* BCG intradermal vaccination and shuttle live bacilli to the draining lymph nodes. *Blood* **106**: 1843-1850.

41. Sani, M., E. N. Houben, J. Geurtsen, J. Pierson, K. de Punder, M. van Zon, B. Wever, S. R. Piersma, C. R. Jimenez, M. Daffe, B. J. Appelmelk, W. Bitter, N. van der Wel and P. J. Peters. 2010. Direct visualization by cryo-EM of the mycobacterial capsular layer: a labile structure containing ESX-1-secreted proteins. *PLoS Pathog.* **6**: e1000794.

42. Minnikin, D. E., J. H. Parlett, M. Magnusson, M. Ridell and A. Lind. 1984. Mycolic acid patterns of representatives of *Mycobacterium bovis* BCG. *J. Gen. Microbiol.* **130**: 2733-2736.

43. Davis, J. M. and L. Ramakrishnan. 2009. The role of the granuloma in expansion and dissemination of early tuberculous infection. *Cell* **136**: 37-49.

44. Puissegur, M. P., C. Botanch, J. L. Duteyrat, G. Delsol, C. Caratero and F. Altare. 2004. An i*n vitro* dual model of mycobacterial granulomas to investigate the molecular interactions between mycobacteria and human host cells. *Cell. Microbiol.* **6**: 423-433.

45. Venugopal, A., R. Bryk, S. Shi, K. Rhee, P. Rath, D. Schnappinger, S. Ehrt and C. Nathan. 2011. Virulence of *Mycobacterium tuberculosis* depends on lipoamide dehydrogenase, a member of three multienzyme complexes. *Cell Host Microbe* **9**: 21-31.

46. Singh, V., S. Jamwal, R. Jain, P. Verma, R. Gokhale and K. V. Rao. 2012. *Mycobacterium tuberculosis*-driven targeted recalibration of macrophage lipid homeostasis promotes the foamy phenotype. *Cell Host Microbe* **12**: 669-681.

47. Huang, Z., Q. Luo, Y. Guo, J. Chen, G. Xiong, Y. Peng, J. Ye and J. Li. 2015. *Mycobacterium tuberculosis*-induced polarization of human macrophage orchestrates the formation and development of tuberculous granulomas i*n vitro*. *PLoS One* **10**: e0129744. doi:0129710.0121371/journal.pone.0129744.

48. Krahmer, N., Y. Guo, R. V. Farese, Jr. and T. C. Walther. 2009. SnapShot: Lipid Droplets. *Cell* **139**: DOI 10.1016/j.cell.2009.1011.1023.

49. Lovewell, R. R., C. M. Sassetti and B. C. VanderVen. 2016. Chewing the fat: lipid metabolism and homeostasis during *M. tuberculosis* infection. *Curr. Opin. Microbiol.* **29**: 30-36.

50. Daniel, J., H. Maamar, C. Deb, T. D. Sirakova and P. E. Kolattukudy. 2011. *Mycobacterium tuberculosis* uses host triacylglycerol to accumulate lipid droplets and acquires a dormancy-like phenotype in lipid-loaded macrophages. *PLoS Pathog*. **7**: doi:10.1371/journal.ppat.1002093.

51. Kim, M. J., H. C. Wainwright, M. Locketz, L. G. Bekker, G. B. Walther, C. Dittrich, A. Visser, W. Wang, F. F. Hsu, U. Wiehart, L. Tsenova, G. Kaplan and D. G. Russell. 2010. Caseation of human tuberculosis granulomas correlates with elevated host lipid metabolism. *EMBO Mol*. *Med*. **2**: 258-274.

52. Deb, C., C.-M. Lee, V. M. Dubey, J. Daniel, B. Abomoelak, T. D. Sirakova, S. Pawar, L. Rogers and P. E. Kolattukudy. 2009. A novel *in vitro* multiple-stress dormancy model for *Mycobacterium tuberculosis* generates a lipid-loaded, drug-tolerant, dormant pathogen. *PLoS One* **6**: 1-15.

53. D'Avila, H., R. C. N. Melo, G. G. Parreira, E. Werneck-Barroso, H. C. Castro-Faria-Neto and P. T. Bozza. 2006. *Mycobacterium bovis* Bacillus Calmette-Guerin induces TLR2-mediated formation of lipid bodies: intracellular domains for eicosanoid synthesis *in vivo*. *J*. *Immunol*. **176**: 3087-3097.

54. Fruman, D. A. and C. Rommel. 2014. PI3K and cancer: lessons, challenges and opportunities. *Nat*. *Rev*. *Drug Discov*. **13**: 140-156.

55. Mattos, K. A., F. A. Lara, V. G. Oliveira, L. S. Rodrigues, H. D'Avila, R. C. Melo, P. P. Manso, E. N. Sarno, P. T. Bozza and M. C. Pessolani. 2011. Modulation of lipid droplets by *Mycobacterium leprae* in Schwann cells: a putative mechanism for host lipid acquisition and bacterial survival in phagosomes. *Cell*. *Microbiol*. **13**: 259-273.

56. Anes, E., M. P. Kuhnel, E. Bos, J. Moniz-Pereira, A. Habermann and G. Griffiths. 2003. Selected lipids activate phagosome actin assembly and maturation resulting in killing of pathogenic mycobacteria. *Nat*. *Cell Biol*. **5**: 793-802.

57. van Meer, G. 2011. Dynamic transbilayer lipid asymmetry. *Cold Spring Harb*. *Perspect*. *Biol*. **3**: 1-11.

58. Pol, A., S. P. Gross and R. G. Parton. 2014. Biogenesis of the multifunctional lipid droplet: lipids, proteins, and sites. *J*. *Cell Biol*. **204**: 635-646.

59. Schuster, G. U. 2002. Accumulation of foam cells in liver X receptor-deficient mice. *Circulation* **106**: 1147-1153.

60. Korf, H., S. Vander Beken, M. Romano, K. R. Steffensen, B. Stijlemans, J. A. Gustafsson, J. Grooten and K. Huygen. 2009. Liver X receptors contribute to the protective immune response against *Mycobacterium tuberculosis* in mice. *J*. *Clin*. *Invest*. **119**: 1626-1637.

61. Nataraj, V., C. Varela, A. Javid, A. Singh, G. S. Besra and A. Bhatt. 2015. Mycolic acids: deciphering and targeting the Achilles' heel of the tubercle bacillus. *Mol*. *Microbiol*. **98**: 7-16.

62. Slama, N., S. Jamet, W. Frigui, A. Pawlik, D. Bottai, F. Laval, P. Constant, A. Lemassu, K. Cam, M. Daffe, R. Brosch, N. Eynard and A. Quemard. 2016. The changes in mycolic acid structures caused by hadC mutation have a dramatic effect on the virulence of *Mycobacterium tuberculosis*. *Mol*. *Microbiol*. **99**: 794-807.

CHAPTER III |

Lipidome immunomodulation of murine macrophages by chemically synthetic mycobacterial mycolates

Ilke Vermeulen[1,2], Mark Baird[3], Juma Al-Dulayymi[3], Katarzyna Bloch[4], Rita Derua[5], Etienne Waelkens[5], Johannes V. Swinnen[4], Johan Grooten[2], and Jan Verschoor[1]

[1]Department of Biochemistry, University of Pretoria, Pretoria 0002, South Africa

[2]Laboratory of Molecular Immunology, Department of Biomedical Molecular Biology, Ghent University, Technologiepark 927, Ghent Zwijnaarde 9052, Belgium

[3]School of Chemistry, Bangor University, Bangor, Gwynedd, Wales, LL57 2UW, UK

[4]Laboratory of Lipid Metabolism and Cancer, Department of Oncology, Leuven Cancer Institute, University of Leuven, O&N I Herestraat 49, Leuven 3000, Belgium

[5]Laboratory of Protein Phosphorylation and Proteomics, Department of Cellular and Molecular Medicine, University of Leuven, Leuven 3000, Belgium

Manuscript submitted to the *Journal of Lipid Research*: currently under peer review

Author contributions: IV conducted the experimental work, analysed the results, compiled the figures and wrote the complete first draft of the manuscript. JV and JG conceptualised the research and share senior authorship. MB oversaw the MA synthesis and JAD provided the synthetic MAs. JVS, KB, RD and EW performed the lipidomics analyses on experimental samples provided by IV.

1. Introduction

Tuberculosis (TB) is a deadly airborne disease of mainly the respiratory organs and is transmitted by the bacterial pathogen *Mycobacterium tuberculosis* (Mtb)[1]. Mtb bacilli target macrophage mononuclear phagocytes that are instrumental in mediating innate and adaptive protective immune functions[2]. Macrophages are associated with every phase of TB progression, including the establishment of a primary infection, latent persistence in granulomas, and reactivation[3, 4]. Granulomas constitute the histopathological hallmark of pulmonary TB. The intricate granuloma environment holds a balance of ongoing bacillary replication that is characterised by high bacterial load, and an immune cell-induced growth suppression demonstrated by non-replicating drug-resistant bacilli, also known as latent TB[5].

Mtb is known for inducing multiple changes to the host cell lipidome. For example, the depletion of sphingosine or phosphatidylinositide (PI) lipid mediators from the vacuolar envelope hinders phagosome maturation and fusion with acidic lysosomes by interfering with actin assembly[6, 7]. Mycobacterial factors can furthermore alter the molecular packaging of cholesterol and sphingomyelin (SM) in host membrane lipid rafts[8], mediate fatty acid acquisition via the hydrolysing activity of Mtb lipases[9] and effect membrane changes by manipulating the degree of unsaturation of phospholipid species of host cells[10]. Host lipids may also serve as nutrients for the bacilli during the various stages of infection. Initial evidence for this was provided by the enhanced respiration of Mtb bacilli isolated from murine lungs following growth on fatty acids, rather than carbohydrates[11]. More recent work highlighted the close association of mycobacteria with host-derived cholesterol, shown to be essential for entry into host cells and to support mycobacterial proliferation and pathogenicity[12-14]. Cholesterol is an abundant structural sterol distributed within cell membranes[15]. Yet the induction of cytosolic lipid droplets (LDs) by Mtb bacilli may also sustain an important esterified cholesterol reservoir. Natural Mtb infection or exposure to

Mtb-derived MAs can drive macrophage differentiation to the foam phenotype, which is characterised by accumulation of intracellular vacuoles and cholesterol entrapped in cytosolic LDs[16-18].

A distinctive feature of Mtb is a waxy cell envelope that lends an acid fast property to the bacillus. A lipid-rich cell wall is essential for survival and virulence and provides protection against degradation by host immune defence chemicals as well as antibiotics[19]. The outer membrane of Mtb is rich in highly branched long-chain lipids known as mycolic acids (MAs)[20]. The general structure of MA lipids consists of a branched mycolic motif (with a non-functionalised long alkyl chain) and a functional group-containing meromycolate chain[21]. The meromycolate chain can be either oxygenated or unoxygenated. The three main MA classes of Mtb consist of the abundant (fixed at ~53%) unoxygenated alpha-MA (αMA) and the less abundant (variable, totalling ~47%) oxygenated keto- (kMA) and methoxy-MA (mMA)[22] (Fig. 1). The three MA classes are further subdivided based on the configuration of the proximal cyclopropane: though a small amount of *trans*- may be present, αMA essentially exhibits a *cis*-configuration whereas kMA and mMA can contain *cis*- or *trans*-cyclopropanation and an adjoining methyl branch[20]. Each is also present as a complex mixture of homologues with chains of different lengths.

Qualitative and quantitative investigation of lipids can lead to an enhanced comprehension of disease mechanisms and the identification of diagnostic markers, which has important significance in disease diagnosis and drug development[23, 24]. Electrospray ionisation tandem mass spectrometry (ESI-MS/MS) lipidomics has greatly improved earlier detection methods and now allows for a robust and reliable analysis of complex lipidomes[25-28]. Whole system lipidomics of host cells in the context of bacterial invasion constitutes an emerging field. Several contributions by Dennis and co-workers highlighted the utility of lipidomics to study

disease. For example by assessing changes in essential fatty acids[29], eicosanoid metabolism[30, 31] and in 2010 a comprehensive analysis of changes to a macrophage lipidome and transcriptome following inflammatory insult in primary and immortalised macrophages was reported[32]. As the first documented study on quantitative immune cell lipidome dynamics, the work by Dennis *et al*.[32] greatly contributed to a better understanding of the lipid response of host cells to inflammatory activation and metabolic inhibition. Examining pathogen-induced changes in host cell lipidomes is a powerful approach for discovering new druggable targets that result from host-pathogen interaction. Here we applied a lipidomics approach to improve our understanding of TB, as various acquired drug resistant strains are developing owing to poor drug quality and non-compliance with use[33].

2. Research aims

- In Chapter II of this thesis, we report how MAs differentially change the phenotype of macrophages to facilitate mycobacterial survival and proliferation. By using individual chemically synthetic MAs, each with a defined stereochemistry, representative of the three main classes of natural MA[34-36], mMA was found to cause vacuolation while kMA induced cholesteryl ester rich LD accumulation in murine macrophages. Only macrophages associated with kMA, but not mMA treatment, could sustain intracellular mycobacterial growth. αMA had no notable effect on macrophage physiology. We therefore hypothesised that the induction of phenotypically and functionally distinct macrophage populations by the oxygenated MAs could be accompanied by unique lipidome profiles. Employing an ESI-MS/MS lipidomics approach, we therefore studied changes in the lipidome of murine peritoneal macrophages following *in vivo* treatment with chemically synthetic representatives of the major classes of Mtb MAs. We report here on changes in the composition of glycerophospholipids (PLs), lysophospholipids (LPLs) and

sphingolipids among the lipidomes of murine peritoneal macrophages differentially treated with each of the MA classes.

3. Materials and methods

3.1 Mycolic acids

Natural MA mixture was isolated and single synthetic MAs synthesised as previously described[22, 34-36]. The MAs used for *in vivo* murine treatment in this study comprised a natural isolated MA mixture similar to the natural MAs in the Mtb cell wall (MA mix), *cis*-αMA, *cis*-mMA, and *cis*-kMA consisting of a mixture of both epimers of the distal α-methyl-ketone group with S- and R-stereochemistry (Fig. 1). *Cis*- refers to the orientation of the proximal cyclopropane.

3.2 Animals

C57BL/6 WT female mice, eight to twelve weeks of age, were used for experiments (Janvier Labs, France). All mice were housed in specific pathogen-free conditions in a controlled animal facility at the Flemish Institute of Biotechnology (Ghent). Mice received mixed ration feed and water *ad libitum*. Experiments were preapproved by the Ghent University Ethical Committee for Animal Experimentation in accordance with current European laws regarding the welfare and humane use of animals.

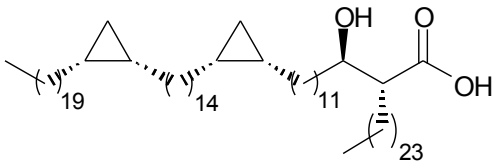

JR1080, **αMA** (19,14,11,23)

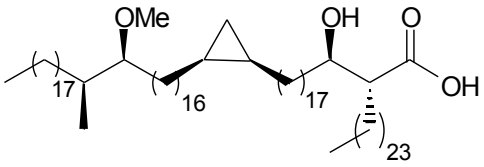

JR1046, **mMA** (17,16,17,23)

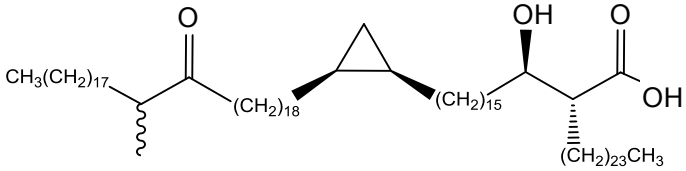

GK324, **kMA** (17,16,17,23)

Figure 1 | Mycolic acid structures. Chemical structures of the synthetic mycolic acids (MAs) containing *cis*-cyclopropanation: alpha (αMA; JR1080), methoxy (mMA; JR1046) and keto (kMA; GK324). Numbers in brackets represent carbon chain lengths and wiggly line indicates a mixture of stereoisomers at that position.

3.3 Injectable solutions and macrophage isolation

Liposomes were used as carrier to deliver the highly hydrophobic MA compounds to target cells. As a first step, L-α-Phosphatidylcholine (PC; Sigma®) powder was dissolved in chloroform at 100 mg/ml (10% w/v). PC and MA stock solutions were vortexed and heated before undergoing dehydration on a heat block (90°C) and the dried lipids recovered in endotoxin-free PBS (Lonza). Solutions underwent a series of vortex and sonication steps at 65°C until homogenous milky consistency. Mice were immediately treated *in vivo* by intraperitoneal (i.p.) injection (25 µg MA/100 µl/mouse). Two days after *in vivo* treatment, mice were terminated via cervical dislocation and peritoneal exudate cells (PECs) harvested by peritoneal lavage for enrichment of F4/80$^+$ macrophages. Mouse abdomens were decontaminated with 70% ethanol and 10 ml ice cold endotoxin-free PBS injected i.p. Following a short abdominal massage PECs were removed into sterile 15 ml tubes and kept on ice until further processing by centrifugation (400xg, 4°C, 10 min) and red blood cell lysis (ACK lysing buffer, Lonza; 50% v/v). PECs were seeded in 250 µl culture medium (5x10^5 cells) in µ-Slide 8-well microscopy plates (ibidi®). Culture medium consisted of RPMI 1640 (Gibco®) supplemented with lipopolysaccharide-free and heat-inactivated foetal calf serum (10%), sodium pyruvate (2 mM), non-essential amino acids (1%), penicillin/streptomycin antibiotics (0.2%), and β-mercaptoethanol (0.1%). Cultures were enriched for macrophages by overnight adherence. All cells were cultured at 37°C and 5% CO_2.

3.4 Magnetic labelling and enrichment of F4/80$^+$ macrophages

For lipidomics analyses, murine F4/80$^+$ macrophages were isolated from total PEC using MACS magnetic cell sorting (Miltenyi Biotech) according to manufacturer's instructions. In short, PECs were labelled with biotinylated anti-F4/80 (AbD Serotec, C1:A31) and subsequently incubated with magnetic anti-biotin Streptavidin microbeads. Cell suspensions were loaded onto a MACS column and magnetically separated with a MACS sorting magnet.

Magnetically retained material was eluted from the column and an aliquot stained with anti-F4/80-APC (eBiosciences, clone BM8) to assess purity on an LSRII flow cytometer (BD Biosciences; FlowJo Software), which was ~68-78% (Supplementary Fig. S1).

3.5 Electrospray ionisation tandem mass spectrometry

Lipids were extracted from F4/80^{+} macrophages and PL, LPL, ceramide (Cer) and sphingomyelin (SM) content quantified by ESI-MS/MS. Cell pellets diluted in PBS were mixed with 800 µl 1 N hydrochloric acid-methanol (1:8, v/v), 900 µl chloroform, and 200 µg/ml butylated hydroxytoluene antioxidant (2,6-di-tert-butyl-4-methylphenol; Sigma Aldrich). Organic fractions were dried at room temperature with a Savant Speedvac spd111v (Thermo Fisher Scientific) and lipid pellets stored under argon gas at -20°C. Lipid pellets were reconstituted in methanol:choloroform:ammonium hydroxide (90:10:1.25, v/v/v) immediately prior to measurement. MS analysis was performed with a triple quadrupole/linear ion trap instrument model 4000 QTRAP (AB SCIEX) equipped with a TriVersa NanoMate (Advion Biosciences) robotic nanosource for automated sample injection and spraying. Lipid species were quantified by multiple reaction monitoring in positive/negative ion mode. Collision energy settings employed were as follows: 50 eV/45 eV (PC/SM), 35 eV (PE), -35 eV (PS), -60 eV (PI) and -35 eV (Cer). Addition of lipid standards was based on the amount of DNA in each sample (nmol/µg DNA) and comprised PC25:0, PC43:6, LPC13:0, LPC17:1, SM d18:1/12:0, PE25:0, PE43:6, LPE13:0, LPE17:1, PS25:0, PS31:1, PS37:4, PS43:6, LPS13:0, LPS17:1, PI25:0, PI43:6, LPI13:0, LPI17:1, and Cer d18:1/17:0 (Avanti Polar Lipids). Cer and SM nomenclature contained the prefix d to illustrate the number of hydroxyl groups in the alkyl chain, which consisted of dihydroxy sphingoid bases[37]. PL summary groups represented the total contributions of two combined fatty acyl chains containing no unsaturation (SFA), one unsaturation (MUFA) or multiple unsaturation (PUFA).

3.6 Arachidonic acid containing phospholipids

To investigate the possible abundance of arachidonic acid (AA) in the PL profiles of murine peritoneal macrophages harvested after treatment with control PBS or various MAs, we based ourselves on the results from a recent publication that employed MS-based lipidomic analyses for identifying the most abundant AA-containing PL species in murine peritoneal macrophages[38]. Of the 23 AA-containing PL species recorded in resting murine peritoneal macrophages by Gil-de-Gómez and team[38], we matched their data with results from our study and identified 15 corresponding PL species that most likely contain AA. These plausible AA-containing PL species were then compared among treatments in the current study.

3.7 Statistical analyses

MS data were corrected for carbon isotope distribution and differences in ionisation efficiency due to chain length. Data were normalised based on the amount of DNA and only lipid species with a 5-fold intensity above blank values were included in analyses. Similarities in the quantitative (nmol/µg DNA) lipid species profiles were assessed by SIMPER (similarity percentage) to identify those species responsible for distinguishing among treatments. Influential lipid species consisted of those contributing at least 75% to dissimilarity among macrophage populations. A one-way ANOSIM (analysis of similarity with treatment as factor) was used to determine if differences among groups were statistically significant (Euclidian similarity matrix; 10,000 permutations). ANOSIM output was reported as an R value and an associated significance (P) value. R values ranged from one (dissimilarity) to zero (similarity) with negative values seldom reported. ESI-MS/MS output was derived from two independent biological experiments that each comprised pooled murine F4/80$^+$ macrophages from ten individual C57BL/6 mice (n = 2 independent experiments, n = 20 mice; αMA n = 10 mice). MS data were analysed with custom made RALP 4.0 software.

All other analyses were performed with PAST 3.0[39] and IBM SPSS Statistics 23 (IBM, Chicago IL, USA).

4. Results

4.1 Glycerophospholipids

PL species analysed were denoted by the number of carbon atoms in both fatty acyl chains, followed by their combined number of double bonds. ESI-MS/MS recorded 47 to 56 individual PL species contributing to the total phosphatidylcholine (PC), -ethanolamine (PE), -inositol (PI) and -serine (PS) content of murine F4/80$^+$ peritoneal macrophages (Supplementary Fig. S2-S5). PC comprised a larger portion of the total PL fraction in macrophages from the mMA treated mice (59.8%) compared to the other treatments (32-39%; Table 1). PE and PI each contributed <20% to the total PL content in cells from all treatments. PS ranged from 33 to 37% of total PL content, but was reduced in macrophages from mMA treated mice (~22%). In comparison to placebo (PBS) treated mice, macrophages from the MA mix treated mice contained 3- to 4-fold more PL content of all four head groups. Quantitatively, mMA contributed most to the increase in typical outer leaflet PL (PC) observed in macrophages, while kMA contributed most to the increases in the classical inner leaflet PS, PI and PE (Table 1).

Upon comparing the relative abundance of PL species belonging to the saturated, monounsaturated and polyunsaturated summary groups among the macrophage populations of the variously treated mice (Fig. 2A-C), it was observed that lipid species containing saturated acyl chains (SFA) associated mainly with PC, polyunsaturated species (PUFA) mainly with PS, and monounsaturated species (MUFA) equally among PC and PS. mMA treatment stimulated more SFA in PC and MUFA in PC and PS, while kMA steered more towards PUFA in PS and PE. In addition, the global lipidomic profiles consisting of all

measured lipid species were assessed by SIMPER analysis to identify the most influential species contributing at least 75% to cumulative dissimilarity among the groups. The influential species were assessed in conjunction with the relative abundance of global species from the three unsaturation summary fractions (Fig. 2D-G, Supplementary Table S1). The MA mix and kMA elicited much more PC, PE, PI and PS synthesis than αMA, but mMA only elicited the synthesis of PC in a pronounced way. For the PC lipid class these were mostly species comprised of 36 carbon atoms combined with one to four unsaturations (Fig. 2D). Multivariate one-way ANOSIM on quantitative data showed that PBS treatment data were dissimilar to that of the MA mix and kMA treatments across PL fractions ($R > 0.75$, $P < 0.01$; Supplementary Table S1). Cells from the oxygenated mMA and kMA treatments were dissimilar in all PL profiles ($R > 0.5$, $P < 0.01$). PL signatures of kMA cells significantly varied from the αMA lipid species ($R > 0.75$, $P < 0.01$). The relative up- and downregulation of PL species in each class was compared between cells from the oxygenated MA treatments to that of the αMA (Fig. 2H, Supplementary Fig. S6-S9). Signatures of PC, the PL predominantly associated with the outer leaflet, were entirely upregulated in cells from the oxygenated MA treatments relative to αMA. Macrophages from the kMA treated mice exhibited respectively 30%, 50% and 80% more upregulation of PI, PS and PE PL species that are primarily associated with the inner leaflet, compared to those from mMA treated mice (Fig. 2H).

Table 1 | Composition of the major glycerophospholipids, lysophospholipids and sphingolipids of murine F4/80$^+$ peritoneal macrophages. The relative contributions (%) of the major head groups to total phospholipid and lysophospholipid content are given for macrophage populations from mice treated with placebo (PBS) or the various mycolic acids (MA). The quantitative contributions to each of the major phospholipid and lysophospholipid head group classes (nmol/µg DNA) are also provided. Phospholipid ratios represent total monounsaturated to saturated lipid species (MUFA/SFA), total polyunsaturated to saturated lipid species (PUFA/SFA), and total phosphatidylcholine to phosphatidylethanolamine lipid species (PC/PE). Total fatty acids (FA), contribution of all lipid species within a lipid category. ESI-MS/MS data are from two independent experiments each comprising pooled F4/80$^+$ macrophages from multiple mice (n = 10; mean ± SEM). PI, phosphatidylinositol; PS, phosphatidylserine.

	Control groups		*Main MA classes (oxygenated*)*		
	PBS	**MA mix**	**αMA**	**kMA***	**mMA***
Phospholipids					
PC (%)	37.1	38.9	32.6	37.6	59.8
PE (%)	10.7	13.9	12.6	12.3	6.8
PI (%)	16.0	14.1	19.1	13.3	10.4
PS (%)	36.2	33.2	35.7	36.8	22.9
Phospholipid species (nmol/µg DNA)					
PC	75.7 ± 18.8	264.4 ± 27.0	97.1	231.0 ± 0.5	271.8 ± 38.7
PE	21.9 ± 2.0	94.1 ± 3.6	37.7	75.6 ± 7.3	31.0 ± 11.1
PI	32.6 ± 0.1	95.5 ± 6.3	56.9	81.8 ± 1.2	47.4 ± 7.7
PS	73.8 ± 13.6	225.2 ± 49.7	106.5	225.7 ± 0.8	104.1 ± 17.3
Total FA	204.0 ± 30.5	679.1 ± 46.6	298.1	614.1 ± 7.5	454.4 ± 7.4
MUFA/SFA ratio					
PC	0.6	1.1	0.9	1.1	1.2
PE	2.1	4.2	2.4	4.3	3.7
PI	0.7	1.6	0.7	1.9	1.6
PS	3.4	3.7	3.0	4.4	4.6
PUFA/SFA ratio					
PC	1.9	2.7	1.6	2.7	2.8
PE	10.9	25.2	14.5	24.6	18.1
PI	8.9	24.7	11.2	22.7	17.0
PS	14.0	14.1	10.7	15.8	12.0
PC/PE ratio	3.5	2.8	2.6	3.1	8.8
Lysophospholipids					
lysoPC (%)	45.5	50.7	59.6	64.1	77.7
lysoPE (%)	8.9	10.0	4.8	8.0	2.6
lysoPI (%)	21.9	15.4	12.6	10.8	7.7
lysoPS (%)	23.7	23.9	23.0	17.1	12.0
Lysophospholipid species (nmol/µg DNA)					
lysoPC	57.2 ± 13.9	83.2 ± 16.6	88.6	157.8 ± 16.7	176.5 ± 17.7
lysoPE	11.2 ± 3.0	16.3 ± 0.2	7.1	19.7 ± 2.9	6.0 ± 1.0
lysoPI	27.4 ± 5.6	25.3 ± 0.1	18.6	26.6 ± 0.7	17.4 ± 0.4
lysoPS	29.7 ± 2.5	39.3 ± 0.8	34.1	42.0 ± 2.1	27.3 ± 1.5
Total FA	125.5 ± 20.0	164.1 ± 15.6	148.4	246.0 ± 22.4	227.3 ± 14.7
Sphingolipids					
Ceramide species (pmol/µg DNA)					
Total FA	123.7 ± 12.2	218.5 ± 7.9	132.2	227.2 ± 35.1	271.3 ± 1.0
Sphingomyelin species (nmol/µg DNA)					
Total FA	63.1 ± 14.3	105.6 ± 6.2	71.5	106.9 ± 1.6	115.2 ± 10.9

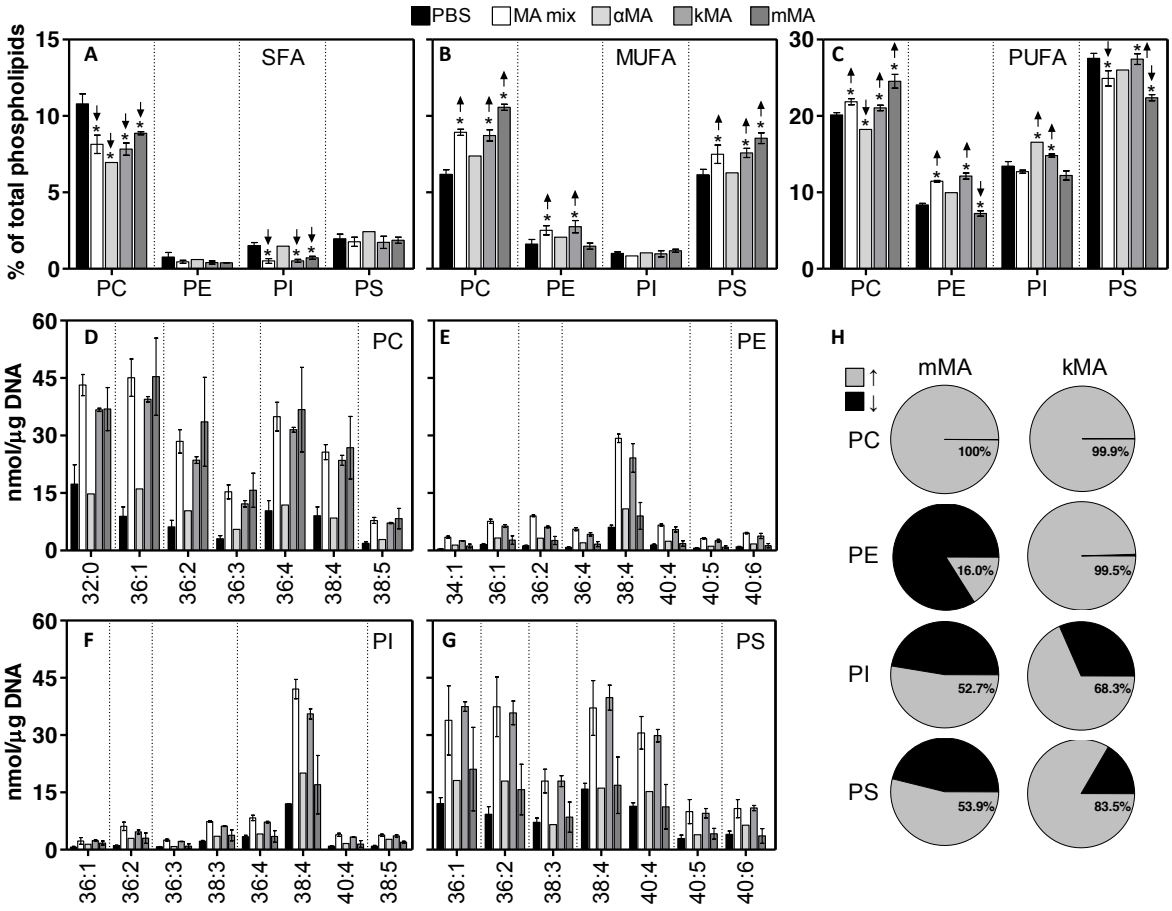

Figure 2 | Glycerophospholipid profiles of murine peritoneal macrophages. Mice were treated with placebo (PBS) or the various mycolic acids (MA) and F4/80$^+$ peritoneal macrophages isolated from total peritoneal exudate cells. The major glycerophospholipid species within each macrophage population were then quantified by ESI-MS/MS. (A-C) Shown for each of the major head group classes, the relative contributions (%) to total phospholipids of saturated lipid species (A) or those with one unsaturation (B) or multiple unsaturations (C). For each treatment, the sum of all bars equals 100%. Significant variation was assessed by an independent samples Kruskal-Wallis test (n = 9 per head group, df = 19) for the saturated (SFA: H = 34.324, $P < 0.05$), monounsaturated (MUFA: H = 34.838, $P < 0.05$) and polyunsaturated (PUFA: H = 34.733, $P < 0.05$) lipid species. (D-G) Quantitative abundance (nmol/µg DNA) of the influential lipid species within the various phospholipid classes. Influential lipid species were identified using SIMPER and significant differences assessed by one-way ANOSIM with post hoc pairwise comparisons (Supplementary Table S1). Lipid species are ranked based on the number of unsaturations and total carbon number of two combined fatty acyl chains. Data are given as mean ± SEM. (H) Proportional contributions are given for the number of phospholipid species (in each head group) of macrophages from mMA- or kMA-treated mice that increased (grey) or decreased (black) relative to cells from the unoxygenated αMA treatment. Data represent relative $\log_2$ change in absolute abundance and indicated values are the proportional upregulation of total lipid species within each phospholipid class (Supplementary Fig. S1-S4). Data are from duplicate experiments (n = 2).

4.2 Arachidonic acid-containing phospholipids

Of the fifteen corresponding PLs species that most likely contain AA (20:4) in this study, the five most abundant species were PC36:4 (indicative of 16:0/20:4), PC38:4 (indicative of 18:0/20:4), PE38:4 (indicative of 18:0/20:4), PI38:4 (indicative of 18:0/20:4) and PS38:4 (indicative of 18:0/20:4) (Fig. 3). MA mix stimulated synthesis or uptake of all these PL species in comparison to placebo (PBS) treatment (Fig. 3). The major contributor to this seemed to be kMA. Besides elevation in the PC species 36:4 and 38:4, hardly any increase in inner leaflet-associated PL species most likely containing AA was observed in cells from mice treated with mMA.

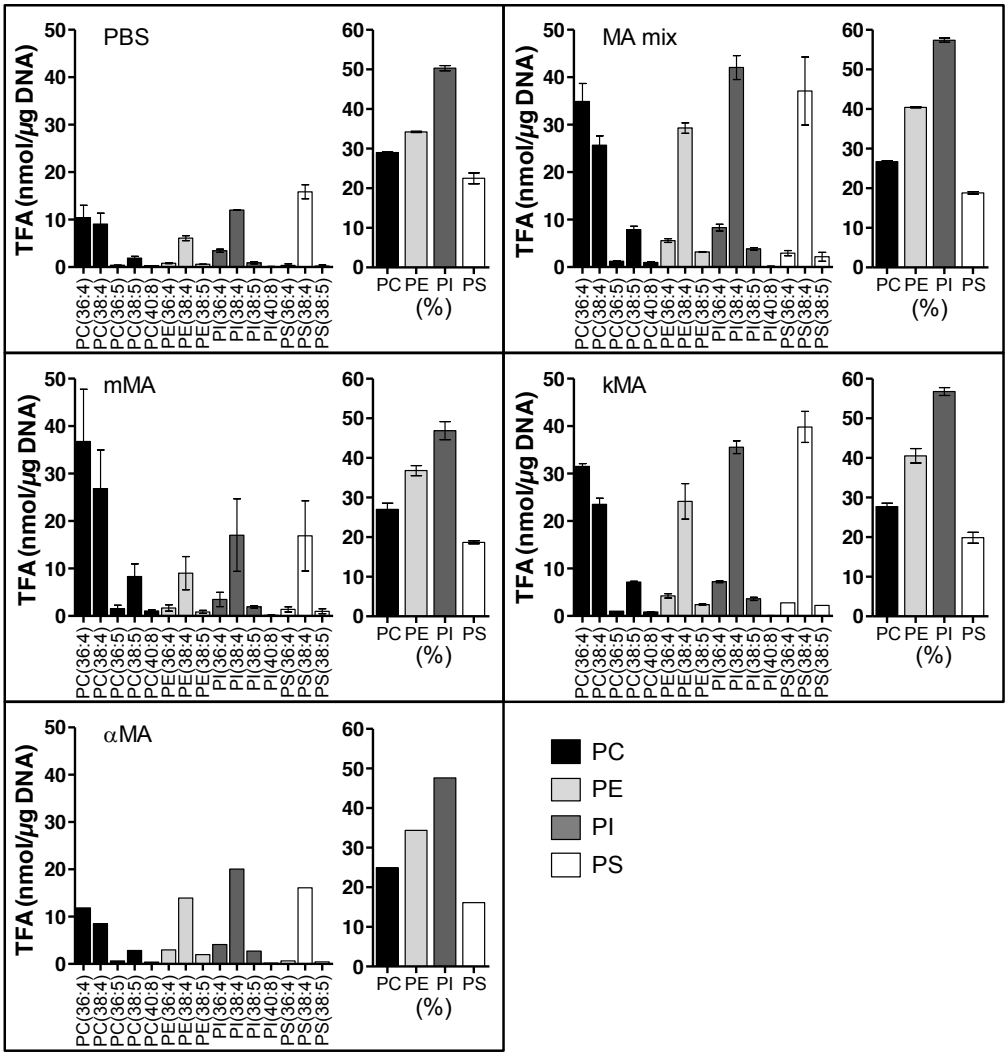

Figure 3 | Murine peritoneal macrophage profiles of glycerophospholipids likely containing arachidonic acid (AA). The profiles of the glycerophospholipid species most likely containing AA (20:4) are given for individual F4/80^{+} peritoneal macrophage populations (nmol/μg DNA; mean ± SEM). Phospholipid summary bars show proportional contributions of likely AA-containing species to each phospholipid class (%). PC, phosphatidylcholine (black); PE, phosphatidylethanolamine (light grey); PI, phosphatidylinositol (dark grey); PS, phosphatidylserine (white).

4.3 Lysophospholipids

A total of 13 to 27 LPL species contributed to the lysophosphatidylcholine (lysoPC), -ethanolamine (lysoPE), -inositol (lysoPI) and -serine (lysoPS) content of murine F4/80$^+$ peritoneal macrophages (Supplementary Fig. S10-S13). The relative contribution of lysoPC to total LPL content was the largest for cells from mice treated with mMA (~77%) followed by kMA (~64%) and the αMA, MA mix and PBS treatments (45-59%; Table 1). As a consequence, levels of lysoPE in cells from mice treated with mMA (2.6%) were clearly lower in comparison to all other groups (5-10%). MA mix treatment did not induce noteworthy LPL changes in macrophages compared to placebo (PBS) treatment (Fig. 4A-G, Table 1). Individual kMA and mMA, however, strongly induced lysoPC PLs with saturated and unsaturated aliphatic chains (Fig. 4A-C). In particular, lysoPC lipid content was comparable between kMA and mMA cells, but was up to 2-fold enriched relative to αMA cells (Fig. 4D). LysoPC is an export immune signaller. This may implicate that kMA and mMA as individual synthetic substances may be bioactive in the body.

The influential fatty acids within each of the LPL classes were determined by SIMPER (Fig. 4D-G, Supplementary Table S2). Multivariate one-way ANOSIM on quantitative data showed that cells from kMA and mMA treatments had similar lysoPC signatures ($R = 0.25$, $P < 0.05$), but different lysoPE, lysoPI or lysoPS profiles ($R = 1$, $P < 0.01$). The lysoPC content of cells from the oxygenated MAs was distinct from all other treatments ($R = 1$, $P < 0.01$; Supplementary Table S2). LPLs of cells from mice treated with unoxygenated αMA were distinct from the oxygenated MAs ($R = 1$, $P < 0.01$), but not lysoPE and lysoPI from mMA cells ($R < 0.25$, $P < 0.01$). Relative to the unoxygenated αMA, all lysoPC signatures were upregulated in cells from the oxygenated MA treatments (Fig. 4H, Supplementary Fig. S14-S17). While less than 45% of species were downregulated in kMA cells, downregulation in

global levels of lysoPE (76.0%), lysoPI (60.9%) and lysoPS (70.4%) was recorded in cells from mice treated with mMA (Fig. 4H).

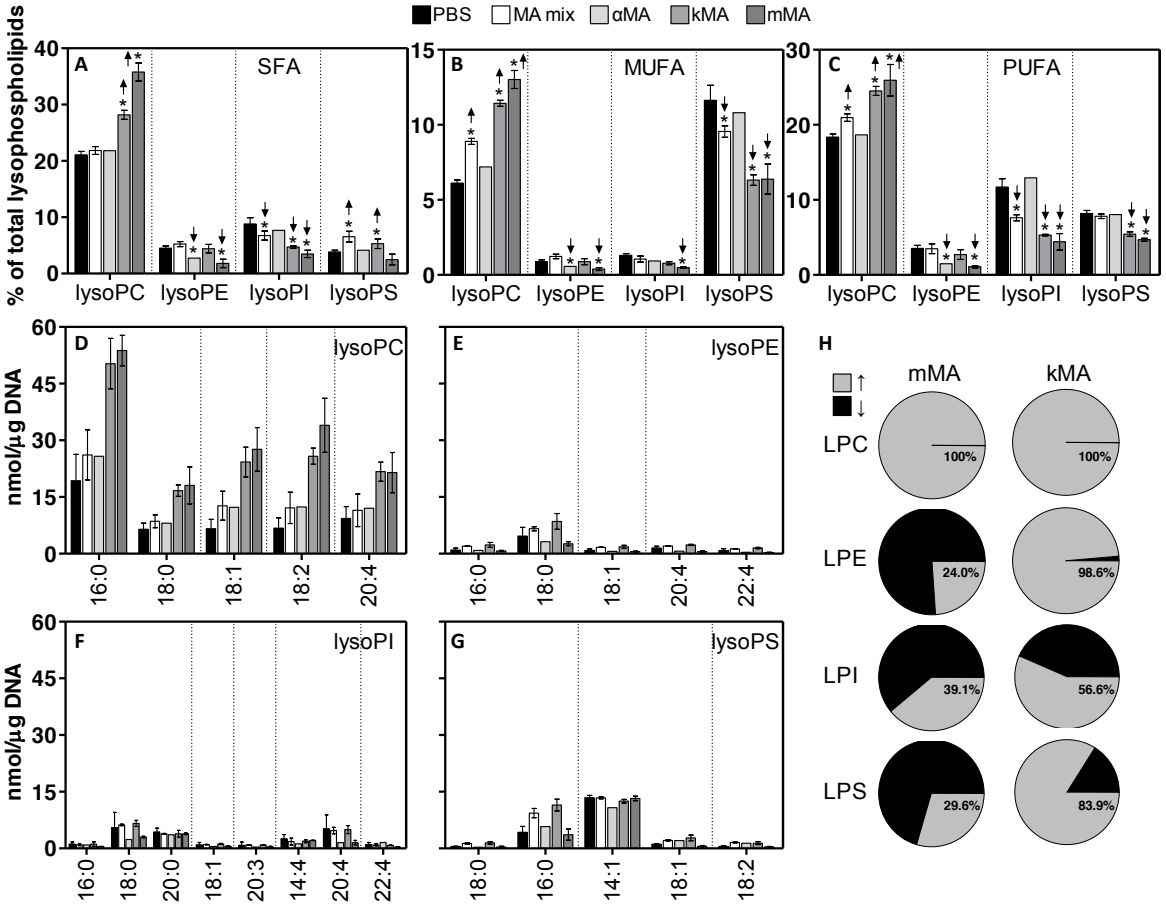

Figure 4 | Lysophospholipid profiles of murine peritoneal macrophages. (A-C) Shown for each of the major head group classes, the relative contributions (%) to total lysophospholipids of saturated lipid species (A) or those with one unsaturation (B) or multiple unsaturations (C). For each treatment, the sum of all bars equals 100%. Significant variation was assessed by an independent samples Kruskal-Wallis test (n = 9 per head group, df = 19) for the saturated (SFA: H = 34.235, $P < 0.05$), monounsaturated (MUFA: H = 34.789, $P < 0.05$) and polyunsaturated (PUFA: H = 34.610, $P < 0.05$) lipid species. (D-G) Quantitative abundance (nmol/µg DNA) of the influential lipid species within the various lysophospholipid head groups. Influential lipid species were identified using SIMPER and significant differences assessed by one-way ANOSIM with post hoc pairwise comparisons (Supplementary Table S2). Lipid species are ranked based on the number of unsaturations and total carbon number of each fatty acyl chain. Data are given as mean ± SEM. (H) Proportional contributions are given for the number of lysophospholipid species (in each head group) of macrophages from mMA- or kMA-treated mice that increased (grey) or decreased (black) relative to cells from the unoxygenated αMA treatment. Data represent relative $\log_2$ change in absolute abundance and indicated values are the proportional upregulation of total lipid species within each lysophospholipid class (Supplementary Fig. S5-S8). Data are from duplicate experiments (n = 2).

4.4 Sphingolipids - ceramide and sphingomyelin

Lipidomic analyses identified 38 Cer and 21 SM lipid species contributing to the sphingolipid content in murine F4/80$^+$ peritoneal macrophages (Supplementary Fig. S18-S19). The 18-carbon sphingoid base of all Cer species consisted of *N*-acylsphingosine (d18:1). SM comprised, in addition to species containing one to four unsaturations in the 18-carbon alkyl chain, species with *N*-acylsphinganine (d18:0, dihydroceramide) backbones, dihydrosphingomyelins. Compared to macrophages from placebo (PBS) treated mice, cells from the MA mix treatment were enriched in sphingolipid content (Table 1). Total Cer and SM species were up to 3-fold higher in cells from mice treated with the oxygenated MAs relative to unoxygenated αMA. SIMPER analysis identified the influential lipid species (Fig. 5A,E; Supplementary Table S3). mMA induced more Cer and SM with saturated acyl chains, compared to kMA that induced these with a higher degree of unsaturation (Fig. 5B). Using quantitative data, ANOSIM analysis showed that cells from the oxygenated MA treatments were dissimilar to each other and to the unoxygenated αMA in all sphingolipid species (R > 0.5, P < 0.01; Supplementary Table S3). Cer and SM lipid species were >93% upregulated in cells from the kMA and mMA treatments, measured against the unoxygenated αMA (Supplementary Fig. S20-S21). Peritoneal macrophages from variously treated mice consisted of C12 to C26 acyl chain Cer species (Fig. 5C), including saturated Cer species from 16 to 26 carbons (Fig. 5D). In comparison to PBS treated control mice, cells from mice that were treated with MA mix were enriched in mainly C16 and C24 Cer species (Fig. 5C), but mostly the C16 saturated species (Fig. 5D). The enrichment shown for cells from the MA mix treated mice was mimicked by the oxygenated mycolates with kMA inducing Cer levels similar to the MA mix treatment, and mMA inducing even higher levels than the MA mix. MA mix treatment also induced ~4-fold more SM lipid species with dihydroceramide (saturated) backbones, of which kMA was the main contributor, as compared with placebo

treatment (Fig. 5E). Macrophages from mice treated with unoxygenated αMA failed to substantially upregulate any of the recorded Cer or SM species (Fig. 5).

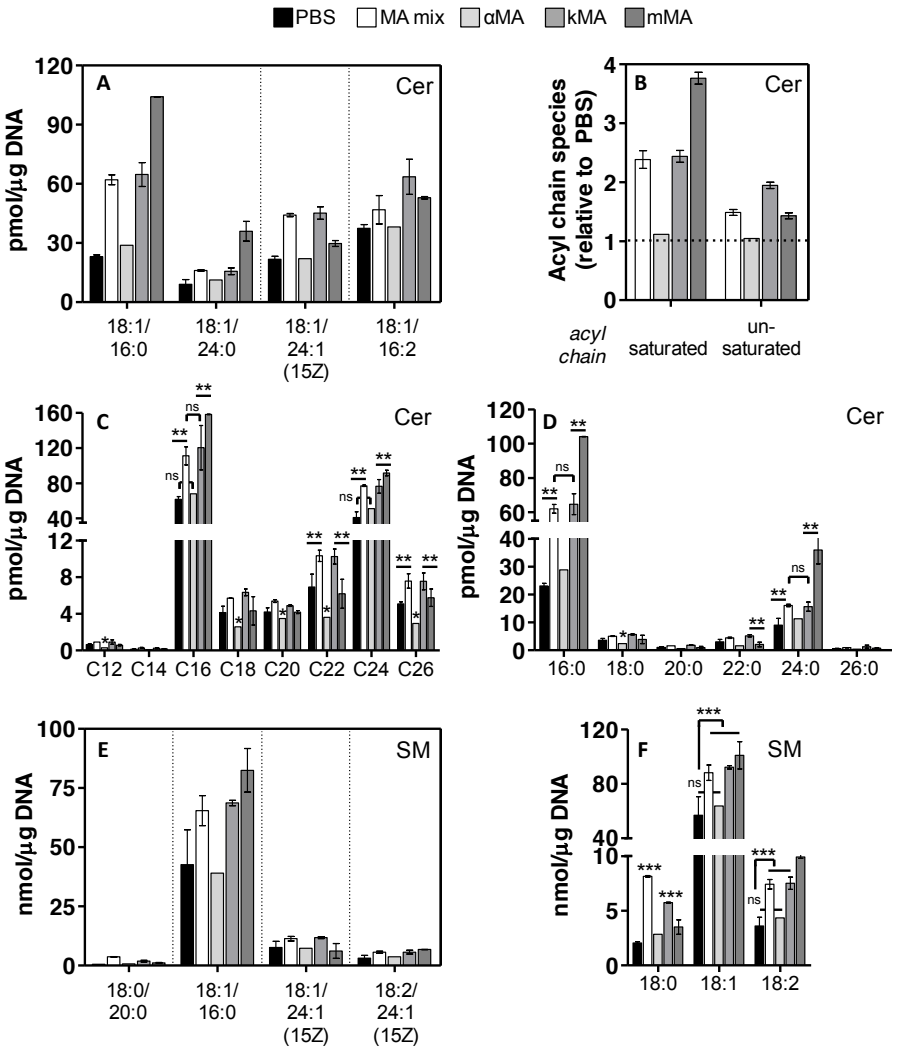

Figure 5 | Sphingolipid profiles of murine peritoneal macrophages. (A, E) Quantitative abundance of the ceramide (Cer, pmol/µg DNA) and sphingomyelin (SM, nmol/µg DNA) influential lipid species within the different murine F4/80$^+$ macrophage populations. Influential lipid species were identified using SIMPER and significant differences assessed by one-way ANOSIM with post hoc pairwise comparisons (Supplementary Table S3). Cer and SM species contained dihydroxy sphingoid bases consisting of 18 carbons in the alkyl chain with either a single (Cer) or zero to four (SM) unsaturations. Lipid species are ranked firstly according to the number of double bonds in the sphingoid base alkyl chain, followed by the number of carbon atoms and unsaturations of the amide-linked fatty acid. (B) Relative induction of Cer lipid species containing a saturated or unsaturated fatty acyl chain as compared to placebo (PBS, broken line). (C-D) Acyl chain and saturated acyl chain profiles of the amide-linked fatty acid of Cer species. Differences are shown for F4/80$^+$ peritoneal macrophages (pmol/µg DNA) in all Cer acyl chain lengths (C) and how the saturated acyl chain lengths are represented (D). (F) Profiles of the SM dihydroxy sphingoid base with zero to two unsaturations in the alkyl chain. Significant differences were determined using independent-samples Kruskal-Wallis tests with pairwise comparisons for Cer acyl chain (H = 133.301, P < 0.001, n = 76 per treatment, df = 39), Cer saturated acyl chain (H = 51.642, P < 0.01, n = 12 per treatment, df = 29) and SM sphingoid base alkyl chain unsaturation groups (H = 35.803, P < 0.01, n = 36 per treatment, df = 14). Cer species: medium-chain (C12), long-chain (C14, C16, C18 and C20), very long-chain (C22, C24 and C26). Data are from duplicate experiments (n = 2) given as mean ± SEM.

5. Discussion

Considering the key importance of the MAs in the mycobacterial cell envelope for virulence[16, 40-42], our lipidomic analyses of macrophages from MA-treated mice aimed to identify the role that various MA classes may play in the establishment of TB through lipid signalling. Employing ESI-MS/MS, we assessed peritoneal macrophages from C57BL/6 mice isolated two days after *in vivo* treatment with MAs. We identified 13 to 56 distinct molecular species across ten lipid categories and highlighted differential steering of lipid homeostasis by MA. The main findings of the current study are that relative to placebo treatment, macrophages from mice treated with the natural mixture of MAs showed greater than 3-fold increases in all of the four main PL fractions, pronounced eicosanoid potential and ~2-fold more sphingolipid content. Hardly any variation was recorded between the macrophage lipidomes from the placebo and αMA treatments. Lipidomics analysis further demonstrated that individual oxygenated kMA or mMA treatment stimulated global PL synthesis and PL species likely containing AA, lysoPC induction of species with saturated and unsaturated aliphatic chains, as well as substantial sphingolipid generation. It is important to note that many of the lipid stimulating effects induced by MA mix treatment can be explained by its relative composition of unoxygenated to oxygenated MA classes. Though unoxygenated αMA predominates with a fixed ratio of ~53% of total natural Mtb MA[22], its abundance did not compensate for the lack of distinct PL or sphingolipid inducing activity recorded in this study. This supports the inflammatory "neutral" characteristic of αMA[17]. Oxygenated MAs make up the other ~47% of the composition of the natural Mtb MA[22], but ratios of mMA to kMA classes are variable depending on the growth stage of the bacilli[42-44]. Individual oxygenated MA treatment did both exhibit pronounced lipid synthesising activity, but dissimilarity in lipidome profiles between macrophages from mice treated with the two oxygenated mycolate compounds was recorded.

Our lipidomics results relate to a differential induction by MAs of granuloma foam cell phenotypes. Using light and laser-scanning-confocal microscopy, we show in Chapter III of this thesis that MA structure influences the induction of granuloma-associated macrophage populations, intracellular cholesterol accumulation and mycobacterial growth. Whereas mMA effected enlarged multi-vacuolar foam cell formation and kMA induced abundant intracellular LDs that were rich in esterified cholesterol, αMA had no notable effects. Results from this study thus show that macrophages from mice treated with mMA contained abundant PC comprising ~60% of the total PL content with a ~3-fold higher PC/PE ratio, associated with outer (convexed) membrane vacuole formation[45]. Cells from kMA-treated mice were rich in PC, PE and PS, associated with inner (concaved) leaflet intracellular LDs[45]. Vacuoles are PL bilayer enveloped structures derived from the ER or the plasma membrane, while LDs come about by fat and cholesterol accumulation in between the leaflets of the double layered PL structure of the ER, budding off as LDs enveloped by a protein impregnated PL monolayer. The PL composition determines the LD-proteome that is taken from the ER, and which provides particular metabolic functions for the types of LDs found in different cell types[46]. Therefore, macrophage populations from kMA and mMA treated mice may have very different biochemical functions, beside their phenotypic differences, indicated by their LD and vacuolar traits. Altered PC/PE ratios have been shown to influence the membrane potential and integrity of hepatocytes, steering inflammation and disease progression from steatosis to steatohepatitis in a murine model of liver disease[47]. The decrease in relative abundances of saturated lipid species versus elevation in monounsaturated species observed for the oxygenated MA treatments, might imply activation of the expression of enzymes involved in fatty acid desaturation such as stearoyl-CoA desaturase 1, the enzyme that converts saturated to monounsaturated fatty acids[48]. Upregulation of PE and PS polyunsaturated species with four to six unsaturations by kMA treatment, furthermore suggests an increase in enzymes involved in fatty acyl chain

elongation such as the fatty acid elongase subtypes (ELOVL 1-7)[48]. The propensity towards elevated PC in macrophages from the mMA treatment, but comprehensively elevated PC/PE/PS in kMA macrophages indicates different lines of maturation of intracellular lipid structures. This may be driven by divergent enzymatic activities along the *de novo* generation pathways, as distinct downregulation of species by mMA in the PE and PS components was also noted. The fine regulation of the differential species composition of the various PLs is remarkable, and indicates pronounced MA induced differences of kinase, acyltransferase or synthase in the endoplasmic reticulum (ER) between the macrophage populations[49, 50].

An important antimicrobial defence and immunoregulatory mechanism that is mediated by lipid pathways in the macrophage is the generation of various eicosanoids derived from AA (20:4)[51-53]. AAs are found esterified to various PLs in especially LDs, but also in nuclear and cytoplasmic membranes[53-55]. Eicosanoid potential was induced by oxygenated MA treatment, mMA associated with PC and kMA with PS and PE. None of the three individual MA types could simulate the potential eicosanoid inducing activity of the natural MA mixture, but kMA had a stronger effect, mMA weaker, and αMA hardly had any effect. This implies synergistic activity of the mMA and kMA classes when combined as it occurs in nature, and testifies to the strong potential of Mtb MA in manipulating host cells towards establishing TB, or triggering of host cells into effective anti-mycobacterial defence. Indeed, in the case of TB it was demonstrated how manipulation of the levels of the eicosanoid prostaglandin E_2 could enhance pathogen survival in a mammalian model of pulmonary Mtb infection[56]. Another example is the demonstration of the fine balance of the eicosanoids Lipoxin A_4 and Leukotriene B_4 for optimal protection in TB[57]. As a result of the potent biological activity of AA, levels are tightly controlled through the activity of phospholipase A $(PLA)_2$ and LPL-acyltransferases that regulate the membrane PL cycle of deacylation-reacylation[58]. In resting cells, reacylation is dominant over deacylation and the majority of AA is esterified to

membrane PLs whilst free AA levels remain small. Activated immune cells react to agonists or pathogenic stimuli by remodelling membrane lipid composition and metabolism, releasing stores of AA and other key lipid intermediates[54, 55, 59].

LPLs may accumulate in significant quantity in LDs[60, 61]. Following insult or cell activation, PLA-mediated PL hydrolysis generates LPLs that may exert diverse biological functions through specific G-protein coupled receptors[62, 63]. LPLs containing PC and PS head groups can stimulate NADPH oxidase and calcium ion mobilisation in activated phagocytes[64, 65]. Translocation and assembly of the membrane-bound NADPH oxidase enzyme complex by activated immune cells is dependent on AA availability, and primarily produces superoxide anion[66]. MA mix treatment did not induce prominent upregulation of LPL species relative to the PBS control, but macrophages from mice treated with either of the individual oxygenated MAs more than doubled their lysoPC content and all measured acylated species were upregulated relative to αMA. Here, the predominance of the αMA class in the MA mix treatment may be responsible for its absence of LPL-stimulating activity, as individual αMA also failed to induce significant LPL generation. LysoPC is a proinflammatory lipid mediator reportedly involved in macrophage activation[67]. As one of several antigenic lipids bound by natural killer T (NKT) cells through the nonclassical antigen-presenting molecule CD1d, lysoPC elicited IFNγ cytokine release upon exposure to antigen presenting cells expressing CD1d[68, 69], suggesting involvement in Th1 proinflammatory steering. Downregulation in relative abundances of unsaturated lysoPS in macrophages from both kMA and mMA treated mice was observed. LysoPS stimulates the Th2 type activity of mast cell degranulation specifically through the serine group, mainly when the associated acyl is unsaturated[63]. Its downregulation by the two oxygenated MAs observed here would then orientate more towards the Th1 mode of response. We previously reported that the natural MA mixture

induces LD-loading in mice during foam cell differentiation and steer host cells to a proinflammatory, Th1-type mode[16].

Cer forms the anchor backbone of all sphingolipids and is delivered to the Golgi for conversion to ceramide-1-phosphate, SM, glucosylceramide or more complex glycosphingolipids[70]. Beyond a structural function, bioactive Cer derivatives largely mediate anti-proliferative effects such as caspase induction, cytochrome release and apoptosis in response to stress or injury stimuli[71, 72]. They also form important precursors for innate signalling metabolites[73]. The balance among autophagy, apoptosis and necrosis plays a crucial role in the pathogenicity of Mtb. Necrosis is a strategy whereby virulent Mtb evades host defences while under pathophysiological conditions, autophagy facilitates antigen presentation[74, 75]. Autophagy is also a key process regulating the turnover of cellular nutrients and lipid metabolism[76]. Here we showed that oxygenated MAs, but not αMA, significantly stimulated the production of Cer and SM with mMA having the stronger effect. mMA induced more Cer and SM with saturated acyl chains, compared to kMA that induced these with a higher degree of unsaturation. Notably, the C16 and C24 acyl chain containing species are elicited in substantial quantity. Rise in endogenous levels of saturated C16 fatty acyl Cer species in particular is strongly associated with induction of apoptosis in cultured, primary and cancer cells[77]. In contrast evidence exists that dihydroceramide, which is present in low cellular abundance, counteract Cer-induced cell death[75]. Notwithstanding the anti-proliferative effects of both saturated and desaturated Cer, dihydroceramides steer towards autophagy whereas Cer induces apoptosis[75]. Apoptosis is an important antimicrobial defence mechanism by which Mtb-infected macrophages liberate bacilli for phagocytic clearance and antigen presentation to stimulate adaptive T cell immunity[74, 78]. In this work we did not record any Cer lipid species with sphinganine backbones, but dihydrosphingomyelins were observed in small quantity. MA mix treatment induced in macrophages ~4-fold the amount of

dihydrosphingomyelin present in control (PBS) cells. Compared with the neutral αMA, kMA stimulated substantially higher levels of dihydrosphingomyelin than mMA. The induction of ~40% more 16:0 Cer by the proinflammatory mMA, likely triggering a proapoptotic host defence, versus stimulation of dihydroceramide-containing SM species by kMA, suggests an interesting and divergent mechanism by which Mtb bacilli could manipulate the host environment. Could it be that stimulation of SM species containing dihydroceramide bases represent a strategy through which Mtb bacilli allow fusion of LDs with vacuoles? It certainly seems plausible that kMA treatment inducing cholesterol ester accrual is able to induce autophagy whereas mMA is not. Interestingly, glycosphingolipids that contain a sugar moiety linked to its sphingoid base are important inducers of Th1 immunity signalling through the CD1d receptor of NKT cells[79]. In this study we did not investigate the presence or absence of sugars among the sphingolipid species; nevertheless, it certainly would provide valuable information for future study regarding steering of immunity by the various MA classes.

6. Conclusion

Though recorded here for murine peritoneal macrophages as the experimental model, this study highlighted key aspects of the manifestation of TB following *in vivo* treatment with Mtb-derived chemically synthetic MAs. ESI-MS/MS measurement clearly showed that the naturally-occurring Mtb MA mixture induces substantial changes to PL and sphingolipid content in macrophage host cells. Whereas αMA treatment had negligible lipid synthesising activity, the oxygenated mMA and kMA divergently steered macrophage lipidomes. PC enrichment was associated with macrophages from the mMA treatment, which mainly induced Cer and SM species containing saturated fatty acyl chains. Macrophages from kMA treatment were rich in PC, PE and PS and primarily stimulated sphingolipids with unsaturated fatty acyls. Macrophage lipidomes from mMA and kMA treated mice firstly stimulated PL species likely containing AA, but with divergent PL head groups; and secondly were

significantly enriched in all measured lysoPC lipid species (even more so than the natural MA mixture). This may imply larger anaphylactic potential of the individual oxygenated MAs that is ameliorated when the oxygenated MA is partnered with αMA as they occur in nature. The differential induction by mMA and kMA of host PL species associated with respectively vacuole and LD containing granuloma cell phenotypes may be correlated with steering of pro- and anti-inflammatory modes, sustained by macrophage polarising signalling lipids like eicosanoid-derived leukotrienes and prostanoids. The lipidomics evidence provided in this study thus corroborates the genetic evidence of host/pathogen coevolution of Mtb[80], wherein Mtb is shown to engage the immune response of the host for its survival. In this context, it is especially kMA that directs host cell lipid signalling for the sustenance and proliferation of Mtb. Selective secretion of various ratios of oxygenated MAs may thus steer innate immunity through the lipidome of macrophages to establish persistent TB.

7. Supplemental data

All supplemental data pertaining to this study have been compiled as an additional chapter, which is provided on a separate compact disc along with this thesis.

7.1 List of supplemental data

Table S1 | SIMPER and ANOSIM output of glycerophospholipid profiles

Table S2 | SIMPER and ANOSIM output of lysophospholipid profiles

Table S3 | SIMPER and ANOSIM output of ceramide and sphingomyelin profiles

Figure S1 | Purity of F4/80^{+} murine peritoneal macrophages

Figure S2-S5 | Profiles of phospholipid species of peritoneal macrophages from mice treated with various MAs

Figure S6-S9 | Change in absolute abundance of glycerophospholipid species

Figure S10-S13 | Profiles of lysophospholipid species of peritoneal macrophages from mice treated with various MAs

Figure S14-S17 | Change in absolute abundance of lysophospholipid species

Figure S18-S19 | Profiles of sphingolipid species of peritoneal macrophages from mice treated with various MAs

Figure S20-S21 | Change in absolute abundance of sphingolipid species

7.2 Additional experiments

Assessment of inflammation and foam cell traits following murine *in vivo* treatment with an acid sphingomyelinase inhibitor (Zoledronic acid)

Figure S22 | Flow cytometry analysis of BAL fluid samples

Figure S23 | Average total and differential BAL fluid cell counts

Figure S24 | Cytokine response of bronchoalveolar infiltrate following treatment with zoledronic acid

Figure S25 | Cytokine response of peritoneal macrophages after ZA treatment and LPS stimulation

Figure S26 | Foam cell traits of murine peritoneal macrophages following ZA treatment and LPS stimulation

Figure S27 | Confocal microscopy images of foam cell morphology after treatment with ZA

Figure S28 | Confocal microscopy images of foam cell morphology after ZA treatment and LPS stimulation

8. References

1. Favrot, L. and D. R. Ronning. 2012. Targeting the mycobacterial envelope for tuberculosis drug development.

Expert Rev. Anti Infect. Ther. **10**: 1023-1036.

2. Glickman, M. S. and W. R. Jacobs, Jr. 2001. Microbial pathogenesis of *Mycobacterium tuberculosis*: dawn of a discipline. *Cell* **104**: 477-485.

3. Cooper, A. M. 2009. Cell-mediated immune responses in tuberculosis. *Annu. Rev. Immunol.* **27**: 393-422.

4. Pieters, J. 2008. *Mycobacterium tuberculosis* and the macrophage: maintaining a balance. *Cell Host Microbe* **3**: 399-407.

5. Kumar, D. and K. V. Rao. 2011. Regulation between survival, persistence, and elimination of intracellular mycobacteria: a nested equilibrium of delicate balances. *Microbes Infect.* **13**: 121-133.

6. Anes, E., M. P. Kuhnel, E. Bos, J. Moniz-Pereira, A. Habermann and G. Griffiths. 2003. Selected lipids activate phagosome actin assembly and maturation resulting in killing of pathogenic mycobacteria. *Nat. Cell Biol.* **5**: 793-802.

7. Thompson, C. R., S. S. Iyer, N. Melrose, R. VanOosten, K. Johnson, S. M. Pitson, L. M. Obeid and D. J. Kusner. 2005. Sphingosine Kinase 1 (SK1) Is Recruited to Nascent Phagosomes in Human Macrophages: Inhibition of SK1 Translocation by *Mycobacterium tuberculosis*. *J. Immunol.* **174**: 3551-3561.

8. Hayakawa, E., F. Tokumasu, G. A. Nardone, A. J. Jin, V. A. Hackley and J. A. Dvorak. 2007. A *Mycobacterium tuberculosis*-derived lipid inhibits membrane fusion by modulating lipid membrane domains. *Biophys. J.* **93**: 4018-4030.

9. Cotes, K., C. Bakala N'goma J, R. Dhouib, I. Douchet, D. Maurin, F. Carriere and S. Canaan. 2008. Lipolytic enzymes in *Mycobacterium tuberculosis*. *Appl. Microbiol. Biotechnol.* **78**: 741-749.

10. Jackson, S. K., J. M. Stark, S. Taylor and J. L. Harwood. 1989. Changes in phospholipid fatty acid composition and triacylglycerol content in mouse tissues after infection with bacille Calmette-Guerin. *Br. J. Exp. Pathol.* **70**: 431-441.

11. Segal, W. and H. Bloch. 1955. Biochemical differentiation of *Mycobacterium tuberculosis* grown *in vivo* and *in vitro*. *J. Bacteriol.* **72**: 132-141.

12. Brzostek, A., J. Pawelczyk, A. Rumijowska-Galewicz, B. Dziadek and J. Dziadek. 2009. *Mycobacterium tuberculosis* is able to accumulate and utilize cholesterol. *J. Bacteriol.* **191**: 6584-6591.

13. Gatfield, J. and J. Pieters. 2000. Essential role for cholesterol in entry of mycobacteria into macrophages. *Science* **288**: 1647-1650.

14. de Chastellier, C. and L. Thilo. 2006. Cholesterol depletion in *Mycobacterium avium*-infected macrophages overcomes the block in phagosome maturation and leads to the reversible sequestration of viable mycobacteria in phagolysosome-derived autophagic vacuoles. *Cell. Microbiol.* **8**: 242-256.

15. Maxfield, F. R. and G. van Meer. 2010. Cholesterol, the central lipid of mammalian cells. *Curr. Opin. Cell Biol.* **22**: 422-429.

16. Korf, J., A. Stoltz, J. Verschoor, P. De Baetselier and J. Grooten. 2005. The *Mycobacterium tuberculosis* cell wall component mycolic acid elicits pathogen-associated host innate immune responses. *Eur. J. Immunol.* **35**: 890-900.

17. Vander Beken, S., J. R. Al Dulayymi, T. Naessens, G. Koza, M. Maza-Iglesias, R. Rowles, C. Theunissen, J. De Medts, E. Lanckacker, M. S. Baird and J. Grooten. 2011. Molecular structure of the *Mycobacterium tuberculosis* virulence factor, mycolic acid, determines the elicited inflammatory pattern. *Eur. J. Immunol.* **41**: 450-460.

18. Russell, D. G., P. J. Cardona, M. J. Kim, S. Allain and F. Altare. 2009. Foamy macrophages and the progression of the human tuberculosis granuloma. *Nat. Immunol.* **10**: 943-948.

19. Glickman, M. S., J. S. Cox and W. R. Jacobs, Jr. 2000. A novel mycolic acid cyclopropane synthetase is required for cording, persistence and virulence of *Mycobacterium tuberculosis*. *Mol. Cell* **5**: 717-727.

20. Jankute, M., J. A. Cox, J. Harrison and G. S. Besra. 2015. Assembly of the mycobacterial cell wall. *Annu. Rev. Microbiol.* **69**: 405-423.

21. Verschoor, J. A., M. S. Baird and J. Grooten. 2012. Towards understanding the functional diversity of cell wall mycolic acids of *Mycobacterium tuberculosis*. *Prog. Lipid Res.* **51**: 325-339.

22. Ndlandla, F. L., V. Ejoh, A. C. Stoltz, B. Naicker, A. D. Cromarty, S. van Wyngaardt, M. Khati, L. S. Rotherham, Y. Lemmer, J. Niebuhr, C. R. Baumeister, J. R. Al-Dulayymi, H. Swai, M. S. Baird and J. A. Verschoor. 2016. Standardization of natural mycolic acid antigen composition and production for use in biomarker antibody detection to diagnose active tuberculosis. *J. Immunol. Methods* **435**: 50-59.

23. Hu, C., R. van der Heijden, M. Wang, J. van der Greef, T. Hankemeier and G. Xu. 2009. Analytical strategies in lipidomics and applications in disease biomarker discovery. *J. Chromatogr. B Analyt. Technol. Biomed. Life Sci.* **877**: 2836-2846.

24. Vihervaara, T., M. Suoniemi and R. Laaksonen. 2014. Lipidomics in drug discovery. *Drug Discov. Today* **19**: 164-170.

25. Han, X. and R. W. Gross. 2003. Global analyses of cellular lipidomes directly from crude extracts of biological samples by ESI mass spectrometry: a bridge to lipidomics. *J. Lipid Res.* **44**: 1071-1079.

26. Layre, E. and D. B. Moody. 2013. Lipidomic profiling of model organisms and the world's major pathogens. *Biochimie* **95**: 109-115.

27. Milne, S., P. Ivanova, J. Forrester and H. Alex Brown. 2006. Lipidomics: an analysis of cellular lipids by ESI-MS. *Methods* **39**: 92-103.

28. Ho, C. S., M. H. M. Chan, R. C. K. Cheung, L. K. Law, L. C. W. Lit, K. F. Ng, M. W. N. Suen and H. L. Tai. 2003. Electrospray ionisation mass spectrometry: Principles and clinical applications. *Clin. Biochem. Rev.* **24**: 3-12.

29. Quehenberger, O., A. Armando, D. Dumlao, D. L. Stephens and E. A. Dennis. 2008. Lipidomics analysis of essential fatty acids in macrophages. *Prostaglandins Leukot. Essent. Fatty Acids* **79**: 123-129.

30. Buczynski, M. W., D. S. Dumlao and E. A. Dennis. 2009. Thematic Review Series: Proteomics. An integrated omics analysis of eicosanoid biology. *J. Lipid Res.* **50**: 1015-1038.

31. Norris, P. C., D. Reichart, D. S. Dumlao, C. K. Glass and E. A. Dennis. 2011. Specificity of eicosanoid production depends on the TLR-4-stimulated macrophage phenotype. *J. Leukoc. Biol.* **90**: 563-574.

32. Dennis, E. A., R. A. Deems, R. Harkewicz, O. Quehenberger, H. A. Brown, S. B. Milne, D. S. Myers, C. K. Glass, G. Hardiman, D. Reichart, A. H. Merrill, Jr., M. C. Sullards, E. Wang, R. C. Murphy, C. R. Raetz, T. A. Garrett, Z. Guan, A. C. Ryan, D. W. Russell, J. G. McDonald, B. M. Thompson, W. A. Shaw, M. Sud, Y. Zhao, S. Gupta, M. R. Maurya, E. Fahy and S. Subramaniam. 2010. A mouse macrophage lipidome. *J. Biol. Chem.* **285**: 39976-39985.

33. Gandhi, N. R., A. Moll, A. W. Sturm, R. Pawinski, T. Govender, U. Lalloo, K. Zeller, J. Andrews and G. Friedland. 2006. Extensively drug-resistant tuberculosis as a cause of death in patients co-infected with tuberculosis and HIV in a rural area of South Africa. *Lancet* **368**: 1575-1580.

34. Al Dulayymi, J. a. R., M. S. Baird and E. Roberts. 2005. The synthesis of a single enantiomer of a major α-mycolic acid of *M. tuberculosis*. *Tetrahedron* **61**: 11939-11951.

35. Al Dulayymi, J. a. R., M. S. Baird, E. Roberts, M. Deysel and J. Verschoor. 2007. The first syntheses of single enantiomers of the major methoxymycolic acid of *Mycobacterium tuberculosis*. *Tetrahedron* **63**: 2571-2592.

36. Koza, G. and M. S. Baird. 2007. The first synthesis of single enantiomers of ketomycolic acids. *Tetrahedron Lett*. **48**: 2165-2169.

37. Sullards, M. C., Y. Liu, Y. Chen and A. H. Merrill, Jr. 2011. Analysis of mammalian sphingolipids by liquid chromatography tandem mass spectrometry (LC-MS/MS) and tissue imaging mass spectrometry (TIMS). *Biochim*. *Biophys*. *Acta* **1811**: 838-853.

38. Gil-de-Gomez, L., A. M. Astudillo, C. Meana, J. M. Rubio, C. Guijas, M. A. Balboa and J. Balsinde. 2013. A phosphatidylinositol species acutely generated by activated macrophages regulates innate immune responses. *J*. *Immunol*. **190**: 5169-5177.

39. Hammer, O., D. A. T. Harper and P. D. Ryna. 2001. PAST - PAlaeontological STatistics, ver. 1.89. *Palaeontol*. *Electronica* **4**: 1-92.

40. Rao, V., F. Gao, B. Chen, W. R. Jacobs, Jr. and M. S. Glickman. 2006. Trans-cyclopropanation of mycolic acids on trehalose dimycolate suppresses *Mycobacterium tuberculosis*-induced inflammation and virulence. *J*. *Clin*. *Invest*. **116**: 1660-1667.

41. Riley, L. W. 2006. Of mice, men and elephants: *Mycobacterium tuberculosis* cell envelope lipids and pathogenesis. *J*. *Clin*. *Invest*. **116**: 1475-1478.

42. Yuan, Y., Y. Zhu, D. D. Crane and C. E. Barry, 3rd. 1998. The effect of oxygenated mycolic acid composition on cell wall function and macrophage growth in *Mycobacterium tuberculosis*. *Mol*. *Microbiol*. **29**: 1448-1458.

43. Watanabe, M., Y. Aoyagi, M. Ridell and D. E. Minniken. 2001. Separation and characterization of individual mycolic acids in representative mycobacteria. *Microbiology* **147**: 1825-1837.

44. Dubnau, E., J. Chan, C. Raynaud, V. P. Mohan, M.-A. Laneelle, K. Yu, A. Quemard, S. Smith and M. Daffe. 2000. Oxygenated mycolic acids are necessary for virulence of *Mycobacterium tuberculosis* in mice. *Mol*. *Microbiol*. **36**: 630-637.

45. van Meer, G. 2011. Dynamic transbilayer lipid asymmetry. *Cold Spring Harb*. *Perspect*. *Biol*. **3**: 1-11.

46. Pol, A., S. P. Gross and R. G. Parton. 2014. Review: biogenesis of the multifunctional lipid droplet: lipids, proteins, and sites. *J*. *Cell Biol*. **204**: 635-646.

47. Li, Z., L. B. Agellon, T. M. Allen, M. Umeda, L. Jewell, A. Mason and D. E. Vance. 2006. The ratio of phosphatidylcholine to phosphatidylethanolamine influences membrane integrity and steatohepatitis. *Cell Metab*. **3**: 321-331.

48. Guillou, H., D. Zadravec, P. G. Martin and A. Jacobsson. 2010. The key roles of elongases and desaturases in mammalian fatty acid metabolism: Insights from transgenic mice. *Prog*. *Lipid Res*. **49**: 186-199.

49. Shindou, H. and T. Shimizu. 2009. Acyl-CoA:lysophospholipid acyltransferases. *J*. *Biol*. *Chem*. **284**: 1-5.

50. Hermansson, M., K. Hokynar and P. Somerharju. 2011. Mechanisms of glycerophospholipid homeostasis in mammalian cells. *Prog*. *Lipid Res*. **50**: 240-257.

51. Norris, P. C. and E. A. Dennis. 2014. A lipidomic perspective on inflammatory macrophage eicosanoid signaling. *Adv*. *Biol*. *Regul*. **54**: 99-110.

52. Divangahi, M., D. Desjardins, C. Nunes-Alves, H. G. Remold and S. M. Behar. 2010. Eicosanoid pathways regulate adaptive immunity to *Mycobacterium tuberculosis*. *Nat*. *Immunol*. **11**: 751-758.

53. Harizi, H., J. B. Corcuff and N. Gualde. 2008. Arachidonic-acid-derived eicosanoids: roles in biology and immunopathology. *Trends Mol. Med.* **14**: 461-469.

54. Astudillo, A. M., G. Perez-Chacon, D. Balgoma, L. Gil-de-Gomez, V. Ruiperez, C. Guijas, M. A. Balboa and J. Balsinde. 2011. Influence of cellular arachidonic acid levels on phospholipid remodeling and CoA-independent transacylase activity in human monocytes and U937 cells. *Biochim. Biophys. Acta* **1811**: 97-103.

55. Balgoma, D., A. M. Astudillo, G. Perez-Chacon, O. Montero, M. A. Balboa and J. Balsinde. 2010. Markers of monocyte activation revealed by lipidomic profiling of arachidonic acid-containing phospholipids. *J. Immunol.* **184**: 3857-3865.

56. Mayer-Barber, K. D., B. B. Andrade, S. D. Oland, E. P. Amaral, D. L. Barber, J. Gonzales, S. C. Derrick, R. Shi, N. P. Kumar, W. Wei, X. Yuan, G. Zhang, Y. Cai, S. Babu, M. Catalfamo, A. M. Salazar, L. E. Via, C. E. Barry, 3rd and A. Sher. 2014. Host-directed therapy of tuberculosis based on interleukin-1 and type I interferon crosstalk. *Nature* **511**: 99-103.

57. Tobin, D. M. and L. Ramakrishnan. 2013. TB: the Yin and Yang of lipid mediators. *Curr. Opin. Pharmacol.* **13**: 641-645.

58. Perez-Chacon, G., A. M. Astudillo, D. Balgoma, M. A. Balboa and J. Balsinde. 2009. Control of free arachidonic acid levels by phospholipases A_2 and lysophospholipid acyltransferases. *Biochim. Biophys. Acta* **1791**: 1103-1113.

59. Fernandis, A. Z. and M. R. Wenk. 2007. Membrane lipids as signaling molecules. *Curr. Opin. Lipidol.* **18**: 121-128.

60. Bartz, R., W. H. Li, B. Venables, J. K. Zehmer, M. R. Roth, R. Welti, R. G. Anderson, P. Liu and K. D. Chapman. 2007. Lipidomics reveals that adiposomes store ether lipids and mediate phospholipid traffic. *J. Lipid Res.* **48**: 837-847.

61. Tauchi-Sato, K., S. Ozeki, T. Houjou, R. Taguchi and T. Fujimoto. 2002. The surface of lipid droplets is a phospholipid monolayer with a unique fatty acid composition. *J. Biol. Chem.* **277**: 44507-44512.

62. Kihara, Y., H. Mizuno and J. Chun. 2015. Lysophospholipid receptors in drug discovery. *Exp. Cell Res.* **333**: 171-177.

63. Makide, K., A. Uwamizu, Y. Shinjo, J. Ishiguro, M. Okutani, A. Inoue and J. Aoki. 2014. Novel lysophosphoplipid receptors: their structure and function. *J. Lipid Res.* **55**: 1986-1995.

64. Silliman, C. C. 2003. Lysophosphatidylcholines prime the NADPH oxidase and stimulate multiple neutrophil functions through changes in cytosolic calcium. *J. Leukoc. Biol.* **73**: 511-524.

65. Frasch, S. C., K. Z. Berry, R. Fernandez-Boyanapalli, H. S. Jin, C. Leslie, P. M. Henson, R. C. Murphy and D. L. Bratton. 2008. NADPH oxidase-dependent generation of lysophosphatidylserine enhances clearance of activated and dying neutrophils via G2A. *J. Biol. Chem.* **283**: 33736-33749.

66. Cathcart, M. K. 2004. Regulation of superoxide anion production by NADPH oxidase in monocytes/macrophages: contributions to atherosclerosis. *Arterioscler. Thromb. Vasc. Biol.* **24**: 23-28.

67. Olofsson, K. E., L. Andersson, J. Nilsson and H. Bjorkbacka. 2008. Nanomolar concentrations of lysophosphatidylcholine recruit monocytes and induce pro-inflammatory cytokine production in macrophages. *Biochem. Biophys. Res. Commun.* **370**: 348-352.

68. Fox, L. M., D. G. Cox, J. L. Lockridge, X. Wang, X. Chen, L. Scharf, D. L. Trott, R. M. Ndonye, N. Veerapen, G. S. Besra, A. R. Howell, M. E. Cook, E. J. Adams, W. H. Hildebrand and J. E. Gumperz. 2009. Recognition of lyso-phospholipids by human natural killer T lymphocytes. *PLoS Biol.* **7**: e1000228.

69. Rossjohn, J., D. G. Pellicci, O. Patel, L. Gapin and D. I. Godfrey. 2012. Recognition of CD1d-restricted antigens by natural killer T cells. *Nat. Rev. Immunol.* **12**: 845-857.

70. Maceyka, M. and S. Spiegel. 2014. Sphingolipid metabolites in inflammatory disease. *Nature* **510**: 58-67.

71. Seumois, G., M. Fillet, L. Gillet, C. Faccinetto, C. Desmet, C. Francois, B. Dewals, C. Oury, A. Vanderplasschen, P. Lekeux and F. Bureau. 2007. *De novo* C_{16}- and C_{24}-ceramide generation contributes to spontaneous neutrophil apoptosis. *J. Leukoc. Biol.* **81**: 1477-1486.

72. Uchida, Y. 2014. Ceramide signaling in mammalian epidermis. *Biochim. Biophys. Acta* **1841**: 453-462.

73. Chalfant, C. E. and S. Spiegel. 2005. Sphingosine 1-phosphate and ceramide 1-phosphate: expanding roles in cell signaling. *J. Cell Sci.* **118**: 4605-4612.

74. Divangahi, M., M. Chen, H. Gan, D. Desjardins, T. T. Hickman, D. M. Lee, S. Fortune, S. M. Behar and H. G. Remold. 2009. *Mycobacterium tuberculosis* evades macrophage defenses by inhibiting plasma membrane repair. *Nat. Immunol.* **10**: 899-906.

75. Siddique, M. M., Y. Li, B. Chaurasia, V. A. Kaddai and S. A. Summers. 2015. Dihydroceramides: From Bit Players to Lead Actors. *J. Biol. Chem.* **290**: 15371-15379.

76. Levine, B., N. Mizushima and H. W. Virgin. 2011. Autophagy in immunity and inflammation. *Nature* **469**: 323-335.

77. Grosch, S., S. Schiffmann and G. Geisslinger. 2012. Chain length-specific properties of ceramides. *Prog. Lipid Res.* **51**: 50-62.

78. Behar, S. M., C. J. Martin, C. Nunes-Alves, M. Divangahi and H. G. Remold. 2011. Lipids, apoptosis, and cross-presentation: links in the chain of host defense against *Mycobacterium tuberculosis*. *Microbes Infect.* **13**: 749-756.

79. Birkholz, A. M., A. R. Howell and M. Kronenberg. 2015. The Alpha and Omega of Galactosylceramides in T Cell Immune Function. *J. Biol. Chem.* **290**: 15365-15370.

80. Gagneux, S. 2012. Host-pathogen coevolution in human tuberculosis. *Philos. Trans. R. Soc. Lond. B Biol. Sci.* **367**: 850-859.

CHAPTER IV |

General Discussion

1. General Discussion

Paleopathological evidence classifies TB as arguably the oldest bacterial infectious disease of humans[1]. The signature trait of active TB is the tubercle, which represents the key localised focal point of the host-pathogen interaction. Following the initial uptake of Mtb bacilli, lung tubercles (or granulomas) develop, comprising structured aggregations of Mtb-infected and non-infected immune cells that surround a lipid-rich caseous centre harbouring extracellular mycobacteria and cellular debris[2]. The cell wall of Mtb contains abundant MA lipids that are not only essential for pathogenicity, but engage with the host innate immune system[3-5] to elicit distinct inflammatory profiles[6]. Natural Mtb MAs comprise a complex mixture of unoxygenated (alpha) and oxygenated (methoxy and keto) homologues that each contains different meromycolic chain lengths[7]. Studying the effects of natural MA mixtures may conceal any potential activity or biological function of the individual components, thus highlighting the necessity for studying single MA molecules. We were privileged with such an opportunity by our collaboration with Professor Mark Baird from Bangor University (Gwynedd, UK) who recently achieved the synthesis and provision of pure chemically synthetic Mtb mycolates, each with a defined stereochemistry. Gaining insight into how Mtb manipulates the host cell is necessary for understanding the complex biochemical interaction inside the granuloma, and may thus aid in the development of novel TB therapies. To better understand the functional diversity of MAs in the manifestation of TB was the focus of this study; in particular, the contribution that examples of individual chemically synthetic mycolates from the major classes of Mtb MAs make towards foamy macrophage induction, intracellular cholesterol accumulation, mycobacterial proliferation and immune lipidomic steering.

MAs are primarily taken up by murine macrophages expressing the F4/80 membrane antigen marker including those from the peritoneal and alveolar lineages[3, 8]. As Mtb inhalation normally occurs via the pulmonary route, this raises the question of the relevance of studying peritoneal versus alveolar macrophage populations. The reasons are twofold. It firstly allowed for faster response times of foamy phenotype induction following intraperitoneal MA treatment[3], relative to intratracheal instillation, which was important for conducting mycobacterial infection experiments. Secondly, larger cellular yields of adherent macrophages could be obtained from the total peritoneal exudate cells harvested, which was a requirement for lipidomics analyses.

It is well known that the Mtb cell wall contains a complex MA organisation of the three main classes and that it not only provides an important lipid barrier, but is essential for survival[9]. Apart from distinct unoxygenated (αMA) versus oxygenated (mMA and kMA) signatures recorded here, the results from this investigation clearly distinguished two unique profiles to the oxygenated MAs. Yuan *et al*. showed that keto mycolates are predominantly produced during the Mtb logarithmic growth phase, in contrast to methoxy mycolates that dominate during persistence[10]. It is thus suggested that Mtb bacilli, through regulation of the proportional prevalence of the MA classes in cell membranes, are able to influence the host environment after infection, first to allow rapid pathogen proliferation and later to subside into a persistent, slow proliferating stage for a long period of active disease when the infection can spread to many new individual hosts.

Foam cell formation strongly relates to a beneficial response for fast proliferating Mtb bacilli[5, 11]. We illustrated that kMA stimulates the host macrophage to a cholesteryl ester rich LD milieu for sustenance of mycobacterial proliferation. Lipidomics analyses provided

further evidence in support of the role of kMA in steering towards LD-mediated mycobacterial growth, with the generation of PL and LPL structural species that are functionally associated with LDs[12, 13]. Also, a propensity towards accumulation of lipid species with strong eicosanoid potential was stimulated by kMA in the macrophages. Neutral lipids are a major source of stored AA in macrophages and monocytes. Eicosanoid synthesis occurs within distinct subcellular domains, namely the nuclear membrane, ER, phagosomes and LDs[14]. Eicosanoids are transitory and synthesised *de novo* as required by the cell. By acting on arachidonyl-containing PLs or DAG, PLA_2 mediated cleavage from the *sn2* position will liberate free AA that is further oxidised by the COX, LOX or CYP450 enzymatic pathways[14]. This depends on the activation status or needs of the cell[15]. In addition to a direct ingestion of neutral LDs by mycobacteria through nutrition[16], LD accumulation by leukocytes mediates inflammation, because important protein mediators for immune dissemination and lipid metabolising enzymes are housed within LDs[17]. Indeed, a strong link between intracellular LDs and the host-pathogen interaction has been established. For example, LDs are sites for eicosanoid/lipid biosynthesis leading to the generation of prostaglandin E_2 and leukotriene B_4, IFN-mediated effector assembly, antigen cross presentation and autophagy (reviewed in[18]). Keto mycolate-induced interference of host lipid machinery and cholesterol export for accumulation of lipid nutrients thus reflects a distinct functionality of MAs to drive macrophages towards inflammation and support of mycobacterial proliferation. Targeting of kMAs and its host target molecules may therefore present a new vision for the development of anti-TB therapeutics.

The mMA oxygenated class did not induce LDs with esterified cholesterol nor facilitated the proliferation of mycobacteria. Macrophages from mice treated with mMA did exhibit a multi-vacuolar phenotype and were enlarged relative to all other macrophage populations studied.

Multinucleated giant 'Langhans' cells (MGCs) are characteristic of the tuberculous granuloma and form as a result of monocyte/macrophage fusion[19]. A previous study illustrated that Mtb-induced giant cells do not support bacterial growth, due to a diminished expression of phagocytic receptors, but retain NADPH oxidase activity and mycobacterial antigen-presentation[20]. Mtb envelope glycolipids stimulate TLR-associated macrophage fusion machinery to form MGCs[21, 22]. Yet Mtb MAs are TLR2/4-independent PAMPs[3], suggesting that the induction of multi-vacuolar giant cells observed after treatment with mMA occurs via an alternate route. Interestingly, Langhans giant cells elicited by inflammatory cytokine stimulation, for example granulocyte macrophage colony stimulating factor (GM-CSF), IL-6 and IFNγ, are representative of M1-polarised macrophages[23]. A precise biological function for MGCs in tuberculous granulomas remains obscure. Even so, it appears that the induction of these cells by methoxy mycolates orients towards an M1 mode, corroborating an earlier report on the involvement of Mtb MAs in Th1 immunity[3]. From a host cell perspective, the stimulation by mMA of enlarged multi-vacuolar cells signifies a microbe elimination response, since the production of NADPH oxidase-dependent ROS is more than 20-fold elevated in MGCs relative to unfused macrophages[24]. These cells robustly present microbial antigens to $CD4^+$ T lymphocytes[25]. During the optimisation of the experimental conditions, comparable phagocytic uptake of Streptavidin microspheres (2-3 beads per cell) and BCG bacilli (~1 bacillus per cell) was confirmed for macrophages from all MA treatment conditions (Appendix: Exploration of comparative *ex vivo* cellular technologies). mMA macrophages therefore are able to facilitate internalisation of mycobacteria, but clearly do not sustain their proliferation. From the pathogen viewpoint, it would be beneficial to not be taken up by these giant microbicidal cells before they mature in the granuloma, but rather effectively exploit the lipid-laden cells induced by kMA. This correlates with the prominent upregulation of the PC content relative to PE in mMA

stimulated macrophages, which reflects a mMA mechanism of induced change in cell membrane conformation. Optimal ratios of PC/PE are essential for maintaining flexibility and function, as the hydrated head region of PC amplifies rigidity and the cone-shaped PE facilitates fusion[26]. One may speculate that methoxy mycolates, by stimulating PC synthesis and/or PE degradation, would reduce the fluidity of host membranes. In this manner, Mtb bacilli may restrict the proportion of macrophages that differentiate into giant cells or manipulate their phagocytic capacity. Assessment of the expression of genes regulating the enzymatic synthesis or degradation of PC or PE may provide clarity on the pathway by which mMA alters the macrophage membrane composition, and warrants further study. The fact that methoxy mycolates become particularly important during the late persistent stage of active TB may be a strong indicator of the role of these Mtb lipids in steering host immunity to sustain infection and encumber microbial destruction.

Understanding the role of MAs in the establishment of TB is important, but not the only application field of this study. While MAs are so cleverly active to manipulate the host immune response to benefit the pathogen, one may ask how this wisdom learnt from the millennia of host-pathogen coevolution in TB can be exploited for human benefit. Ten years ago, a student from our group published her findings on how the MA natural mixture practically "cured" experimental asthma in mice[4], the illustration of which aimed to find fields of application for MAs as potential therapeutic agents against disease. This followed on an earlier finding that the natural MA mixture steered the murine immune system away from the Th2 mode of immunity[3] that is associated with inflammatory diseases such as arthritis and asthma. Vander Beken *et al*. published results that bode well for the use of MAs as vaccine adjuvants for medical and veterinary use[6]. Last year, Dr Yolandy Lemmer, a previous graduate from our research team, reported their discovery that the natural mixture of MAs

acted as a targeting ligand to strongly facilitate uptake of nanoencapsulated anti-TB drugs into macrophages *in vitro*[27]; thereby illustrating how MAs could be used for much improved anti-TB drug delivery. It is not only in TB that a targeted drug transfer mechanism shows promise, but also for the supply of nano-medicines to other macrophage-borne disease. One example is HIV, which partially hides in monocyte/macrophage reservoirs in affected patients, from where they could hitherto not be eradicated[28]. These diverse potential applications for MAs in the medical and veterinary fields, learnt from the mechanism of action of MAs in TB, pose the important question on what MAs may do to the body in terms of undesirable side-effects, while effecting their benefits to the humans or animals undergoing treatment.

From this thesis, potential risks can be identified that may result from MA administration for vaccination or therapeutic purposes. These require careful testing in future animal experiments to determine safety of MA administration and to instruct the design of pharmaceutical delivery strategies to avoid malefaction. In the discussion that follows, the risks are considered, but also how these may be mitigated in cases where benefaction may be gained from particular MA preparations of which the MA class composition is designed to reduce the risk.

The prominent feature of the induction of lipid-filled foamy cells among murine alveolar or peritoneal macrophage populations following administration of the natural MA mixture[3] was shown in this thesis to be ascribed solely to the mycolates from the keto oxygenation class. Catabolism of cholesteryl esters in LDs is a process mediated by autophagy in macrophage foam cells[29]. Even if autophagy is typically a microbicidal function[30], reports exist that intracellular bacteria may utilise autophagosomes as nutrient-rich replicative niches[31]. The

permissiveness of the natural MA mixture and kMA macrophages to facilitate BCG proliferation, relative to mMA which does not, queries the precise biochemical regulation of the macrophage state under each of these conditions. It will also be of interest to assess whether the striking induction of PC and PC metabolites by the methoxy MA class, manifests negatively in the body and if so, whether the keto class that steers away from PC towards PE and PS could improve therapeutic designs of host immunity steering using specific MA classes. Stimulating the macrophages within the body into a cholesterol-rich environment for mycobacteria that may exploit lipid resources, perhaps via an autophagous mechanism, poses a real health risk for therapy development. As we recorded that it is this foamy phenotype in particular that will sustain mycobacterial growth, it creates the possibility of inducing a period of TB susceptibility in patients treated with MA-containing therapies or vaccines.. Fortunately, the foam cell-inducing effect seems transient. The foamy cell population subsided by one third, two days after MA administration. The mice studied showed no outward indication of illness before euthanasia. Nevertheless, the potential danger of foamy phenotype induction can be bypassed by excluding keto and utilising methoxy mycolates in its place as long as this does not negatively affect the beneficent effect of the MA treatment.

Through assessment of the lipidomes of the macrophage populations from differently MA treated mice, we also gained knowledge on the induction of AA-containing PL potential. Liberating membrane-bound AA stores will initiate the generation of eicosanoids that are lipid mediators critically involved in the fine regulation of inflammation and immunity[32]. This includes both anti- and proinflammatory pathways that in macrophages are primarily driven by their state of activation or differentiation, influenced by an extensive array of antigens and cytokines[33]. The natural MA mixture greatly induced eicosanoid potential. kMA exhibited stronger eicosanoid potential associated with lipid species from the PE, PI and PS

head group classes relative to mMA, for which some potential was recorded mainly in PC. Whether the particular AA-inducing responses associated with the methoxy or keto macrophages will manifest risk or beneficent outcomes for the host remains to be determined. Our measurements of BCG proliferation however, suggest that the intracellular milieus of the macrophages from the oxygenated MA treatments differ: mMA treatment prevented mycobacterial growth reflective of a proinflammatory state while kMA macrophages, which permitted mycobacterial replication, rather seem to support an environment of house-keeping or cellular repair. Nevertheless, the potential of kMA to stimulate an eicosanoid storm is worrisome, and an in-depth assessment of their potential effects in the body will thus have to be incorporated into future research.

No significant LPL generation was observed for macrophages from the natural MA treatment. Macrophages from the oxygenated mycolates on the other hand exhibited reduced proportional abundances of unsaturated lysoPS, but strikingly elevated abundances of lysoPC. Should these pose risk, then it could in principle be mitigated by the addition of α-MA.

Natural MA-mixture generally steers towards a Th1 response, supported by lysoPC and lysoPS lipid mediators demonstrated here for treatments also with the two oxygenated MAs. This suggests induction of a broadly proinflammatory state, but in which more lysoPC is induced by mMA and more lysoPS induced by kMA. Cer lipid species were induced by the natural MA mixture as well as the individual oxygenated molecules. These may pose the risk for undue induction of apoptosis or autophagy. In particular mMA treatment was found to induce the highest Cer content of species associated with apoptosis. Natural MA mixture and kMA displayed comparable levels of sphingolipids and were the only treatments that

distinctly induced dihydroceramide backbones, proposing a role in autophagy. Differential induction of Cer and sphingolipids by the two oxygenated MAs may therefore allow for fine tuning the composition of MA-treatments to limit the potential risk.

Any of the conceivable harmful effects induced by either of the MA classes could potentially be compensated for by altering the composition of that element in the drug or vaccine, permitting that it does not take away from the benefit these molecules could offer as therapeutic agents. The testing of new medicines via oral or injectable routes will therefore require the comprehensive evaluation of the macrophage populations and any plausible contraindications associated with MA therapy.

MAs assign a unique fingerprint to mycobacteria and display diverse biological functions[3, 4, 6, 34-36]. This work provided evidence for an improved understanding of the manifestation of TB. The keto and methoxy mycolates studied here, differentially interfere with host lipid homeostasis and materialisation of the TB disease phenotype. We clearly show that the type of oxygenated distal group of the meromycolic moiety influences foamy macrophage regulation, cholesterol accumulation and mycobacterial growth facilitation through the lipidome of its host cell. These are crucial findings, as the Mtb cell envelope displays significant structural variation in MA oxygenation class and proximal cyclopropane configuration[7], which is continuously remodelled in response to growth needs[10, 37, 38]. We show here that kMA transforms the macrophage to a lipidome phenotype that accumulates cholesterol and sustains mycobacterial proliferation, whereby autophagy and eicosanoids potentially play a significant role. The humorally antigenic mMA in contrast, displays strong immune steering capability through the generation of lipid species associated with reduced membrane fluidity and apoptosis, which we reported do not stimulate cholesterol

accumulation or uphold mycobacterial growth. A major lead provided here is the identification of the involvement of the keto class in facilitating BCG growth. While this effect appears transient, keto mycolates pose a risk of modulating host immunity to benefit the mycobacteria; evidently a highly undesirable outcome of TB treatment. Nonetheless, even as considering the risk factors are vitally important for therapeutic design, some of these may be overestimated and should be explicitly tested. Collectively this study provides a molecular basis by which the safety and mechanism of MA biolipids as plausible therapeutic agents may be assessed, and so to provide a starting-point for planning risk assessments for future development of nanomedicines for targeted drug delivery against macrophage borne infectious diseases, asthma and vaccine adjuvants.

2. References

1. Comas, I., M. Coscolla, T. Luo, S. Borrell, K. E. Holt, M. Kato-Maeda, J. Parkhill, B. Malla, S. Berg, G. Thwaites, D. Yeboah-Manu, G. Bothamley, J. Mei, L. Wei, S. Bentley, S. R. Harris, S. Niemann, R. Diel, A. Aseffa, Q. Gao, D. Young and S. Gagneux. 2013. Out-of-Africa migration and Neolithic coexpansion of *Mycobacterium tuberculosis* with modern humans. *Nat. Genet.* **45**: 1176-1182.

2. Russell, D. G. 2007. Who puts the tubercle in tuberculosis? *Nat. Rev. Microbiol.* **5**: 39-47.

3. Korf, J., A. Stoltz, J. Verschoor, P. De Baetselier and J. Grooten. 2005. The *Mycobacterium tuberculosis* cell wall component mycolic acid elicits pathogen-associated host innate immune responses. *Eur. J. Immunol.* **35**: 890-900.

4. Korf, J. E., G. Pynaert, K. Tournoy, T. Boonefaes, A. Van Oosterhout, D. Ginneberge, A. Haegeman, J. A. Verschoor, P. De Baetselier and J. Grooten. 2006. Macrophage reprogramming by mycolic acid promotes a tolerogenic response in experimental asthma. *Am. J. Respir. Crit. Care Med.* **174**: 152-160.

5. Peyron, P., J. Vaubourgeix, Y. Poquet, F. Levillain, C. Botanch, F. Bardou, M. Daffe, J. F. Emile, B. Marchou, P. J. Cardona, C. de Chastellier and F. Altare. 2008. Foamy macrophages from tuberculous patients' granulomas constitute a nutrient-rich reservoir for *M. tuberculosis* persistence. *PLoS Pathog.* **4**: e1000204. doi:1000210.1001371/journal.ppat.1000204.

6. Vander Beken, S., J. R. Al Dulayymi, T. Naessens, G. Koza, M. Maza-Iglesias, R. Rowles, C. Theunissen, J. De Medts, E. Lanckacker, M. S. Baird and J. Grooten. 2011. Molecular structure of the *Mycobacterium tuberculosis* virulence factor, mycolic acid, determines the elicited inflammatory pattern. *Eur. J. Immunol.* **41**: 450-460.

7. Verschoor, J. A., M. S. Baird and J. Grooten. 2012. Towards understanding the functional diversity of cell wall mycolic acids of *Mycobacterium tuberculosis*. *Prog. Lipid Res.* **51**: 325-339.

8. Stoltz, A. C. 2005. *Immunological properties of mycolic acids, the major lipid cell wall component of Mycobacterium tuberculosis*. PhD thesis, University of Pretoria. pp 224.

9. Jankute, M., J. A. Cox, J. Harrison and G. S. Besra. 2015. Assembly of the mycobacterial cell wall. *Annu. Rev. Microbiol.* **69**: 405-423.

10. Yuan, Y., Y. Zhu, D. D. Crane and C. E. Barry, 3rd. 1998. The effect of oxygenated mycolic acid composition on cell wall function and macrophage growth in *Mycobacterium tuberculosis*. *Mol. Microbiol.* **29**: 1448-1458.

11. de Chastellier, C. 2009. The many niches and strategies used by pathogenic mycobacteria for survival within host macrophages. *Immunobiology* **214**: 526-542.

12. Bartz, R., W. H. Li, B. Venables, J. K. Zehmer, M. R. Roth, R. Welti, R. G. Anderson, P. Liu and K. D. Chapman. 2007. Lipidomics reveals that adiposomes store ether lipids and mediate phospholipid traffic. *J. Lipid Res.* **48**: 837-847.

13. Guo, Y., K. R. Cordes, R. V. Farese, Jr. and T. C. Walther. 2009. Lipid droplets at a glance. *J. Cell Sci.* **122**: 749-752.

14. Bozza, P. T., I. Bakker-Abreu, R. A. Navarro-Xavier and C. Bandeira-Melo. 2011. Lipid body function in eicosanoid synthesis: an update. *Prostaglandins Leukot. Essent. Fatty Acids* **85**: 205-213.

15. Murphy, S., S. Martin and R. G. Parton. 2009. Lipid droplet-organelle interactions; sharing the fats. *Biochim. Biophys. Acta* **1791**: 441-447.

16. Daniel, J., H. Maamar, C. Deb, T. D. Sirakova and P. E. Kolattukudy. 2011. *Mycobacterium tuberculosis* uses host triacylglycerol to accumulate lipid droplets and acquires a dormancy-like phenotype in lipid-loaded macrophages. *PLoS Pathog.* **7**: doi:10.1371/journal.ppat.1002093.

17. Bozza, P. T., K. G. Magalhaes and P. F. Weller. 2009. Leukocyte lipid bodies - Biogenesis and functions in inflammation. *Biochim. Biophys. Acta* **1791**: 540-551.

18. Saka, H. A. and R. Valdivia. 2012. Emerging roles for lipid droplets in immunity and host-pathogen interactions. *Annu. Rev. Cell Dev. Biol.* **28**: 411-437.

19. Helming, L. and S. Gordon. 2009. Molecular mediators of macrophage fusion. *Trends Cell Biol.* **19**: 514-522.

20. Lay, G., Y. Poquet, P. Salek-Peyron, M. P. Puissegur, C. Botanch, H. Bon, F. Levillain, J. L. Duteyrat, J. F. Emile and F. Altare. 2007. Langhans giant cells from *M. tuberculosis*-induced human granulomas cannot mediate mycobacterial uptake. *J. Pathol.* **211**: 76-85.

21. Puissegur, M. P., C. Botanch, J. L. Duteyrat, G. Delsol, C. Caratero and F. Altare. 2004. An i*n vitro* dual model of mycobacterial granulomas to investigate the molecular interactions between mycobacteria and human host cells. *Cell. Microbiol.* **6**: 423-433.

22. Puissegur, M. P., G. Lay, M. Gilleron, L. Botella, J. Nigou, H. Marrakchi, B. Mari, J. L. Duteyrat, Y. Guerardel, L. Kremer, P. Barbry, G. Puzo and F. Altare. 2007. Mycobacterial Lipomannan Induces Granuloma Macrophage Fusion via a TLR2-Dependent, ADAM9- and 1 Integrin-Mediated Pathway. *J. Immunol.* **178**: 3161-3169.

23. Quinn, M. T. and I. A. Schepetkin. 2009. Role of NADPH oxidase in formation and function of multinucleated giant cells. *J. Innate Immun.* **1**: 509-526.

24. Kreipe, H., H. J. Radzun, P. Rudolph, J. Barth, M.-L. Hansmann, K. Heidorn and M. R. Parwaresch. 1988. Multinucleated giant cells *in vitro*. *Am. J. Pathol.* **130**: 232-243.

25. Russell, D. G. 2001. *Mycobacterium tuberculosis*: here today, and here tomorrow. *Nat. Rev. Mol. Cell Biol.* **2**: 1-9.

26. Holthuis, J. C. and A. K. Menon. 2014. Lipid landscapes and pipelines in membrane homeostasis. *Nature* **510**: 48-57.

27. Lemmer, Y., L. Kalombo, R. D. Pietersen, A. T. Jones, B. Semete-Makokotlela, S. Van Wyngaardt, B. Ramalapa, A. C. Stoltz, B. Baker, J. A. Verschoor, H. S. Swai and C. de Chastellier. 2015. Mycolic acids, a promising mycobacterial ligand for targeting of nanoencapsulated drugs in tuberculosis. *J. Control. Release* **211**: 94-104.

28. Le Douce, V., G. Herbein, O. Rohr and C. Schwartz. 2010. Molecular mechanisms of HIV-1 persistence in the monocyte-macrophage lineage. *Retrovirology* **7**: 1-16.

29. Ouimet, M. and Y. L. Marcel. 2012. Regulation of lipid droplet cholesterol efflux from macrophage foam cells. *Arterioscler. Thromb. Vasc. Biol.* **32**: 575-581.

30. Mizushima, N., B. Levine, A. M. Cuervo and D. J. Klionsky. 2008. Autophagy fights disease through cellular self-digestion. *Nature* **451**: 1069-1075.

31. Huang, J. and D. J. Klionsky. 2007. Autophagy and human disease. *Cell Cycle* **6**: 1837-1849.

32. Harizi, H., J. B. Corcuff and N. Gualde. 2008. Arachidonic-acid-derived eicosanoids: roles in biology and immunopathology. *Trends Mol. Med.* **14**: 461-469.

33. Norris, P. C. and E. A. Dennis. 2014. A lipidomic perspective on inflammatory macrophage eicosanoid signaling. *Adv. Biol. Regul.* **54**: 99-110.

34. Benadie, Y., M. Deysel, D. G. Siko, V. V. Roberts, S. Van Wyngaardt, S. T. Thanyani, G. Sekanka, A. M. Ten Bokum, L. A. Collett, J. Grooten, M. S. Baird and J. A. Verschoor. 2008. Cholesteroid nature of free mycolic acids from *M. tuberculosis*. *Chem. Phys. Lipids* **152**: 95-103.

35. Deysel, M. S. M. 2008. *Structure-function relationships of mycolic acid in tuberculosis*. PhD thesis, University of Pretoria. pp 178.

36. Beukes, M., Y. Lemmer, M. Deysel, J. R. Al Dulayymi, M. S. Baird, G. Koza, M. M. Iglesias, R. R. Rowles, C. Theunissen, J. Grooten, G. Toschi, V. V. Roberts, L. Pilcher, S. Van Wyngaardt, N. Mathebula, M. Balogun, A. C. Stoltz and J. A. Verschoor. 2010. Structure-function relationships of the antigenicity of mycolic acids in tuberculosis patients. *Chem*. *Phys*. *Lipids* **163**: 800-808.

37. Riley, L. W. 2006. Of mice, men and elephants: *Mycobacterium tuberculosis* cell envelope lipids and pathogenesis. *J*. *Clin*. *Invest*. **116**: 1475-1478.

38. Dubnau, E., J. Chan, C. Raynaud, V. P. Mohan, M.-A. Laneelle, K. Yu, A. Quemard, S. Smith and M. Daffe. 2000. Oxygenated mycolic acids are necessary for virulence of *Mycobacterium tuberculosis* in mice. *Mol*. *Microbiol*. **36**: 630-637.

Curriculum Vitae |

Ilke Vermeulen

PERSONAL DETAILS

Place and date of birth:	Cape Town, 14 March 1984
Gender:	Female
Nationality:	South African
Identity number:	8403140218080
Marital status:	Married (married name *Roelofse*)
Driver's license:	Code 8 and Code A1
Residential address:	1004 Galjoen Road, 28 The Shades, Garsfontein east, 0081, Pretoria
Postal address:	Suite 10, Private Bag X1, Moreleta Plaza, 0167, Pretoria
E-mail:	ilke.vermeulen@gmail.com
Mobile phone:	+27 (0)82 072 6712
Native languages:	Afrikaans (L1) and English (L2)
Foreign language:	Dutch (fluent)

SYNOPSIS

I recently completed a joint PhD in Biochemistry and Biotechnology at Ghent University (Department of Life Sciences and Medicine, Belgium) and in Biochemistry at the University of Pretoria (Department of Biochemistry, South Africa). The doctorate formed part of an interuniversity 'Flanders-South Africa' PhD programme. Since January 2015, I have been working as a researcher in the Antiviral Gene Therapy Research Unit (Department of Molecular Medicine and Haematology) at the University of the Witwatersrand in Johannesburg, South Africa. My main managerial responsibility entails overseeing the running of our laboratory's two tissue culture facilities that are utilised by all group members for maintenance of healthy cultured cells, preparation of native viral stocks or recombinant viral vectors, and for assessment of anti-hepatitis B virus efficacy. Research contributions include the development of an in-house chromatin immunoprecipitation (ChIP) method to assess mechanisms of targeted viral epigenome modifications, cloning and assembly of mammalian expression plasmids, production of recombinant adeno-associated virus (rAAV) for *in vivo* and *in vitro* experimental use, as well as participation in weekly lab meetings whereby progress reports and scientific journal articles are presented. I am focussed, highly motivated and eager to broaden my knowledge and skills in molecular biology and diverse medical disciplines.

EDUCATION

2012-2016 **Ghent University, Belgium** and **University of Pretoria, Pretoria** **PhD**

Supervisors: Professors Johan Grooten and Jan Verschoor

Tuberculosis: How different synthetic analogues of pathogen associated mycolates affect lipid homeostasis of murine host macrophages.

2010 **University of Pretoria, Pretoria** **Science Special**

Formed part of the BSc Veterinary Biology II. Gene and Chromosome Organisation, Genetic Analysis and Manipulation, Animal Science, Nutrition.

2009-2010 **Rhodes University, Grahamstown** **MSc**

Supervisors: Dr Nicole B. Richoux and Professor P. William Froneman

Trophic dynamics of suspension-feeders in the nearshore marine environment with the use of fatty acid and stable isotope tracer techniques.

2008 **Rhodes University, Grahamstown** **BSc Honours**

Supervisor: Professor P. William Froneman

Research Methodology, Primary Production, Marine Fringing Communities, Zooplankton Dynamics, Benthic Communities, Invertebrate Life Histories, Experimental design, Scientific writing, Research letters.

2007 **University of Pretoria, Pretoria** **Veterinary Nursing I**

Anatomy, Physiology, Laboratory Technique, Microbiology, Pharmacology, Parasitology, General, Reproductive and Medical Nursing, Theatre Practice, Veterinary Ethology.

2006 **Nelson Mandela Metropolitan University, George** **B.Tech**

Research Methodology, Conservation Management, Coastal and Marine Management, Fresh Water Management, Plant Studies, Resource Management.

2005 **Cape Peninsula University of Technology, Cape Town** **National Diploma**

Plant Studies, Animal Studies, Conservation Ecology, Conservation Development, Administration and Communication, Resource Management, Soil Science.

2001 **Pretoria College, South Africa** **Gauteng Senior Certificate**

English, Afrikaans, Mathematics, Science, Biology, Business Economics.

QUALIFICATIONS

PhD Joint PhD: Doctor of Science in **Biochemistry and Biotechnology** at Ghent University (Belgium), and Doctor of Philosophy in **Biochemistry** at the University of Pretoria (South Africa). The doctoral defence was held on 3 March 2017 at the Council for Scientific and Industrial Research (CSIR) in Pretoria.

MSc Master of Science in marine biology

BSc. H Bachelor of Science with Honours in marine biology (*cum laude*)

B.Tech Bachelor of Technology in nature conservation (*cum laude*)

Instructor NAUI Certified Scuba Diving Instructor

AWARDS AND SCHOLARSHIPS

2012-2014	Ghent University	FWO Vlaanderen – PhD scholarship
2009-2010	Rhodes University	DAAD and Ernst & Ethel Eriksen Trust – MSc scholarships
2009	Rhodes University	Academic Colours
2008	Rhodes University	Duerden Scholarship – BSc Honours
2007	NMMU	Golden Key International Honour Society
2006	NMMU	Merit award for academic excellence
2006	NMMU	Special award for top bachelor student
2005	CPUT	Best resource management student award

CERTIFIED COURSES

2013	Ghent University, Belgium	Leadership Foundation Course, by Dan Steer (3d)
2013	Ghent University, Belgium	Project Management, by Tom Jacobs (3d)
2012	Ghent University, Belgium	Bio-Imaging, organised by Saskia Lippens (1w)
2012	Ceppellini, Naples Italy	Advanced Course in Immunology Level II, by the Ceppellini Advanced School of Immunology (1w)
2012	Ghent University, Belgium	Laboratory Animal Science I and II (2w)
2011	Ghent University, Belgium	Advanced Academic English Conference Skills, by Katelijne Verstraete (3d)
2007	Competency Alignment Ltd., Pretoria	Management & Leadership Awareness Workshop, by Louis Odendaal (1w)
2007	Hill's Pet Nutrition Ltd., Pretoria	Hill's Veterinary Nutrition Advisor Programme Level 1, by Hill's Pet Nutrition (2d)

COMPUTER LITERACY

Microsoft Word, Excel and PowerPoint
PAST 1.42
STATISTICA v8
SYSTAT v12.0
SigmaPlot 10.0
GenStat 16
Image J
GraphPad Prism V6
Volocity 3D image analysis
CorelDRAW V12

WORK EXPERIENCE

2015-2017 **Wits/SAMRC Antiviral Gene Therapy Research Unit** **Researcher**

Research scientist in the Antiviral Gene Therapy Research Unit (AGTRU). AGTRU is dedicated to the development of therapies using targeted viral genome and epigenome technologies to cure viral diseases. Molecular biology skills include standard cell culture, sterile technique, cultures of human hepatoma and embryonic kidney cell lines, PCR, real-time qPCR, agarose gel electrophoresis, multiplex assay, immunoassays, fluorescence or immunofluorescence imaging, DNA isolation, RNA isolation, reverse transcription and cDNA synthesis, nucleic acid manipulation, cloning, bacterial transformation, production of hepatitis B virus, preparation of recombinant viral vectors (AAVs), cell transfection, genome editing technologies, ChIP, transgenic and NMRI mouse models.

2011-2014 **Ghent University, Belgium** **PhD Researcher**

Full-time doctoral researcher in the Laboratory of Molecular Immunology at Ghent University, Belgium. Key research focus: *Mycobacterium tuberculosis* host-pathogen interactions. Obtained a working knowledge of an immunology laboratory and diverse molecular biology techniques: certified experiment leader in mouse models, general tissue culture, sterile technique, primary macrophage cultures, mycobacteriology, lipidomics, immunoassays, fluorescence labelling, and specialised microscopy.

2013-2014 **Ghent University, Belgium** **GLP-Representative**

Good laboratory practice liaison for the Laboratory of Molecular Immunology.

2012-2013 **Ghent University, Belgium** **Room Manager in Tissue Culture Lab**

Responsible for general management and organisation of a room in the Tissue Culture Laboratory at the Flemish Institute of Biotechnology.

2009 **Rhodes University, Grahamstown** **Postgraduate representative**

Main communication liaison for postgraduate students in the Department of Zoology and Entomology. Monthly staff meetings, organisation of the annual departmental function.

2008-2009 **Rhodes University, South Africa** **Teaching Assistant**

Assisted in tutoring and coordinated practical courses in Cell Biology to undergraduate BSc students.

2008-2009 **Rhodes University, South Africa** **Scuba Diving Instructor**

Planned and headed scuba diving courses and trips whilst training students for the NAUI scuba diver and advanced scuba diver courses at the university Underwater Club.

2005 **Blaauwberg Conservation Area, South Africa** **Conservation Intern**

General administration and team management, marine and coastal reserve resource management, communication to public and educational school groups, conservation compliance, invasive alien clearing, research and monitoring of an endangered species.

2002-2003 **Paindaine Scuba Diving Camp, Mozambique** **Manager & Dive Instructor**

Three month summer holiday employment. General dive camp management, scuba instruction and training; including the organising of scuba diving trips, night diving, snorkelling, dolphin and whale shark watching.

PUBLICATIONS

1. **Vermeulen, I.**, Baird, M., Al-Dulayymi, J., Smet, M., Verschoor, J. and Grooten, J. **2017**. Mycolates of *Mycobacterium tuberculosis* modulate the flow of cholesterol for bacillary proliferation in murine macrophages. *Journal of Lipid Research*, doi: 10.1194/jlr.M073171 (in Press). IF = 4.56
2. Maepa, M.B., **Roelofse, I.**, Ely, A. & Arbuthnot, P. **2015**. Progress and prospects of anti-HBV gene therapy development. *International Journal of Molecular Sciences* **16**: 17589-17610.
3. Richoux, N.B., **Vermeulen, I**. & Froneman, P.W. **2014**. Fatty acid profiles reveal temporal and spatial differentiation in diets within and among sympatric rocky shore suspension-feeders. *Marine Ecology Progress Series* **495**: 143-160.
4. Richoux, N.B., **Vermeulen, I**. & Froneman, P.W. **2014**. Stable isotope ratios indicate differential omnivory among sympatric rocky shore suspension-feeders. *Marine Biology* **161**(5): 971-984.

5. **Vermeulen, I**. & Heyns, E. **2009**. The hyperbenthos: overlooked component of South African estuaries? *The Aardvark*, April: 6-7. Popular magazine, Zoological Society of Southern Africa.

CONFERENCES

1. Optimisation of a chromatin immunoprecipitation method to investigate epigenome changes effected by transcription activator-like effector repressors. **Biennual Wits Faculty of Health Sciences Research Day and Postgraduate Expo**, 1 September 2016, Wits University, Johannesburg, South Africa. *Poster presentation*.
2. Chemically synthetic oxygenated mycolic acids and the liver X receptor regulate cholesterol export in macrophages: how does this relate to tuberculosis? **European Molecular Biology Organisation (EMBO) Global Exchange Lecture Course: Frontiers in Innate Immunity and Drug Discovery**, 8 July 2015, Wits University, Johannesburg, South Africa. *Oral presentation*.
3. *Mycobacterium tuberculosis* mycolic acid and its role in foam cell formation. **6th Benelux Nuclear Receptor Meeting**, 21 November 2013, Utrecht, Netherlands. *Poster presentation*.
4. *Mycobacterium tuberculosis* mycolic acids at the host-pathogen immune interface. **Flanders Inter-University Attraction Poles kick-off meeting P7/32**, 30 January 2013, Ghent, Belgium. *Oral presentation*.
5. Spatial and temporal changes in the diets of rocky shore invertebrates along the coast of South Africa: a fatty acid perspective. **31st Congress of the International Limnological Society**, 16 August 2010, Cape Town, South Africa. *Oral presentation*.

REFEREES

1. **Professor Patrick Arbuthnot**
   Director of the Wits/SAMRC Antiviral Gene Therapy Research Unit, University of the Witwatersrand, Faculty of Health Sciences, 7 York Road, JOHANNESBURG, 2193. Tel.: +27 (0)11 717 2365 and E-mail: Patrick.Arbuthnot@wits.ac.za
2. **Professor Johan Grooten**
   Head of Department of Molecular Biology, Ghent University. Technologiepark 927, GHENT, 9052, Belgium. Tel.: +32 (0)9 331 3650 and E-mail: johan.grooten@irc.ugent.be
3. **Professor Jan Verschoor**
   Department of Biochemistry, University of Pretoria, cnr Lynnwood Road and Roper Street, PRETORIA, 0083. . Tel.: +27 (0)12 420 2477 and E-mail: Jan.Verschoor@up.ac.za
4. **Professor William Froneman**
   Head of Department of Zoology and Entomology, Rhodes University. P. O. Box 94, GRAHAMSTOWN, 6140. Tel.: +27 (0)46 603 8525 and E-mail: W.Froneman@ru.ac.za

CHAPTER II |

Mycolates of *Mycobacterium tuberculosis* modulate the flow of cholesterol for bacillary proliferation in murine macrophages

---

Supplemental data

---

1. Supplemental data

Table S1 | Sequential Sidak pairwise comparisons showing within- and between-group differences in the proportion of enlarged vacuole-positive (V+) cells induced by mycolic acid (MA). In the GLM, treatment and time point were the independent predictors while the proportion of enlarged V+ cells was the dependent variable (GLM: Wald Chi-Square = 753.924, $P < 0.001$, $df = 14$, $n = 5$ per time point). Results were significant at $P < 0.05$ (bolded).

PBS			Lipo			αMA			mMA			kMA		
0h	**24h**	**48h**	**0h**	**24h**	**48h**	**0h**	**24h**	**48h**	**0h**	**24h**	**48h**	**0h**	**24h**	**48h**
0h	1.000	1.000	0.999	0.999	0.954	1.000	1.000	1.000	**<0.001**	**<0.001**	**<0.001**	**<0.001**	**<0.01**	1.000
	24h	0.948	1.000	1.000	1.000	0.990	0.999	1.000	**<0.001**	**<0.001**	**<0.001**	**<0.01**	**<0.01**	1.000
		48h	1.000	1.000	1.000	1.000	1.000	1.000	**<0.001**	**<0.001**	**<0.001**	**<0.001**	**<0.01**	0.999
			0h	1.000	1.000	0.904	0.983	1.000	**<0.001**	**<0.001**	**<0.001**	**<0.001**	**<0.001**	0.983
				24h	1.000	0.904	0.983	1.000	**<0.001**	**<0.001**	**<0.001**	**<0.001**	**<0.001**	0.983
					48h	0.589	0.825	1.000	**<0.001**	**<0.001**	**<0.001**	**<0.001**	**<0.001**	0.825
						0h	1.000	0.990	**<0.001**	**<0.001**	**<0.001**	**<0.01**	**<0.05**	1.000
							24h	0.999	**<0.001**	**<0.001**	**<0.001**	**<0.01**	**<0.05**	1.000
								48h	**<0.001**	**<0.001**	**<0.001**	**<0.001**	**<0.01**	1.000
									0h	0.087	0.997	**<0.001**	**<0.001**	**<0.001**
										24h	0.952	**<0.001**	**<0.001**	**<0.001**
											48h	**<0.001**	**<0.001**	**<0.001**
												0h	1.000	**<0.01**
													24h	**<0.05**
														48h

Table S2 | Sequential Sidak pairwise comparisons showing within- and between-group differences in the induction of lipid droplets (LDs) by mycolic acid (MA). In the GLM, treatment and time point were the independent predictors while the number of LDs per 100 cells was the dependent variable (GLM: Wald Chi-Square = 353.662, $P < 0.001$, $df = 14$, $n = 5$ per time point). Results were significant at $P < 0.05$ (bolded).

PBS			Lipo			αMA			mMA			kMA		
0h	**24 h**	**48h**	**0h**	**24h**	**48h**	**0h**	**24h**	**48h**	**0h**	**24h**	**48h**	**0h**	**24h**	**48h**
0h	0.979	1.000	0.971	0.078	1.000	1.000	0.378	1.000	1.000	0.999	1.000	**<0.001**	**<0.001**	**<0.001**
	24h	0.875	1.000	0.995	0.999	0.964	1.000	1.000	1.000	1.000	0.757	**<0.001**	**<0.001**	**<0.01**
		48h	0.847	**<0.05**	1.000	1.000	0.179	0.999	0.997	0.986	1.000	**<0.001**	**<0.001**	**<0.001**
			0h	0.996	0.998	0.955	1.000	1.000	1.000	1.000	0.725	**<0.001**	**<0.001**	**<0.05**
				24h	1.000	0.060	1.000	0.684	0.815	0.933	**<0.05**	**<0.001**	**<0.001**	**<0.01**
					48h	1.000	0.734	1.000	1.000	1.000	1.000	**<0.001**	**<0.001**	**<0.001**
						0h	0.313	1.000	1.000	0.997	1.000	**<0.001**	**<0.001**	**<0.001**
							24h	1.000	0.995	0.999	0.109	**<0.001**	**<0.001**	**<0.05**
								48h	1.000	1.000	0.997	**<0.001**	**<0.001**	**<0.001**
									0h	1.000	0.989	**<0.001**	**<0.001**	**<0.01**
										24h	0.952	**<0.001**	**<0.001**	**<0.01**
											48h	**<0.001**	**<0.001**	**<0.001**
												0h	1.000	**<0.05**
													24h	**<0.01**
														48h

Table S3 | Cellular cholesterol levels of murine peritoneal macrophages. Cellular cholesterol content of primary peritoneal murine macrophages was determined using the Calbiochem® cholesterol/cholesteryl ester quantitation kit. The concentration of esterified cholesterol was determined by subtracting the free cholesterol from the total cholesterol, and the ratios of esterified-to-free cholesterol by dividing the values of esterified with free cholesterol. Values represent the total, free and esterified cholesterol reported as $\mu g/10^6$ cells (mean ± SEM; n = 12 mice).

	Placebo	MA-treated			LXR	
	PBS	**αMA**	**mMA**	**kMA**	**WT**	**KO**
Total cholesterol	16.2 ± 3.2	12.1 ± 1.1	13.0 ± 3.3	18.1 ± 3.5	14.6 ± 3.4	49.4 ± 3.7
Free cholesterol	11.8 ± 1.1	9.1 ± 0.9	10.2 ± 3.3	4.1 ± 0.7	12.8 ± 6.1	6.2 ± 1.0
Cholesterol ester	4.4 ± 1.6	2.9 ± 0.1	3.6 ± 2.8	14.0 ± 3.7	3.4 ± 0.6	43.8 ± 8.6
Ratio (ester:free)	0.4 ± 0.1	0.4 ± 0.1	0.4 ± 0.1	3.8 ± 1.6	0.3 ± 0.0	7.6 ± 0.9

Table S4 | Sequential Sidak pairwise comparisons showing differences among treatments in lipid droplet (LD) induction and mycobacterial replication of murine peritoneal macrophages. In the GLM, treatment was the independent predictor while LDs (GLM: Wald Chi-Square = 219.619, $P < 0.001$, $df = 5$, $n = 5$ confocal images) and BCG-dsRed bacilli (GLM: Wald Chi-Square = 54.723, $P < 0.001$, $df = 5$, $n = 5$ confocal images) were the dependent variables. Results were significant at $P < 0.05$ (bolded). Mock, macrophages from placebo (PBS) treated mice that were mock-infected with a PBS solution containing no BCG-dsRed. Macrophages from all other treatments were *ex vivo* infected with BCG-dsRed (MOI: 1).

Predictor		LDs		Mycobacteria	
Treatment		*df*	*P*	*df*	*P*
Mock	PBS	1	0.631	1	**<0.001**
	MA mix	1	**<0.001**	1	**<0.001**
	αMA	1	0.518	1	**<0.001**
	mMA	1	0.518	1	**<0.001**
	kMA	1	**<0.001**	1	**<0.001**
PBS	MA mix	1	**<0.001**	1	**<0.05**
	αMA	1	0.277	1	0.853
	mMA	1	0.631	1	0.234
	kMA	1	**<0.001**	1	0.114
MA mix	αMA	1	**<0.001**	1	**<0.05**
	mMA	1	**<0.001**	1	**<0.001**
	kMA	1	**<0.05**	1	0.799
αMA	mMA	1	**<0.05**	1	0.259
	kMA	1	**<0.001**	1	0.087
mMA	kMA	1	**<0.001**	1	**<0.01**

Table S5 | Sequential Sidak pairwise comparisons showing within- and between-group differences in lipid droplet (LD) induction and mycobacterial replication of murine peritoneal macrophages. In the GLM, treatment and time point were the independent predictors while LDs (GLM: Wald Chi-Square = 636.496, $P < 0.001$, $df = 17$, $n = 5$ per time point) and BCG-dsRed bacilli (GLM: Wald Chi-Square = 250.303, $P < 0.001$, $df = 17$, $n = 5$ per time point) were the dependent variables. Results were significant at $P < 0.05$ (bolded). Mock, macrophages from placebo (PBS) treated mice that were mock-infected with a PBS solution containing no BCG-dsRed. Macrophages from all other treatments were *ex vivo* infected with BCG-dsRed (MOI: 1).

Lipid droplets

Mock			PBS			MA mix			αMA			mMA			kMA		
0h	**48h**	**96h**	**0h**	**48h**	**96h**	**0h**	**48h**	**96h**	**0h**	**48h**	**96h**	**0h**	**48h**	**96h**	**0h**	**48h**	**96h**
0h	0.992	0.993	1.000	0.992	0.644	**<0.05**	**<0.001**	**<0.001**	1.000	1.000	1.000	1.000	1.000	**<0.01**	0.947	**<0.001**	**<0.001**
	48h	1.000	0.997	1.000	1.000	0.984	**<0.001**	**<0.001**	0.977	1.000	0.997	1.000	0.998	0.221	1.000	**<0.001**	**<0.01**
		96h	0.997	1.000	1.000	0.981	**<0.001**	**<0.001**	0.980	1.000	0.997	1.000	0.998	0.208	1.000	**<0.001**	**<0.001**
			0h	0.997	0.741	0.057	**<0.001**	**<0.001**	1.000	1.000	1.000	1.000	1.000	**<0.01**	0.977	**<0.001**	**<0.001**
				48h	1.000	0.984	**<0.001**	**<0.001**	0.977	1.000	0.997	1.000	0.998	0.220	1.000	**<0.001**	**<0.001**
					96h	1.000	**<0.001**	**<0.001**	0.484	1.000	0.736	1.000	0.800	0.823	1.000	**<0.001**	**<0.001**
						0h	**<0.01**	**<0.001**	**<0.05**	**<0.05**	**<0.05**	**<0.05**	**<0.05**	1.000	**<0.05**	**<0.001**	**<0.001**
							48h	**<0.05**	**<0.001**	**<0.001**	**<0.001**	**<0.001**	**<0.001**	**<0.05**	**<0.001**	**<0.001**	**<0.001**
								96h	**<0.001**	**<0.001**	**<0.001**	**<0.001**	**<0.001**	**<0.001**	**<0.001**	0.120	**<0.001**
									0h	1.000	1.000	0.999	1.000	**<0.001**	**<0.05**	**<0.001**	**<0.001**
										48h	1.000	1.000	1.000	**<0.05**	**<0.05**	**<0.001**	**<0.001**
											96h	1.000	1.000	**<0.01**	**<0.05**	**<0.001**	**<0.001**
												0h	1.000	0.059	**<0.05**	**<0.001**	**<0.001**
													48h	0.051	**<0.05**	**<0.001**	**<0.001**
														96h	0.429	**<0.001**	**<0.001**
															0h	**<0.001**	**<0.001**
																48h	**<0.001**
																	96h

Mycobacteria

Mock			PBS			MA mix			αMA			mMA			kMA		
0h	**48h**	**96h**	**0h**	**48h**	**96h**	**0h**	**48h**	**96h**	**0h**	**48h**	**96h**	**0h**	**48h**	**96h**	**0h**	**48h**	**96h**
0h	-	-	-	-	-	-	-	-	-	-	-	-	-	-	-	-	-
	48h	-	-	-	-	-	-	-	-	-	-	-	-	-	-	-	-
		96h	-	-	-	-	-	-	-	-	-	-	-	-	-	-	-
			0h	1.000	1.000	1.000	0.803	**<0.001**	1.000	1.000	1.000	1.000	1.000	1.000	0.974	**<0.05**	**<0.001**
				48h	1.000	1.000	1.000	**<0.001**	1.000	1.000	1.000	0.995	0.926	1.000	**<0.05**	0.950	**<0.001**
					96h	1.000	1.000	**<0.01**	1.000	1.000	1.000	0.974	0.812	1.000	**<0.05**	0.214	**<0.001**
						0h	0.947	**<0.001**	1.000	1.000	1.000	1.000	1.000	1.000	**<0.05**	**<0.05**	**<0.001**
							48h	**<0.05**	0.967	0.974	1.000	0.448	0.199	0.998	**<0.05**	1.000	**<0.001**
								96h	**<0.001**	**<0.001**	**<0.01**	**<0.001**	**<0.001**	**<0.001**	**<0.001**	**<0.01**	**<0.001**
									0h	1.000	1.000	1.000	1.000	1.000	0.817	**<0.05**	**<0.001**
										48h	1.000	1.000	1.000	1.000	0.812	**<0.05**	**<0.001**
											96h	0.982	0.831	1.000	**<0.05**	0.837	**<0.001**
												0h	1.000	1.000	1.000	**<0.05**	**<0.001**
													48h	0.994	1.000	**<0.05**	**<0.001**
														96h	0.580	**<0.05**	**<0.001**
															0h	**<0.01**	**<0.001**
																48h	**<0.001**
																	96h

Table S6 | Sequential Sidak pairwise comparisons showing differences in lipid droplet (LD) induction and mycobacterial growth at various MOIs of WT and LXR-deficient mouse macrophages. In the GLM, treatment and MOI were the independent predictors while LDs (Wald Chi-Square = 601.675, $P < 0.001$, $df = 5$; $n = 6$ per MOI) and mycobacteria (Wald Chi-Square = 517.150, $P < 0.001$, $df = 5$; $n = 6$ per MOI) were the dependent variables. Results were significant at $P < 0.05$ (bolded).

Predictors		LDs		Mycobacteria	
Treatment*MOI	**Treatment*MOI**	***df***	***P***	***df***	***P***
WT, 0.25	WT, 0.5	1	0.637	1	**<0.01**
	WT, 1	1	0.637	1	**<0.001**
	KO, 0.25	1	**<0.001**	1	**<0.001**
	KO, 0.5	1	**<0.001**	1	**<0.001**
	KO, 1	1	**<0.001**	1	**<0.001**
WT, 0.5	WT, 1	1	0.791	1	**<0.001**
	KO, 0.25	1	**<0.001**	1	**<0.001**
	KO, 0.5	1	**<0.001**	1	**<0.001**
	KO, 1	1	**<0.001**	1	**<0.001**
WT, 1	KO, 0.25	1	**<0.001**	1	**<0.001**
	KO, 0.5	1	**<0.001**	1	0.259
	KO, 1	1	**<0.001**	1	**<0.001**
KO, 0.25	KO, 0.5	1	0.115	1	**<0.001**
	KO, 1	1	0.637	1	**<0.001**
KO, 0.5	KO, 1	1	**<0.01**	1	**<0.001**

Table S7 | Sequential Sidak pairwise comparisons depicting within- and between-group differences in mycobacterial MOI over time for WT and LXR-deficient macrophages. In the GLM treatment, MOI and time point were the independent predictors while BCG-dsRed bacilli was the dependent variable (Wald Chi-Square = 576.689, $P < 0.001$, $df = 17$; $n = 6$ per MOI per time point). Results were significant at $P < 0.05$ (bolded).

WT									KO								
0.25			0.5			1			0.25			0.5			1		
0h	48h	96h	0h	48h	96h	0h	48h	96h	0h	48h	96h	0h	48h	96h	0h	48h	96h
0h	0.999	0.986	0.910	0.521	**<0.05**	**<0.01**	**<0.001**	**<0.001**	0.809	**<0.05**	**<0.01**	**<0.001**	**<0.001**	**<0.001**	**<0.001**	**<0.001**	**<0.001**
	48h	1.000	0.998	0.968	0.286	**<0.01**	**<0.001**	**<0.001**	0.996	0.172	**<0.05**	**<0.01**	**<0.001**	**<0.001**	**<0.001**	**<0.001**	**<0.001**
		96h	1.000	0.997	0.694	**<0.05**	**<0.01**	**<0.001**	1.000	0.521	0.138	**<0.05**	**<0.001**	**<0.001**	**<0.001**	**<0.001**	**<0.001**
			0h	1.000	0.909	0.101	**<0.01**	**<0.001**	1.000	0.809	0.332	0.119	**<0.001**	**<0.001**	**<0.001**	**<0.001**	**<0.001**
				48h	0.996	0.410	**<0.05**	**<0.01**	1.000	0.988	0.809	0.484	**<0.001**	**<0.001**	**<0.001**	**<0.001**	**<0.001**
					96h	0.983	0.575	0.093	0.972	1.000	0.999	0.993	**<0.001**	**<0.001**	**<0.001**	**<0.001**	**<0.001**
						0h	1.000	0.982	0.176	0.994	1.000	1.000	0.809	**<0.05**	**<0.001**	**<0.001**	**<0.001**
							48h	1.000	**<0.05**	0.754	0.980	0.997	0.996	0.356	**<0.01**	**<0.001**	**<0.001**
								96h	**<0.01**	0.161	0.553	0.842	1.000	0.899	**<0.05**	**<0.001**	**<0.001**
									0h	0.910	0.509	0.209	**<0.001**	**<0.001**	**<0.001**	**<0.001**	**<0.001**
										48h	1.000	0.997	**<0.05**	**<0.001**	**<0.001**	**<0.001**	**<0.001**
											96h	1.000	0.127	**<0.001**	**<0.001**	**<0.001**	**<0.001**
												0h	0.358	**<0.01**	**<0.001**	**<0.001**	**<0.001**
													48h	0.966	**<0.01**	**<0.001**	**<0.001**
														96h	0.553	**<0.01**	**<0.001**
															0h	0.988	**<0.05**
																48h	0.803
																	96h

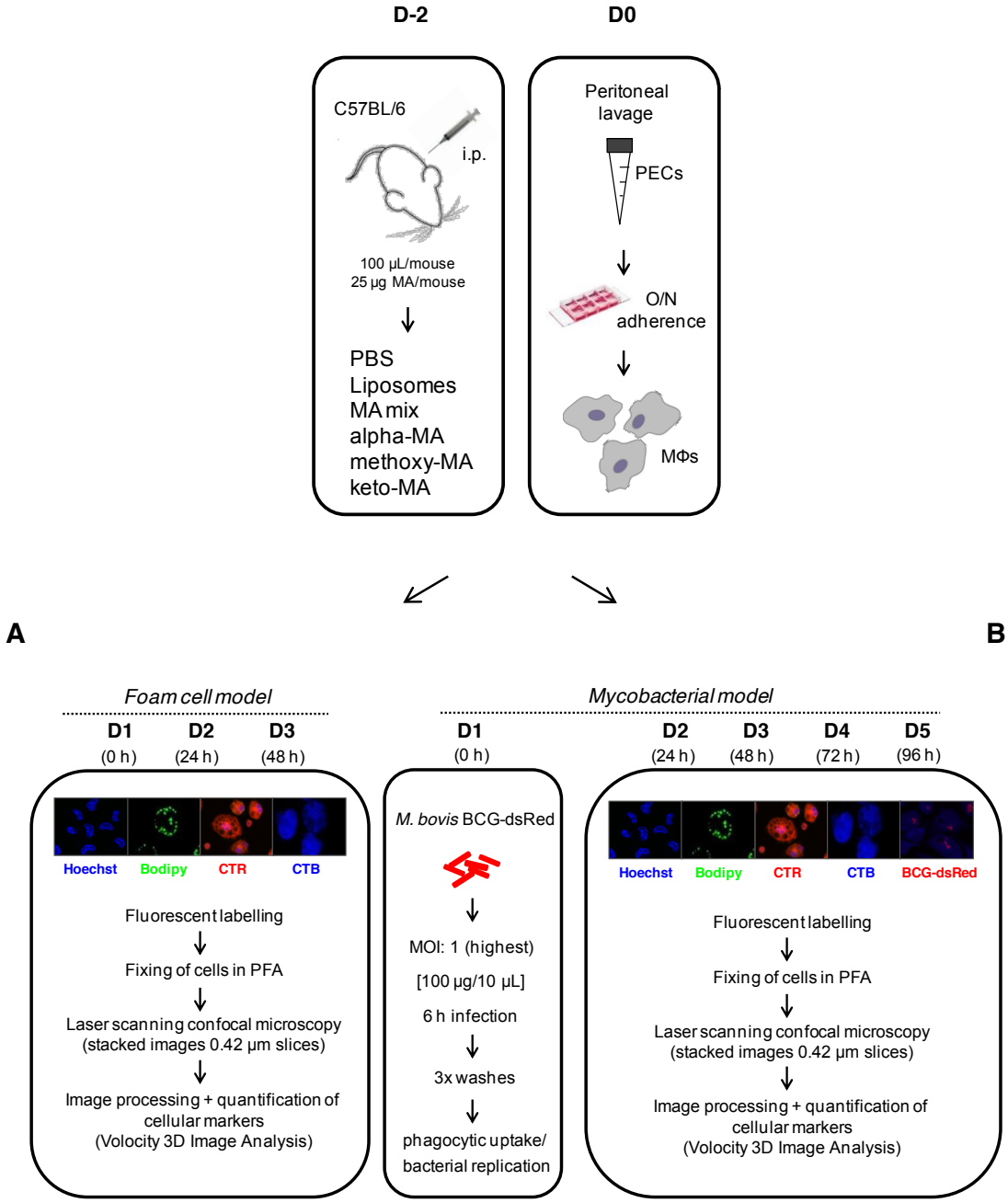

Figure S1 | Schematic overview of the experimental design of the foam cell and mycobacterial models. Two days prior to harvesting of the peritoneal exudate cells (PECs), mice were treated intraperitoneally (i.p.) with PBS, empty liposome carrier or either of various MAs (25 µg/100 µL/mouse). Mice were sacrificed on D0 and PECs collected through peritoneal lavage with 10 mL ice cold PBS. Cells were seeded into µ-Slide 8-well microscopy plates (ibidi®) and macrophages selected for with an overnight adherence step. ***A***, *Foam cell model*. Macrophages were incubated for a further three days. On each day, live cells were fluorescently labelled for 30 min at 37°C then fixed for 15 min each in 2% then 4% paraformaldehyde (PFA). Fixed cells were immediately imaged by laser-scanning-confocal microscopy (Z-stacked images of 0.42 µm slices). All images were processed and analysed for quantification of intracellular markers with the use of Volocity 3D Image Analysis Software. ***B***, *Mycobacterial model*. Following overnight adherence, macrophages were infected for 6 h with *M. bovis* BCG-dsRed at an MOI of 1:1 (100 µg/10 µL). After infection, cells were washed three times in endotoxin-free PBS and either stained and imaged (phagocytic uptake) or cultured for up to five days (replication).

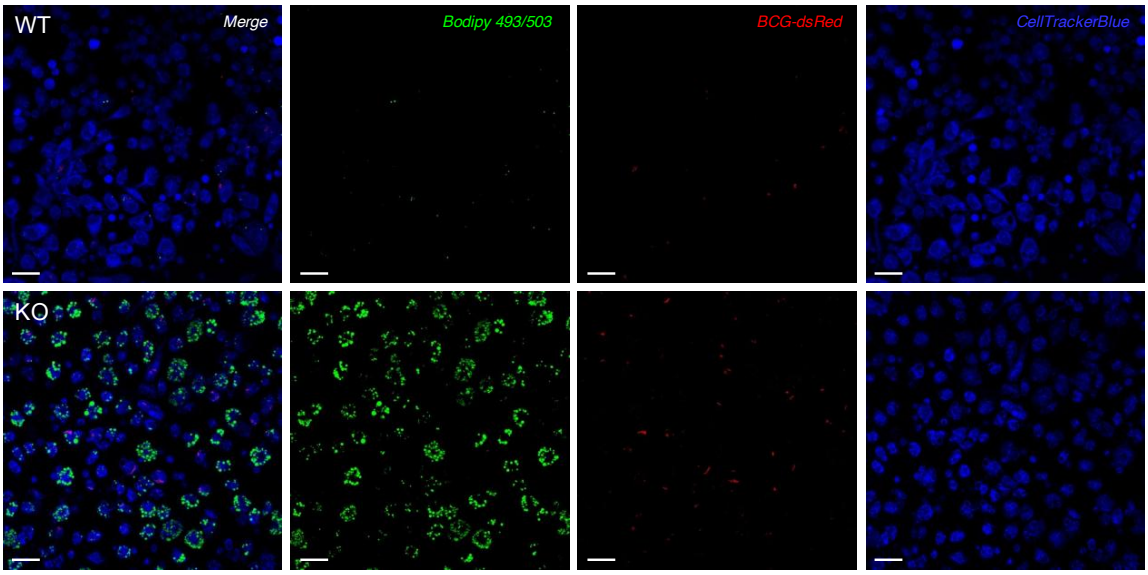

Figure S2 | Fluorescently-labelled macrophages from WT and LXR-deficient mice after five days of culture. Laser-scanning-confocal microscopy was used to measure intracellular LDs and mycobacterial growth (BCG-dsRed bacilli MOI: 1) in macrophages from WT and LXR$\alpha^{-/-}\beta^{-/-}$ KO mice. Neutral LDs were fluorescently labelled with Bodipy®493/503 and cytoplasm with CellTracker™Blue. Scale bar: 24 µm.

2. Additional experiments

2.1 Screen for LXR target genes and ER stress markers in MA-treated macrophages

Materials and methods

C57BL/6 mice were treated intraperitoneally (i.p.) with liposome-formulated MAs (Mtb mixture; Sigma) and peritoneal exudate cells (PECs) isolated at specific time points (4, 12, 24, 48 and 96 h). Primary macrophages were enriched through magnetic cell sorting with biotin-labelled F4/80 antibody (clone CI:A3-1, AbD Serotec) and anti-biotin microbeads (Miltenyi Biotec), used according to the manufacturer's instructions. Flow cytometry was used to assess purity of the F4/80-enriched samples (~60 %). The RNeasy Mini Kit (Qiagen) was used to extract total RNA and complementary DNA was prepared with Superscript II (Invitrogen). Quantitative PCR (qPCR) was performed with a SYBRGreen mixture (GC Biotech) on a Roche LightCycler 480 system (Applied Biosystems). The sequences of the primers used were as follows:

Liver X receptor (LXR) target genes

mLXRα (fwd): 5'-TCATGCTTCTGGAGACGT-3'

mLXRα (rvse): 5'-CTCAGCATCATTGAGTTGC-3'

mAbcg1 (fwd): 5'-GGCAGGCTCCTCCCAGACTTC-3'

mAbcg1 (rvse): 5'-GGCAGGCTCCTCCCAGACTTC-3'

mAbca1 (fwd): 5'-CGCAAGCATATGCCTCAT-3'

mAbca1 (rvse): 5'-CCCATTACATAACACATGGCT-3'

mScd1 (fwd): 5'-TGGGGCTGCTAATCTCTGGGTGTA-3'

mScd1 (rvse): 5'-GGCTTTATCTCTGGGGTGGGTTTG-3'

Endoplasmic reticulum (ER) stress markers

mPerk (fwd): 5'-GTAGCCACGACCTTCATCG-3'

mPerk (rvse): 5'-TTTCAGTCTGGCACTGAGTTTC-3'

mIre1 (fwd): 5'-GACATGGCTACCATTATCCTGAG-3'

mIre1 (rvse): 5'-CTGACGCTGCTGATGCAC-3'

mAtf6a (fwd): 5'-CCACCAGAAGTATGGGTTCG-3'

mAtf6a (rvse): 5'-CAGACTCTCGGTTCTTTATCATCC-3'

mGrp78/mBiP (fwd): 5'-ATGAGGCTGTAGCCTATGGTG-3'

mGrp78/mBiP (rvse): 5'-GGGGACAAACATCAAGCAG-3'

mChop (fwd): 5'-CCACCACACCTGAAAGCAG-3'

mChop (rvse): 5'-TCCTGCAGATCCTCATACCAG-3'

mGADD34 (fwd): 5'-TTCCTCTAAAAGCTCGGAAGG-3'

mGADD34 (rvse): 5'-CAAAGCGGCTTCGATCTC-3'

mGrp94 (fwd): 5'-CAGTATGGATGGTCTGGCAAC-3'

mGrp94 (rvse): 5'-ACGTTTTCTTTTGACTGGCATAG-3'

mCalr (fwd): 5'-TGGCAAATTTGTCCTCAGTTC-3'

mCalr (rvse): 5'-TGCGTAAAATCGGGCATC-3'

mXbp1 unspliced (fwd): 5'-CACGCTTGGGAATGGACACGCT-3'

mXbp1 unspliced (rvse): 5'-TGCACATAGTCTGAGTGCTGCGC-3'

mXbp1 spliced (fwd): 5'-CACGCTTGGGAATGGACACGCT-3'

mXbp1 spliced (rvse): 5'-GCCTGCACCTGCTGCGGACTC-3'

Results and discussion

(A) LXR target genes

In comparison to a control treatment of liposomes containing no MA, a 4-fold induction of relative mRNA expression was recorded for the murine nuclear receptor Lxrα in F4/80$^+$ macrophages from two days of treatment with the Mtb MA mixture (Fig. S3). Though a marked down-regulation in relative mRNA expression was recorded for the cellular cholesterol export genes Abcg1 and Abca1 after one day, there was no distinct expression pattern recorded in F4/80$^+$ macrophages at the other time points. The gene encoding stearoyl-CoA desaturase-1 (Scd1), a key enzyme of fatty acid metabolism producing monounsaturated from saturated fatty acid species[1], was downregulated by Mtb MAs (Fig. S3).

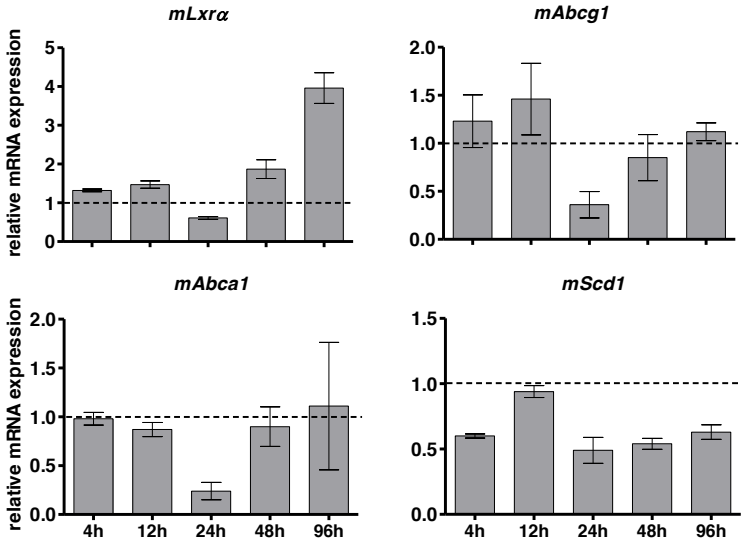

Figure S3 | LXR target genes. Mouse peritoneal exudate cells harvested after two days of treatment with empty liposome carrier containing no MA (dotted line) or MA-liposomes (Mtb mixture, Sigma Aldrich), were enriched for F4/80$^+$ macrophages with magnetic cell sorting. RNA was extracted from F4/80+ macrophages and LXR target genes analysed by qPCR. Lxrα, liver X receptor alpha; Abcg1 and Abca1, ATP-binding cassette transporters G1 and A1; SCD1, stearoyl-CoA desaturase-1.

The LXRs are key transcriptional regulators of cellular cholesterol balance[2-4]. Upon activation by oxysterol ligands, LXRs induce an array of genes involved in cholesterol transport[5]. The ATP-binding cassette transporters A1 (ABCA1) and G1 (ABCG1) are crucial in maintenance of sterol homeostasis through the efflux of excess cholesterol to lipid-poor apolipoproteins or high density lipoproteins[3]. A strong induction of the nuclear receptor Lxrα following treatment with Mtb MA mixture (that should induce abundant LDs) was not mirrored by the cellular cholesterol exporters Abcg1 and Abca1, which should be upregulated following abundant lipid loading. The gene encoding the key enzyme involved in the desaturation of stearic acid to oleic acid (Scd1) was also downregulated in cells from Mtb MA-treated mice. SCD1 activity is important in cellular cholesterol metabolism as it provides the monounsaturated fatty acids needed for synthesis of cholesteryl esters[6], while also maintaining membrane lipid content and fluidity[7]. SCD1 has been shown to inhibit ABCA1-mediated cholesterol efflux (through membrane domain reorganisation) and to be a source of fatty acyl-CoAs that could be easily incorporated into phospholipids[8]. This strategy of preventing LD export and utilising host SCD1-derived acyl-CoAs would surely benefit mycobacteria. Though Scd1 was not upregulated following Mtb MA treatment, neither were the cholesterol transporters. This hints towards a plausible inhibition by Mtb of host cholesterol export, and warranted further investigation. As a result of time constraints we were unable to assess the expression of cholesterol-associated target genes following treatment with the oxygenated MAs or BCG.

(B) ER stress markers

No major mRNA expression patterns were observed in ER stress markers in F4/80^{+} murine macrophages. Our results did show that Mtb MAs decreased the expression of the integral ER membrane protein Perk (protein kinase R-like ER kinase) from two days of MA treatment (Fig. S4). On day two following Mtb MA treatment, thus coinciding with the distinct induction of cellular vacuoles and LDs, Ire1 mRNA was reduced by 50% while Grp78 and Calr mRNA was ~50% upregulated (yet followed no clear expression pattern). The ubiquitously expressed unspliced isoform of Xbp1 was 50% upregulated after four hours of Mtb MA treatment, but was followed by a gradual downregulation (Fig. S4).

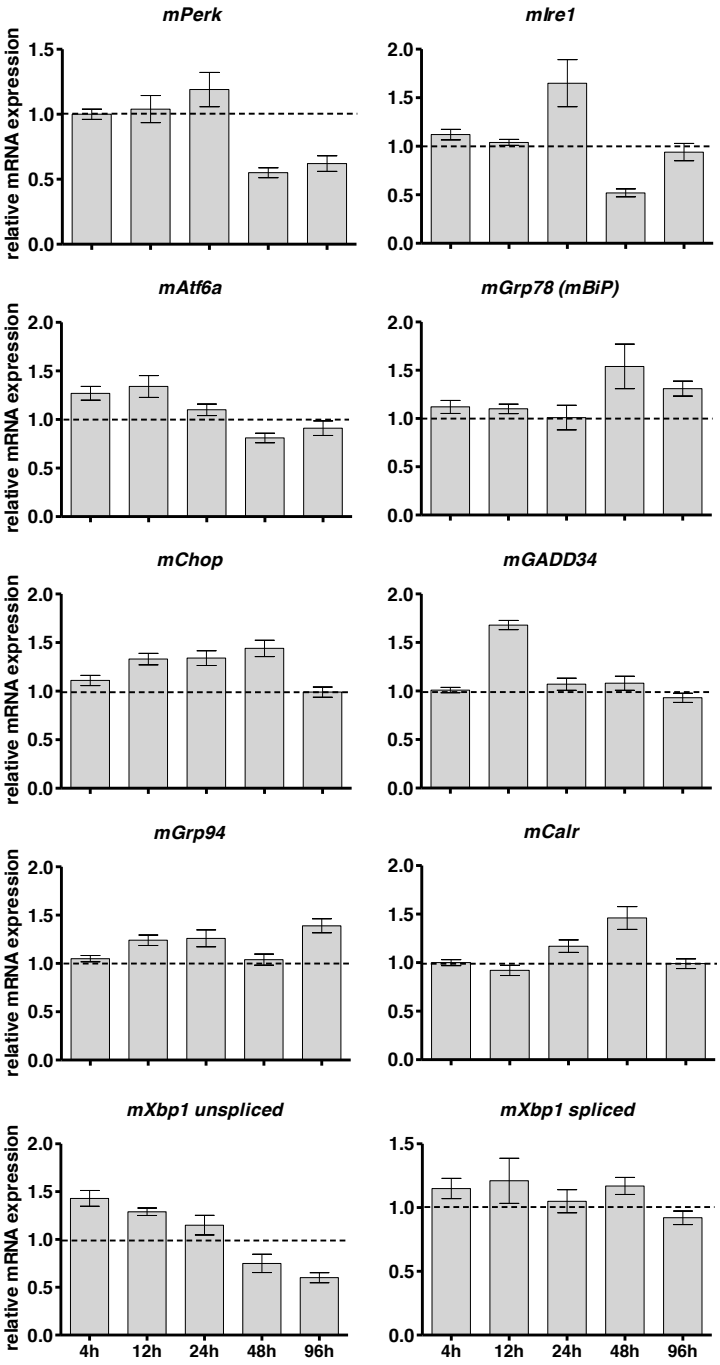

Figure S4 | ER stress markers. Mice were treated with empty liposome carrier containing no MA (dotted line) or MA-liposomes (Mtb mixture, Sigma Aldrich) for 48 h and peritoneal exudate cells enriched for F4/80$^+$ macrophages with magnetic cell sorting. RNA was extracted and LXR target genes analysed by qPCR. Perk, protein kinase R (PKR)-like ER kinase; Ire1, inositol-requiring enzyme-1; Atf6a, activating transcription factor-6; Grp78 (BiP), 78 kDa glucose-related protein (binding immunoglobulin protein); Chop, CCAAT/enhancer-binding protein (C/EBP) homologous protein; GADD34, 34 kDa growth arrest and DNA damage-inducible protein; Grp94, 94 kDa glucose-related protein; Calr, calreticulin; Xbp1, X-box binding protein-1 (ubiquitously expressed unspliced and Ire1-mediated spliced isoforms).

The ER lumen regulates folding of proteins and acts as a quality-control checkpoint to ensure only properly folded proteins are secreted or delivered to transmembrane locations[9, 10]. ER stress can result from exogenous or endogenous stimuli thus activating the unfolded protein response (UPR) to restore balance to the ER machinery[11]. First, through expression of ER transmembrane proteins (IRE1 and ATF) to stimulate molecular chaperones and protein folding enzymes to raise ER folding capacity (Grp78, Grp94, Calr); and second by activation of the resident ER transmembrane protein PERK (PKR-like ER kinase) to reduce the unfolded protein load by preventing protein synthesis[10]. The Mtb MA mixture did not bring about a significant UPR in murine F4/80^{+} macrophages. Mtb infection, however, elicits ER stress in macrophages from mouse and human tuberculous granulomas and effects ER stress-induced apoptosis[12, 13]. Considering the intricacy of Mtb entry into host cells and the vast array of mediators involved in the resultant immune response, our model of using only the MA mixture to replicate the complex TB environment may not have been sufficient to elicit an ER stress response. In this study we reported on progress of the functional diversity of Mtb MAs, and showed that each of the major classes of Mtb MAs elicits distinct foam cell responses that either facilitated or prevented mycobacterial growth. The lack of ER stress induction by the combined MA mixture in this experiment may thus reflect the compositions of the three major MA classes as they occur in nature. The inflammatory neutral alpha-MA (~53% of total MAs) being the dominant constituent, whereas the bioactive oxygenated methoxy and keto MAs (totalling ~47%) make up the other portion[14]. Due to time constraints we were unable to further investigate ER stress in mycobacteria-infected foam cells from mice treated with the individual MA classes. Future study may therefore enable a better understanding of the underlying mechanisms involved in TB-induced ER stressors.

3. References

1. Sampath, H. and J. M. Ntambi. 2011. The role of stearoyl-CoA desaturase in obesity, insulin resistance, and inflammation. *Ann. N. Y. Acad. Sci.* **1243**: 47-53.

2. Peet, D. J., B. A. Janowski and D. J. Mangelsdorf. 1998. The LXRs: a new class of oxysterol receptors. *Curr. Opin. Genet. Dev.* **8**: 571-575.

3. Jakobsson, T., E. Treuter, J. A. Gustafsson and K. R. Steffensen. 2012. Liver X receptor biology and pharmacology: new pathways, challenges and opportunities. *Trends Pharmacol. Sci.* **33**: 394-404.

4. Wojcicka, G., A. Jamroz-Wisniewska, K. Horoszewicz and J. Beltowski. 2007. Liver X receptors (LXRs). Part I: structure, function, regulation of activity, and the role in lipid metabolism. *Postepy Hig. Med. Dosw.* **61**: 736-759.

5. Ignatova, I. D., J. Angdisen, E. Moran and I. G. Schulman. 2013. Differential regulation of gene expression by LXRs in response to macrophage cholesterol loading. *Mol. Endocrinol.* **27**: 1036-1047.

6. Hodson, L. and B. A. Fielding. 2013. Stearoyl-CoA desaturase: rogue or innocent bystander? *Prog. Lipid Res.* **52**: 15-42.

7. Ntambi, J. M. 1999. Regulation of stearoyl-CoA desaturase by polyunsaturated fatty acids and cholesterol. *J. Lipid Res.* **40**: 1549-1558.

8. Sun, Y., M. Hao, Y. Luo, C. P. Liang, D. L. Silver, C. Cheng, F. R. Maxfield and A. R. Tall. 2003. Stearoyl-CoA desaturase inhibits ATP-binding cassette transporter A1-mediated cholesterol efflux and modulates membrane domain structure. *J. Biol. Chem.* **278**: 5813-5820.

9. Cao, S. S. and R. J. Kaufman. Unfolded protein response. *Curr. Biol.* **22**: R622-R626.

10. Ron, D. and P. Walter. 2007. Signal integration in the endoplasmic reticulum unfolded protein response. *Nat. Rev. Mol. Cell Biol.* **8**: 519-529.

11. Takayanagi, S., R. Fukuda, Y. Takeuchi, S. Tsukada and K. Yoshida. 2013. Gene regulatory network of unfolded protein response genes in endoplasmic reticulum stress. *Cell Stress Chaperones* **18**: 11-23.

12. Seimon, T. A., M. J. Kim, A. Blumenthal, J. Koo, S. Ehrt, H. Wainwright, L. G. Bekker, G. Kaplan, C. Nathan, I. Tabas and D. G. Russell. 2010. Induction of ER stress in macrophages of tuberculosis granulomas. *PLoS One* **5**: e12772.

13. Choi, H. H., D. M. Shin, G. Kang, K. H. Kim, J. B. Park, G. M. Hur, H. M. Lee, Y. J. Lim, J. K. Park, E. K. Jo and C. H. Song. 2010. Endoplasmic reticulum stress response is involved in Mycobacterium tuberculosis protein ESAT-6-mediated apoptosis. *FEBS Lett.* **584**: 2445-2454.

14. Ndlandla, F. L., V. Ejoh, A. C. Stoltz, B. Naicker, A. D. Cromarty, S. van Wyngaardt, M. Khati, L. S. Rotherham, Y. Lemmer, J. Niebuhr, C. R. Baumeister, J. R. Al-Dulayymi, H. Swai, M. S. Baird and J. A. Verschoor. 2016. Standardization of natural mycolic acid antigen composition and production for use in biomarker antibody detection to diagnose active tuberculosis. *J. Immunol. Methods* **435**: 50-59.

CHAPTER III |

Lipidome immunomodulation of murine macrophages by chemically synthetic mycobacterial mycolates

---

Supplemental data

---

1. Supplemental data

Table S1 | SIMPER and ANOSIM output of glycerophospholipid profiles. *Glycerophospholipid profiles:* SIMPER analyses identified global and between-group average dissimilarity (%). For pairwise comparisons, one-way ANOSIM output of quantitative data (nmol/µg DNA) is reported as an R value from one (dissimilar) to zero (similar) with an associated significance value (brackets: $P \leq 0.05$, bolded). The global significance and R value are also reported for each ANOSIM test. The number of phospholipid species included in each analysis is indicated. *Influential lipid species:* SIMPER identified the influential phospholipid species contributing at least 75% to global cumulative group dissimilarity (all treatments). Influential lipid species responsible for significant pairwise differences (as identified by ANOSIM) are given to highlight the effect of natural MA treatment (PBS vs. MA mix) or differences between the oxygenated MAs (kMA vs. mMA). PC, phosphatidylcholine; PE, phosphatidylethanolamine; PI, phosphatidylinositol; PS, phosphatidylserine.

Glycerophospholipid profiles				
	PC	**PE**	**PI**	**PS**
Lipid species analysed	56	50	50	47
Total *n*	504	450	450	423
Global dissimilarity	34.1%	38.3%	34.5%	35.9%
Global R value	0.4688	0.6406	0.6719	0.4375
Global significance (*P*)	0.00604**	0.00259**	0.00223**	0.00118**
PBS/MA mix	55.7% **|** 1(**<0.01**)	62.3% **|** 1 (**<0.01**)	51.1% **|** 1 (**<0.01**)	50.1% **|** 0.75 (**0.01**)
PBS/αMA	20.2% **|** -1 (0.66)	28.4% **|** 0.25 (0.32)	32.7% **|** 1 (**<0.01**)	22.1% **|** 0 (0.62)
PBS/kMA	51.2% **|** 1 (**<0.01**)	55.1% **|** 1 (**<0.01**)	46.4% **|** 1 (**<0.01**)	51.5% **|** 1 (**<0.01**)
PBS/mMA	55.2% **|** 0.75 (**<0.01**)	21.4% **|** 0 (0.67)	29.1% **|** 0.25 (**<0.01**)	29.5% **|** 0 (0.07)
MA mix/αMA	46.0% **|** 1 (**<0.01**)	42.9% **|** 1 (**<0.01**)	35.5% **|** 1 (**<0.01**)	37.2% **|** 1 (**<0.01**)
MA mix/kMA	7.2% **|** 0.5 (**<0.01**)	11.2% **|** 0.5 (**<0.05**)	11.7% **|** 0.5 (**<0.01**)	12.4% **|** 0 (**<0.01**)
MA mix/mMA	13.8% **|** -0.25 (0.11)	51.6% **|** 1 (**<0.01**)	39.5% **|** 0.75 (**<0.01**)	40.6% **|** 0.5 (**<0.01**)
αMA/kMA	40.8% **|** 1 (**<0.01**)	33.4% **|** 1 (**<0.05**)	30.5% **|** 1 (**<0.01**)	38.6% **|** 1 (**<0.01**)
αMA/mMA	45.9% **|** 0.75 (**<0.01**)	18.9% **|** 0 (0.07)	28.0% **|** -1 (0.67)	27.6% **|** -1 (0.17)
kMA/mMA	13.4% **|** 0.5 (**<0.05**)	43.3% **|** 1 (**<0.01**)	34.6% **|** 0.5 (**<0.01**)	40.6% **|** 0.5 (**<0.01**)

Influential lipid species				
Glycerophospholipid species (% cumulative contribution to dissimilarity) **|** contribution factor				
	PC	**PE**	**PI**	**PS**
All treatments	**36:1** (19.1%) **|** 6.6	**38:4** (31.3%) **|** 12.2	**38:4** (41.6%) **|** 14.4	**36:2** (16.4%) **|** 5.9
**global dissimilarity*	**36:4** (32.9%) **|** 4.8	**36:2** (41.0%) **|** 3.8	**36:4** (49.1%) **|** 2.6	**38:4** (31.8%) **|** 5.5
	36:2 (45.0%) **|** 4.2	**36:1** (49.2%) **|** 3.2	**38:3** (55.9%) **|** 2.3	**36:1** (46.9%) **|** 5.4
	32:0 (56.8%) **|** 4.1	**40:4** (56.3%) **|** 2.8	**36:2** (62.3%) **|** 2.2	**40:4** (59.9%) **|** 4.7
	38:4 (65.9%) **|** 3.2	**36:4** (62.4%) **|** 2.4	**40:4** (66.6%) **|** 1.5	**38:3** (67.2%) **|** 2.6
	36:3 (72.3%) **|** 2.2	**40:6** (67.6%) **|** 2.0	**38:5** (70.6%) **|** 1.4	**40:6** (71.9%) **|** 1.7
	38:5 (75.6%) **|** 1.2	**34:1** (71.5%) **|** 1.5	**36:3** (73.2%) **|** 0.9	**40:5** (76.2%) **|** 1.5
		40:5 (75.1%) **|** 1.4	**36:1** (75.8%) **|** 0.9	
PBS/MA mix	**36:1** (19.1%) **|** 10.6	**38:4** (32.1%) **|** 20.0	**38:4** (45.9%) **|** 23.4	**36:2** (18.6%) **|** 9.3
**effect of natural MA*	**32:0** (33.0%) **|** 7.7	**36:2** (42.9%) **|** 6.7	**38:3** (53.7%) **|** 4.0	**36:1** (32.7%) **|** 7.0
treatment	**36:4** (46.0%) **|** 7.3	**36:1** (51.2%) **|** 5.2	**36:2** (61.4%) **|** 3.9	**38:4** (46.6%) **|** 6.9
	36:2 (57.8%) **|** 6.6	**40:4** (58.4%) **|** 4.5	**36:4** (68.8%) **|** 3.8	**40:4** (59.3%) **|** 6.4
	38:4 (66.6%) **|** 4.9	**36:4** (64.9%) **|** 4.1	**40:4** (73.4%) **|** 2.4	**38:3** (66.5%) **|** 3.6
	36:3 (73.1%) **|** 3.6	**40:6** (69.9%) **|** 3.1	**38:5** (77.8%) **|** 2.3	**34:1** (71.3%) **|** 2.4
	38:5 (76.2%) **|** 1.8	**34:1** (74.1%) **|** 2.6		**40:5** (75.9%) **|** 2.3
		38:5 (77.7%) **|** 2.2		
kMA/mMA	**36:4** (15.6%) **|** 2.1	**38:4** (33.6%) **|** 14.5	**38:4** (44.6%) **|** 15.4	**38:4** (%) **|** 7.4
**effect of oxygenated MA*	**36:2** (31.1%) **|** 2.1	**36:1** (41.9%) **|** 3.6	**36:4** (53.6%) **|** 3.1	**36:2** (%) **|** 6.5
treatment	**36:1** (45.1%) **|** 2.0	**40:4** (50.0%) **|** 3.5	**38:3** (59.5%) **|** 2.1	**40:4** (%) **|** 6.0
	38:4 (55.8%) **|** 1.8	**36:2** (57.9%) **|** 3.4	**40:4** (63.9%) **|** 1.5	**36:1** (%) **|** 5.6
	32:0 (63.5%) **|** 1.5	**36:4** (63.3%) **|** 2.5	**36:2** (68.3%) **|** 1.5	**38:3** (%) **|** 3.1
	36:3 (70.1%) **|** 1.3	**40:6** (69.1%) **|** 2.4	**38:5** (72.1%) **|** 1.3	**40:6** (%) **|** 2.4
	38:5 (74.2%) **|** 0.8	**40:5** (73.0%) **|** 1.6	**36:3** (75.1%) **|** 1.0	
	34:1 (77.9%) **|** 0.4	**38:3** (76.5%) **|** 1.5		

Table S2 | SIMPER and ANOSIM output of lysophospholipid profiles. *Lysophospholipid profiles:* SIMPER analyses identified global and between-group average dissimilarity (%). For pairwise comparisons, one-way ANOSIM output of quantitative data (nmol/µg DNA) is reported as an R value from one (dissimilar) to zero (similar) with an associated significance value (brackets: $P \leq 0.05$, bolded). The global significance and R value are also reported for each ANOSIM test. The number of lysophospholipid species included in each analysis is indicated. *Influential lipid species:* SIMPER identified the influential lysophospholipid species contributing at least 75% to global cumulative group dissimilarity (all treatments). Influential lipid species responsible for significant pairwise differences (as identified by ANOSIM) are given to highlight the effect of natural MA treatment (PBS vs. MA mix) or differences between the oxygenated MAs (kMA vs. mMA). lysoPC, lysophosphatidylcholine; lysoPE, lysophosphatidylethanolamine; lysoPI, lysophosphatidylinositol; lysoPS, lysophosphatidylserine; n.s., not significant.

Lysophospholipid profiles

	lysoPC	**lysoPE**	**lysoPI**	**lysoPS**
Lipid species analysed	27	13	23	22
Total *n*	243	117	207	198
Global dissimilarity	30.6%	31.5%	24.5%	14.7%
Global R value	0.4219	0.5469	0.3594	0.6094
Global significance (*P*)	0.01038*	0.00464**	0.01364*	0.00272**
PBS/MA mix	21.5% **|** 0.5 (**<0.05**)	22.6% **|** 0.5 (**<0.01**)	22.4% **|** 0 (0.67)	15.0% **|** 1 (**<0.01**)
PBS/αMA	22.7% **|** 0 (**<0.05**)	24.0% **|** -1 (0.051)	28.7% **|** 0 (0.63)	9.9% **|** 0 (**<0.01**)
PBS/kMA	47.1% **|** 1 (**<0.01**)	29.2% **|** 0.5 (**<0.01**)	21.5% **|** 0 (0.63)	20.5% **|** 1 (**<0.01**)
PBS/mMA	51.4% **|** 1 (**<0.01**)	29.4% **|** 0.25 (**<0.01**)	26.5% **|** 0. 5 (**<0.01**)	7.7% **|** -0.5 (0.11)
MA mix/αMA	10.5% **|** -1 (0.31)	39.6% **|** 1 (**<0.01**)	31.3% **|** 1 (**<0.05**)	9.9% **|** 1 (**<0.01**)
MA mix/kMA	31.2% **|** 1 (**<0.01**)	10.3% **|** 0.25 (0.07)	10.6% **|** -0.5 (0.69)	7.4% **|** 0.25 (0.33)
MA mix/mMA	36.2% **|** 1 (**<0.01**)	46.6% **|** 1 (**<0.01**)	26.8% **|** 1 (**<0.01**)	18.8% **|** 1 (**<0.01**)
αMA/kMA	27.8% **|** 1 (**<0.01**)	46.4% **|** 1 (**<0.01**)	33.4% **|** 1 (**<0.01**)	14.7% **|** 1 (**<0.01**)
αMA/mMA	32.9% **|** 1 (**<0.01**)	11.9% **|** 0 (**<0.01**)	19.3% **|** 0.25 (**<0.01**)	13.2% **|** 1 (**<0.01**)
kMA/mMA	10.6% **|** 0.25 (**<0.05**)	53.0% **|** 1 (**<0.01**)	27.9% **|** 1 (**<0.01**)	24.1% **|** 1 (**<0.01**)

Influential lipid species

Lysophospholipid species (% cumulative contribution to dissimilarity) **|** contribution factor

	lysoPC	**lysoPE**	**lysoPI**	**lysoPS**
All treatments	**16:0** (29.9%) **|** 10.2	**18:0** (39.8%) **|** 12.5	**18:0** (24.2%) **|** 6.5	**18:0** (44.0%) **|** 6.5
**global dissimilarity*	**18:1** (46.3%) **|** 5.6	**20:4** (53.0%) **|** 4.1	**20:4** (48.0%) **|** 5.8	**18:1** (55.7%) **|** 1.7
	18:2 (61.8%) **|** 5.3	**16:0** (64.8%) **|** 3.7	**14:4** (55.0%) **|** 3.7	**18:2** (62.8%) **|** 1.0
	20:4 (73.8%) **|** 4.1	**18:1** (74.4%) **|** 3.0	**20:0** (63.3%) **|** 2.6	**16:0** (69.4%) **|** 1.0
	18:0 (84.4%) **|** 3.6	**22:4** (83.1%) **|** 2.8	**22:4** (66.6%) **|** 1.2	**14:1** (75.7%) **|** 0.9
			20:3 (69.1%) **|** 1.2	
			16:0 (73.1%) **|** 1.1	
			18:1 (76.7%) **|** 1.0	
PBS/MA mix	**16:0** (27.7%) **|** 5.9	**18:0** (34.9%) **|** 7.9		**18:0** (49.5%) **|** 7.4
**effect of natural MA*	**18:1** (47.9%) **|** 4.3	**16:0** (51.8%) **|** 3.8		**18:2** (59.7%) **|** 1.5
treatment	**18:2** (65.6%) **|** 3.8	**18:1** (65.4%) **|** 3.1	n.s.	**18:1** (69.9%) **|** 1.5
	20:4 (77.7%) **|** 2.6	**20:4** (74.1%) **|** 2.0		**16:0** (77.7%) **|** 1.2
		18:2 (82.6%) **|** 1.9		
kMA/mMA	**18:2** (29.8%) **|** 3.2	**18:0** (43.0%) **|** 22.8	**18:0** (29.3%) **|** 8.2	**18:0** (47.0%) **|** 11.3
**effect of oxygenated MA*	**16:0** (45.7%) **|** 1.7	**20:4** (56.0%) **|** 6.9	**20:4** (57.3%) **|** 7.8	**18:1** (60.3%) **|** 3.2
treatment	**18:1** (59.9%) **|** 1.5	**16:0** (67.6%) **|** 6.1	**20:0** (62.4%) **|** 1.4	**16:0** (66.8%) **|** 1.6
	20:4 (70.6%) **|** 1.1	**18:1** (76.8%) **|** 4.9	**18:1** (67.3%) **|** 1.4	**20:4** (73.0%) **|** 1.5
	18:0 (80.6%) **|** 1.1		**16:0** (72.2%) **|** 1.4	**18:2** (79.0%) **|** 1.4
			20:3 (76.1%) **|** 1.1	

Table S3 | SIMPER and ANOSIM output of ceramide and sphingomyelin profiles. *Sphingolipid profiles:* SIMPER analyses identified global and between-group average dissimilarity (%). For pairwise comparisons, one-way ANOSIM output of quantitative data (nmol/µg DNA) is reported as an R value from one (dissimilar) to zero (similar) with an associated significance value (brackets: $P \leq 0.05$, bolded). The global significance and R value are also reported for each ANOSIM test. The number of lipid species included in each analysis is indicated. *Influential lipid species:* SIMPER identified the influential sphingolipid species contributing at least 75% to global cumulative group dissimilarity (all treatments). Influential lipid species responsible for significant pairwise differences (as identified by ANOSIM) are given to highlight the effect of natural MA treatment (PBS vs. MA mix) or differences between the oxygenated MAs (kMA vs. mMA). Cer, ceramide; SM, sphingomyelin.

Sphingolipid profiles		
	Cer	**SM**
Lipid species analysed	38	21
Total *n*	342	189
Global dissimilarity	25.6%	19.8%
Global R value	0.7656	0.4688
Global significance (*P*)	0.00125**	0.00315**
PBS/MA mix	27.9% **|** 1 (**<0.01**)	26.0% **|** 0.5 (**<0.01**)
PBS/αMA	12.6% **|** 1 (**<0.01**)	12.6% **|** 0 (0.06)
PBS/kMA	30.2% **|** 0.75 (**<0.01**)	26.7% **|** 0.5 (**<0.01**)
PBS/mMA	40.0% **|** 1 (**<0.01**)	32.9% **|** 1 (**<0.01**)
MA mix/αMA	25.3% **|** 1 (**<0.05**)	19.2% **|** 1 (**<0.01**)
MA mix/kMA	8.7% **|** -0.25 (0.065)	4.5% **|** 0 (**<0.01**)
MA mix/mMA	22.9% **|** 1 (**<0.01**)	16.2% **|** 0.75 (**<0.01**)
αMA/kMA	28.1% **|** 1 (**<0.01**)	19.9% **|** 1 (**<0.01**)
αMA/mMA	34.7% **|** 1 (**<0.01**)	25.9% **|** 1 (**<0.01**)
kMA/mMA	24.8% **|** 1 (**<0.01**)	13.7% **|** 0. 5 (**<0.01**)

Influential lipid species		
Sphingolipid species (% cumulative contribution to dissimilarity) **|** contribution factor		
	Cer	**SM**
All treatments	**18:1/16:0** (40.0%) **|** 10.2	**18:1/16:0** (61.4%) **|** 15.9
**global dissimilarity*	**18:1/24:1(15Z)** (53.8%) **|** 3.5	**18:1/24:1(15Z)** (70.9%) **|** 2.5
	18:1/16:2 (67.0%) **|** 3.4	**18:2/24:1(15Z)** (76.2%) **|** 1.4
	18:1/24:0 (78.8%) **|** 3.0	
PBS/MA mix	**18:1/16:0** (39.6%) **|** 11.6	**18:1/16:0** (54.3%) **|** 14.1
**effect of natural MA*	**18:1/24:1(15Z)** (62.2%) **|** 6.7	**18:1/24:1(15Z)** (63.0%) **|** 2.3
treatment	**18:1/16:2** (71.7%) **|** 2.8	**18:0/20:0** (70.2%) **|** 1.8
	18:1/24:0 (78.7%) **|** 2.1	**18:2/24:1(15Z)** (76.1%) **|** 1.5
kMA/mMA	**18:1/16:0** (31.2%) **|** 8.0	**18:1/16:0** (44.5%) **|** 6.1
**effect of oxygenated MA*	**18:1/24:0** (47.6%) **|** 4.2	**18:1/24:1(15Z)** (63.4%) **|** 2.6
treatment	**18:1/16:2** (62.2%) **|** 3.8	**18:1/24:0** (69.3%) **|** 0.8
	18:1/24:1(15Z) (74.3%) **|** 3.1	**18:2/22:1** (73.7%) **|** 0.6
	18:1/24:2 (85.5%) **|** 2.9	**18:1/22:1** (77.9%) **|** 0.6

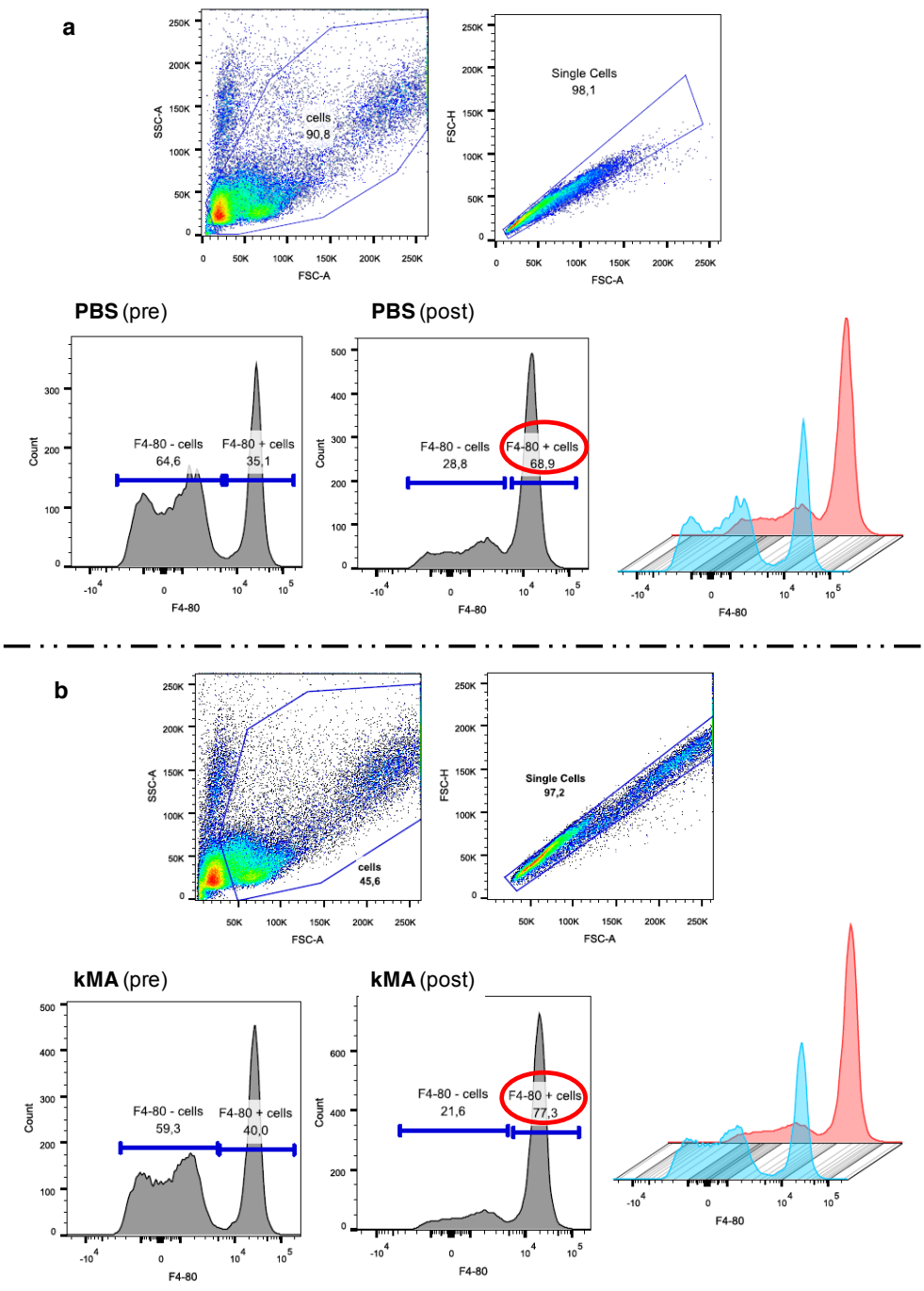

Figure S1 | Purity of F4/80$^+$ murine peritoneal macrophages. Murine F4/80$^+$ macrophages were isolated using MACS magnetic cell sorting and the purity of magnetically labelled cells assessed by flow cytometry. Flow cytometry output represents the pre- and post-sorting fractions of F4/80$^+$ macrophages in murine PECs for the (a) PBS and (b) kMA treatments. Single cells were gated by forward and side scatter and F4/80$^+$ macrophages identified by staining with anti-F4/80-APC (eBiosciences, clone BM8).

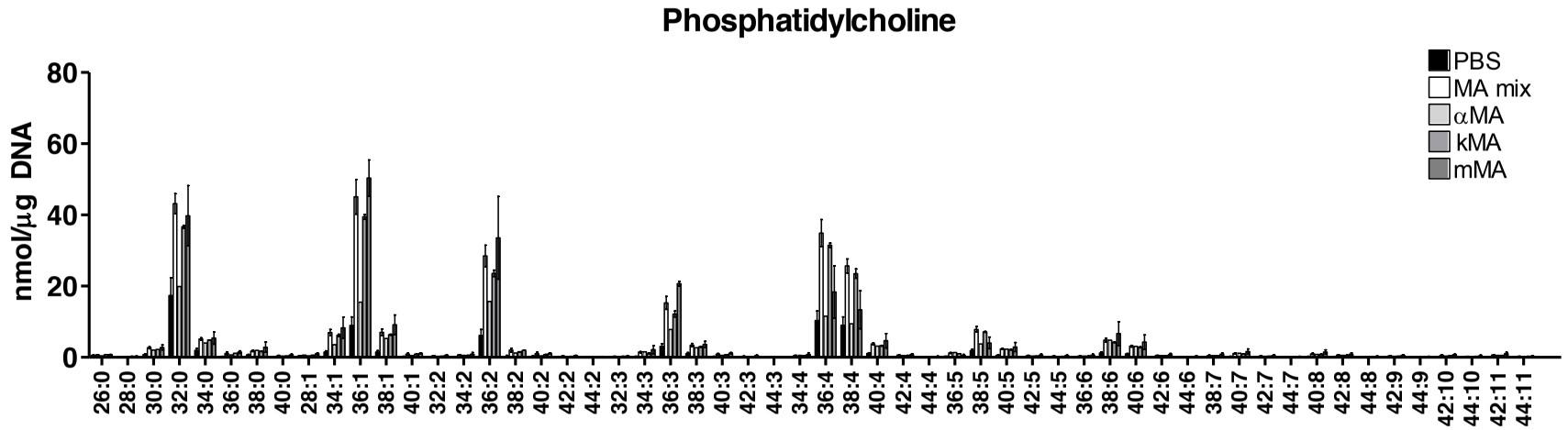

Figure S2 | Phosphatidylcholine lipid species profiles of peritoneal macrophages from mice treated with various MAs. The absolute levels (nmol/µg DNA) are given for the phosphatidylcholine fatty acid species of F4/80$^+$ macrophages from mice treated with PBS (-control), MA mix (+control), unoxygenated αMA, or the oxygenated kMA or mMA. Values are expressed as mean ± SEM. Data are from two independent experiments (n = 2) each comprising pooled F4/80$^+$ macrophages from multiple mice (n = 10).

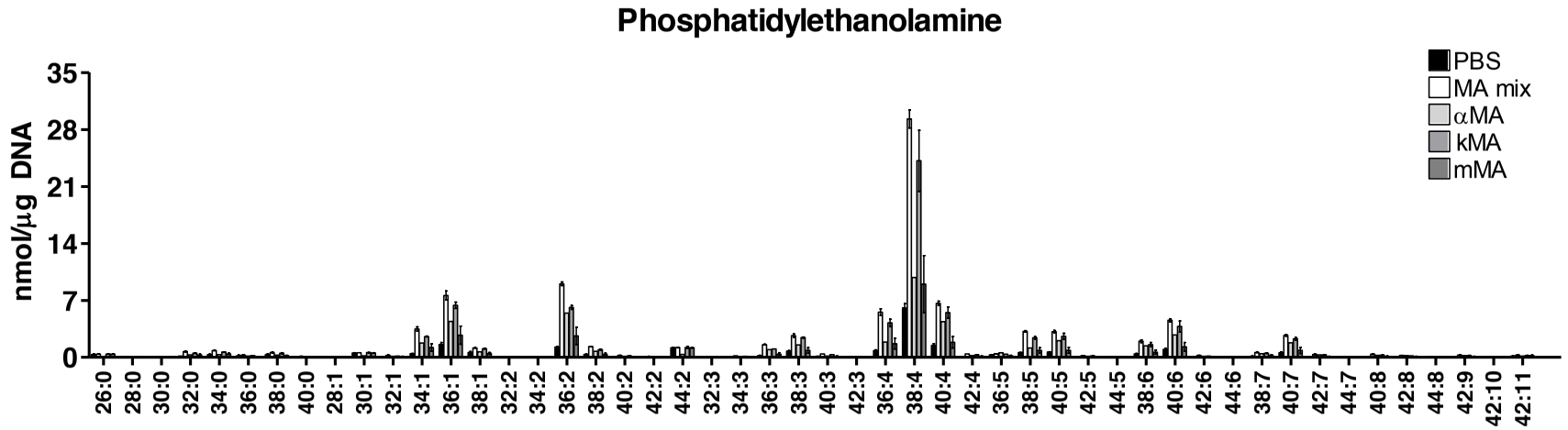

Figure S3 | Phosphatidylethanolamine lipid species profiles of peritoneal macrophages from mice treated with various MAs. The absolute levels (nmol/µg DNA) are given for the phosphatidylethanolamine fatty acid species of F4/80$^+$ macrophages from mice treated with PBS (-control), MA mix (+control), unoxygenated αMA, or the oxygenated kMA or mMA. Values are expressed as mean ± SEM. Data are from two independent experiments (n = 2) each comprising pooled F4/80$^+$ macrophages from multiple mice (n = 10).

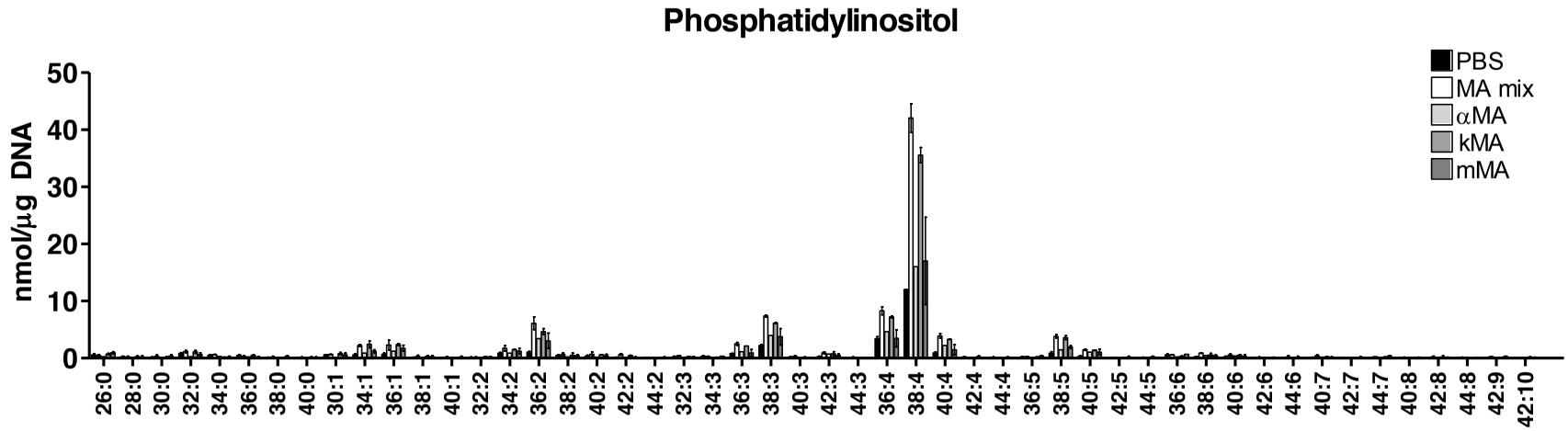

Figure S4 | Phosphatidylinositol lipid species profiles of peritoneal macrophages from mice treated with various MAs. The absolute levels (nmol/µg DNA) are given for the phosphatidylinositol fatty acid species of F4/80$^+$ macrophages from mice treated with PBS (-control), MA mix (+control), unoxygenated αMA, or the oxygenated kMA or mMA. Values are expressed as mean ± SEM. Data are from two independent experiments (n = 2) each comprising pooled F4/80$^+$ macrophages from multiple mice (n = 10).

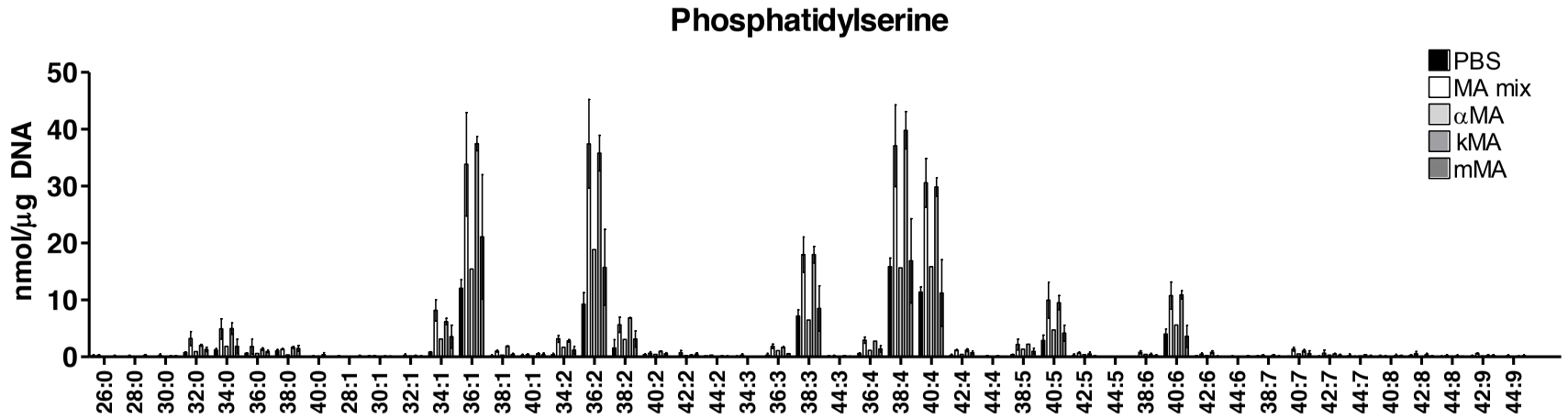

Figure S5 | Phosphatidylserine lipid species profiles of peritoneal macrophages from mice treated with various MAs. The absolute levels (nmol/µg DNA) are given for the phosphatidylserine fatty acid species of F4/80$^+$ macrophages from mice treated with PBS (-control), MA mix (+control), unoxygenated αMA, or the oxygenated kMA or mMA. Values are expressed as mean ± SEM. Data are from two independent experiments (n = 2) each comprising pooled F4/80$^+$ macrophages from multiple mice (n = 10).

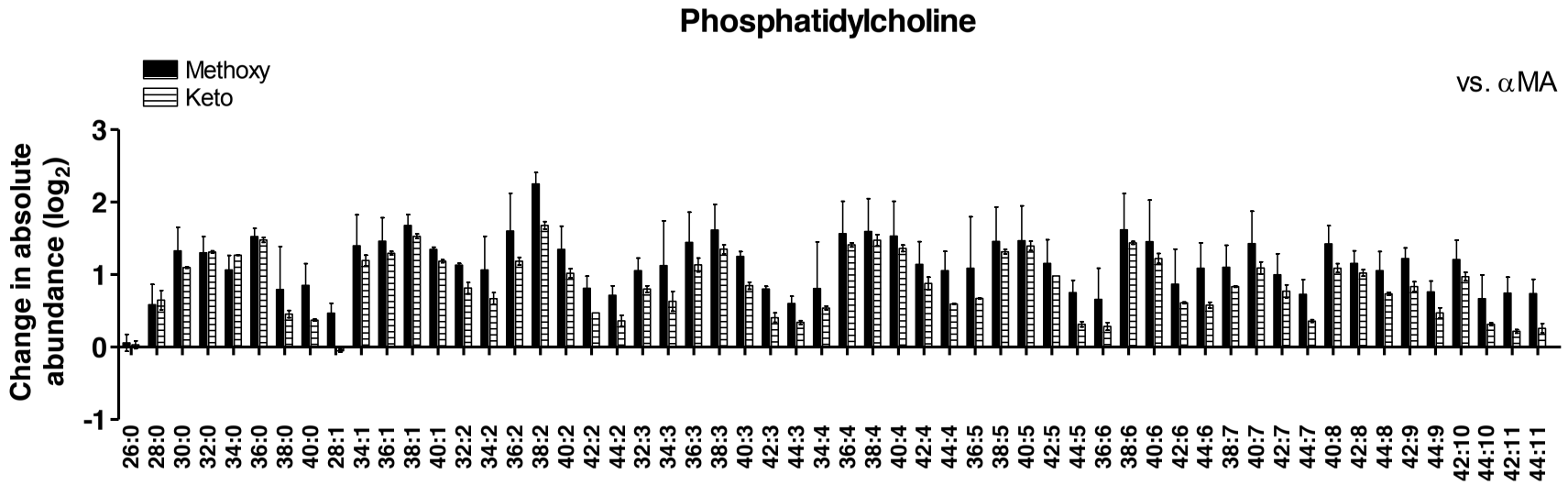

Figure S6 | Change in absolute abundance of phosphatidylcholine lipid species. The change in phosphatidylcholine composition is given for F4/80$^+$ macrophages from mice treated with the oxygenated mMA or kMA. Quantitative fatty acid values (nmol/µg DNA) are expressed as a ratio (log_2) of mMA or kMA over control unoxygenated αMA. Data are from two independent experiments (n = 2) each comprising pooled F4/80$^+$ macrophages from multiple mice (n = 10).

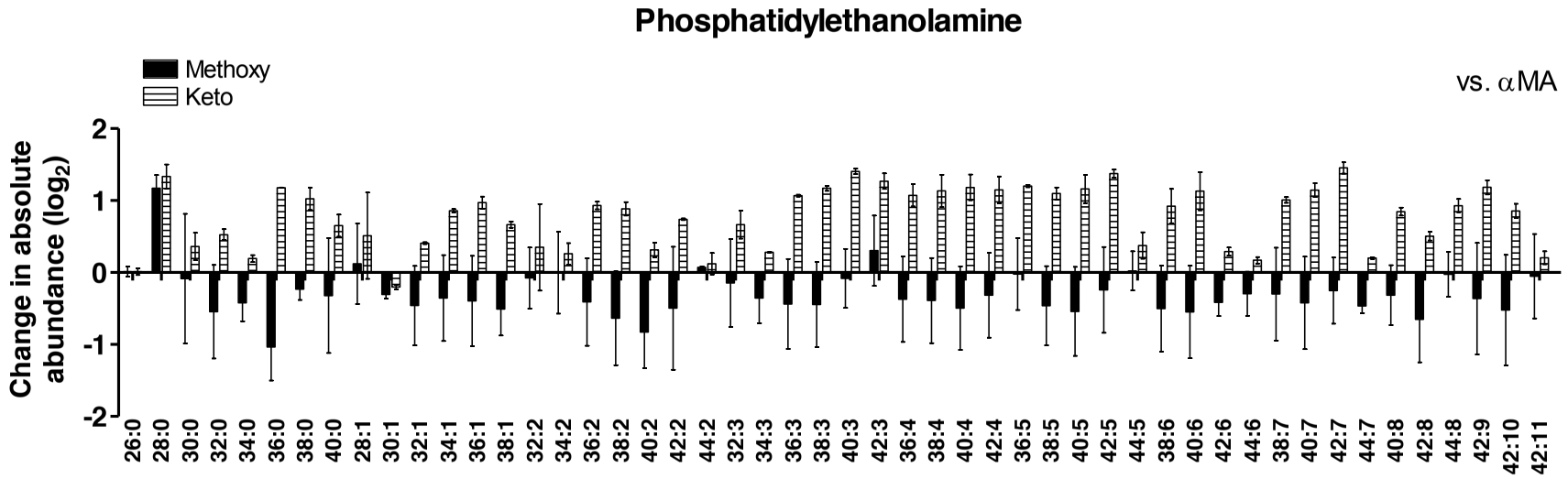

Figure S7 | Change in absolute abundance of phosphatidylethanolamine lipid species. The change in phosphatidylethanolamine composition is given for F4/80$^+$ macrophages from mice treated with the oxygenated mMA or kMA. Quantitative fatty acid values (nmol/μg DNA) are expressed as a ratio (log_2) of mMA or kMA over control unoxygenated αMA. Data are from two independent experiments (n = 2) each comprising pooled F4/80$^+$ macrophages from multiple mice (n = 10).

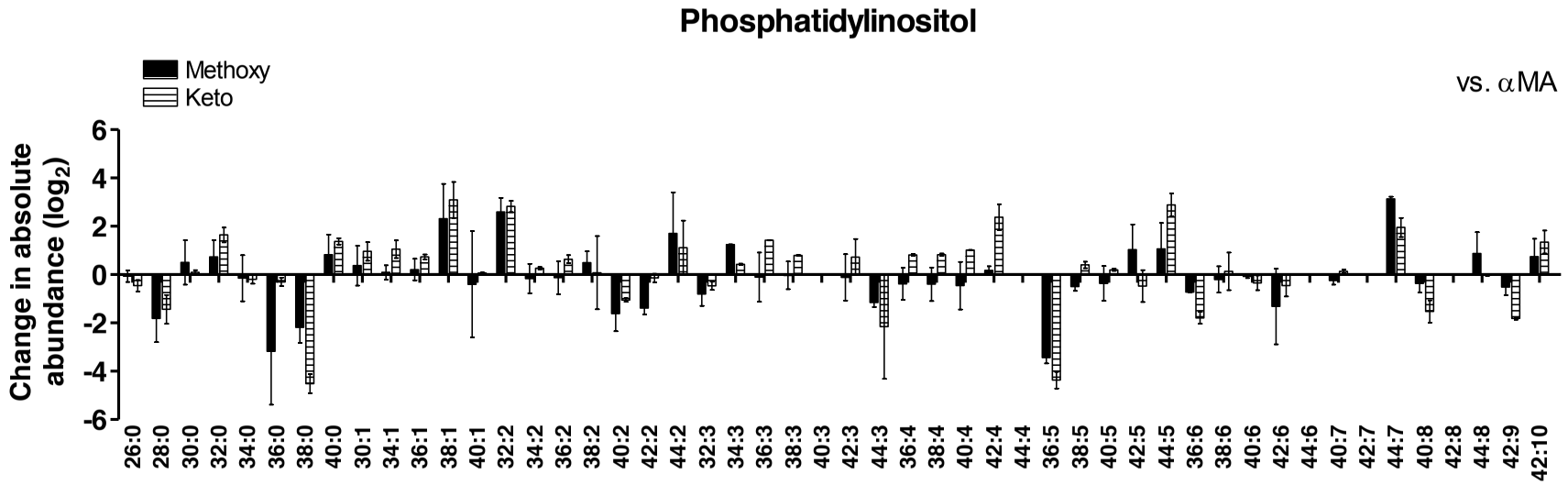

Figure S8 | Change in absolute abundance of phosphatidylinositol lipid species. The change in phosphatidylinositol composition is given for F4/80$^+$ macrophages from mice treated with the oxygenated mMA or kMA. Quantitative fatty acid values (nmol/µg DNA) are expressed as a ratio (log_2) of mMA or kMA over control unoxygenated αMA. Data are from two independent experiments (n = 2) each comprising pooled F4/80$^+$ macrophages from multiple mice (n = 10).

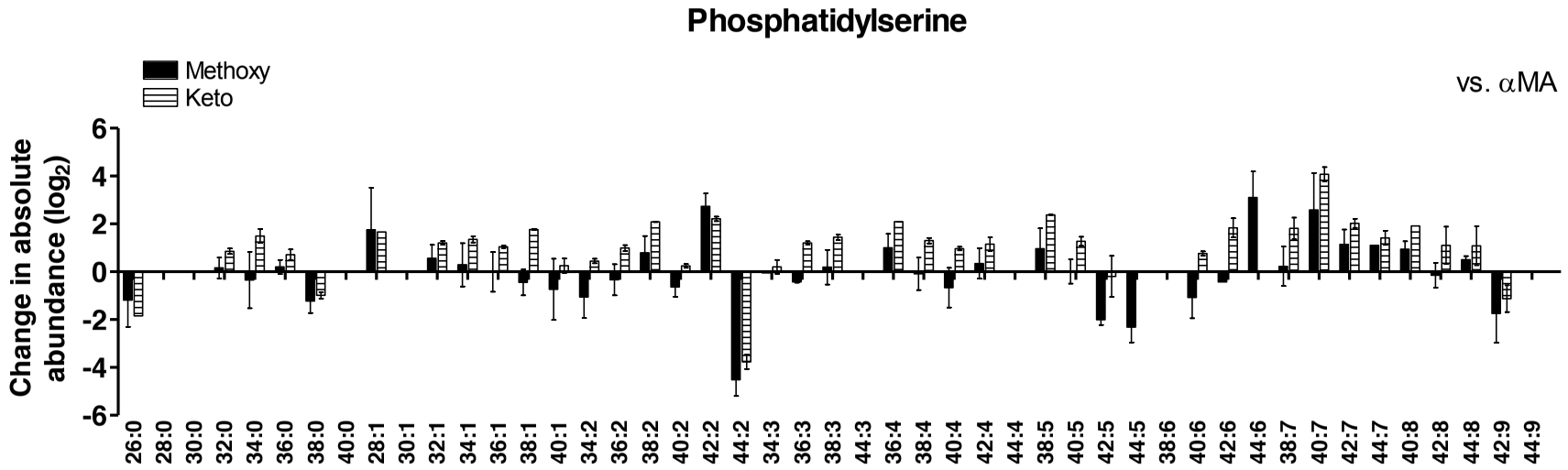

Figure S9 | Change in absolute abundance of phosphatidylserine lipid species. The change in phosphatidylserine composition is given for F4/80$^+$ macrophages from mice treated with the oxygenated mMA or kMA. Quantitative fatty acid values (nmol/μg DNA) are expressed as a ratio (log_2) of mMA or kMA over control unoxygenated αMA. Data are from two independent experiments (n = 2) each comprising pooled F4/80$^+$ macrophages from multiple mice (n = 10).

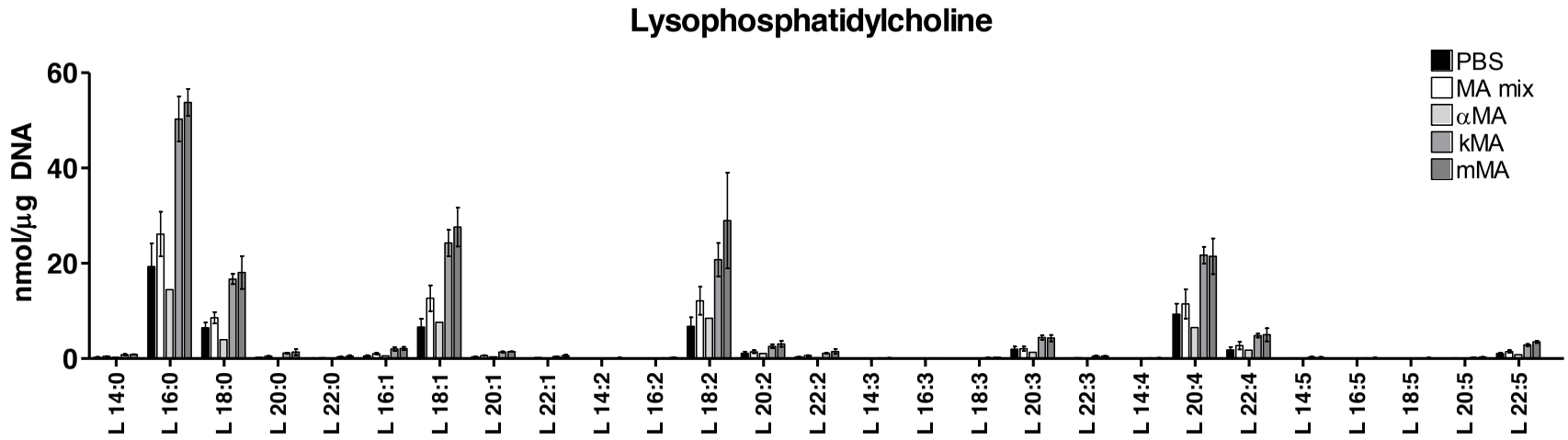

Figure S10 | Lysophosphatidylcholine fatty acid profiles of peritoneal macrophages from mice treated with various MAs. The absolute levels (nmol/µg DNA) are given for the lysophosphatidylcholine fatty acid species of F4/80$^+$ macrophages from mice treated with PBS (-control), MA mix (+control), unoxygenated αMA, or the oxygenated kMA or mMA. Values are expressed as mean ± SEM. Data are from two independent experiments (n = 2) each comprising pooled F4/80$^+$ macrophages from multiple mice (n = 10).

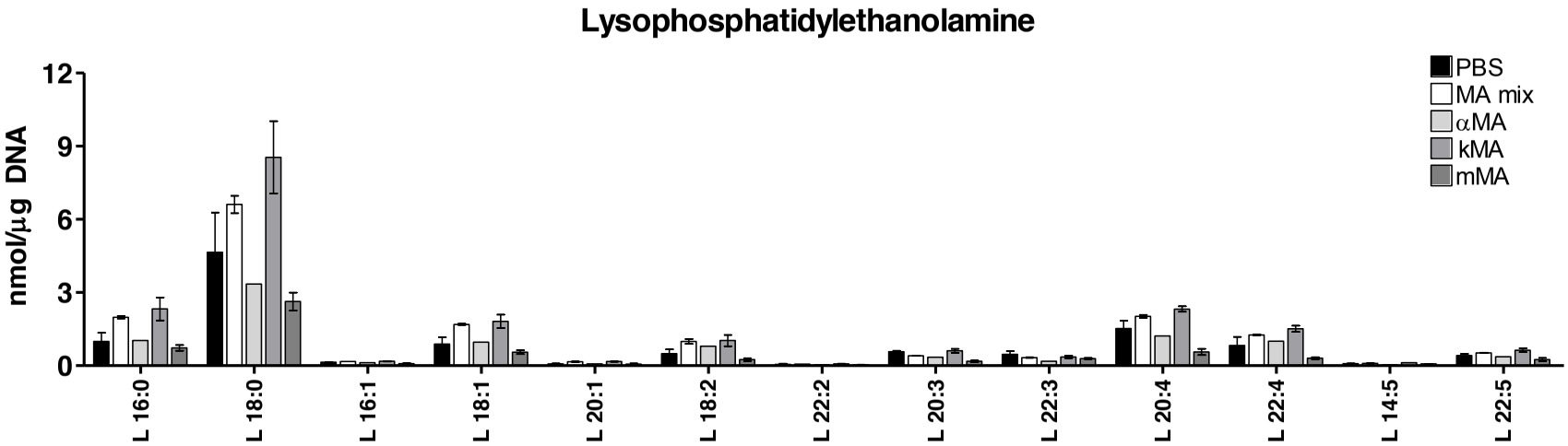

Figure S11 | Lysophosphatidylethanolamine fatty acid profiles of peritoneal macrophages from mice treated with various MAs. The absolute levels (nmol/µg DNA) are given for the lysophosphatidylethanolamine fatty acid species of F4/80$^+$ macrophages from mice treated with PBS (-control), MA mix (+control), unoxygenated αMA, or the oxygenated kMA or mMA. Values are expressed as mean ± SEM. Data are from two independent experiments (n = 2) each comprising pooled F4/80$^+$ macrophages from multiple mice (n = 10).

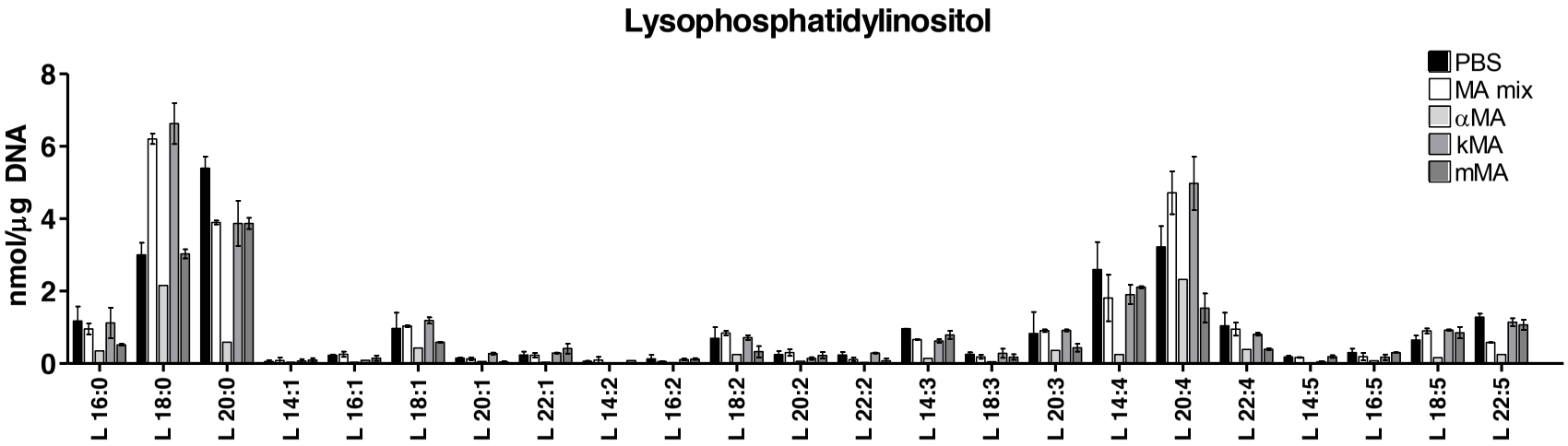

Figure S12 | Lysophosphatidylinositol fatty acid profiles of peritoneal macrophages from mice treated with various MAs. The absolute levels (nmol/µg DNA) are given for the lysophosphatidylinositol fatty acid species of F4/80^{+} macrophages from mice treated with PBS (-control), MA mix (+control), unoxygenated αMA, or the oxygenated kMA or mMA. Values are expressed as mean ± SEM. Data are from two independent experiments (n = 2) each comprising pooled F4/80^{+} macrophages from multiple mice (n = 10).

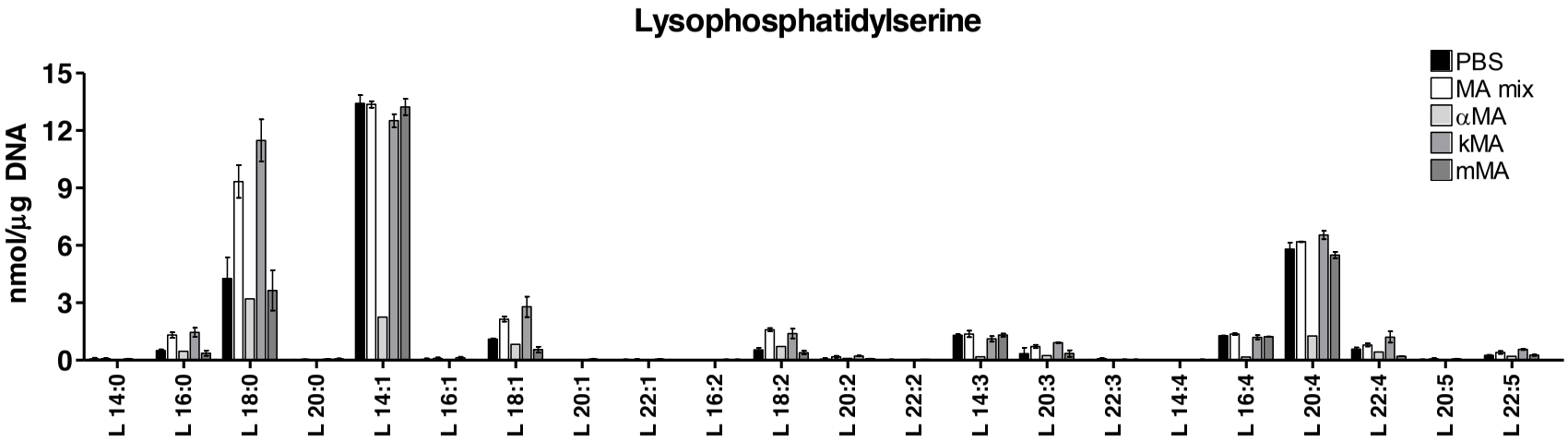

Figure S13 | Lysophosphatidylserine fatty acid profiles of peritoneal macrophages from mice treated with various MAs. The absolute levels (nmol/µg DNA) are given for the lysophosphatidylserine fatty acid species of F4/80$^+$ macrophages from mice treated with PBS (-control), MA mix (+control), unoxygenated αMA, or the oxygenated kMA or mMA. Values are expressed as mean ± SEM. Data are from two independent experiments (n = 2) each comprising pooled F4/80$^+$ macrophages from multiple mice (n = 10).

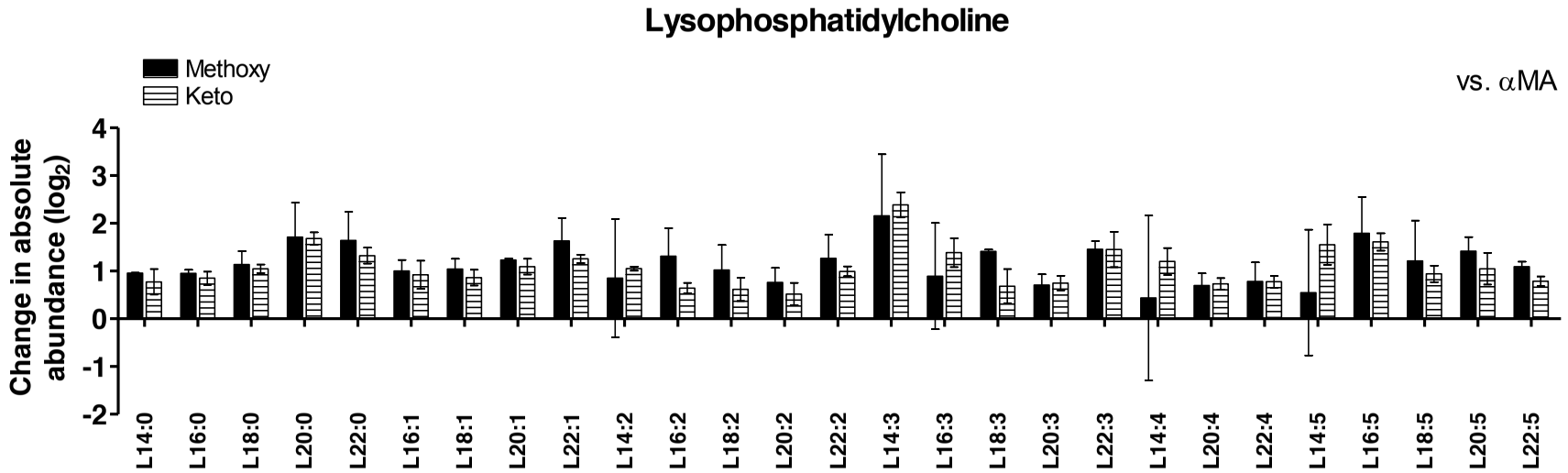

Figure S14 | Change in absolute abundance of lysophosphatidylcholine fatty acid species. The change in lysophosphatidylcholine composition is given for F4/80$^+$ macrophages from mice treated with the oxygenated mMA or kMA. Quantitative fatty acid values (nmol/µg DNA) are expressed as a ratio (log_2) of mMA or kMA over control unoxygenated αMA. Data are from two independent experiments (n = 2) each comprising pooled F4/80$^+$ macrophages from multiple mice (n = 10).

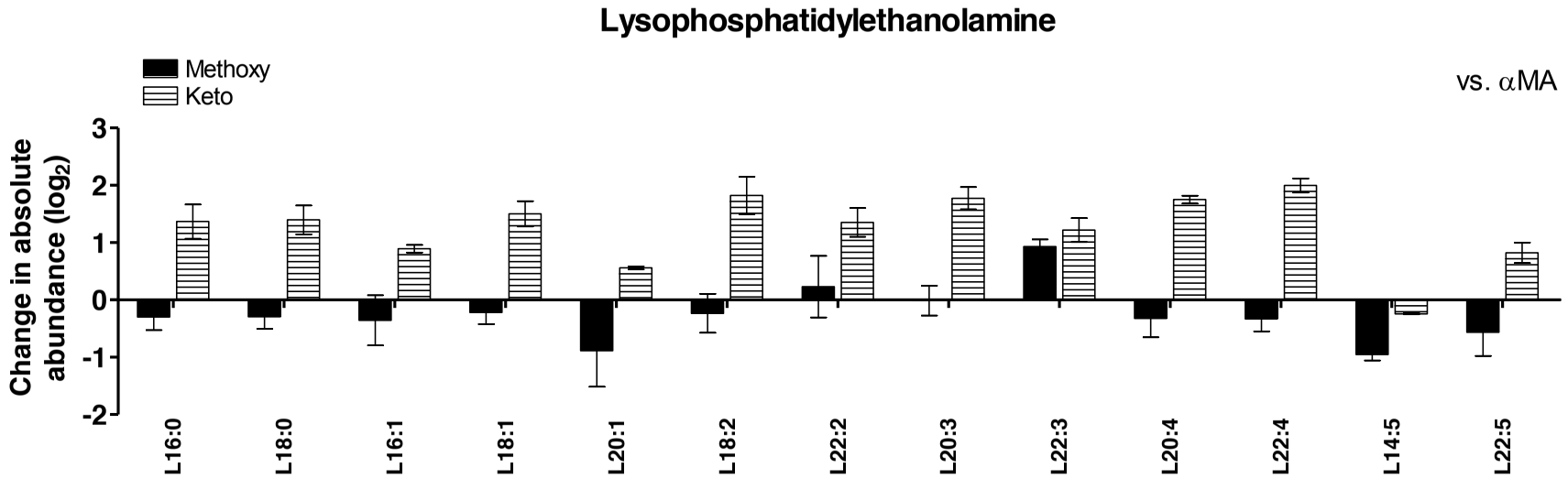

Figure S15 | Change in absolute abundance of lysophosphatidylethanolamine fatty acid species. The change in lysophosphatidylethanolamine composition is given for F4/80$^+$ macrophages from mice treated with the oxygenated mMA or kMA. Quantitative fatty acid values (nmol/μg DNA) are expressed as a ratio (log_2) of mMA or kMA over control unoxygenated αMA. Data are from two independent experiments (n = 2) each comprising pooled F4/80$^+$ macrophages from multiple mice (n = 10).

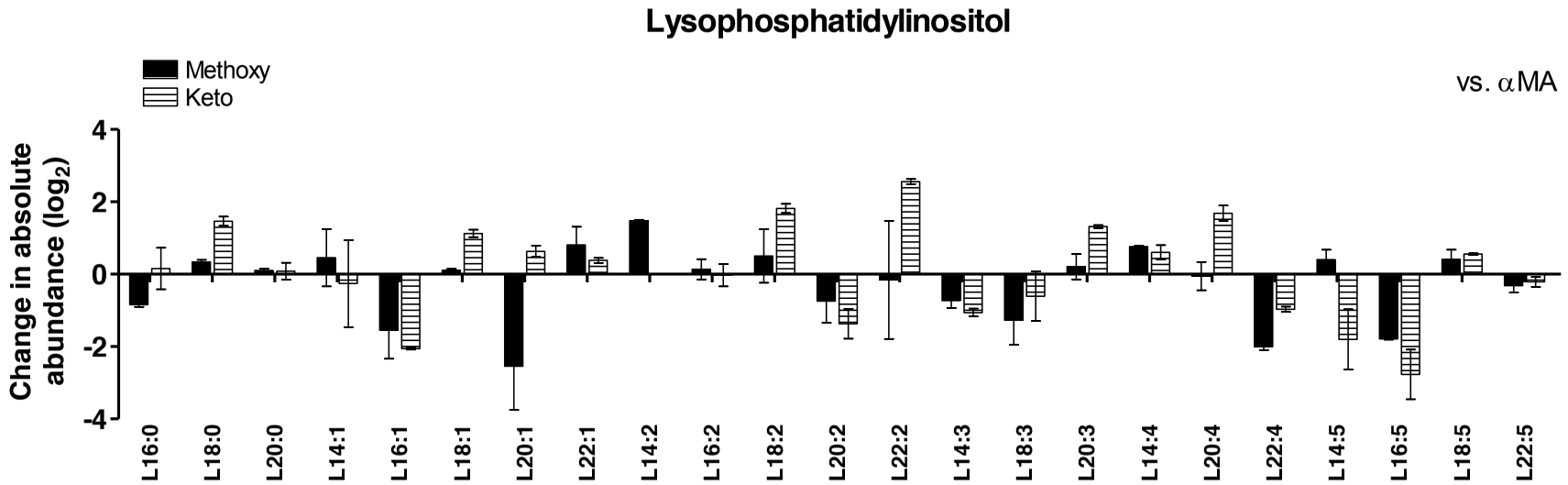

Figure S16 | Change in absolute abundance of lysophosphatidylinositol fatty acid species. The change in lysophosphatidylinositol composition is given for F4/80$^+$ macrophages from mice treated with the oxygenated mMA or kMA. Quantitative fatty acid values (nmol/µg DNA) are expressed as a ratio (log_2) of mMA or kMA over control unoxygenated αMA. Data are from two independent experiments (n = 2) each comprising pooled F4/80$^+$ macrophages from multiple mice (n = 10).

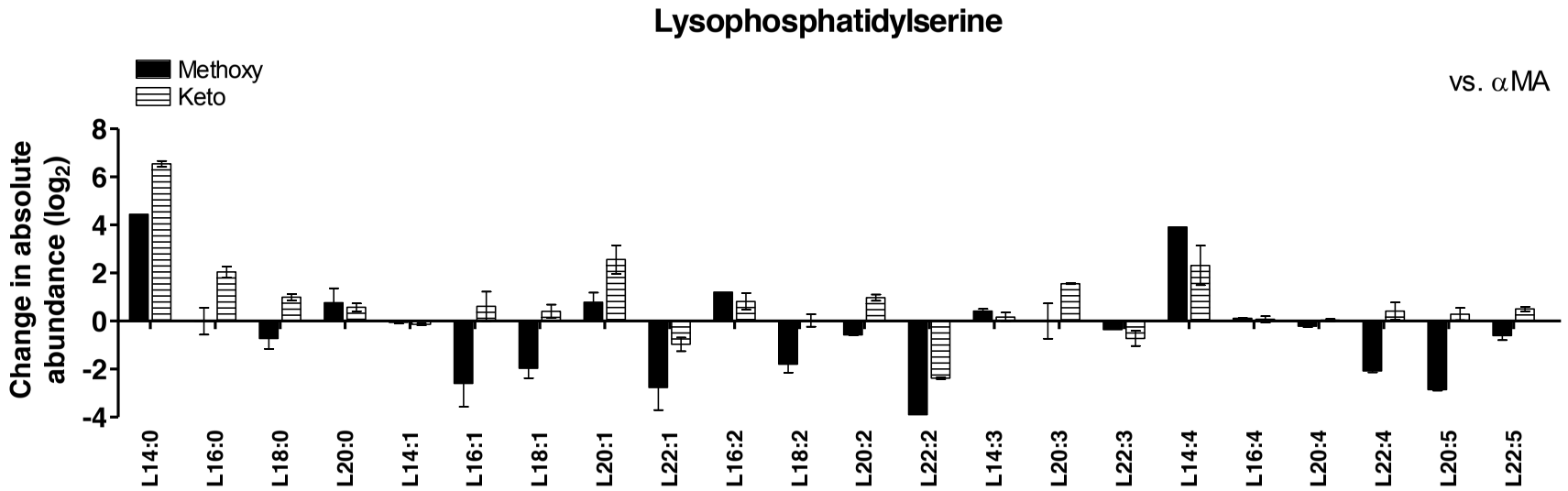

Figure S17 | Change in absolute abundance of lysophosphatidylserine fatty acid species. The change in lysophosphatidylserine composition is given for F4/80$^+$ macrophages from mice treated with the oxygenated mMA or kMA. Quantitative fatty acid values (nmol/μg DNA) are expressed as a ratio (log_2) of mMA or kMA over control unoxygenated αMA. Data are from two independent experiments (n = 2) each comprising pooled F4/80$^+$ macrophages from multiple mice (n = 10).

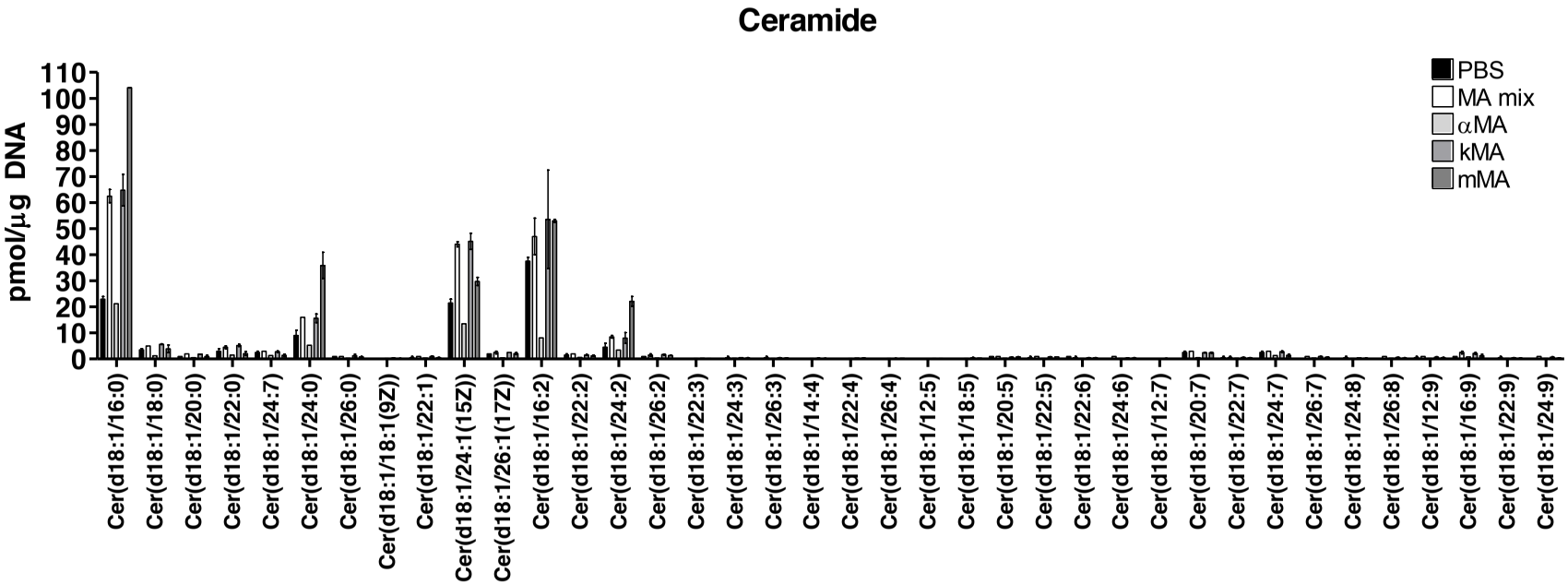

Figure S18 | Ceramide lipid species profiles of peritoneal macrophages from mice treated with various MAs. The absolute levels (nmol/µg DNA) are given for the ceramide fatty acid species of F4/80$^+$ macrophages from mice treated with PBS (-control), MA mix (+control), unoxygenated αMA, or the oxygenated kMA or mMA. Values are expressed as mean ± SEM. Data are from two independent experiments (n = 2) each comprising pooled F4/80$^+$ macrophages from multiple mice (n = 10).

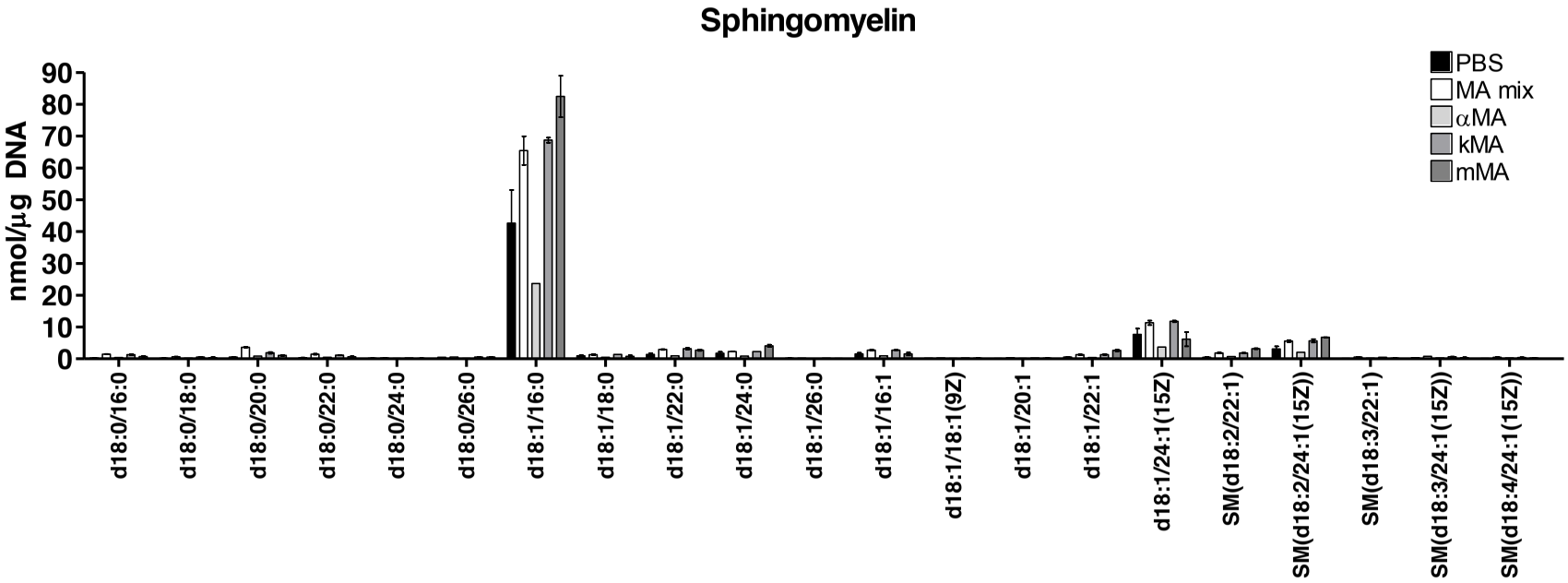

Figure S19 | Sphingomyelin lipid species profiles of peritoneal macrophages from mice treated with various MAs. The absolute levels (nmol/µg DNA) are given for the sphingomyelin fatty acid species of F4/80^{+} macrophages from mice treated with PBS (-control), MA mix (+control), unoxygenated αMA, or the oxygenated kMA or mMA. Values are expressed as mean ± SEM. Data are from two independent experiments (n = 2) each comprising pooled F4/80^{+} macrophages from multiple mice (n = 10).

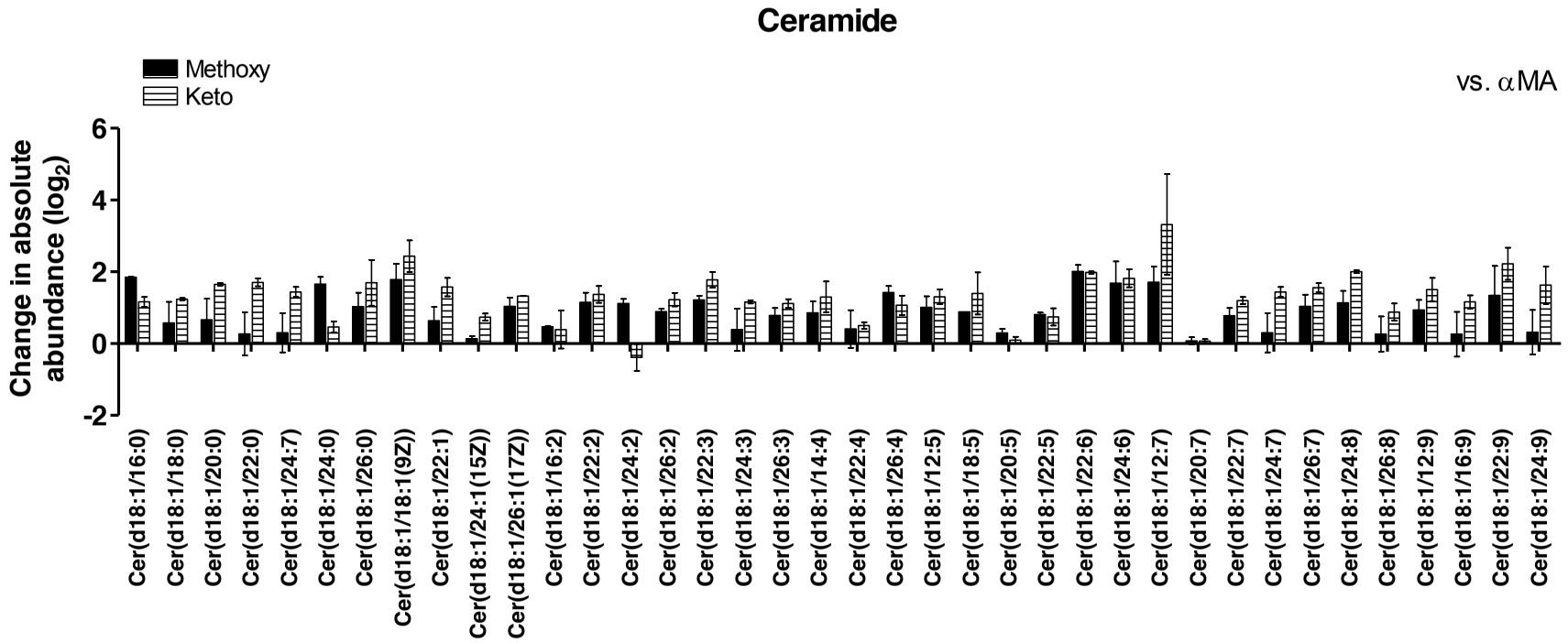

Figure S20 | Change in absolute abundance of ceramide lipid species. The change in ceramide composition is given for F4/80^{+} macrophages from mice treated with the oxygenated mMA or kMA. Quantitative fatty acid values (nmol/μg DNA) are expressed as a ratio (log_2) of mMA or kMA over control unoxygenated αMA. Data are from two independent experiments (n = 2) each comprising pooled F4/80^{+} macrophages from multiple mice (n = 10).

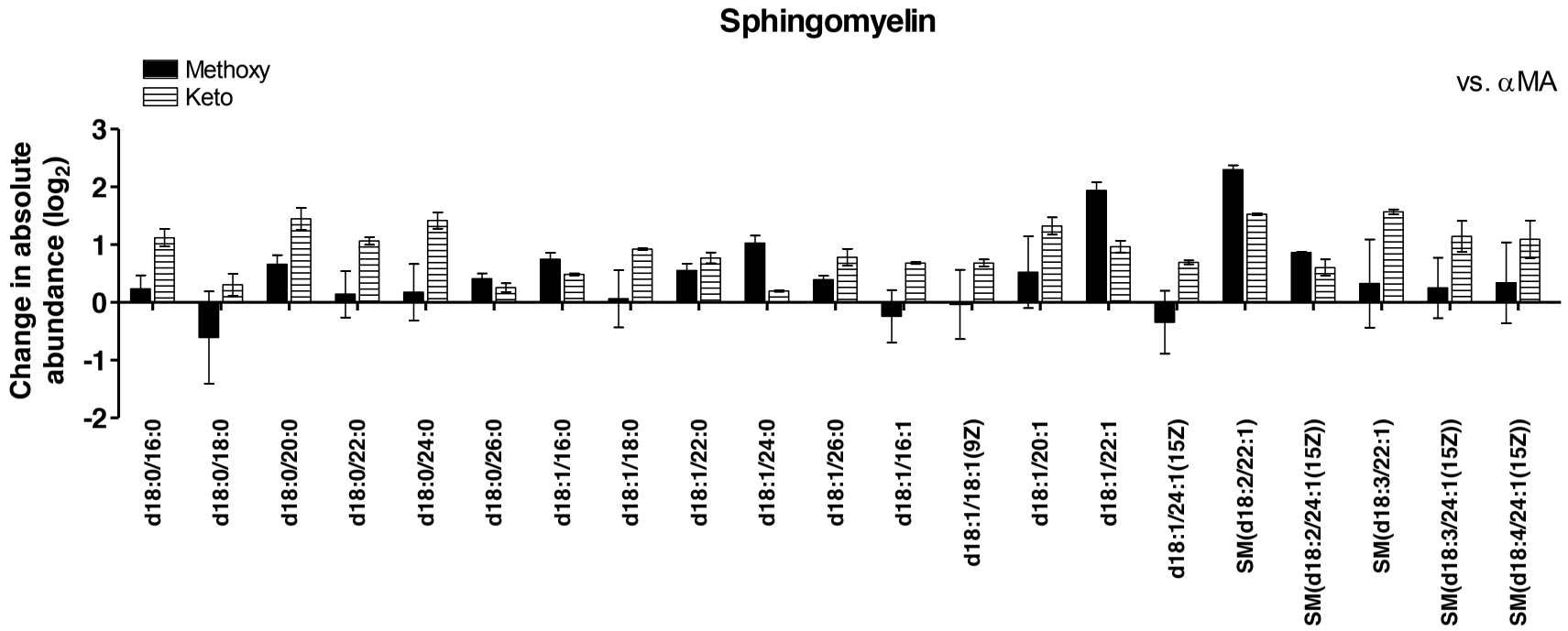

Figure S21 | Change in absolute abundance of sphingomyelin lipid species. The change in sphingomyelin composition is given for F4/80$^+$ macrophages from mice treated with the oxygenated mMA or kMA. Quantitative fatty acid values (nmol/μg DNA) are expressed as a ratio (log_2) of mMA or kMA over control unoxygenated αMA. Data are from two independent experiments (n = 2) each comprising pooled F4/80$^+$ macrophages from multiple mice (n = 10).

2. Additional experiments

2.1 Assessment of inflammation and foam cell traits following murine in vivo treatment with an acid sphingomyelinase inhibitor (Zoledronic acid)

Zoledronic acid (ZA) is a potent nitrogen-containing bisphosphonate generally used to treat malignant hypercalcaemia, osteoporosis and bone-related cancers[1]. Bisphosphonates like ZA also display strong inhibition of acid sphingomyelinase (aSMase)[2], a key phosphodiesterase in the catabolism of sphingomyelin (SM) to ceramide (Cer) and phosphorylcholine[3]. Cer form integral structural components of cellular membranes and are important signalling lipids that regulate cell function[4]. Our lipidomics data showed that Cer species significantly contributed to the lipid composition of macrophages from mice treated with the natural MA mixture (Chapter III: Fig. 5). This Cer enrichment was mimicked by the individual oxygenated MA classes with macrophages from kMA-treated mice recording levels comparable to the MA mix, but mMA inducing even higher levels of total Cer, as well as C16 and C24 fatty acid species, relative to the MA mixture. Several intracellular bacterial pathogens manipulate Cer metabolism to uphold virulence. For example, through generation of plasma membrane Cer-enriched platforms to gain entry into host cells[5-7] or by scavenging and incorporation of host sphingolipids to evade detection after infection[8]. The bioactive lipid messenger, sphingosine-1-phosphate (S1P), is involved in regulation of Ca^{2+} levels in activated macrophages after phagocytosis of opsonised organisms, a strategy employed to allow maturation of lysosomal compartments[9]. *Mycobacterium tuberculosis* (Mtb) can suppress the rise in Ca^{2+} through inhibition of sphingosine kinase translocation, which mediates sphingosine phosphorylation, thus decreasing S1P and preventing acidification of host phagolysosomes[10]. Identification of the molecular mechanisms employed by Mtb to

manipulate host sphingolipids would aid in the understanding of its pathogenesis and allow for the development of novel anti-TB drugs. We postulated that mMA from Mtb triggers aSMase to generate Cer, thus leading to enhanced inflammation. To address this hypothesis, we investigated the involvement of aSMase in the induction of inflammation by mMA. We used different modes of MA and ZA treatment (i.e. intratracheal and intraperitoneal) and assessed bronchoalveolar lavage fluid (BALF) and lipopolysaccharide (LPS) stimulated culture supernatant for inflammatory cytokines. LPS stimulated macrophages were also investigated by confocal microscopy to measure foam cell traits following MA and/or ZA treatment.

Materials and methods

ZA [1-Hydroxy-2-(1*H*-imidazol-1-yl)ethane-1,1-diyl]bis(phosphonic acid) was purchased as a hydrated disodium salt (Enzo Life Sciences). ZA stock solution was prepared in calcium- and endotoxin-free PBS (1 mg/mL, pH 7.4; Lonza) and aliquots filter-sterilised prior to use. C57BL/6 mice (n = 5 per experimental condition) were sedated intraperitoneally (i.p.) with 150 µL anaesthetic solution consisting of ketamine (100 mg/kg) and xylazine (10 mg/kg). Sedated mice were then instilled intratracheally (i.t.) with a lipid backbone control (MA-bb) or the *cis*-isomer of methoxy-MA (mMA; 25 µg/mouse) with or without ZA (2.5 µg/mouse). Mice were terminally sedated after 48 h with Nembutal (sodium pentobarbital; 50 mg/kg) and cells harvested by bronchoalveolar lavage (BAL). Cell supernatant was stored for multiplex assay while pellets were resuspended in 100 µL PBS containing purified anti-mouse CD16/CD32 (blocks high-affinity Fcγ receptors; BD Biosciences), the live/dead marker Sytox red (eBiosciences) and selected fluorescent surface markers for 30 min at 4°C. Cell surface markers were purchased from BD Biosciences and comprised MHC II (I-A, eFluor® 450), CD3ε (Alexa Fluor® 488), Siglec-F (PE), CD11c (PE-Texas red), CD8a (PE-Cyanine7),

CD4 (PerCP), and CD11b (APC-eFluor® 780; eBiosciences). BAL extruded cells were counted and cell type composition analysed by flow cytometry (LSRII flow cytometer, BD Biosciences). Analyses were performed with BD FACS Diva or FlowJo software.

Mice were treated i.p. as described above for assessment of cytokine levels and macrophage morphology (25 µg MA-bb or mMA, +/- ZA). Peritoneal exudate cells (PEC) were harvested after two days by peritoneal lavage and cells seeded into 96-well plates for multiplex assay ($1x10^5$ cells/well) and 8-well ibidi® plates for confocal microscopy ($5x10^5$ cells/well). Peritoneal macrophages were enriched by an overnight adherence then treated with or without *Escherichia coli* LPS-containing medium for 24 h (0.1 µg/mL; LPS 0111:B4, Sigma-Aldrich). Culture supernatants were removed and centrifuged, and aliquots stored at -80°C or processed for multiplex assay as described below. Cells for confocal analyses (+/-LPS) were fluorescently labelled with CellTracker™Violet (10 mM stock, 1:1000) and Bodipy 493/503. Supernatant from BAL extruded cells and LPS-treated peritoneal macrophages were processed for multiplex assay measurement of cytokines using the Bio-Plex Pro™ kit (Bio-Rad). In brief, 100 µL assay buffer was used to pre-wet wells of a 96-well filter plate and 50 µL magnetic beads mixture added of detection antibodies against the mouse cytokines IL-6, KC, MCP-1 and TNFα (Grp1, Bio-Rad; 2.5 µL/bead/well). Wells were washed with wash buffer (2x 200 µL) and 50 µL added of standard, control or treatment sample. Sample and beads were briefly resuspended on a shaking platform (1000 rpm) then covered and incubated for 30 min by rotation at room temperature (300 rpm). After washing (3x 200 µL) 25 µL of detection antibody mixture was added and the plate incubated by rotation for 30 min (1.25 µL/antibody/well). Wells were washed (3x 200 µL) and 50 µL streptavidin-PE/assay buffer solution added (0.25 µL streptavidin-PE/well). Following a 10 min rotation and wash (3x 200

µL), wells were resuspended in 125 µL assay buffer and immediately measured using a Bio-Plex® 200 System with Luminex xMap Technology (Bio-Rad).

Results and discussion

Following murine i.t. instillation with control MA-bb or mMA solutions (+/-ZA), the inflammatory BAL infiltrate was assessed by flow cytometry analysis (Fig. S22). Higher total cell numbers were recorded in BALF from mMA treated lungs (Fig. S23, insert). Resident alveolar macrophages (rAMs) and neutrophils constituted the main components of inflammatory infiltrate in lungs from both MA-bb and mMA treated mice (Fig. S23, upper panel). Recruitment of neutrophils was substantially elevated in the bronchoalveolar lumen of mMA treated lungs with an approximate 30-fold elevation compared to the MA-bb treatment. ZA pretreatment did not significantly change alveolar recruitment of rAMs, dendritic cells (DCs), recruited monocytes and eosinophils (Fig. S23, lower panel). Yet T lymphocytes and neutrophils were reduced in lungs that collectively received ZA and mMA. BALF isolated from mMA treated lungs also contained some infiltration of monocytic myeloid cells (non-rAMs) and eosinophils (Fig. S23).

Cytokine responses of bronchoalveolar infiltrate following MA-bb or mMA instillation and concomitant ZA priming showed a distinct difference for mMA treated lungs (Fig. S24). Though higher for mMA than MA-bb, cytokine levels of IL-6, MCP-1 and TNFα were generally low (<20 pg/mL). Compared to MA-bb, KC levels from lungs of mMA treated mice was significantly elevated (>75 pg/mL). ZA did not have a major effect on cytokine expression though an almost 2-fold reduction in MCP-1 levels was recorded in BALF from mMA (+ZA) treated lungs (Fig. S24).

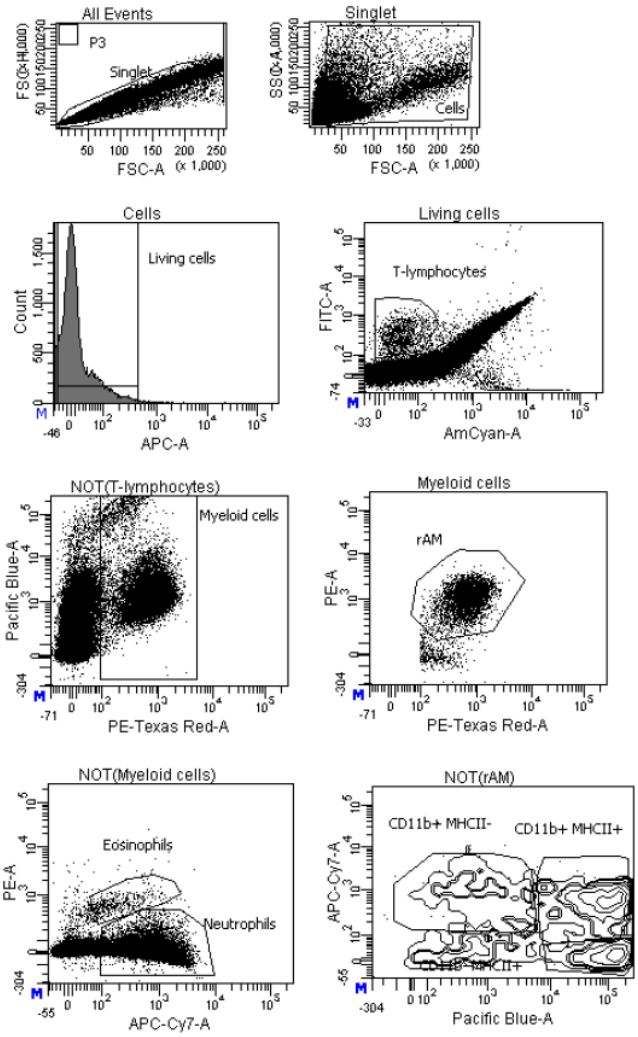

Figure S22 | Flow cytometry analysis of BAL fluid samples. Representation of the flow cytometry analysis of gated leukocyte populations from lungs of mice instilled intratracheally with 25 µg MA-bb or *cis*-mMA solutions with or without zoledronic acid (+/-ZA). Living cells stained negative for Sytox red and distinguished T lymphocytes (CD3ε+) from those of the monocytic myeloid lineage (CD11c+). As a result of failure of the anti-CD4 (PerCP) antibody, no distinction could be made between CD4 (PerCP+) and CD8 (PE-Cy7+) T cells. Within the myeloid cell population rAMs (CD11c+, Siglec-F+, MHC II+), dendritic cells (CD11c+, CD11b+, MHC II+) and recruited monocytes (CD11c+, CD11b+, MHC II-) were distinguished. The granulocytes (CD11c-) comprised the neutrophils (Siglec-F-, CD11b+) and eosinophils (Siglec-F+, CD11b+).

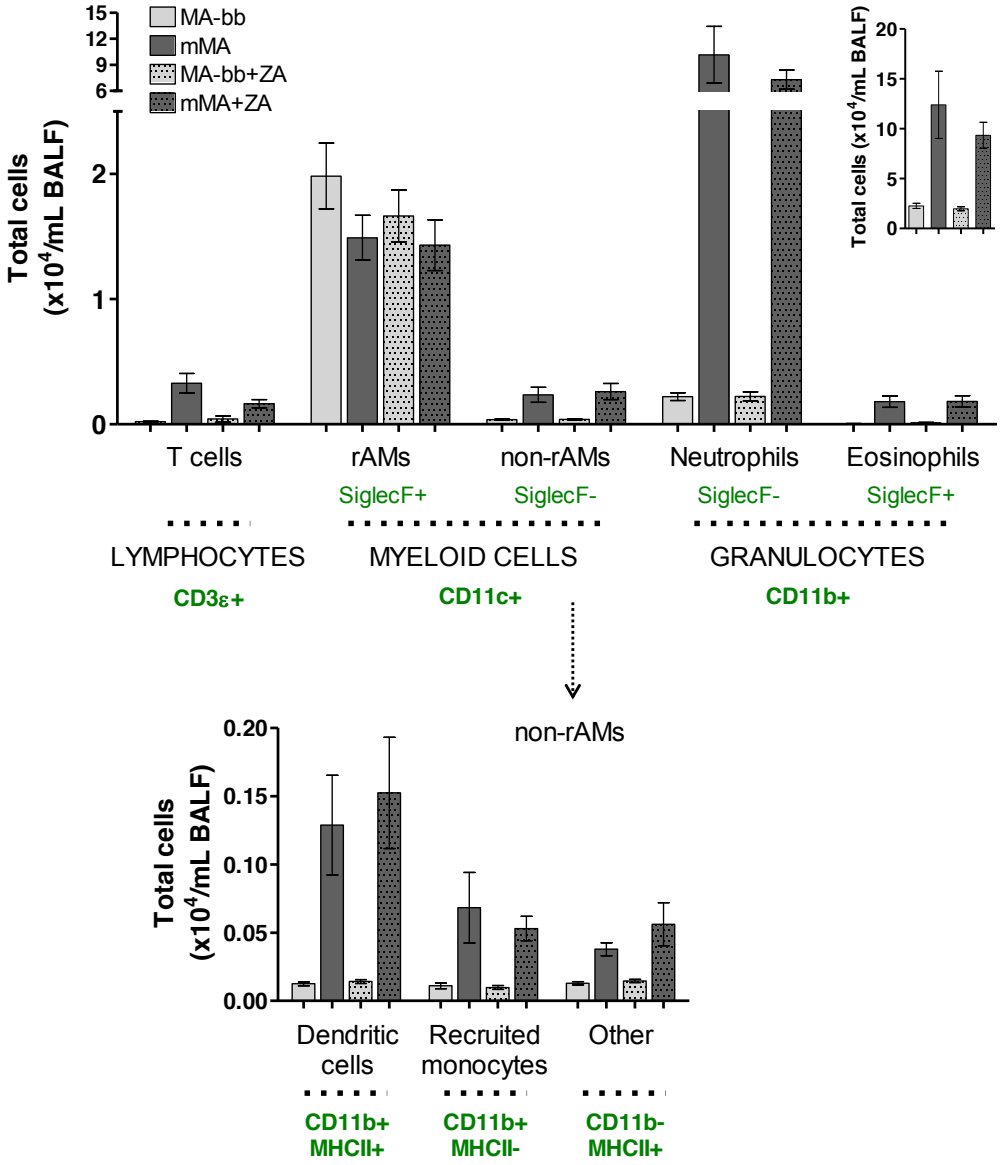

Figure S23 | Average total and differential BAL fluid cell counts. Mice were instilled intratracheally with 25 µg MA-bb or mMA solutions with or without zoledronic acid (+/-ZA). Cells were collected after 48 h by bronchoalveolar lavage (BAL) and total (insert) and differential cell counts measured in BAL fluid by flow cytometry (mean ± SEM). Cell surface markers are shown in green. rAMs, resident alveolar macrophages.

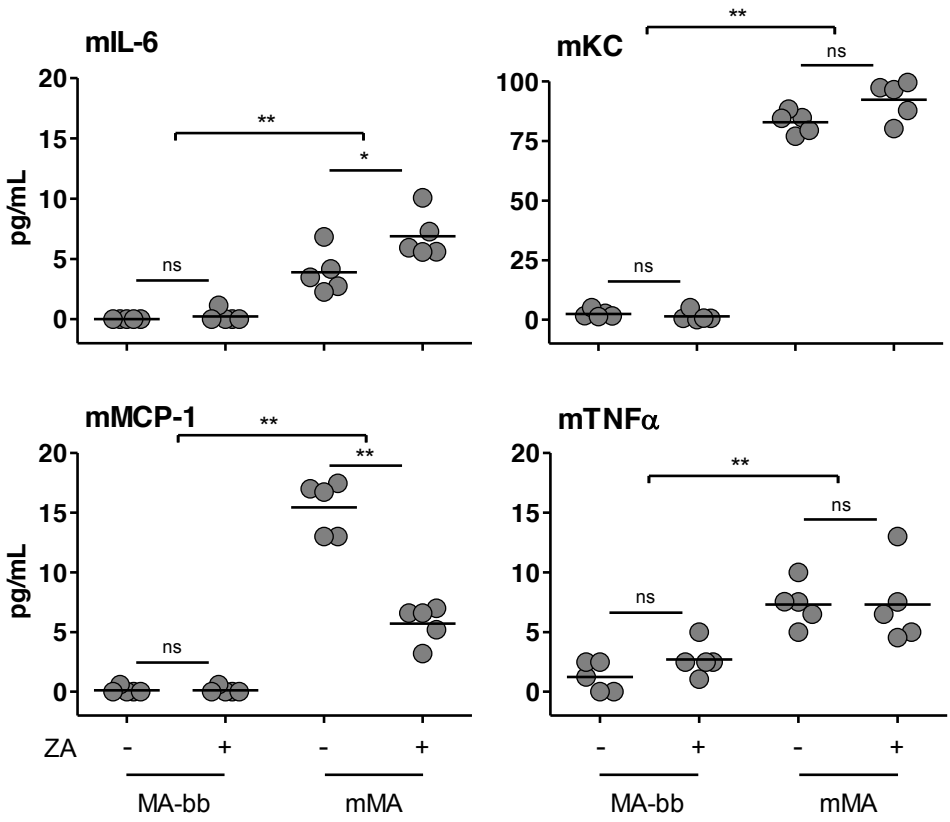

Figure S24 | Cytokine response of bronchoalveolar infiltrate following treatment with zoledronic acid. Mice were treated intratracheally with 25 µg MA-bb or mMA solutions (+/- 2.5 µg ZA). Cells were collected after 48 h by bronchoalveolar lavage and assessed for cytokines (murine IL-6, KC, MCP-1, TNFα) by multiplex immunoassay using a Bio-Plex® 200 system with Luminex xMap Technology (n = 5 mice). Statistical differences were assessed by an independent samples Kruskal-Wallis test for mIL-6 (H = 16.915, P < 0.01, df = 3) mKC (H = 15.754, P < 0.01, df = 3), mMCP-1 (H = 17.196, P < 0.01, df = 3) and mTNFα (H = 14.238, P < 0.01, df = 3).

Peritoneal macrophages from mice harvested after i.p. ZA treatment and *ex vivo* stimulation with LPS, exhibited different cytokine responses to bronchoalveolar cells. In peritoneal macrophages from mice that received the control MA-bb treatment no distinct pattern in cytokine expression was recorded between LPS groups, but ZA pretreatment significantly increased levels of all measured cytokines (Dunn's ranked sum multiple comparisons $P < 0.01$; Fig. S25). ZA treatment noticeably elevated IL-6, KC and TNFα cytokine expression in peritoneal macrophages from mice treated with mMA. Whereas LPS stimulation resulted in decreased MCP-1 levels in cells from mice that received mMA *in vivo*, this effect was reversed with higher levels of MCP-1 in LPS-stimulated cells following ZA treatment (Fig. S25). Bronchoalveolar and peritoneal cells from mice that received mMA exhibited elevated expression of IL-6 and diverse effects on MCP-1 levels in response to ZA treatment (Fig. S24-S25).

Peritoneal macrophages were next assessed by laser scanning confocal microscopy for differences in foam cell traits after differential treatment with MA, ZA and LPS (Fig. S26). In macrophages from MA-bb and mMA treated mice that were not exposed to LPS, ZA treatment induced LD accumulation yet had no effect on the proportion of enlarged V+ cells (Fig. S27). Exposure of the macrophages (from both treatments) to LPS in culture led to a significant reduction in the proportion of enlarged V+ cells (Fig. S28). Interestingly, in LPS-activated macrophages from the mMA treatment LD accumulation decreased following ZA treatment.

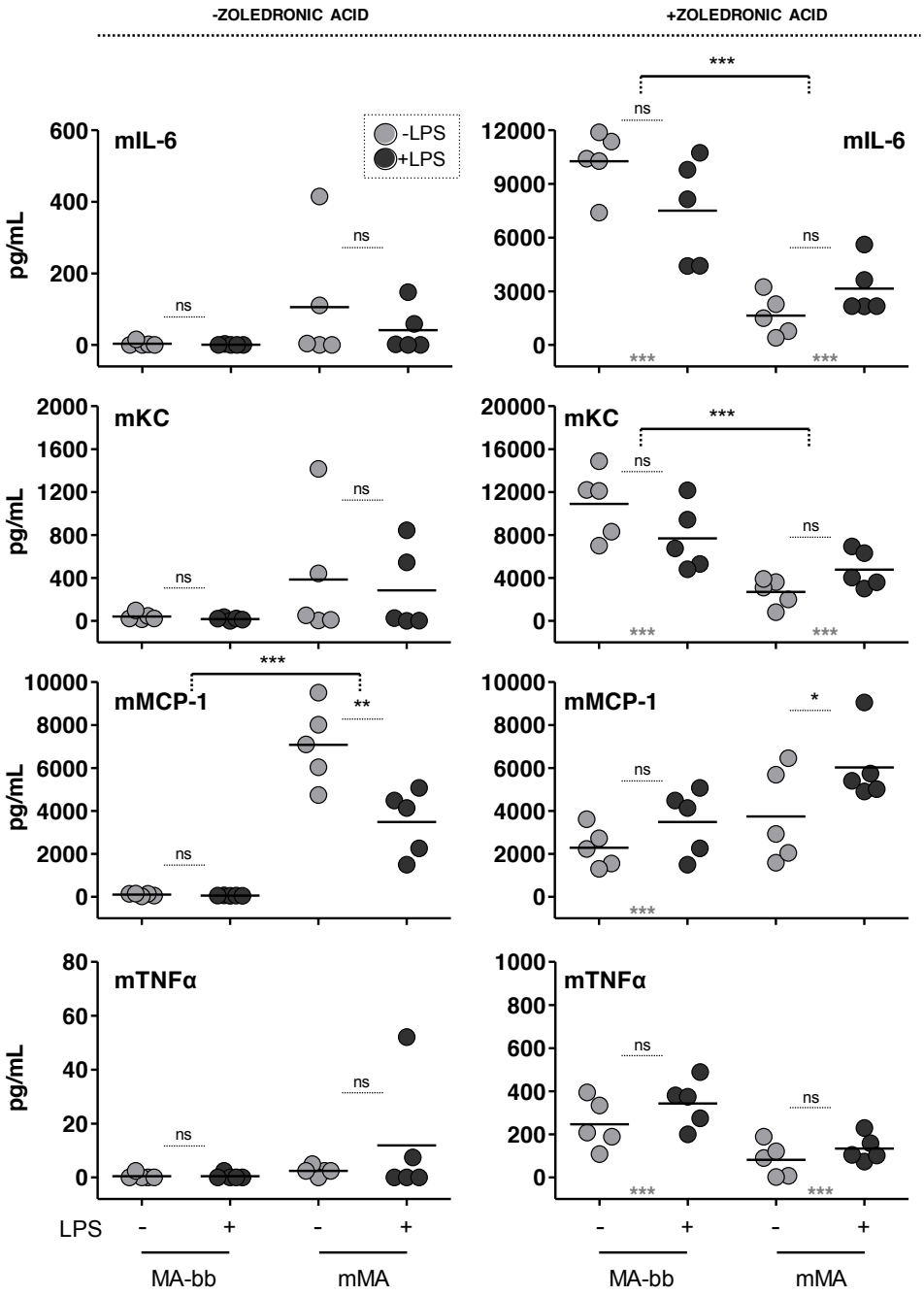

Figure S25 | Cytokine response of peritoneal macrophages after zoledronic acid treatment and LPS stimulation. Mice were treated intraperitoneally with 25 µg MA-bb or mMA solutions (+/- 2.5 µg ZA). Cells were collected after 48 h by peritoneal lavage and stimulated with or without *E.coli* LPS (0.1 µg/mL). Cytokines (murine IL-6, KC, MCP-1, TNFα) were assessed by multiplex immunoassay using a Bio-Plex® 200 system with Luminex xMap Technology (n = 5 mice). Significant differences were assessed with an independent-samples Kruskal-Wallis test for mIL-6 (H = 33.254, P < 0.001, df = 7), mKC (H = 32.885, P < 0.001, df = 7), mMCP-1 (H = 31.097, P < 0.001, df = 7) and mTNFα (H = 32.821, P < 0.001, df = 7). Dunn's ranked sum multiple comparisons recorded a significant rise in cytokine levels in peritoneal macrophages following ZA treatment (indicated by grey bolded asterisks at bottom of graph; P < 0.001***).

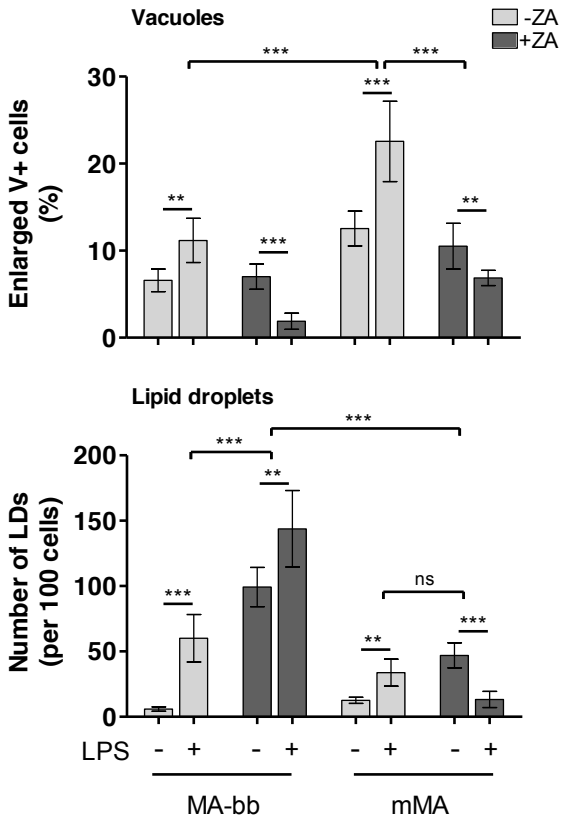

Figure S26 | Foam cell traits of murine peritoneal macrophages following zoledronic acid treatment and LPS stimulation. Mice were treated intraperitoneally with 25 µg MA-bb or mMA (+/- 2.5 µg ZA). Cells were collected after 48 h by peritoneal lavage and stimulated with or without *E.coli* LPS (0.1 µg/mL). Intracellular foam cell traits, namely the accumulation of LDs and vacuoles, were assessed by laser-scanning-confocal microscopy and quantified using Volocity 3D Image Analysis software (mean ± SEM; $n = 5$ mice). Statistical differences were analysed by independent samples Kruskal-Wallis tests for enlarged V+ cells ($H = 36.954$, $P < 0.001$, $df = 7$) and LDs ($H = 48.308$, $P < 0.001$, $df = 7$).

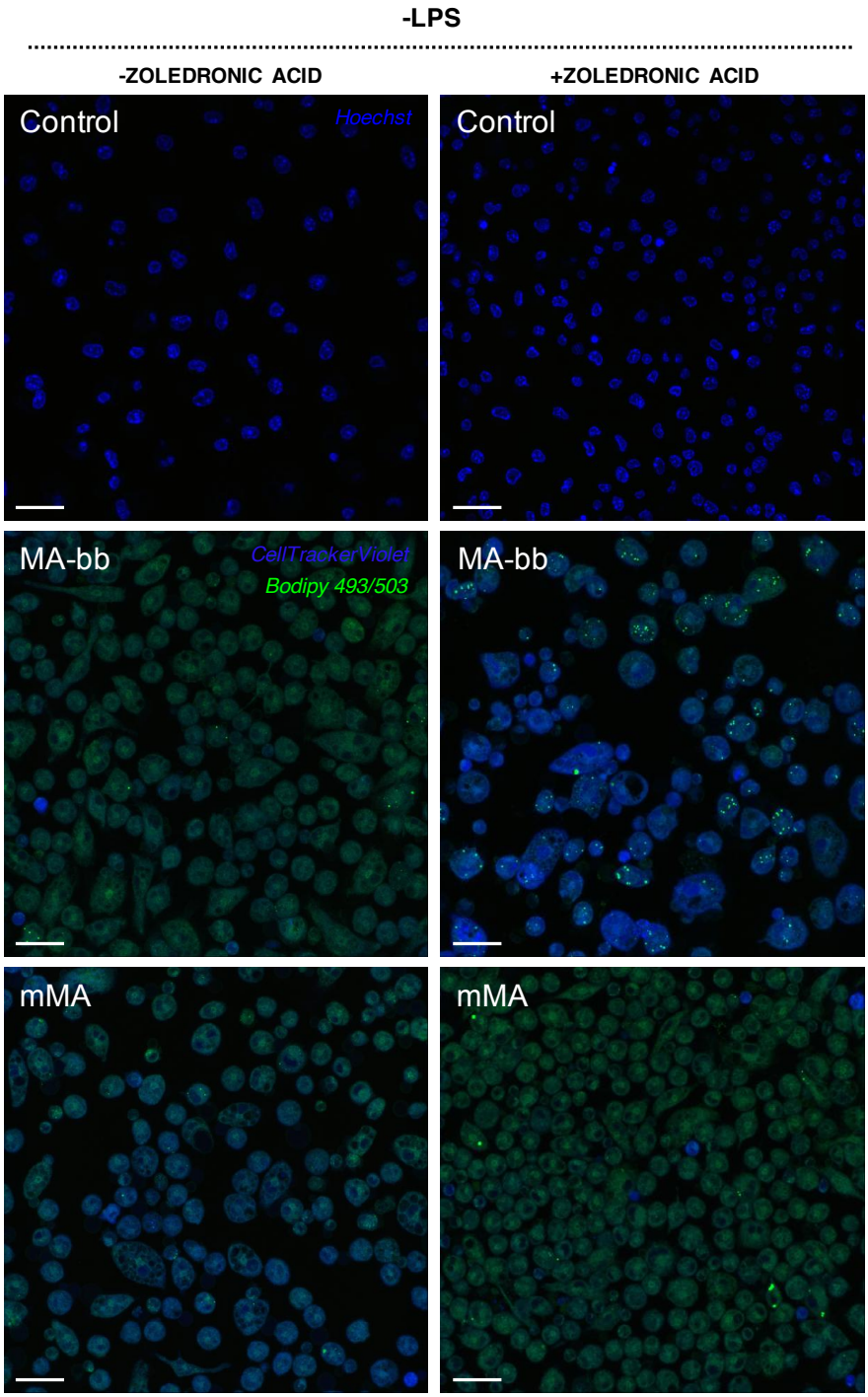

Figure S27 | Confocal microscopy images of foam cell morphology after treatment with zoledronic acid. Mice (n = 5) were treated intraperitoneally with 25 µg MA-bb or mMA (+/- 2.5 µg ZA) for 48 h. PECs were harvested and peritoneal macrophages enriched by overnight adherence. Peritoneal macrophages were mock-treated with PBS containing no *E. coli* LPS for 24 h and intracellular foam cell traits assessed by laser-scanning-confocal microscopy. Whole cells were fluorescently labelled with CellTracker™Violet and neutral LDs with Bodpiy 493/503. Control cells were stained with the nucleic acid marker Hoechst® only (auto-fluorescence control). Scale bar: 24 µm.

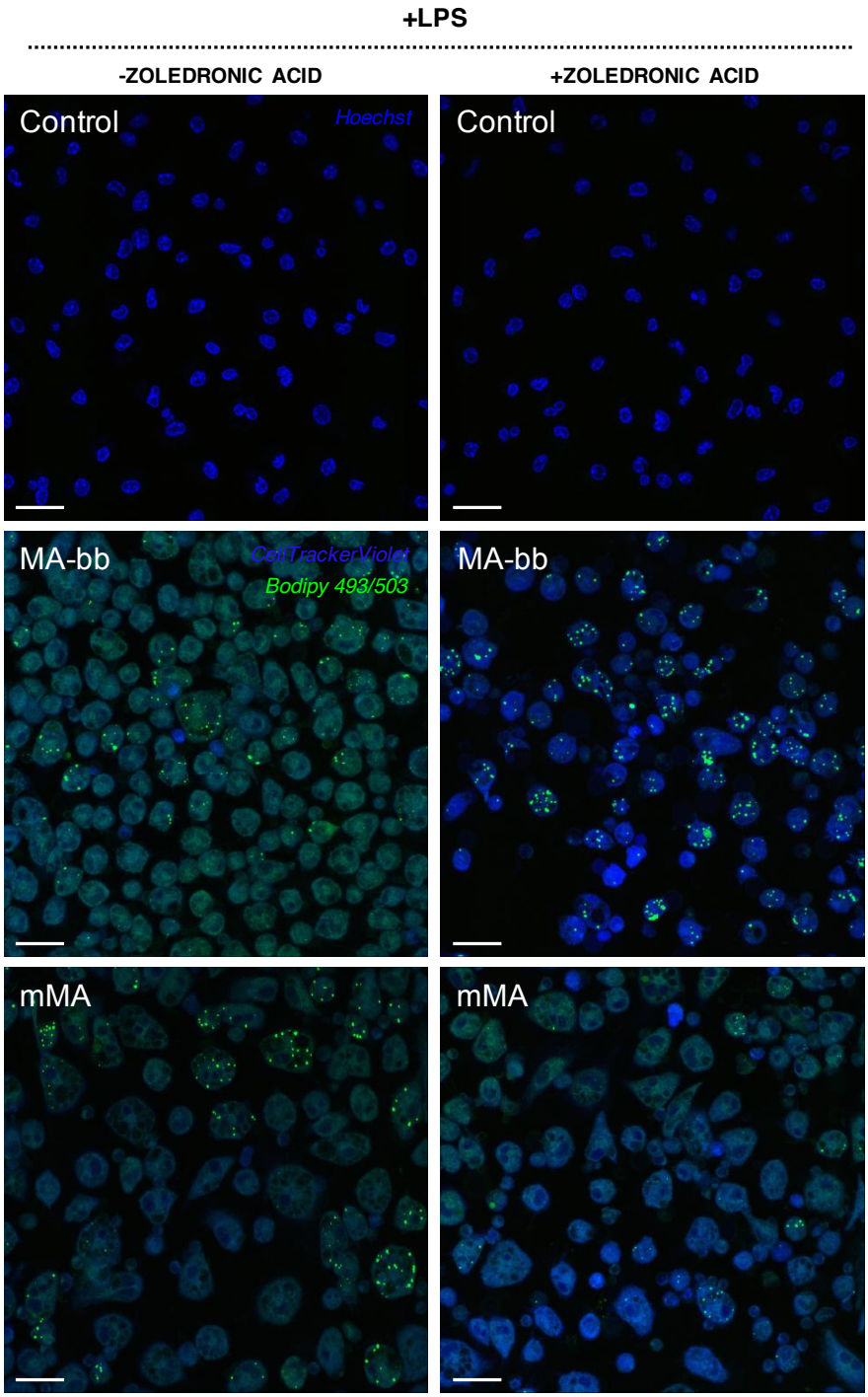

Figure S28 | Confocal microscopy images of foam cell morphology after zoledronic acid treatment and LPS stimulation. Mice (n = 5) were treated intraperitoneal with 25 µg MA-bb or mMA (+/- 2.5 µg ZA) for 48 h. PECs were harvested and peritoneal macrophages enriched by overnight adherence. Peritoneal macrophages were treated *ex vivo* with *E. coli* LPS (0.1 µg/mL) for 24 h and intracellular foam cell traits assessed by laser-scanning-confocal microscopy. Whole cells were fluorescently labelled with CellTracker™Violet and neutral LDs with Bodpiy 493/503. Control cells were stained with the nucleic acid marker Hoechst® only (auto-fluorescence control). Scale bar: 24 µm.

Average total and differential cell counts of neutrophils and monocytic cells are similar to a previous report from our group[11]. The reduction in T lymphocytes, neutrophils, and MCP-1 cytokine levels in the BALF from mMA-exposed lungs after ZA treatment is surely interesting. In LPS-stimulated cells a strong rise in cytokine levels was observed for macrophages from mice that were treated with MA-bb and mMA after ZA treatment, though IL-6, KC and TNFα remained lower in cells from the mMA treatment than those recorded for MA-bb control cells. Varied reports on the role of aSMase in inflammation exist. While ZA treatment can down-modulate inflammation by lowering migration towards, or expression of, various chemokine receptors[12], ZA can distinctly elevate proinflammatory activity in LPS-stimulated macrophages by enhancing NF-κB and reducing negative regulators of MyD88-signalling[13]. A general reduction in proinflammatory markers following aSMase inhibition in cells from mice that received mMA identified an involvement of this enzyme during inflammatory signalling, though further investigation is needed. It would have been interesting to assess aSMase cell surface exposure in unoxygenated (alpha) and oxygenated (keto and methoxy) MA treated cells after aSMase stimulation. Measurement of aSMase translocation from intracellular to plasma membrane compartments could have been assessed by flow cytometry and immunofluorescence following labelling of cells with anti-aSMase primary antibody and conjugated secondary Alexa Fluor antibodies. However, as a result of time constraints we were not able to further directly explore aSMase activity.

3. References

1. Heymann, D., B. Ory, F. Gouin, J. R. Green and F. Redini. 2004. Bisphosphonates: new therapeutic agents for the treatment of bone tumors. *Trends Mol. Med.* **10**: 337-343.

2. Roth, A. G., D. Drescher, Y. Yang, S. Redmer, S. Uhlig and C. Arenz. 2009. Potent and selective inhibition of acid sphingomyelinase by bisphosphonates. *Angew. Chem. Int. Ed. Engl.* **48**: 7560-7563.

3. Smith, E. L. and E. H. Schuchman. 2008. The unexpected role of acid sphingomyelinase in cell death and the pathophysiology of common diseases. *FASEB J.* **22**: 3419-3431.

4. Perry, D. K. and Y. A. Hannun. 1998. The role of ceramide in cell signaling. *Biochim. Biophys. Acta* **1436**: 233-243.

5. Hauck, C. R., H. Grassme, J. Bock, V. Jendrossek, K. Ferlinz, T. F. Meyer and E. Gulbins. 2000. Acid sphingomyelinase is involved in CEACAM receptor-mediated phagocytosis of *Neisseria gonorrhoeae*. *FEBS Lett.* **478**: 260-266.

6. Grassme, H., E. Gulbins, B. Brenner, K. Ferlinz, K. Sandhoff, K. Harzer, F. Lang and T. F. Meyer. 1997. Acid sphingomyelinase mediates entry of *N. gonorrhoeae* into nonphagocytic cells. *Cell* **91**: 605-615.

7. Heung, L. J., C. Luberto and M. Del Poeta. 2006. Role of sphingolipids in microbial pathogenesis. *Infect. Immun.* **74**: 28-39.

8. Wylie, J. L., G. M. Hatch and G. McClarty. 1997. Host cell phospholipids are trafficked to and then modified by *Chlamydia trachomatis*. *J. Bacteriol.* **179**: 7233-7242.

9. Malik, Z. A., G. M. Denning and D. J. Kusner. 2000. Inhibition of Ca^{2+} signaling by *Mycobacterium tuberculosis* is associated with reduced phagosome-lysosome fusion and increased survival within human macrophages. *J. Exp. Med.* **191**: 287-302.

10. Thompson, C. R., S. S. Iyer, N. Melrose, R. VanOosten, K. Johnson, S. M. Pitson, L. M. Obeid and D. J. Kusner. 2005. Sphingosine Kinase 1 (SK1) Is Recruited to Nascent Phagosomes in Human Macrophages: Inhibition of SK1 Translocation by *Mycobacterium tuberculosis*. *J. Immunol.* **174**: 3551-3561.

11. Vander Beken, S., J. R. Al Dulayymi, T. Naessens, G. Koza, M. Maza-Iglesias, R. Rowles, C. Theunissen, J. De Medts, E. Lanckacker, M. S. Baird and J. Grooten. 2011. Molecular structure of the *Mycobacterium tuberculosis* virulence factor, mycolic acid, determines the elicited inflammatory pattern. *Eur. J. Immunol.* **41**: 450-460.

12. Fowler, D. W., J. Copier, A. G. Dalgleish and M. D. Bodman-Smith. 2014. Zoledronic acid causes gammadelta T cells to target monocytes and down-modulate inflammatory homing. *Immunology* **143**: 539-549.

13. Muratsu, D., D. Yoshiga, T. Taketomi, T. Onimura, Y. Seki, A. Matsumoto and S. Nakamura. 2013. Zoledronic acid enhances lipopolysaccharide-stimulated proinflammatory reactions through controlled expression of SOCS1 in macrophages. *PLoS One* **8**: e67906.

APPENDIX I

Exploration of comparative *ex vivo* cellular technologies

1. Chapter aims

This chapter provides detailed information on the experimental techniques that were explored throughout this study. Considering the complex and diverse nature of immunological reactions and the need for experimental animals to simulate mammalian immune response models, for example mycobacterial infection, widespread optimisation of experimental conditions and protocols had to be completed. Here we describe these optimisation conditions and resultant findings, which led to our eventual working experimental models.

For all exploratory experiments the mycolic acids (MAs), animals, experimental design, preparation of injectable solutions and macrophage isolation, cell harvesting and culture, mycobacterial culture and infection with *Mycobacterium bovis* bacille Calmette-Guérin (BCG), and microscopy were as described (Chapter II: Materials and methods). Treatment groups consisted of placebo (PBS), empty liposome carrier (Lipo), MA lipid backbone (MA-bb), *cis*-alpha MA (αMA), natural Mtb MA mixture (MA mix; Sigma), methoxy MA (*cis*- and *trans*-mMA), or keto MA (*cis*- epimeric, *trans*-, and *cis*-monomeric-kMA). Standard fluorescence microscopy was conducted using a CellM Olympus BX61 upright microscope with DIC, equipped with halogen light (brightfield) and 100 W mercury lamp (fluorescence). Variation to any of the described protocols is summarised in each section.

2. Visualisation of mycobacteria in the absence of MA co-staining

2.1 Aim of technology

The aim of the technologies explored in this section was to enable visualisation of mycobacterial bacilli in infected primary murine macrophages, and tracking of bacillary replication over time. Staining conditions had to be optimised to ensure that mycobacteria

from the infection were discernible, and that the Mtb-associated natural and synthetic free MAs used to treat mice *in vivo* did not interfere with bacillary quantification.

2.2 Auramine-Rhodamine T staining

Materials and methods

Control groups were PBS and Lipo while the treatment group was the natural Mtb MA mix (Sigma). Mice were terminated and PECs harvested after 24 h of treatment. PECs were seeded at a final concentration of $1x10^6$ cells in 1 ml complete medium without phenol red in 24-well plates. Cells were incubated at 37°C and 5% CO_2 and the macrophage fraction selected for by 2 h adherence. Following adherence, cells were washed three times in endotoxin-free PBS (Lonza) and either remained unfixed or were fixed in 2% then 4% paraformaldehyde for 15 min each at room temperature. For mycobacteria detection, cells were infected at a multiplicity of infection (MOI) of 10:1 (10 bacilli to 1 cell) for 4 h at a final concentration of 400 µg/10 µl (40 mg/ml). The remainder of the infection protocol was as described (Chapter II: Mycobacterial culture and infection).

The TB Fluorescent Stain Kit T (TB Auramine-Rhodamine T; Cat. no 212515, Becton Dickinson) was used to stain cells *ex vivo* for detection of free MAs or mycobacteria. Cells (unfixed and fixed) were stained with Auramine-Rhodamine T (1:20) for 25 min, then washed twice with endotoxin-free PBS. Cells were decolourised for 2-3 min (TB Decolorizer), washed twice and counterstained for 4-5 min (TB potassium permanganate). Following PBS washes, nuclei were stained with Hoechst® (1:1000) for 15 min at room temperature and mounting medium added (anti-fade agent; KPL). Cells were immediately viewed with a standard fluorescent microscope.

Results and discussion

No Auramine-Rhodamine fluorescence was detected in any of the MA treatments from both cell fixation conditions (Fig. 1 and 2). Fixed cells were clearly more visible than unfixed cells, but intracellular free MAs did not stain yellow-red with Auramine-Rhodamine T. Mycobacteria stained positive with Auramine-Rhodamine T, yet cell viability was fatally affected (Fig. 3). Replication could therefore not be quantitatively measured. Macrophages underwent necrosis after staining with Auramine-Rhodamine T.

Our initial optimisation experiments for *ex vivo* detection of intracellular free MAs and mycobacteria in murine macrophages illustrated that Auramine-Rhodamine T stain is not a suitable application. Auramine O or basic yellow 2 is a diarylmethane dye and is soluble in water and ethanol (460/550 nm) while Rhodamine B or basic violet 10 is a chemical compound and laser dye (540/625 nm)[1]. Auramine O and Rhodamine B bind mycobacterial MAs[2] and our initial thinking was that we could use this staining technique to detect MAs *in vitro*. TB Stain Kits (Becton Dickinson) contain harsh reagents most commonly applied to specimen smears and cultures for tubercle bacillus detection during presumptive diagnosis of mycobacterial infection[3]. We established that Auramine-Rhodamine T stain can successfully distinguish acid-fast mycobacteria, yet is not suitable for staining live cells *in vitro*. This method was therefore not selected for further mycobacterial detection in this study. It was also observed that mycobacterial infection at an MOI of 10 was far exceeding physiological capacity of murine host cells and caused severe necrosis. The mycobacterial MOI was subsequently optimised and these results will be discussed later in this chapter (6. Optimisation of mycobacterial MOI).

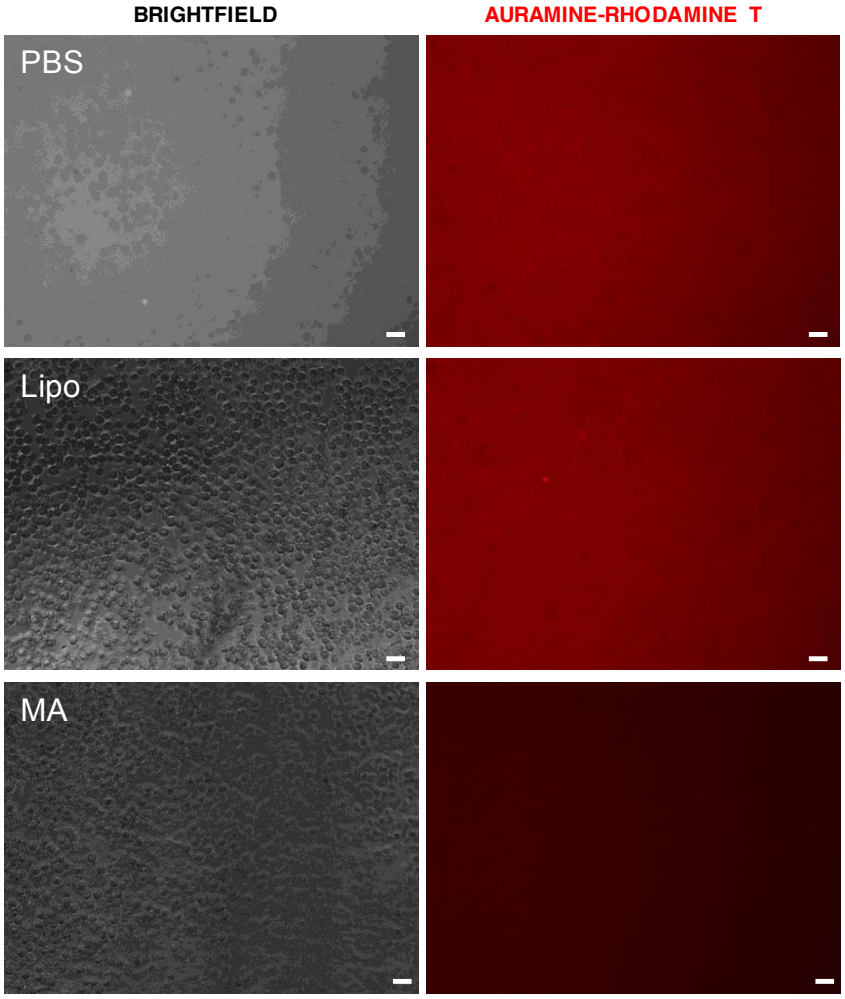

Figure 1 | Auramine-Rhodamine T staining for detection of free MAs in unfixed macrophages. Peritoneal macrophages harvested 24 h after *in vivo* murine control (PBS, Lipo) or MA treatment were left unfixed then stained with Auramine-Rhodamine T. Cells were viewed by standard fluorescence microscopy for detection of intracellular free MAs. Objective: 20x. Scale bar: 20 µm

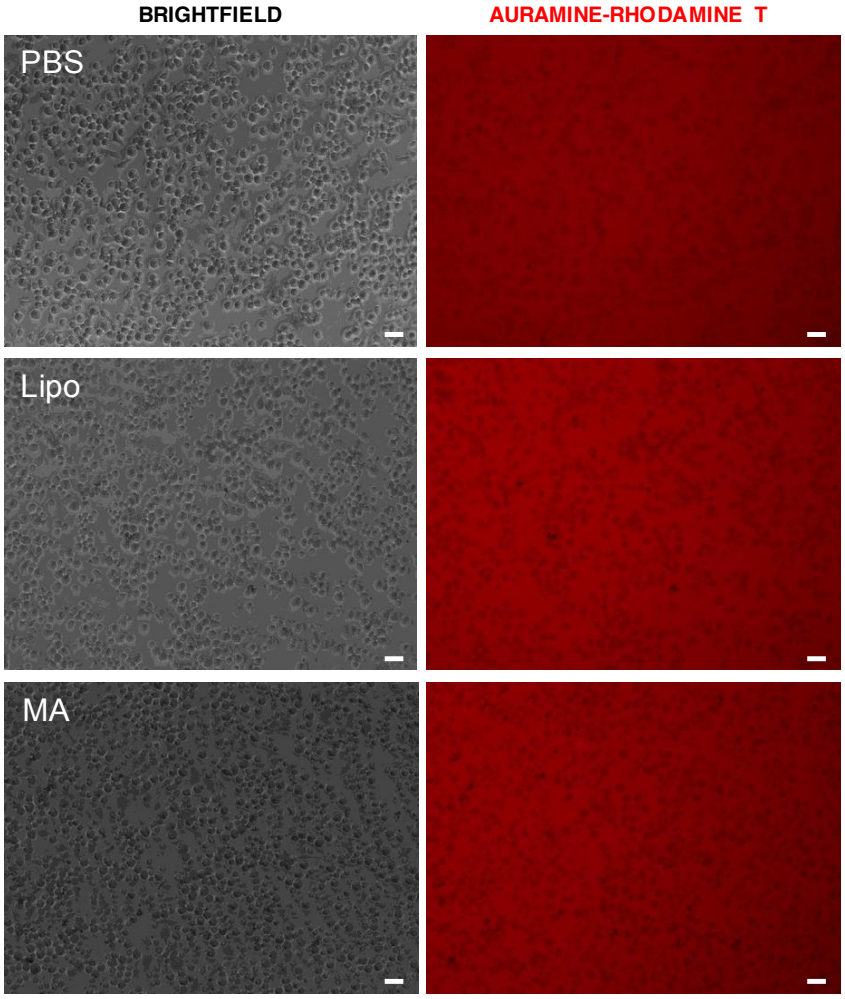

Figure 2 | Auramine-Rhodamine T staining for detection of free MAs in fixed macrophages. Peritoneal macrophages harvested 24 h after *in vivo* murine control (PBS, Lipo) or MA treatment were fixed in 4% paraformaldehyde (PFA) then stained with Auramine-Rhodamine T. Cells were viewed by standard fluorescence microscopy for detection of intracellular free MAs. Objective: 20x. Scale bar: 20 µm

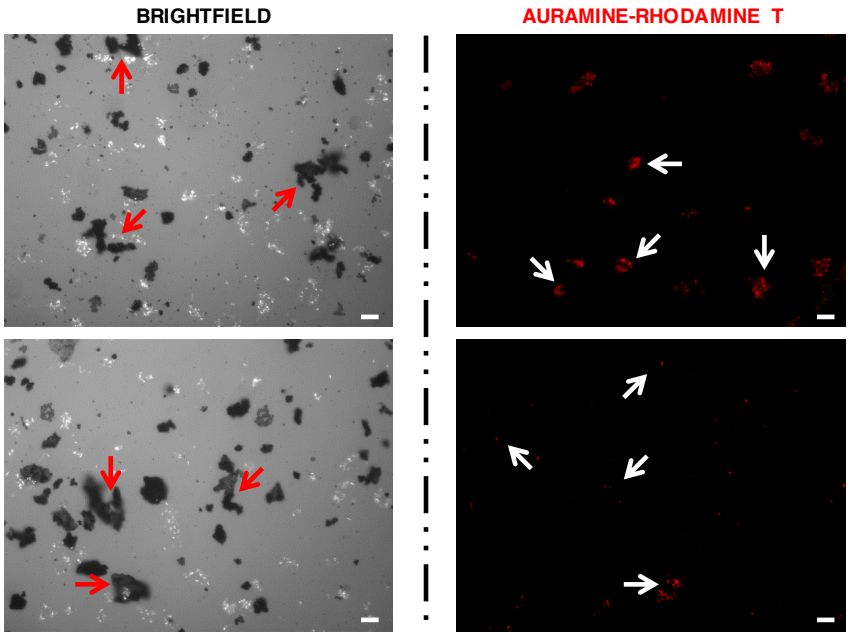

Figure 3 | Auramine-Rhodamine T staining for detection of intracellular mycobacteria. Murine primary peritoneal macrophages were infected *ex vivo* with BCG (MOI: 10) for 4 h then fixed in 4% paraformaldehyde (PFA) and stained with Auramine-Rhodamine T. Red arrows, necrotic macrophages; white arrows, mycobacteria staining bright red with Auramine-Rhodamine T. Cells were viewed and imaged with a standard fluorescent microscope. Objective: 40x. Scale bar: 10 µm

2.3 Mycobacterial nucleic acid staining

Materials and methods

Mice (n = 5 per experimental group) were injected with control (PBS, Lipo or MA-bb) or MA solutions at 25 µg per 100 µl per mouse (αMA, mMA and kMA isomers). Cells were harvested after 48 h and seeded into µ-Slide 8-well microscopy plates (ibidi®; $5x10^5$ cells/well). After overnight adherence, cells were infected with BCG for 6 h (MOI: 1), washed three times with endotoxin-free PBS and incubated 48 h prior to fluorescent labelling with Hoechst®, CellTracker™Red and Bodipy 493/503 as described (Chapter II: Light and laser-scanning-confocal microscopy). In order to detect intracellular bacilli, cells were first stained with Hoechst® for 30 min at 37°C to allow nucleic acid labelling of BCG bacilli prior to staining with other fluorescent dyes. Bacilli were analysed by adjustment of the ultraviolet (UV) laser of the confocal microscope. As morphology assessment control, cells from untreated mice were infected with PBS (mock, no BCG) or BCG and cultured for five days.

Results and discussion

Mock- and BCG-infected control cells remained viable and morphologically intact over the five days of culture though some cell death was observed in the BCG-infected cells (Fig. 4). We labelled mycobacterial nucleic acids by staining with Hoechst®, the same fluorescent probe used to stain cellular nuclei. We confirmed that mycobacteria were stained by excitation of the ~405 nm UV laser at 90%, which was substantially higher than the standard excitation at 3-5% UV for detection of nucleic acids (Fig. 5). Bacilli were visible in BCG-infected macrophages, yet were not easily quantifiable from background UV (Fig. 6). Whilst it was possible to recognise fluorescently-labelled bacterial nucleic acids at 90% UV, measuring individual bacilli at 20, 25 and 30% UV was not successful

(Fig. 6). As a consequence, individual mycobacteria could not be sufficiently exposed in macrophages for quantification and hence only merged images are shown for all conditions (Fig. 7 and 8).

The bisbenzamide derivative Hoechst® is a DNA-specific fluorochrome widely applied to determining abundances of bacteria using various fluorescence microscopy techniques[4]. We attempted to fluorescently label mycobacterial nucleic acids with Hoechst® stain to assess replication by laser-scanning-confocal microscopy. This staining technique, however, did not work well as individual bacilli could not be clearly distinguished or counted using Volocity 3D Image Analysis software.

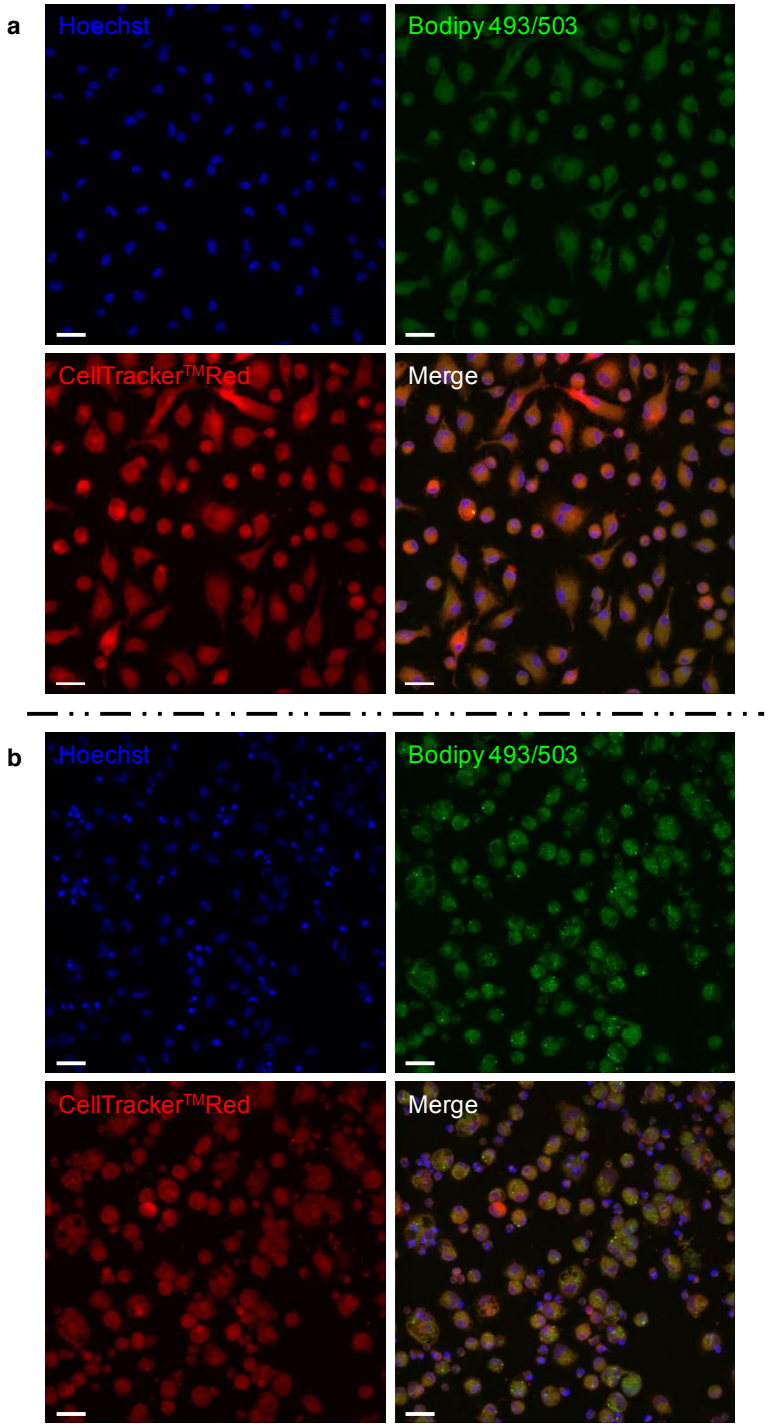

Figure 4 | Comparison of control and BCG-infected cells after five days of culture. Murine peritoneal macrophages were infected *ex vivo* with (a) mock PBS or (b) BCG (MOI: 1) and cultured for five days. Cells were fluorescently labelled with Hoechst®, CellTracker™Red and Bodipy 493/503 and assessed by laser-scanning-confocal microscopy. Panels depict separate fluorescent dyes and combined (merge) images. Scale bar: 10 µm.

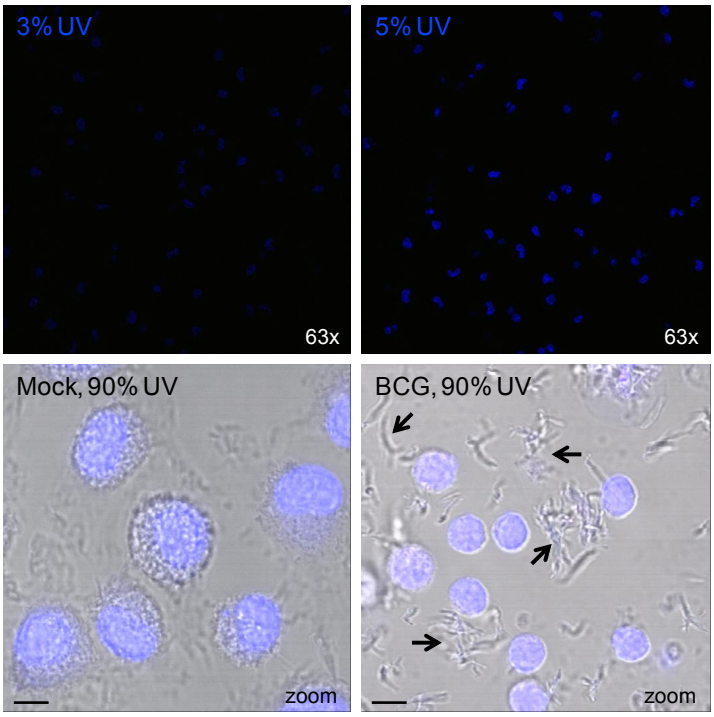

Figure 5 | Optimisation of mycobacterial detection. Top panel images (63x) depict standard excitation of the ~405 nm UV laser at 3% and 5% by laser-scanning-confocal microscopy. Lower panel images (zoom) show brightfield/UV overlays of mock- and BCG-infected peritoneal macrophages assessed for the presence of mycobacteria at 90% excitation. Arrows indicate bacilli. Objective: 63x (2.65x zoom). Scale bar: 5 µm.

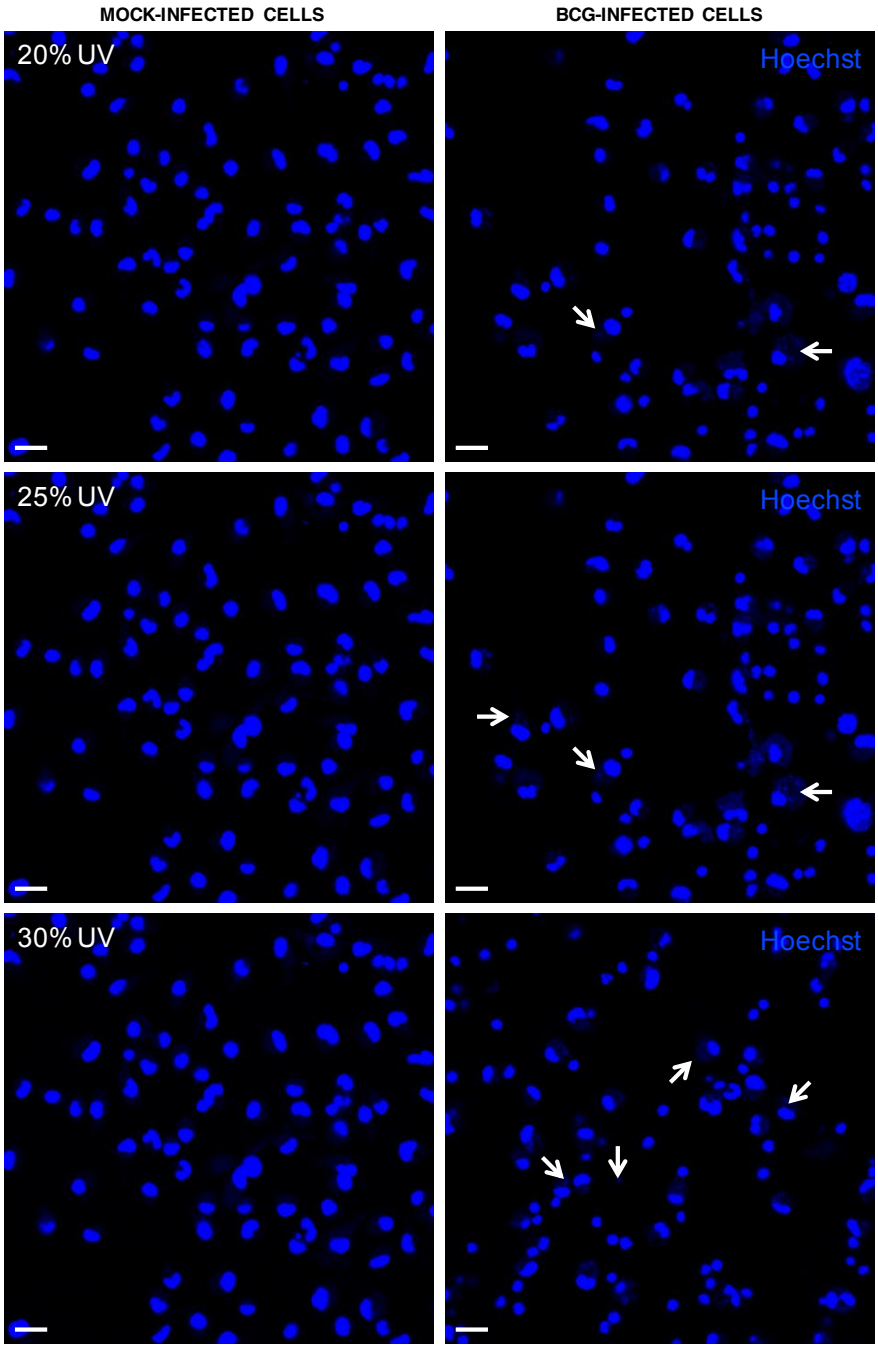

Figure 6 | Detection of mycobacteria by UV laser. *Ex vivo* mock- and BCG-infected murine peritoneal macrophages were stained with the nucleic acid dye Hoechst® and assessed for intracellular bacilli by excitation of the ~405 nm UV laser at 20, 25 and 30%. Arrows indicate fluorescently-labelled yet faintly visible BCG bacilli. Objective: 63x. Scale bar: 10 µm.

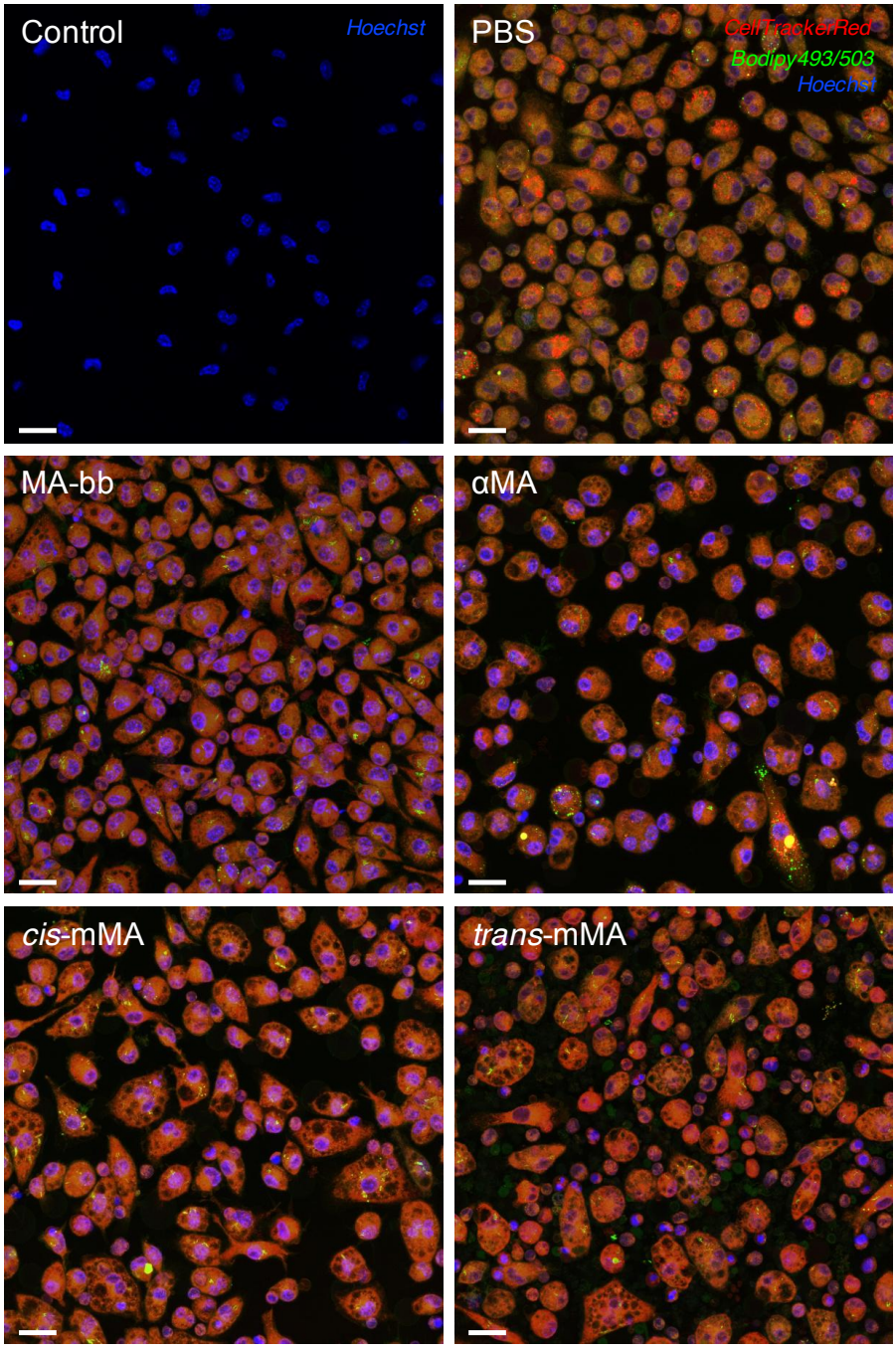

Figure 7 | Detection of mycobacteria through nucleic acid labelling. Mice were treated with placebo (PBS), control (Lipo, MA-bb) or MA solutions and cells harvested and seeded after 48 h. Peritoneal macrophages were infected *ex vivo* with BCG for 6 h (MOI: 1) and analysed by laser-scanning-confocal microscopy after two days of culture. Cells were labelled with the fluorescent dyes Hoechst®, CellTracker™Red and Bodipy 493/503. Merge images are shown. Objective: 63x. Scale bar: 10 µm.

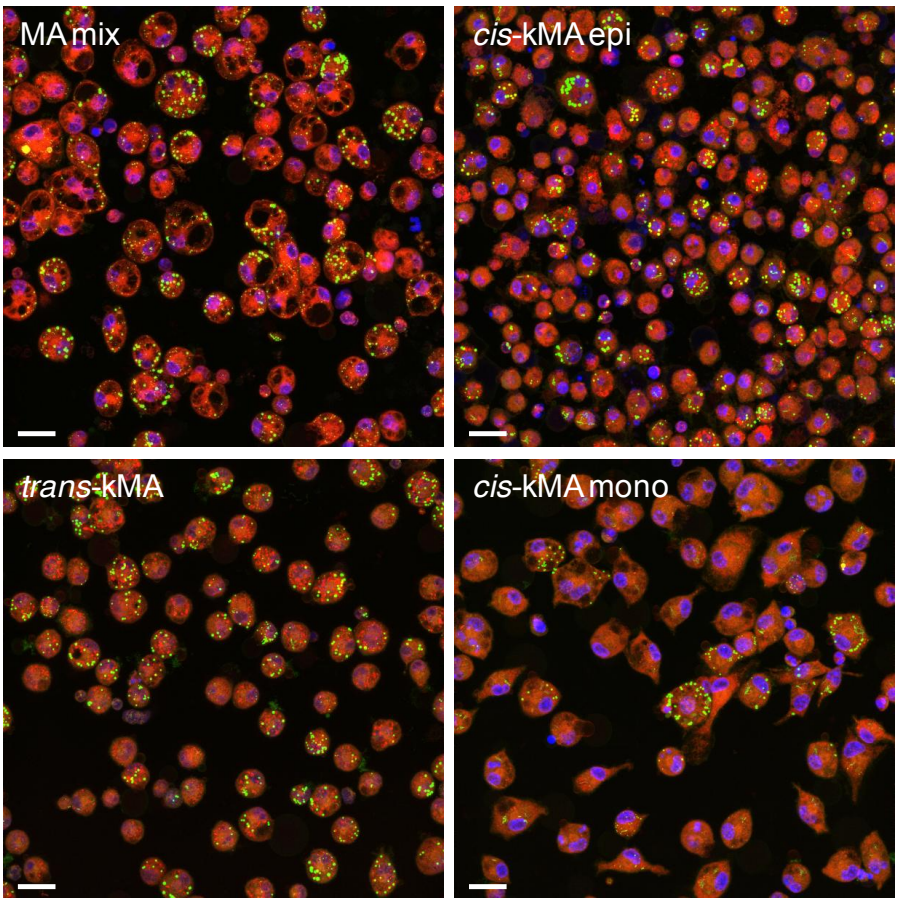

Figure 8 | Detection of mycobacteria through nucleic acid labelling (continued). Mice were treated with MA solutions and cells harvested and seeded after 48 h. Peritoneal macrophages were infected *ex vivo* with BCG for 6 h (MOI: 1) and analysed by laser-scanning-confocal microscopy after two days of culture. Cells were labelled with the fluorescent dyes Hoechst®, CellTracker™Red and Bodipy 493/503. Merge images are shown. Objective: 63x. Scale bar: 10 µm.

2.4 Bodipy 493/503 lipophilic dye

Materials and methods

In order to assess whether intracellular BCG bacilli that have lipid-rich cell envelopes stain positive with the green fluorescent lipophilic dye Bodipy 493/503, murine peritoneal macrophages were harvested and seeded into µ-Slide 8-well microscopy plates (ibidi®; $5x10^5$ cells/well). Cells were infected the next day for 6 h with BCG at a high MOI of 10 (to have abundant bacilli for staining) and were cultured overnight prior to fluorescent labelling (Chapter II: Light and laser-scanning-confocal microscopy). Cells were first stained with Bodipy 493/503 for 30 min at 37°C followed by Hoechst® stain for 15 min. Cells were immediately viewed by laser-scanning-confocal microscopy.

Results and discussion

Upon overexposure of the confocal microscope's yellow-green (543 nm) laser, it was shown that BCG bacilli stained bright green with the lipophilic dye Bodipy 493/503 (Fig. 9). The Mtb cell envelope comprises multiple layers of distinct and diverse lipids and lipoproteins[5-8]. It was important for this study to visualise countable bacilli for growth measurements in MA-treated macrophages. However, quantification of individual foam cell traits like lipid droplets (LDs) and vacuoles were also essential aims of this study. LDs are packed with sterol esters and triacylglycerol that are hydrophobic neutral lipids lacking charged groups[9]. As the neutral lipid dye Bodipy 493/503 was the ideal stain for identification of intracellular LDs with the 543 nm laser, we selected an alternative BCG strain for our mycobacterial experimental model. This BCG strain contained a reporter gene expressing a red fluorescent protein (BCG-dsRed), which allowed us to identify intracellular bacilli with the red (633 nm) laser (2.5 BCG-dsRed).

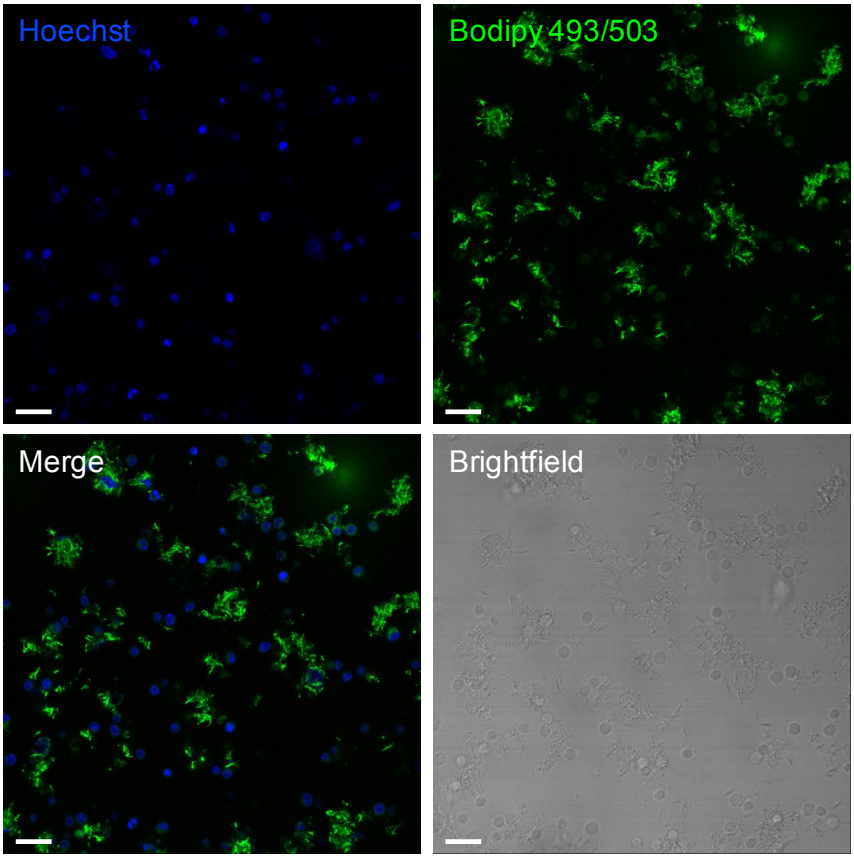

Figure 9 | Mycobacteria stain green with the lipophilic dye Bodipy 493/503. Murine peritoneal macrophages were infected *ex vivo* for 6 h with BCG (MOI: 10) and assessed by laser-scanning-confocal microscopy for detection of fluorescently-labelled mycobacteria. BCG bacilli stained bright green with the lipophilic dye Bodipy 493/503, which was clearly visible upon overexposure of the 488 nm laser. Objective: 63x. Scale bar: 10 µm.

2.5 BCG-dsRed

Materials and methods

BCG-dsRed with red fluorescent reporter gene was a gift from Dr Erica Houthuys from the Unit of Medical Biotechnology (Inflammation Research Center, Ghent, Belgium). To investigate whether red fluorescent BCG bacilli can be detected in macrophages with normal morphology and foam cells brought about by MA exposure, mice were treated with placebo (PBS) or Mtb MA (Sigma) two days prior to harvesting of PECs. After an overnight adherence step, peritoneal macrophages were infected for 6 h with BCG-dsRed (MOI: 1) and cultured overnight prior to fluorescent staining with Hoechst® or CellTracker™Blue and Bodipy 493/503 (Chapter II: Light and laser-scanning-confocal microscopy). Cells were immediately viewed by laser-scanning-confocal microscopy.

Results and discussion

BCG-dsRed bacilli were clearly detectable by laser-scanning-confocal microscopy in peritoneal macrophages from mice treated with PBS and thus having a normal morphology, as well as in foam cells containing intracellular LDs and vacuoles from Mtb MA-treated mice (Fig. 10). We therefore used the BCG strain with reporter gene expressing a red fluorescent protein for all subsequent experimental work.

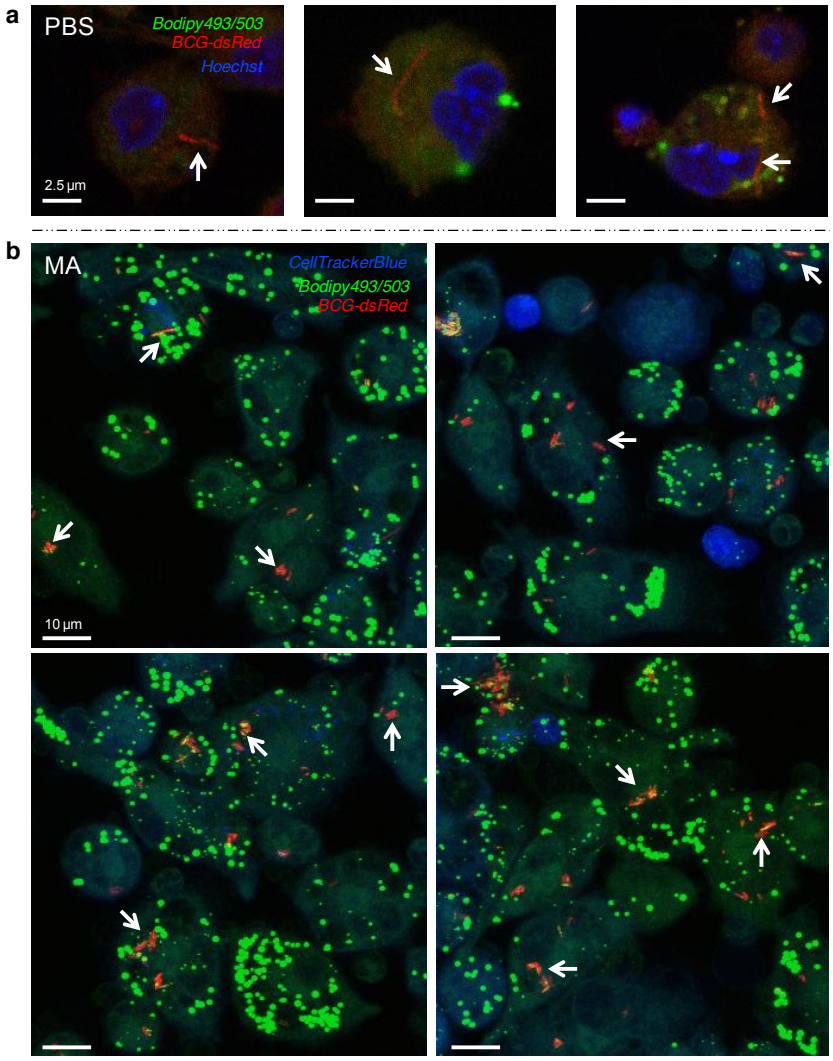

Figure 10 | Detection of BCG-dsRed bacilli by laser-scanning-confocal microscopy. Murine peritoneal macrophages from mice treated with (a) placebo PBS or (b) Mtb MA (Sigma) were infected *ex vivo* for 6 h with BCG-dsRed (MOI: 1). Cells were stained with the fluorescent probes Hoechst® or CellTracker™Blue and Bodipy 493/503. Assessment by laser-scanning-confocal microscopy detected macrophages (405 nm laser), LDs (543 nm laser) and red fluorescent bacilli (633 nm laser). Arrows indicate red fluorescent BCG bacilli. Objective: 63x. Scale bar: (a) 2.5 µm and (b) 10 µm.

3. Visualisation of intracellular neutral lipids

3.1 Aim of technology

Foam cells, a key macrophage population of Mtb-associated granulomas, are characterised by the presence of intracellular LDs and vacuoles. In order to quantify these foam cell traits separately in macrophages brought about by the diverse MA treatments, the aim of this technology was to optimise the staining conditions for detection of intracellular neutral LDs by laser-scanning-confocal microscopy.

3.2 Nile red and Bodipy 493/503

Materials and methods

Cells from untreated mice were harvested and processed as described (Chapter II: Injectable solutions and macrophage isolation) and seeded into 96-well ($1.6x10^5$ cells/well) and 24-well plates ($1x10^6$ cells/well). Macrophages were stained with Hoechst® and either of the lipophilic fluorescent dyes used to detect intracellular neutral LDs: Nile Red (9-diethylamino-5-benzo[α]phenoxazinone; Sigma) or Bodipy 493/503 (8-Bromomethyl-4,4-Difluoro-1,3,5,7,8-Pentamethyl-4-Bora-3a,4a-Diaza-*s*-Incacene; Molecular Probes). Stock solutions of Nile Red (1 mg/ml in acetone) and Bodipy 493/503 (1 mg/ml in DMSO) were tested in serial dilution (1:62.5 to 1:1000) and examined by standard fluorescent and laser-scanning-confocal microscopy.

Results and discussion

No marked differences in standard fluorescence were observed in the tested serial dilutions (1:62.5 to 1:250) of the neutral lipid stains Nile Red and Bodipy 493/503 (Fig. 11). The lower concentrations (1:500 and 1:1000) of lipid stains were faint when viewed by a standard fluorescence microscope (Fig. 11). The 1:125 lipid dye dilution was the most

suited for assessment of intracellular neutral LDs by laser-scanning-confocal microscopy (Fig. 12). It was also observed that whereas the red fluorochrome (Nile Red) immediately bleached upon confocal emission, this was not the case for the bright green fluorophore (Bodipy 493/503).

LDs are dynamic cell organelles with important physiological attributes[10, 11]. Their biogenesis and catabolism are strongly regulated with key functions in cellular lipid metabolism, homeostasis and inter-membrane lipid trafficking[12-15]. Intracellular pathogens like Mtb modify the host cell lipidome for its own benefit by, for example, inducing lipid loading in macrophages[16]. It was thus of key importance to select a suitable fluorescent probe for intracellular assessment of neutral lipids by laser-scanning-confocal microscopy. Compared to the commonly used Nile Red stain, the green fluorophore Bodipy 493/503 was identified as the preferred probe. Bodipy-stained LDs fluoresced bright green, were clearly distinct from cell background and did not bleach when viewed by laser-scanning-confocal microscopy. This is in accordance with previous reports that Bodipy dyes can be used for quantitative analysis of lipids[17]. For our work we applied Bodipy 493/503 at a concentration of 1:125 from 1 mg/ml stock solution.

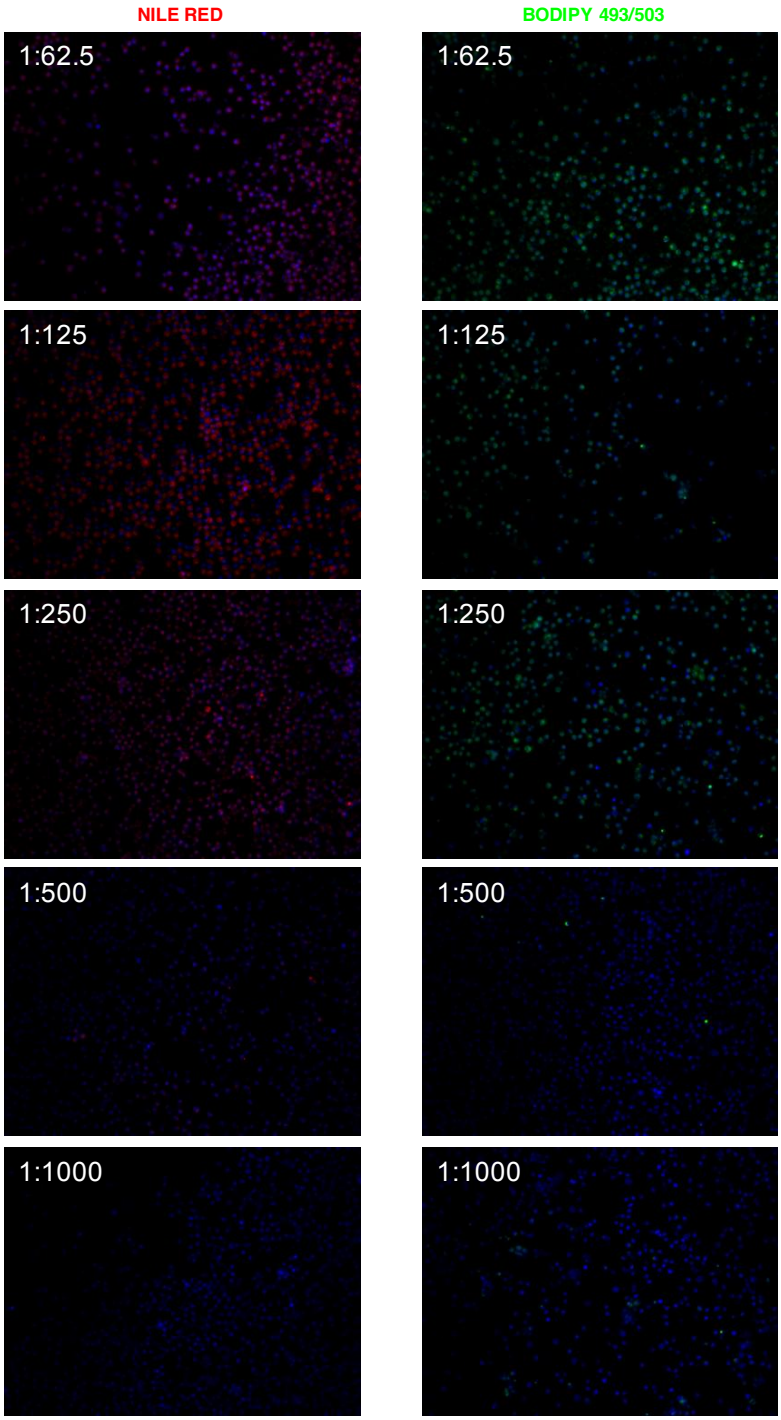

Figure 11 | Optimisation of lipophilic stain concentrations by standard fluorescence microscopy. Murine peritoneal macrophages were stained with Hoechst® and serial dilutions of Nile Red and Bodipy 493/503 lipid dyes (from 1 mg/ml stock) and assessed with a standard fluorescent microscope. Objective: 20x.

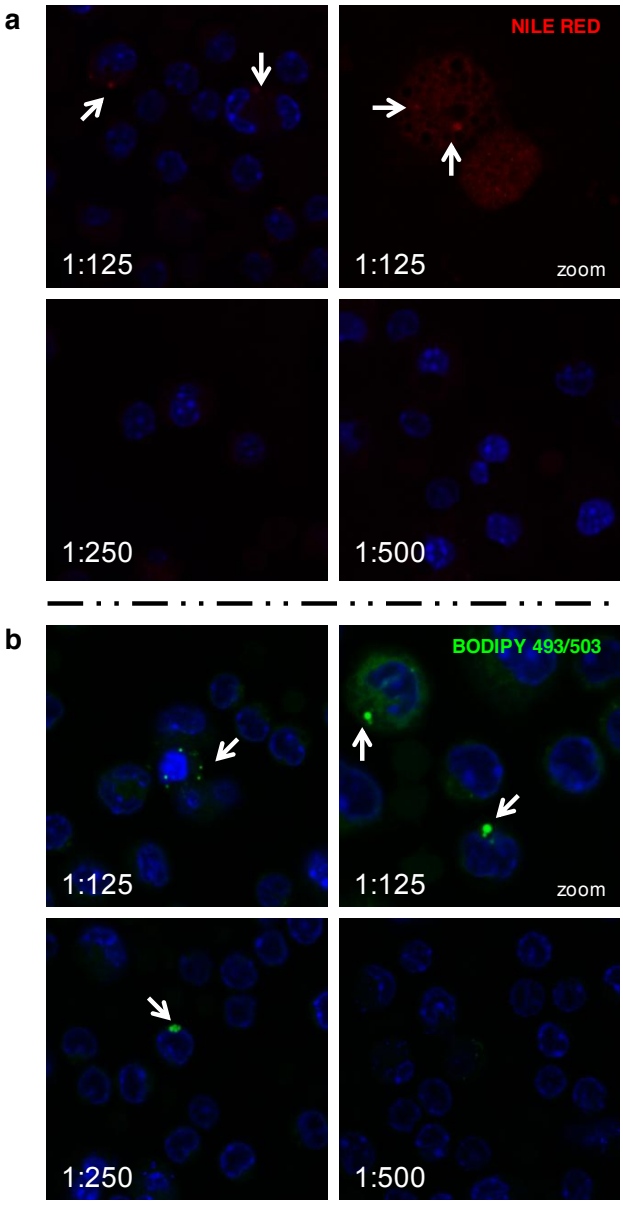

Figure 12 | Optimisation of lipophilic stain concentrations by laser-scanning-confocal microscopy. Murine peritoneal macrophages were stained with serial dilutions of (a) Nile Red and (b) Bodipy 493/503 lipid dyes 503 (from 1 mg/ml stock) and assessed by laser-scanning-confocal microscopy. Arrows indicate intracellular neutral LDs. Objective: 63x (2.65x zoom).

4. Assessment of vacuole formation following MA treatment

4.1 Aim of technology

The aim of this technology was to optimise detection of the second foam cell trait brought about by *in vivo* murine treatment with various MAs, namely the induction of multiple intracellular vacuoles, by laser-scanning-confocal microscopy.

4.2 Vacuole counterstaining with CellTracker™

Materials and methods

Mice were treated with control solutions (PBS, Lipo) or Mtb MA (Sigma). Peritoneal macrophages were harvested, cultured and stained with Hoechst, CellTracker™Red and Bodipy 493/503 as described (Chapter II: Injectable solutions and macrophage isolation). Cell size measurements were taken from laser-scanning-confocal microscopy images using Volocity 3D Image Analysis software. Size measurement was used to determine the threshold value for macrophages with a normal morphology (PBS treated mice) as compared to enlarged vacuole positive cells (V+; induced by treatment with MA). Once the threshold size for enlarged V+ macrophages was established, mice were treated with 100 or 400 µl endotoxin-free PBS or liposome carrier, while those treated with Mtb MA received 25 µg (standard) or 100 µg MA per mouse. Cells were stained with CellTracker™Blue and Bodipy 493/503 and assessed by laser-scanning-confocal microscopy for the induction of enlarged V+ cells.

Results and discussion

The size of macrophages from placebo treated mice that have a normal morphology ranged from 8-15 µm (Fig. 13A). Macrophages containing abundant intracellular vacuoles induced by treatment of mice with Mtb MA were 24 µm or larger (Fig. 13B). The

threshold value for quantifying enlarged V+ cells was therefore set at ≥24 μm. The induction of enlarged V+ cells from mice treated with Mtb MA was distinct from those of PBS or Lipo treated mice (Fig. 14A). Mice injected with different volumes of PBS or liposome carrier concentrations exhibited a morphology that remained a normal rounded shape with negligible enlarged V+ cells. Macrophages from mice treated with Mtb MA exhibited a dose-dependent induction of V+ cells (Fig. 14B).

Our assessment of intracellular vacuoles showed that macrophages from Mtb MA-treated mice effected prominent induction of enlarged cells containing multiple vacuoles when compared to control PBS or Lipo treatments. In addition, these MA-induced intracellular vacuoles were deficient in lipid and protein as they did not stain with either of the respective fluorescent probes, namely Bodipy 493/503 or CellTracker™. Our group previously demonstrated that Mtb MAs induce vacuole formation in host macrophages[18], a hallmark trait of foam cell formation during Mtb infection[19]. The induction of distinct morphological features by MA in host cells affirmed our initial findings and thus allowed us to exploit, in addition to the feature of LD accumulation, the formation of intracellular vacuoles as quantitative foam cell traits for this study.

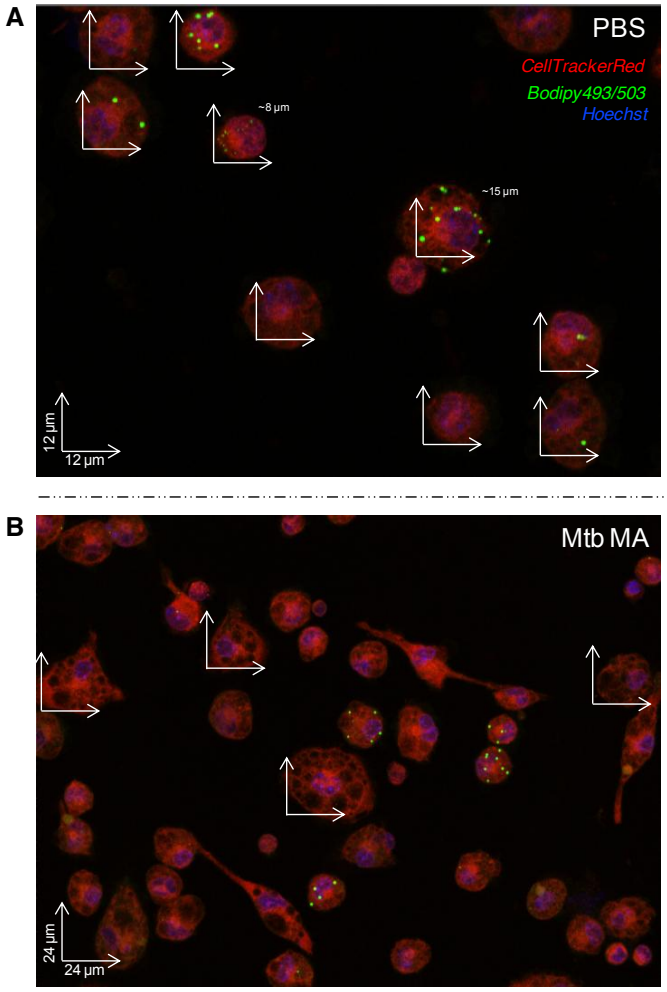

Figure 13 | Determination of threshold value for enlarged V+ macrophages. Mice were treated with (a) placebo (PBS) or (b) Mtb MA (25 µg/mouse) and peritoneal macrophages fluorescently labelled *ex vivo* with Hoechst®, CellTracker™Red and Bodipy 493/503. Laser-scanning-confocal microscopy images showing (a) macrophages with a normal morphology (~12 µm) and negligible enlarged V+ cells, and (b) enlarged V+ macrophages (≥24 µm). Objective: 63x. Scale bars: (a) 12 µm and (b) 24 µm.

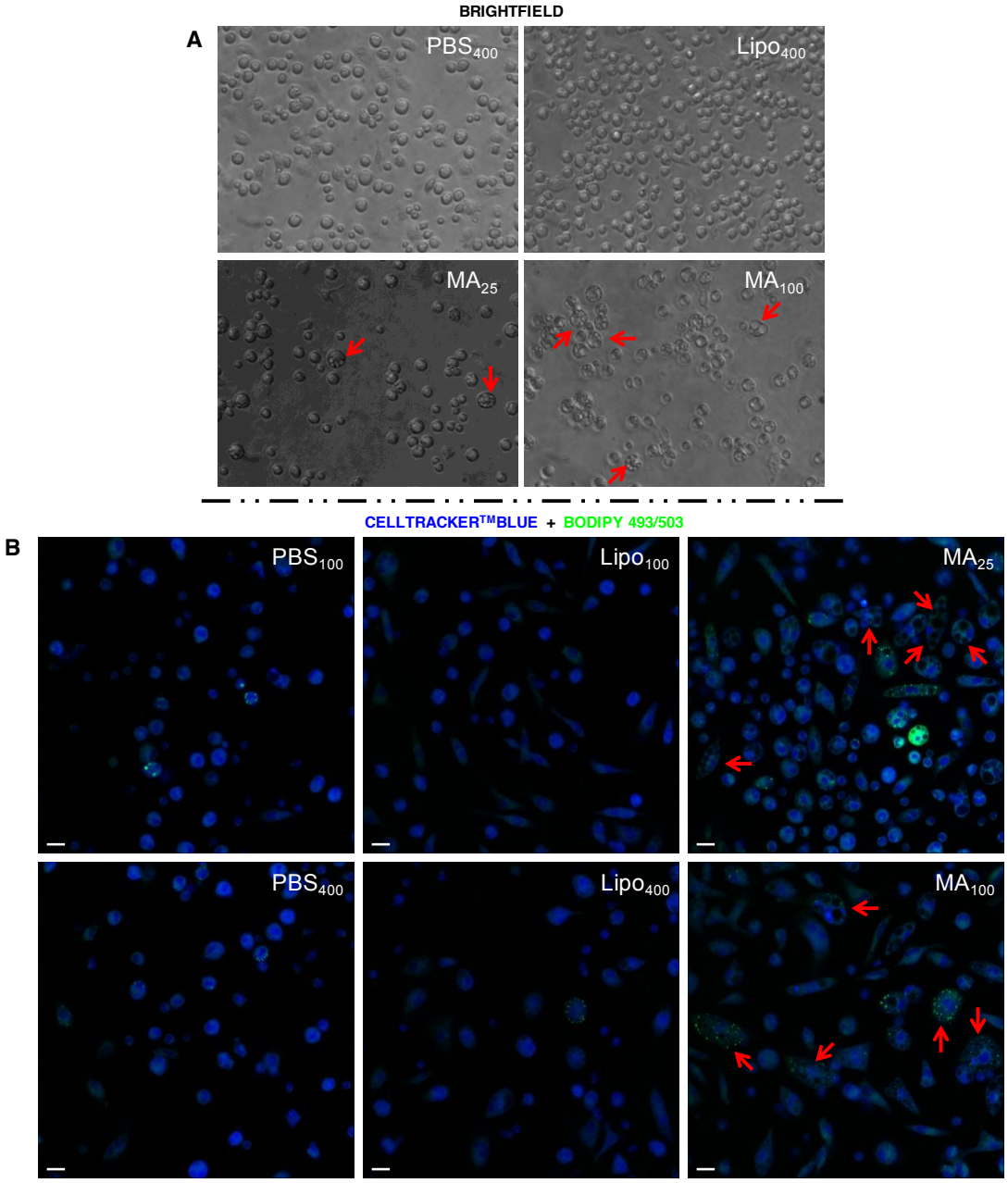

Figure 14 | Assessment of enlarged V+ macrophages following MA treatment. Mice were treated with PBS or Lipo (100 or 400 µl) or Mtb MA (25 or 100 µg/mouse). Peritoneal macrophages were fluorescently labelled *ex vivo* with CellTracker™Blue and Bodipy 493/503. (a) Brightfield images depicting absence or presence of enlarged V+ cells (red arrows) in peritoneal macrophage populations from mice treated with PBS, Lipo or MA. (b) Laser-scanning-confocal microscopy images showing distinct macrophage populations from variously treated mice and enlarged V+ cells induced by Mtb MA (red arrows). Objective: (a) 40x brightfield and (b) 63x. Scale bar: 12 µm.

5. Correlated quantification of multiple morphological foam cell traits

5.1 Aim of technology

During active TB, granulomas are characterised by large cell aggregates of which lipid-filled foam cells and those containing multiple vacuoles form key macrophage populations. MA is the dominant constituent of the Mtb cell envelope and induces a macrophage foam phenotype in mice similar to that observed in TB lung granulomas. Though it is not exactly clear which MAs contribute to the differentiation of macrophages into lipid-loaded and vacuolar cells, it possibly reflects a perturbation of host cell lipid homeostasis to support the infection. To further explore the contribution of each of the main MA classes to the induction of distinct granuloma cell populations, we explored in this section two technologies that could be applied for visualisation and quantification of macrophage foam cell traits.

5.2 High-content imaging analysis and laser-scanning-confocal microscopy

Materials and methods

Mice (n = 3 per experimental group) were treated intraperitoneally (i.p.) with PBS, Lipo, MA-bb, αMA, MA mix (Sigma), mMA (*cis*- and *trans*-), or kMA (*cis*- epimeric, *trans*-, and *cis*-monomeric-). Mice received either 400 µl PBS, 100 or 400 µl Lipo, or 25 or 100 µg MA/100 µl injection. Cells were harvested after 24 h and prepared in black 96-well plates ($5x10^5$ cells/well in 200 µl). Fluorescent probes were CellTracker^{TM}Blue and Bodipy 493/503. Whole cells were analysed by high-content (wide-field) imaging using a BD Pathway 435 benchtop system equipped with mercury halide lamp for capture of brightfield images (360-700 nm). Images were divided into regions of interest (ROI) using the BD Pathway Object Counting Tool for analysis of sub-cellular organelles through segmentation. Key measurements included fluorescence intensity and sub-object counts of

LDs and vacuoles. The proportions of >2 vacuoles and >3 LDs per cell, and the total area of vacuoles (μm) in each treatment were quantified using BD AttoVision Software (Version 1.7; BD Biosciences). Foam cell morphology was simultaneously assessed by laser-scanning-confocal microscopy using Volocity 3D Image Analysis Software (PerkinElmer Inc.; described in Chapter II: Statistical analyses). Gaussian distribution was checked with a Shapiro-Wilk test. Independent samples Kruskal-Wallis tests were used to assess differences in fluorescence intensity of whole cells and neutral LDs, vacuole total area in μm, and the number of LDs per 100 cells. Generalised linear models (GLM) with sequential Sidak pairwise comparisons analysed variation in the proportion of cells containing >2 vacuoles or >3 LDs per cell, and sub-object counts of vacuoles and LDs. Statistics were performed with SPSS 23 (IBM, Chicago IL, USA) or GraphPad Prism 5 (GraphPad Software, La Jolla CA, USA) and differences were significant at $P < 0.05$.

Results and discussion

For high-content imaging analyses with the BD Pathway, whole cells were stained with the fluorescent probe CellTracker^{TM}Blue (CTB) to identify the ROI. Segmentation then discerned among neutral LDs and unstained vacuoles within the ROI (Fig. 15). The $\lambda max^{emission}$ fluorescence intensity of whole cells (CTB) was comparable among treatments (Fig. 16). The $\lambda max^{emission}$ fluorescence intensity of neutral LDs (Bodipy) was significantly lower in cells from mice treated with Lipo (100 μl), MA mix (100 μg), and mMA (25 and 100 μg; Fig. 16). A significant dose-response in the proportions of cells with >2 vacuoles was recorded for the MA-bb, αMA, MA mix, *cis*-kMA (epi) and *trans*-kMA treatments (Fig. 17). Macrophages from mice that received mMA treatment had distinctly more cells with >2 vacuoles in comparison to cells from mice that received kMA treatment. Cells from the oxygenated MA treatments significantly differed in their proportion of cells containing LDs as compared to macrophages from mice treated with PBS, Lipo, MA-bb,

αMA and MA mix (Fig. 17). Vacuole counts distinguished PBS and Lipo control solutions from *cis*-kMA (mono) and all remaining MA treatments (Fig. 18). Cells from the kMA treatments contained significantly more LDs than those from other treatments (Fig. 18). The total area of vacuoles fluctuated among treatments (Fig. 19). While a dose-response in vacuole total area was discernible in cells from mice treated with various MAs, values from the PBS and Lipo controls (45-50 μm) were comparable to the 25 μg αMA and kMA treatments (45-65 μm). Of the 25 μg MA treatments, macrophages from mice treated with MA mix and *cis*-mMA contained the highest vacuole total area (~84 μm) whereas cells from the *trans*-mMA treatment had significantly less vacuoles (~46 μm). The highest vacuole total area was recorded for the 100 μg treatment of *cis*-mMA (115-127 μm) followed by the MA mix (85-99 μm) and all other MA treatments (66-82 μm; Fig. 19). We identified a limitation in the segmentation of sub-cellular organelles for analysis by the BD AttoVision software as it failed to successfully separate all touching cells and consequently underestimated the number of cells analysed (Fig. 20).

Foam cell traits were also analysed by laser-scanning-confocal microscopy (Fig. 21 to 24). Cells from mice treated with *cis*-epimeric and *trans*-kMA contained distinctly more LDs (circa 700 per 100 cells) followed by cells from the MA mix (circa 600 per 100 cells) and those from all other treatments (circa <400 per 100 cells; Fig. 25, upper panel). MA dose did not have an effect on the number of cytosolic LDs. Macrophages from mice that received MA mix and mMA treatments contained significantly more enlarged V+ cells (~25%) in comparison to all other treatments (<11%; Fig. 25, lower panel). MA dose significantly increased the number of V+ cells in the MA mix and *cis*-mMA treatments (Fig. 22 and 25).

High-content image analyses recorded similar whole cell fluorescence among treatments while neutral LD fluorescence varied among groups. Though these findings were as expected, the mean $\lambda max^{emission}$ fluorescence intensity of Bodipy 493/503 from the PBS and Lipo control cells was comparable to the fluorescence of the αMA and kMA treatments. This finding did not match actual data as confocal images clearly distinguished the kMA treatments in their number of LDs from all other groups. Sub-object counts from high-content imaging and confocal microscopy identified kMA as a significant inducer of LDs with 2- to 3-fold more LDs per 100 cells versus other treatments. Analyses of cellular vacuoles by high-content imaging (~25% cells with >2 vacuoles) and confocal microscopy (~25% V+ cells) identified mMA as a significant inducer of vacuoles. The vacuole results from the diverse imaging methods, however, did not entirely correlate. No dose-response was recorded for the mMA treatments in their proportions of cells containing >2 vacuoles while the confocal images showed a small, yet significant, increase in V+ cells from the 100 μg MA mix and *cis*-mMA groups. A strange result from high-content imaging was a dose-response for cells from mice treated with MA-bb or αMA (Fig. 17) with higher proportions of cells containing vacuoles relative to other control treatments (confocal microscopy did not corroborate these findings). In addition, sub-object counts recorded weak group differences in the number of cellular vacuoles and remarkably did not discern mMA as an inducer of vacuoles (Fig. 18). We subsequently quantified the total area of vacuoles from all cells within each treatment and recorded a significantly larger vacuole total area for cells from *cis*-mMA treated mice.

High-content imaging and confocal microscopy are powerful tools for a wide range of fluorescence intensity and morphological measurements of live or fixed cells using superior image quality processing[20]. Our results showed that high-content image analysis may be useful for measuring the number of neutral LDs, but not cellular vacuoles as

distinct discrepancies were recorded that did not correlate with data from the confocal images. This may partly be as a result of disproportionate number of total cells measured through segmentation by high-content imaging, which did not always precisely separate neighbouring cells (Fig. 20). While the discrepancy with segmentation also affected the proportion of cells with >3 LDs as it did not distinguish kMA from mMA groups (Fig. 17), the main concern was that vacuoles were not fluorescently stained and thus challenging to measure using software programmes. Laser-scanning-confocal microscopy allowed clear visual distinction among treatment groups and illustrated that kMA induces LD accumulation while mMA effects vacuole formation. The Volocity software analysis programme could effortlessly measure the total number of cells and cytosolic LDs, and high quality stacked images allowed precise (manual) counting of V+ cells using the predetermined size parameters. Cells were classified as enlarged V+ when their size was ≥24 μm and they contained abundant vacuoles. For these reasons, we consequently selected laser-scanning-confocal microscopy analyses to investigate foam cell morphological traits throughout this study.

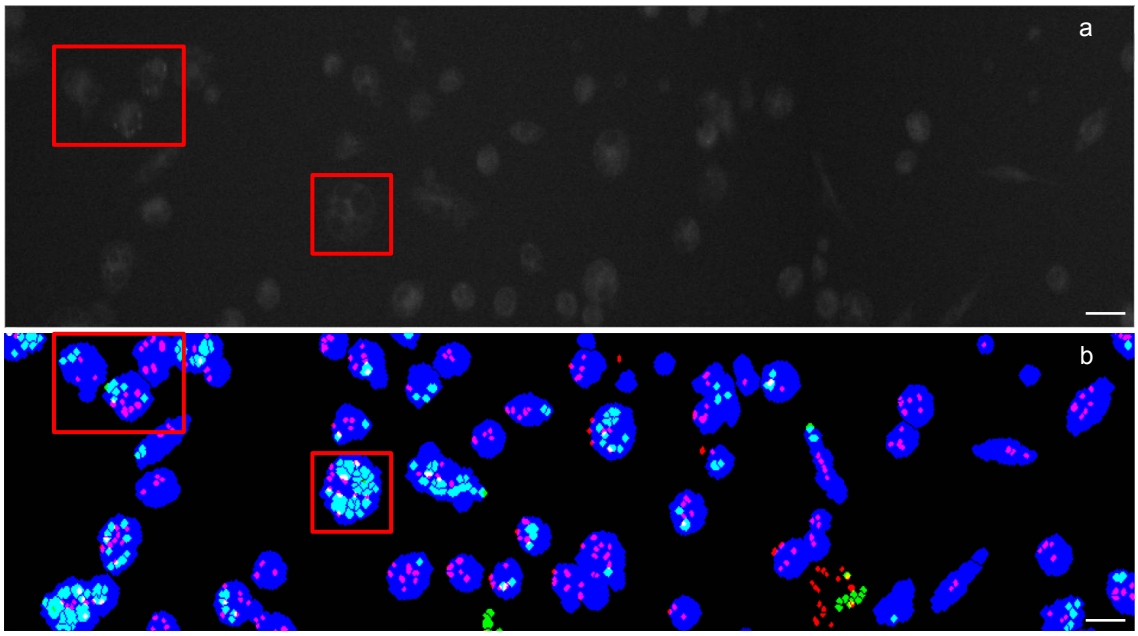

Figure 15 | Representation of high-content image analysis of sub-cellular organelles. (a) Brightfield image of murine peritoneal macrophages. (b) Segmented brightfield image (red squares) showing vacuoles (light blue) and LDs (magenta). Cells were fluorescently labelled with CellTracker™Blue to capture the ROI. Neutral LDs were stained with Bodipy 493/503 and vacuoles identified by unstained voids within the ROI. Both sub-cellular organelles were discernible through segmentation. Scale bar: 10 µm.

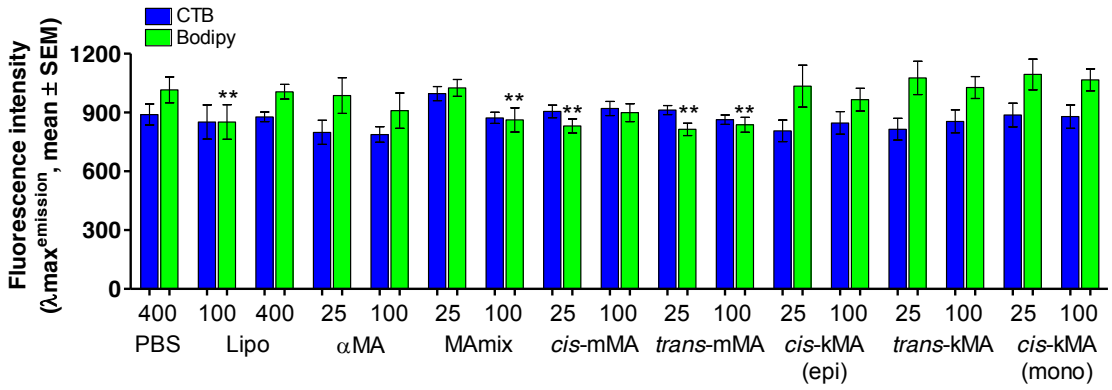

Figure 16 | Fluorescence intensity of mycolic acid-treated murine macrophages. Primary peritoneal macrophages were stained with CellTracker™Blue and the green lipophilic dye Bodipy 493/503, and fluorescence measured by high-content image analysis. Data represent $\lambda max^{emission}$ fluorescence intensity (mean ± SEM) of macrophages from three individual mice per treatment and were analysed with an independent samples Kruskal-Wallis test (CTB: $H = 19.588$, $n = 146$, $df = 16$, $P = 0.239$; Bodipy: $H = 32.612$, $n = 146$, $df = 16$, $P < 0.01$).

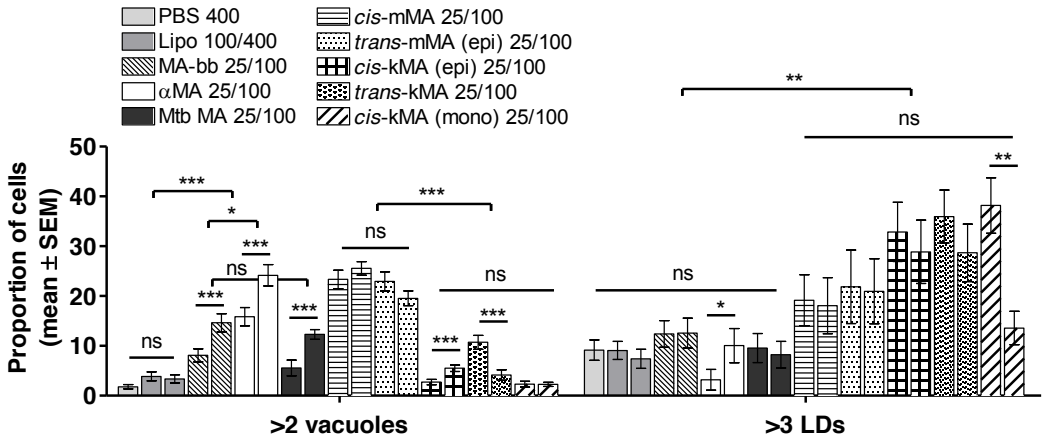

Figure 17 | Assessment of cytosolic vacuoles and LDs. Mice were treated with different volumes of control solutions (100 or 400 µl) or two concentrations of MA (25 or 100 µg), and cytosolic vacuoles and LDs quantified by high-content image analysis. Significant differences among treatments were determined with GLM analyses for cells containing >2 vacuoles (Wald Chi-Square = 835.502, n = 187, df = 18, $P < 0.001$) or >3 LDs (Wald Chi-Square = 86.991, n = 187, df = 18, $P < 0.001$). Data represent the proportion (%) of murine macrophages containing >2 vacuoles or >3 LDs per cell (mean ± SEM; n = 3 mice).

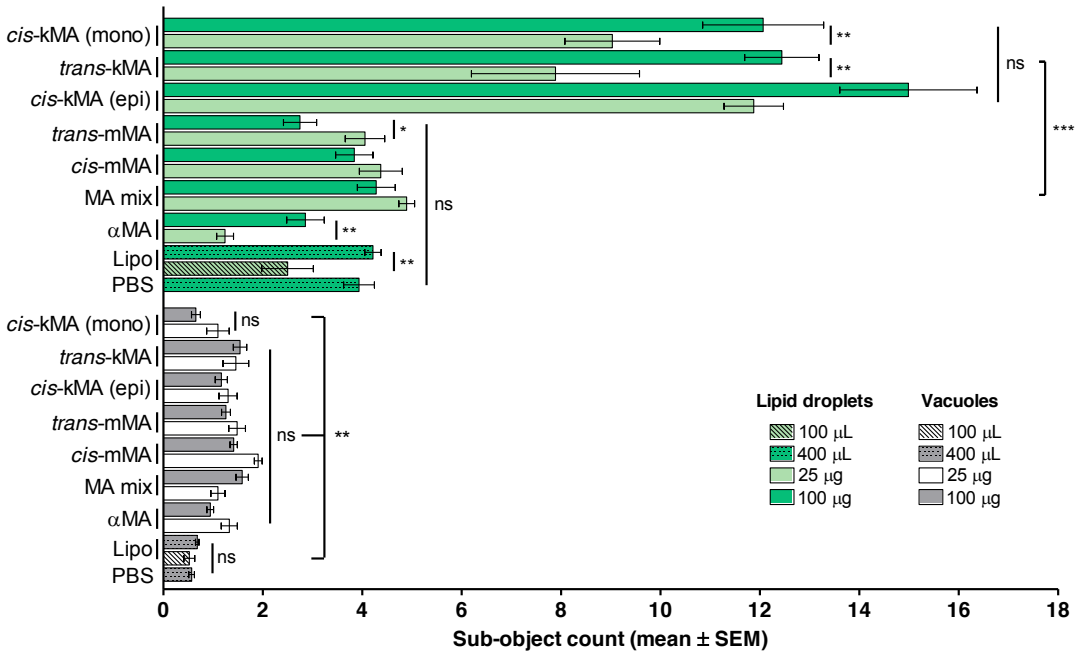

Figure 18 | Sub-object counts of LDs and vacuoles. Mice were treated with control solutions or various MAs and fluorescently labelled *ex vivo* with CellTracker™Blue and Bodipy 493/503. Sub-objects were measured by high-content image analysis and the number of LDs and vacuoles (mean ± SEM) determined through ROI segmentation using BD AttoVision software (BD Biosciences). Significant differences among treatments were determined with GLM analyses for LDs (Wald Chi-Square = 540.811, n = 148, df = 16, $P < 0.001$) or vacuoles (Wald Chi-Square = 129.452, n = 148, df = 16, $P < 0.001$).

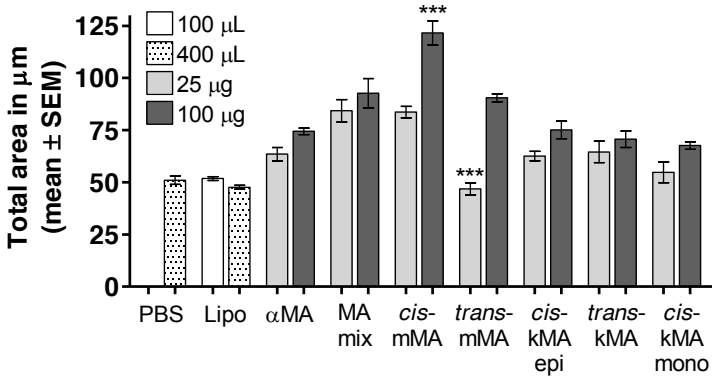

Figure 19 | Total area of intracellular vacuoles. Murine macrophages were injected with different volumes of control solutions: 400 µl PBS; 100 µl (white bar) or 400 µl (black bar) Lipo; and either of two concentrations of MA (25 or 100 µg). Through addition of all vacuole sub-objects from each treatment, differences in the total area (µm; mean ± SEM) of intracellular vacuoles were determined using the BD Pathway high-content image analyser. Significant variation among treatments were determined with a Kruskal-Wallis test ($H = 150.855$, $n = 270$, $df = 16$, $P < 0.001$).

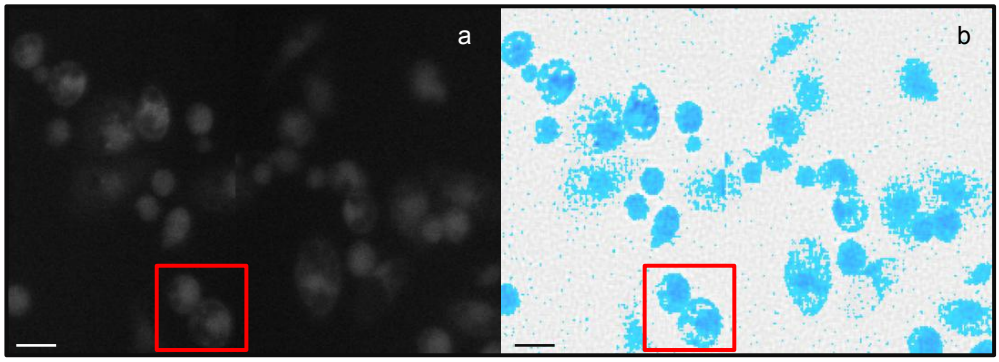

Figure 20 | Segmentation reference image. (a) Brightfield image of murine peritoneal macrophages. (b) Segmented image showing bordering cells (red squares) measured by BD AttoVision software as a single cell. Scale bar: 10 µm.

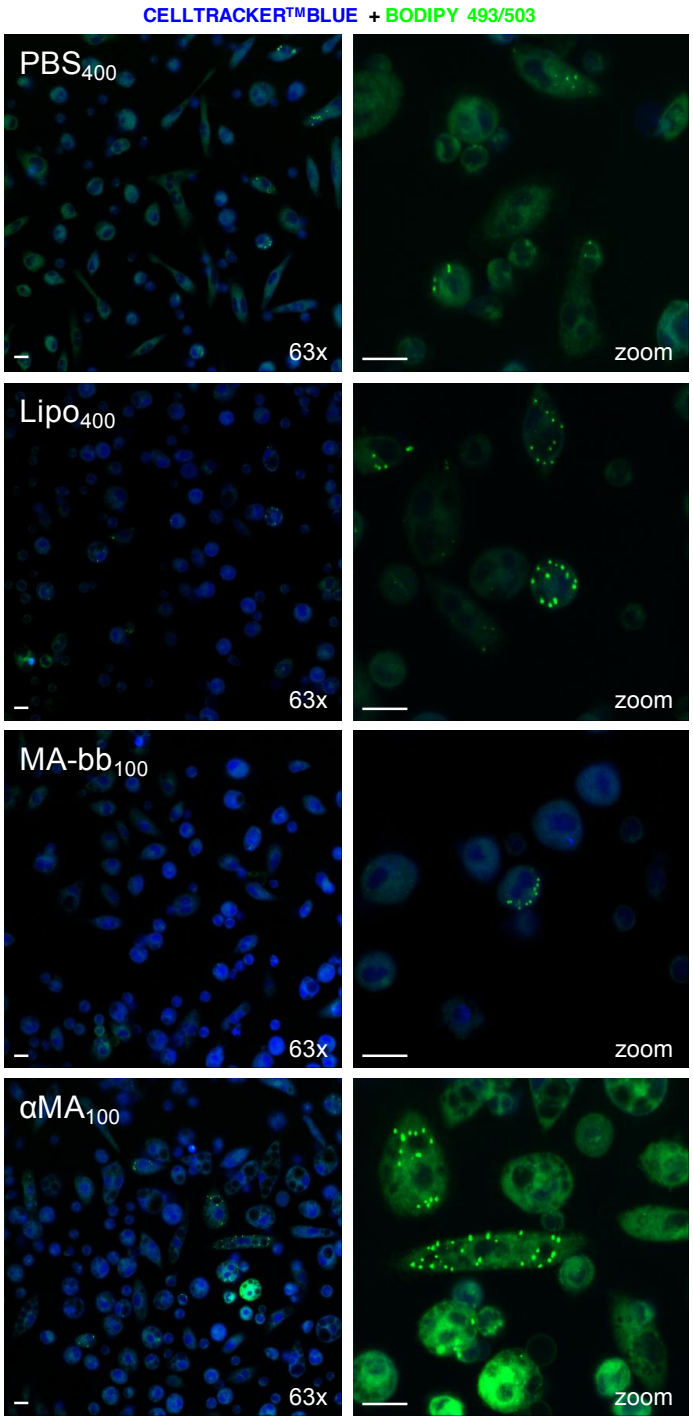

Figure 21 | Assessment of macrophage foam cells by laser-scanning-confocal microscopy. Mice were treated with 100 or 400 µl control solutions (PBS and Lipo), or received a 25 or 100 µg MA/100 µl i.p. injection. No distinct differences were recorded in volumes or MA concentration for these groups therefore only the larger volume or concentration is shown. Peritoneal macrophages were then analysed for vacuoles and LDs by laser-scanning-confocal microscopy. Fluorescent probes were CellTracker™Blue (whole cells) and Bodipy 493/503 (neutral LDs). Objective: 63x (2.65x zoom). Scale bar: 10 µm.

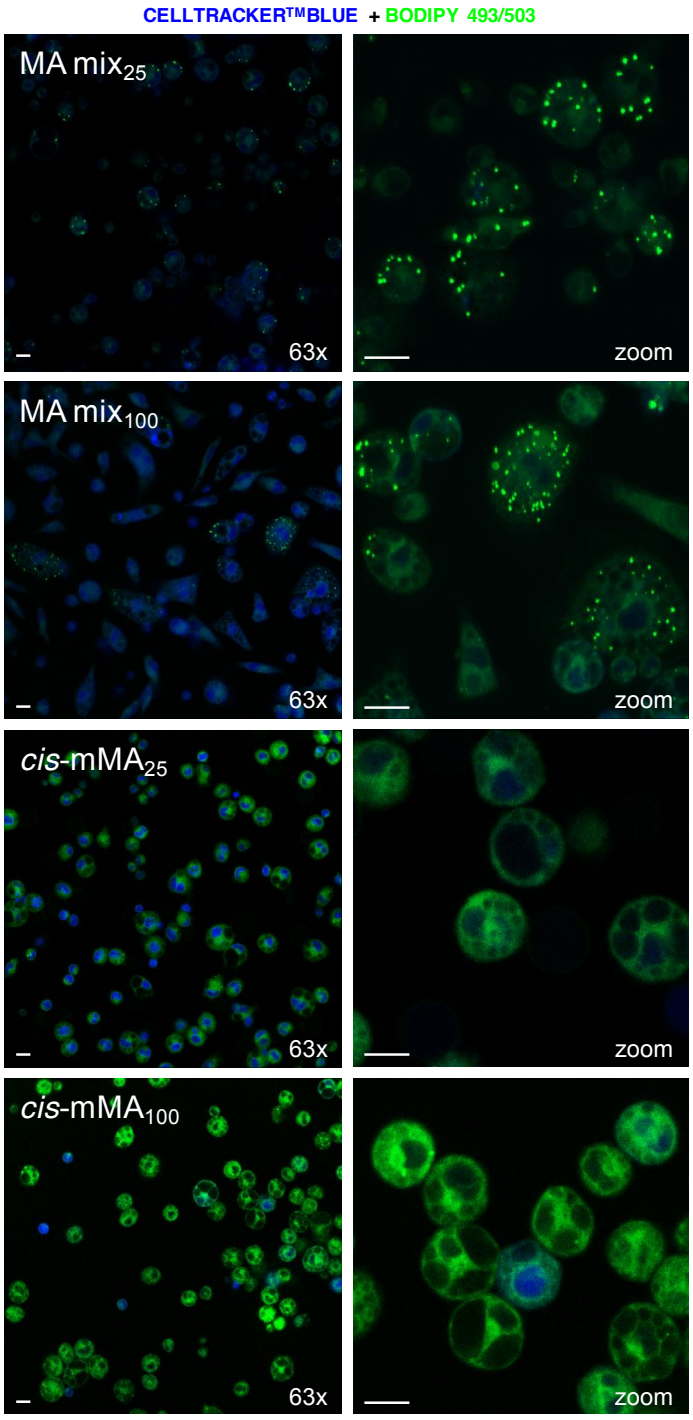

Figure 22 | Assessment of macrophage foam cells by laser-scanning-confocal microscopy. Mice received a 25 or 100 µg MA/100 µl i.p. injection. Peritoneal macrophages were then analysed for vacuoles and LDs by laser-scanning-confocal microscopy. Fluorescent probes were CellTracker™Blue (whole cells) and Bodipy 493/503 (neutral LDs). Objective: 63x (2.65x zoom). Scale bar: 10 µm.

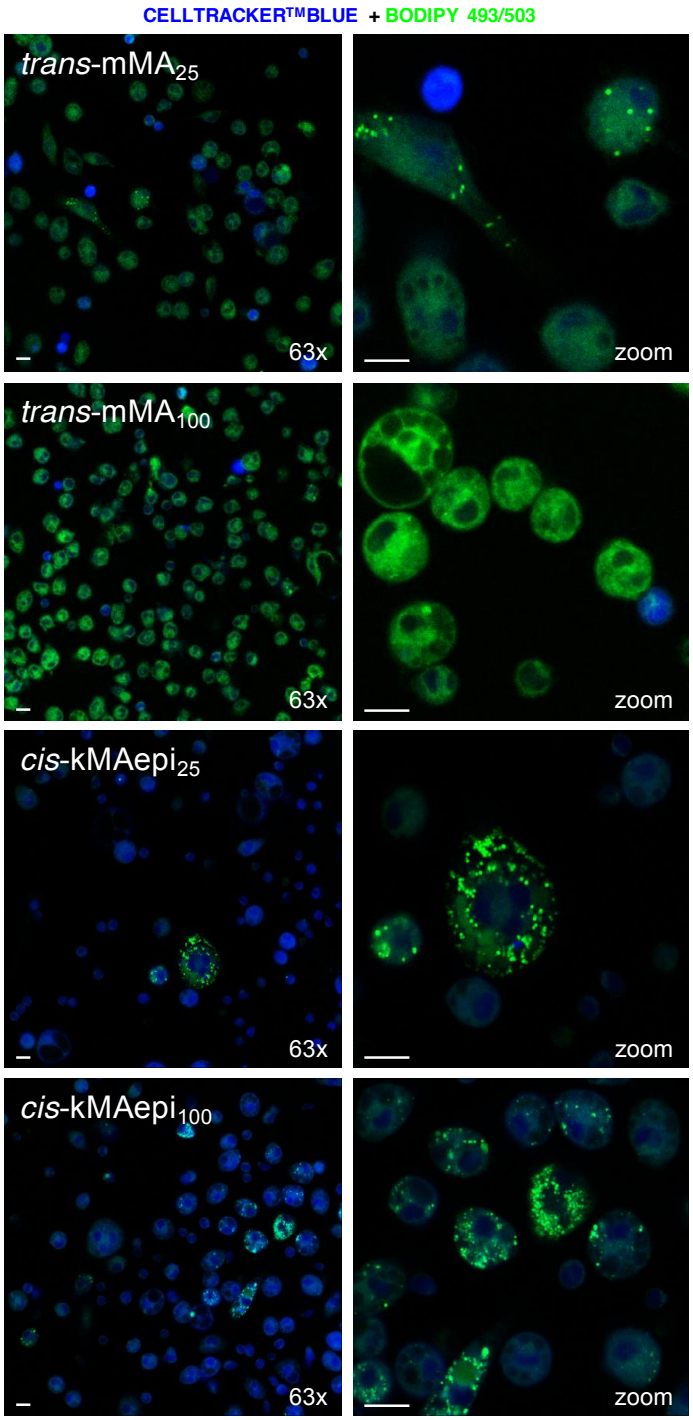

Figure 23 | Assessment of macrophage foam cells by laser-scanning-confocal microscopy. Mice received a 25 or 100 µg MA/100 µl i.p. injection. Peritoneal macrophages were then analysed for vacuoles and LDs by laser-scanning-confocal microscopy. Fluorescent probes were CellTracker™Blue (whole cells) and Bodipy 493/503 (neutral LDs). Objective: 63x (2.65x zoom). Scale bar: 10 µm.

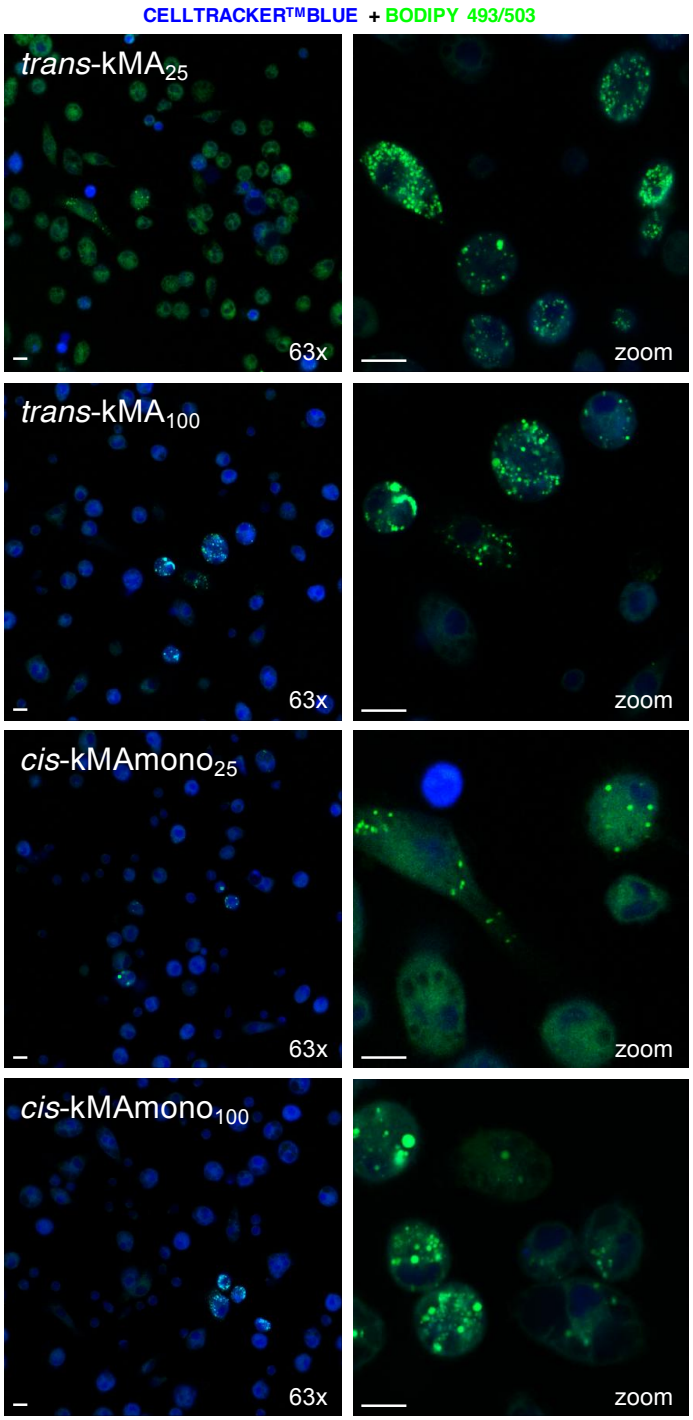

Figure 24 | Assessment of macrophage foam cells by laser-scanning-confocal microscopy. Mice received a 25 or 100 µg MA/100 µl i.p. injection. Peritoneal macrophages were then analysed for vacuoles and LDs by laser-scanning-confocal microscopy. Fluorescent probes were CellTracker™Blue (whole cells) and Bodipy 493/503 (neutral LDs). Objective: 63x (2.65x zoom). Scale bar: 10 µm.

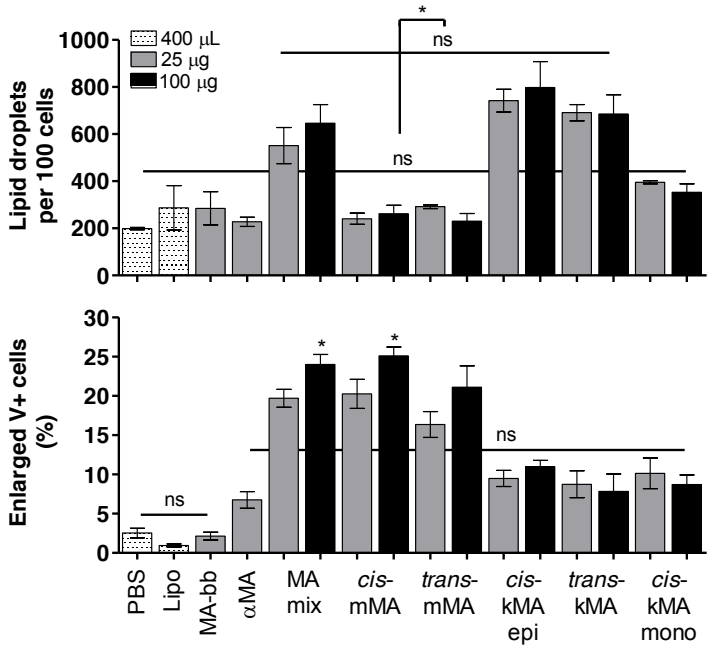

Figure 25 | Measurement of LDs and enlarged V+ cells by laser-scanning-confocal microscopy. Murine peritoneal macrophages were harvested and seeded after 24 h of treatment with placebo, control or various MAs. Following a 2 hour adherence, cells were stained with CellTracker™Blue and Bodipy 493/503. Neutral LDs (green lipophilic dye) and the proportion of enlarged V+ cells (≥24 µm) were analysed by laser-scanning-confocal microscopy. Significant differences among treatments were determined with independent Kruskal-Wallis tests for LDs ($H = 36.833$, $n = 48$, $df = 33$, $P < 0.05$) or enlarged V+ cells ($H = 45.577$, $n = 48$, $df = 33$, $P < 0.05$).

6. Optimisation of mycobacterial multiplicity of infection

6.1 Aim of technology

We aimed here to optimise the ideal mycobacterial MOI for *ex vivo* infection of murine primary peritoneal macrophages. This was optimised to ensure that cell viability, reproducibility and experimental integrity were maintained.

6.2 BCG MOI of peritoneal macrophage cultures

Materials and methods

Murine peritoneal macrophages were seeded into 24-well plates ($0.2x10^6$ to $0.5x10^6$ cells per well) for infection at MOI of 1, 3, 5 and 10 (25-400 µg/10 µl). Following overnight adherence, cells were infected with PBS (mock) or BCG for 6 h then cultured a further 60 h. Cells were labelled with the fluorescent probes Hoechst® (nucleic acids), CellTracker™Red (cytoplasm) and Bodipy 493/503 (LDs) and assessed by laser-scanning-confocal microscopy. The proportion of live versus dead cells was calculated by subtracting the total number of cells measured at 60 h after mycobacterial infection from the total cells at time point 0 h (just prior infection). Normality and significant differences were respectively assessed by Shapiro-Wilk and Kruskal-Wallis tests.

Results and discussion

Laser-scanning-confocal microscopy confirmed that BCG infection causes cell death in a dose-dependent manner with increasing MOI (Fig. 26). Macrophages without BCG (93.4% live cells) and those infected with 1 bacterium per cell (78.2% live cells) remained viable. Viability was distinctly decreased in cells infected with three (57.3% live cells), five (24.8% live cells) or ten bacilli per cell (5% live cells) after 60 h of mycobacterial infection (Fig. 26). It was an aim to measure differences in cytosolic vacuole and LD

formation, but as a result of substantial cytolysis in treatments above an MOI of 1, this was not feasible.

Avirulent or attenuated mycobacterial strains differ in their bacterial regulation of host cell apoptosis[21, 22]. Naive macrophages are resistant to tumour necrosis factor (TNF)-mediated cytotoxicity unless infected with avirulent of attenuated Mtb, which primes cells for TNF death signals involving caspases[23, 24]. Virulence-associated apoptosis suppression relates to interference of TNFα signalling via the TNF-receptor[25]. At high bacillary load (MOI ≥25), virulent Mtb causes strong apoptosis that upholds bacterial viability as a means of dissemination into host tissues[21]. Virulent mycobacteria do not, however, induce strong apoptosis at MOI ≤10 though avirulent or attenuated strains (like BCG) initiate substantial cell death[23], reflecting a host innate immune defence to bacterial invasion. Numerous authors have reported on the manner of induced apoptotic cell death (rather than necrosis) in host macrophages by mycobacteria[21-23, 25, 26]. As a result we did not measure apoptosis directly (i.e. using propidium iodide staining of dead cells), but used time course variation in total cell number as quantitative measure of BCG-associated cell death. Our data strongly reflect previous findings that BCG-treated macrophages undergo cytotoxicity at an MOI of 5 to 10 within three days of infection[23]. As cells infected with 1 mycobacterium remained viable over time and foam cell traits could be well distinguished, the highest MOI used for mycobacterial experiments in this study was 1 bacillus to 1 cell.

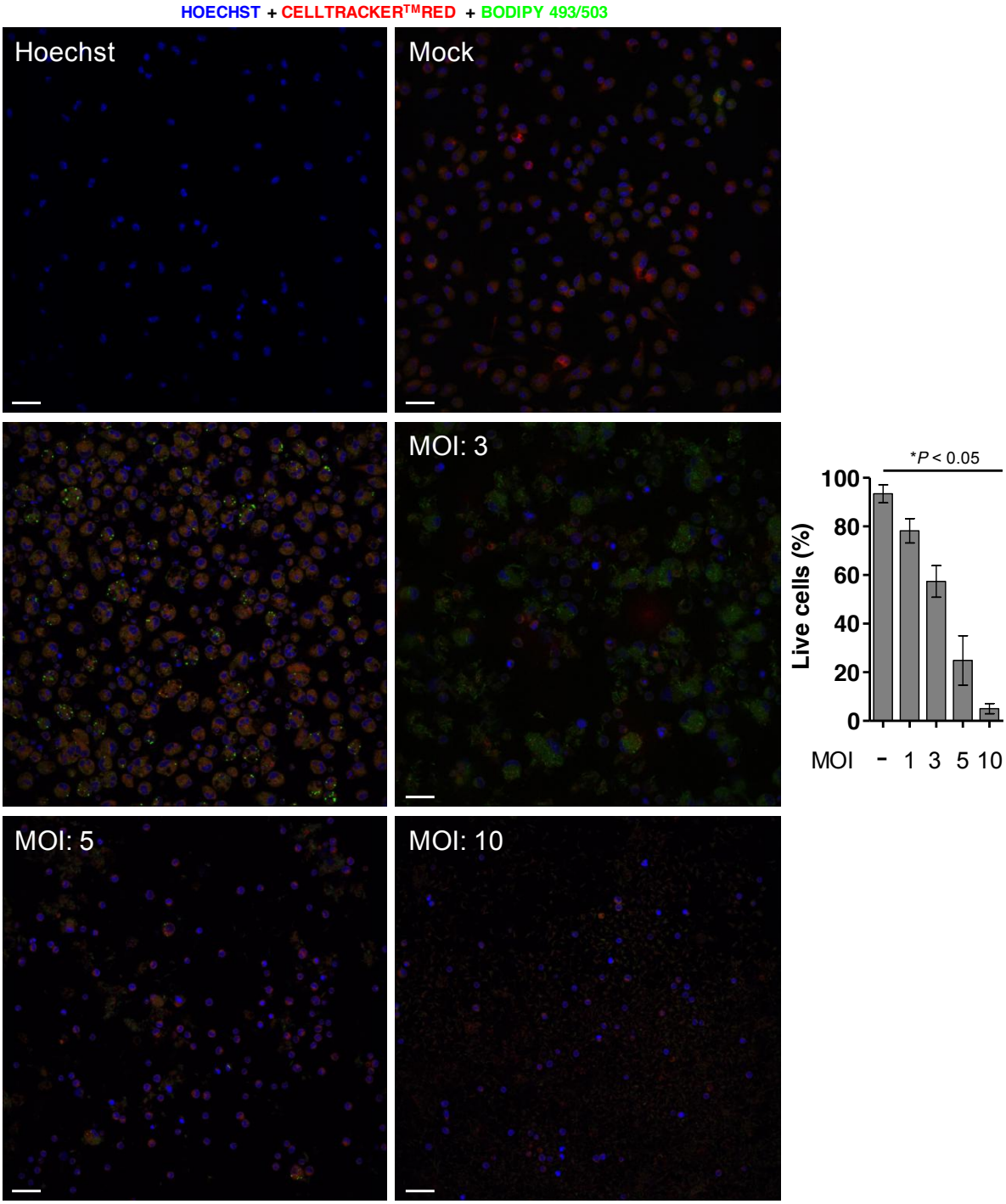

Figure 26 | Cell viability after 2.5 days of mycobacterial infection with different MOI. Peritoneal macrophages were infected *ex vivo* with PBS (mock) or BCG for 6 h at various MOIs. Cells were fluorescently labelled with Hoechst®, CellTracker™Red and Bodipy 493/503. Laser-scanning-confocal images show differences in cell viability after infection with mycobacteria with resultant cytolysis in treatments above an MOI of 1. Objective: 40x. Scale bar: 12 µm. The number of live versus dead cells was assessed by difference in total cells at the 0 h (following overnight adherence) and 60 h (2.5 days of culture) time points. Data are from three independent confocal images and have been normalised to the number of total cells before BCG infection for each treatment (mean ± SEM). Significance was determined by an independent samples Kruskal-Wallis test ($H = 13.115$, $n = 15$, $df = 4$, $^*P < 0.05$).

7. Phagocytic uptake assessment of murine peritoneal macrophages

7.1 Aim of technology

To ensure that following murine i.p. injection peritoneal macrophages exhibited comparable *in vivo* phagocytic uptake of liposome formulations containing either control compounds or the various MAs, it was necessary to assess the phagocytic capacity of these cells *ex vivo* using fluorescent microspheres. Similarly, to warrant consistency of mycobacterial uptake among peritoneal macrophages harvested from variously treated mice, *ex vivo* cultured peritoneal macrophages were assessed for BCG bacilli uptake.

7.2 Uptake of Streptavidin Fluoresbrite™ YG⁺ microspheres and BCG-dsRed by ex vivo cultured peritoneal macrophages

Materials and methods

Primary macrophages, harvested from mice after treatment with placebo (PBS), Lipo carrier or various MAs, were cultured *ex vivo* with Fluoresbrite® fluorescent microspheres (10 beads per cell; Polysciences) or BCG-dsRed (MOI: 1) for 6 h at 37°C. Immediately after three consecutive endotoxin-free PBS washes, cells were imaged by laser-scanning-confocal microscopy. The amount of beads or bacilli per cell and the proportions of fluorescent bead-positive (fb+) or BCG+ cells were quantified using Volocity 3D Image Analysis Software. Significance was assessed with independent-samples Kruskal-Wallis tests ($P < 0.05$).

Results and discussion

No less than half of the peritoneal macrophages from all treatments contained fluorescent microspheres (50-75% fb+ cells; Fig. 27A). Cells from all treatments displayed comparable phagocytic uptake of 2-3 beads per cell (Fig. 27A and 28). For the *ex vivo*

mycobacterial experiments, phagocytic uptake was determined after a 6 h infection with BCG-dsRed. For all treatments but PBS (<35 %), at least half of the peritoneal macrophages contained mycobacteria (49-65 % BCG+ cells; Figure 27B). Peritoneal macrophages exhibited equivalent phagocytic uptake of ~1 bacillus per cell, which was representative of the MOI. We thus concluded with confidence that the results obtained for the murine peritoneal macrophages used throughout this study, were not confounded by treatment and could be compared among the different groups.

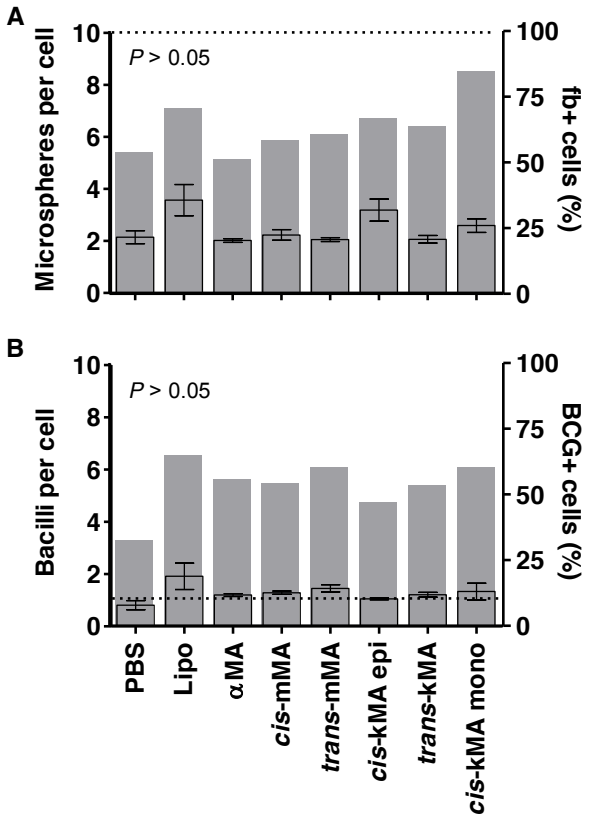

Figure 27 | Phagocytic capacity of murine peritoneal macrophages. The phagocytic capacity of peritoneal macrophages harvested from mice treated with placebo (PBS), liposome carrier (Lipo) or various MAs was determined *ex vivo* after a (**A**) 6 h incubation with Streptavidin Fluoresbrite^{TM} YG^{+} fluorescent microspheres (10 beads per cell, broken line) or (**B**) 6 h infection with BCG-dsRed (MOI: 1, broken line). Values represent mean ± SEM. Left axis, number of beads or bacilli per cell. Right axis, the proportion of fluorescent bead positive (fb+) or bacilli positive (BCG+) cells (grey bars). Significance was assessed with an independent-samples Kruskal-Wallis test for phagocytic uptake of microspheres (n = 5 confocal images; Kruskal-Wallis: H = 10.823, P = 0.147, df = 7) or BCG bacilli (n = 5 confocal images; Kruskal-Wallis: H = 13.499, P = 0.061, df = 7).

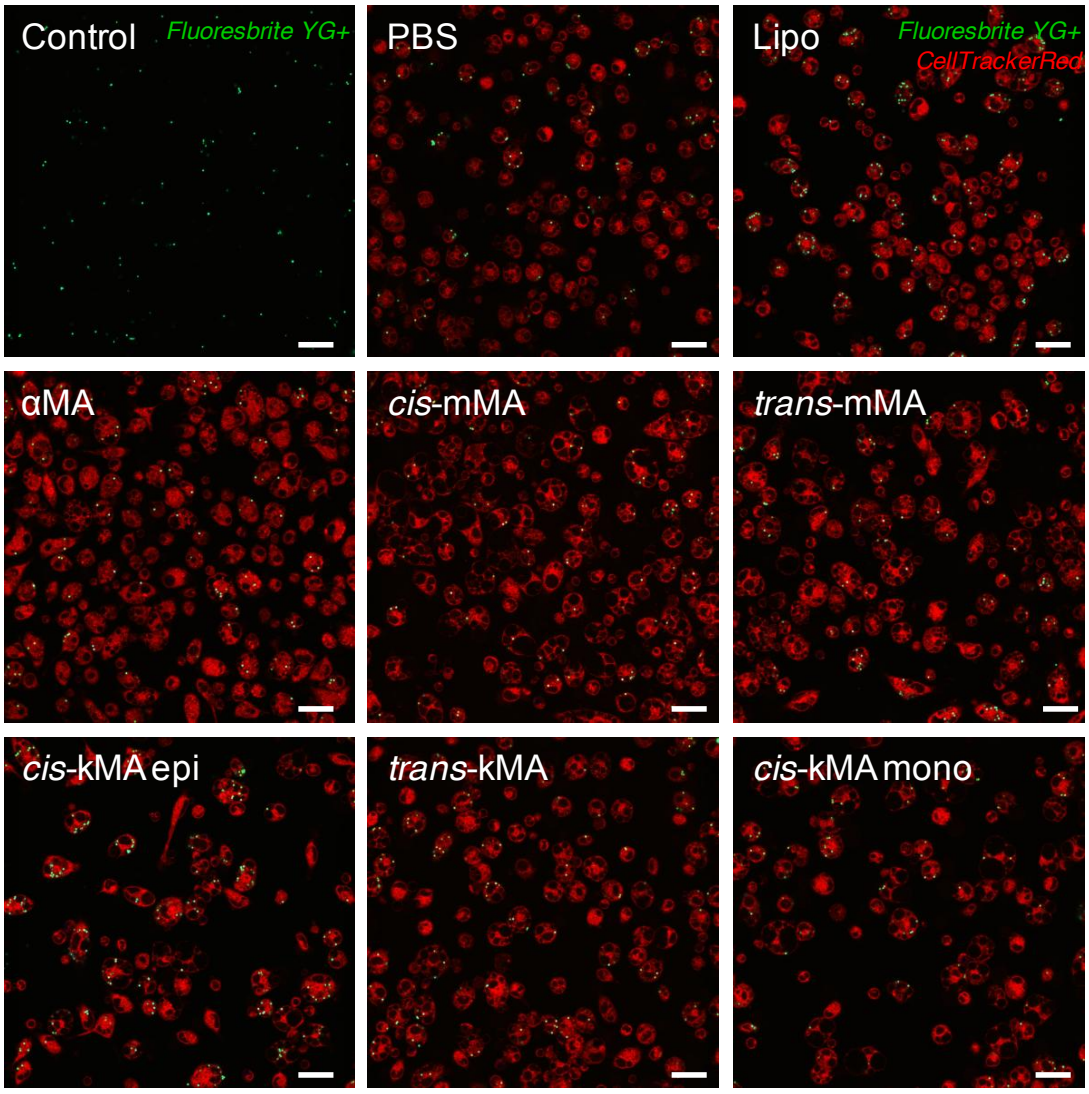

Figure 28 | Phagocytic uptake of fluorescent microspheres by murine peritoneal macrophages. Laser-scanning-confocal microscopy images depicting CellTracker™Red-stained macrophages with intracellular Streptavidin Fluoresbrite™ YG^{+} microspheres. Scale bar: 20 µm.

8. Conclusion

Like for all research undertakings, intensive optimisation of experimental conditions had to be completed. These included optimising the fluorescent probes used for visualisation of intracellular (1) mycobacteria in the absence of MA co-staining, (2) neutral LDs, and (3) vacuoles following MA treatment. The most appropriate technology for (4) quantifying multiple morphological foam cell traits was also established; while the (5) ideal MOI was optimised to ensure cell viability in all experiments and the (6) phagocytic capacity assessed to guarantee liposome formulations consistently reached target cells *in vivo* and BCG uptake of murine macrophages from variously treated mice was comparable among treatments.

We had initially planned to use quick and simple staining techniques of mycobacteria for quantification assays. Incompatibility of harsh reagents with live cell analyses and weak detection of bacterial nucleic acids using the DNA-fluorescent probe Hoechst® necessitated the acquirement of a BCG bacterial strain with a red fluorescent reporter gene. This therefore allowed direct visualisation of mycobacteria without the need for using toxic cellular staining techniques. High-content image analysis is a powerful technique for probing multiple morphological traits on a large scale. However, results from the exploratory experiments identified limitations in using this technique to quantify cytosolic LDs and vacuoles. Though laser-scanning-confocal microscopy is more laborious than high-content image analysis, it provided clear displays of cellular morphology. Volocity 3D Image Analysis software thus enabled fluorescent detection and quantification of sub-cellular organelles (i.e. LDs, vacuoles and mycobacteria) during assessment of macrophage foam cell morphology, lipid homeostasis, and mycobacterial infection.

9. References

1. Becton-Dickinson. 2014. *BD TB Stain Kits and Reagents*. Becton, Dickinson and Company, Sparks, USA. pp 42

2. Finegold, S. M., E. J. Baron and W. R. Bailey. 1990. *Bailey and Scott's Diagnostic Microbiology*, Mosby, St. Louis, MO. pp 861.

3. Nolte, F. S. and B. Metcheck. 1995. *Manual of Clinical Microbiology*, Sixth ed., American Society for Microbiology Press, Washington. pp 400-436.

4. Monger, B. C. and M. R. Landry. 1993. Flow cytometric analysis of marine bacteria with Hoechst 33342. *Appl. Environ. Microbiol.* **59**: 905-911.

5. Brennan, P. J. 2003. Structure, function, and biogenesis of the cell wall of *Mycobacterium tuberculosis*. *Tuberculosis* **83**: 91-97.

6. Riley, L. W. 2006. Of mice, men and elephants: *Mycobacterium tuberculosis* cell envelope lipids and pathogenesis. *J. Clin. Invest.* **116**: 1475-1478.

7. Jankute, M., J. A. Cox, J. Harrison and G. S. Besra. 2015. Assembly of the mycobacterial cell wall. *Annu. Rev. Microbiol.* **69**: 405-423.

8. Sartain, M. J., D. L. Dick, C. D. Rithner, D. C. Crick and J. T. Belisle. 2011. Lipidomic analyses of *Mycobacterium tuberculosis* based on accurate mass measurements and the novel "Mtb LipidDB". *J. Lipid Res.* **52**: 861-872.

9. Guo, Y., K. R. Cordes, R. V. Farese, Jr. and T. C. Walther. 2009. Lipid droplets at a glance. *J. Cell Sci.* **122**: 749-752.

10. Gao, Q. and J. M. Goodman. 2015. The lipid droplet-a well-connected organelle. *Front Cell Dev Biol* **3**: 49.

11. Olofsson, S. O., P. Bostrom, L. Andersson, M. Rutberg, J. Perman and J. Boren. 2009. Lipid droplets as dynamic organelles connecting storage and efflux of lipids. *Biochim. Biophys. Acta* **1791**: 448-458.

12. Ouimet, M. and Y. L. Marcel. 2012. Regulation of lipid droplet cholesterol efflux from macrophage foam cells. *Arterioscler. Thromb. Vasc. Biol.* **32**: 575-581.

13. Walther, T. C. and R. V. Farese, Jr. 2012. Lipid droplets and cellular lipid metabolism. *Annu. Rev. Biochem.* **81**: 687-714.

14. Penno, A., G. Hackenbroich and C. Thiele. 2013. Phospholipids and lipid droplets. *Biochim. Biophys. Acta* **1831**: 589-594.

15. Zehmer, J. K., Y. Huang, G. Peng, J. Pu, R. G. Anderson and P. Liu. 2009. A role for lipid droplets in inter-membrane lipid traffic. *Proteomics* **9**: 914-921.

16. Daniel, J., H. Maamar, C. Deb, T. D. Sirakova and P. E. Kolattukudy. 2011. *Mycobacterium tuberculosis* uses host triacylglycerol to accumulate lipid droplets and acquires a dormancy-like phenotype in lipid-loaded macrophages. *PLoS Pathog.* **7**: doi:10.1371/journal.ppat.1002093.

17. Ranall, M. V., B. G. Gabrielli and T. J. Gonda. 2011. High-content imaging of neutral lipid droplets with 1,6-diphenylhexatriene. *Biotechniques* **51**: 35-36, 38-42.

18. Korf, J., A. Stoltz, J. Verschoor, P. De Baetselier and J. Grooten. 2005. The *Mycobacterium tuberculosis* cell wall component mycolic acid elicits pathogen-associated host innate immune responses. *Eur. J. Immunol.* **35**: 890-900.

19. Singh, V., S. Jamwal, R. Jain, P. Verma, R. Gokhale and K. V. Rao. 2012. *Mycobacterium tuberculosis*-driven targeted recalibration of macrophage lipid homeostasis promotes the foamy phenotype. *Cell Host Microbe* **12**: 669-681.

20. Becton-Dickinson. (2009) BD Pathway Bioimaging Systems. BD Biosciences, San Jose, CA.

21. Keane, J., H. G. Remold and H. Kornfeld. 2000. Virulent *Mycobacterium tuberculosis* Strains Evade Apoptosis of Infected Alveolar Macrophages. *J*. *Immunol*. **164**: 2016-2020.

22. Lee, J., H. G. Remold, M. H. Ieong and H. Kornfeld. 2006. Macrophage Apoptosis in Response to High Intracellular Burden of *Mycobacterium tuberculosis* Is Mediated by a Novel Caspase-Independent Pathway. *J*. *Immunol*. **176**: 4267-4274.

23. Riendeau, C. J. and H. Kornfeld. 2003. THP-1 Cell Apoptosis in Response to Mycobacterial Infection. *Infect*. *Immun*. **71**: 254-259.

24. Jayaraman, P., I. Sada-Ovalle, T. Nishimura, A. C. Anderson, V. K. Kuchroo, H. G. Remold and S. M. Behar. 2013. IL-1beta promotes antimicrobial immunity in macrophages by regulating TNFR signaling and caspase-3 activation. *J*. *Immunol*. **190**: 4196-4204.

25. Spira, A., J. D. Carrol, G. Lui, Z. Aziz, V. Shah, H. Kornfeld and J. Keane. 2003. Apoptosis genes in human alveolar macrophages infected with virulent or attenuated *Mycobacterium tuberculosis*. *Am*. *J*. *Respir*. *Cell Mol*. *Biol*. **29**: 545-551.

26. Keane, J., M. K. Balcewics-Sablinska, H. G. Remold, G. L. Chupp, B. B. Meek, M. J. Fenton and H. Kornfeld. 1997. Infection by *Mycobacterium tuberculosis* Promotes Human Alveolar Macrophage Apoptosis. *Infect*. *Immun*. **65**: 298-304.